Biopolymer based structures for biological tissue reconstruction

Cristinel-Nicolae Degeratu

Thèse de Doctorat

Cristinel-Nicolae DEGERATU

Mémoire présenté en vue de l'obtention du
grade de Docteur de l'Université d'Angers
sous le label de L'Université Nantes Angers Le Mans
et
grade de Docteur de l'Université POLITEHNICA de Bucarest

École doctorale : *Biologie santé (section CNU 65)*
Discipline : *Biologie Cellulaire*
Unité de recherche : ***GEROM*** *: Groupe d'Etudes sur le Remodelage Osseux et les bioMatériaux - UPRES EA 4658*
et Département des Bioresources et Science des Polymères - UPB Bucarest
Soutenue le *19.07.2013*
Thèse N° : ***1346***

Structures de biopolymères pour la reconstruction de tissus biologiques

Biopolymer based structures for biological tissue reconstruction

JURY

Rapporteurs :	**Elena PREOTEASA**, *Professeur, Université de Médicine et Pharmacie "Carol Davila" Bucarest* **Gabriela BĂNCASCU**, *Maitre de conférences, Université de Médicine et Pharmacie "Carol Davila" Bucarest*
Examinateurs :	**Elena PREOTEASA,** ***Professeur, Université de Médicine et Pharmacie "Carol Davila" Bucarest*** **Gabriela BĂNCASCU,** ***Maitre de conférences, Université de Médicine et Pharmacie "Carol Davila" Bucarest*** **Guillaume MABILLEAU**, Ingénieur de Recherche, *Université d'Angers* **Gheorghe HUBCA**, *Professeur*, *Université POLITEHNICA de Bucarest*
Directeur de Thèse :	**Daniel CHAPPARD**, *Professeur, Université d'Angers*
Co-directeur de Thèse :	**Corneliu CINCU**, *Professeur, Université POLITEHNICA de Bucarest*

FONDUL SOCIAL EUROPEAN
Investeşte în oameni!
Programul Operaţional Sectorial pentru Dezvoltarea Resurselor Umane 2007 – 2013
Proiect POSDRU/88/1.5/S/61178 – *Competitivitate şi performanţă în cercetare prin programe doctorale de calitate (ProDOC)*

UNIVERSITATEA POLITEHNICA DIN BUCUREŞTI
Facultatea Chimie Aplicată și Știința Materialelor
Departamentul de Bioresurse și Știința Polimerilor

Université D'Angers
Faculté de médecine

TEZĂ DE DOCTORAT

(Teză în cotutelă)

Structuri pe bază de biopolimeri pentru reconstrucţia ţesuturilor biologice

Biopolymers based structures for biological tissue reconstruction

Autor: ing. Cristinel-Nicolae DEGERATU

Conducător de doctorat: **Prof. dr. ing. Corneliu CINCU**

Prof. dr. Daniel CHAPPARD

Bucharest 2013

Acknowledgments

First and foremost I would like to thank my two promoters, Prof. Dr. Eng. Corneliu CINCU from the University Politehnica of Bucharest and Prof. Dr. MD Daniel CHAPPARD for their valuable scientific guidance and support throughout my PhD programme. Their mentorship has greatly contributed to my development as a researcher. Special thanks to Guillaume Mabilleau for his invaluable support and expert supervision during my stage in France.

Special thanks to Dr. Eng. Cătălin ZAHARIA, lecturer at University Politehnica of Bucharest for his guidance in key moments during the development of my thesis.

I would also like to express my thanks to Sonia GEORGEAULT and Romain MALLET for their support in performing SEM investigations, as well as to the entire staff of INSER-U922: Helene LIBOUBAN, Elodie FIOLEAU, Christine GAUDIN and Florence PASCARETTI for welcoming me in their team during my stage in Angers. Special thanks to Laurence LECHAT for her support with crucial administrative matters.

My appreciation goes also to my PhD fellows: Beatrice BOUVARD, Florence MALLARD and Mambaye N'DIAYE at the University of Angers, Aurel DIACON – special thanks for his constant help and encouragements, Alexandra MOCANU, Diana DRĂGUŞIN, Andrada SERAFIM, and Ramona TUDORA for their team spirit.

Last but certainly not least, I would like to thank my family and especially my wife, who has always believed in me and provided essential help and reassurance, despite her very busy schedule.

The present thesis has been funded by the Sectoral Operational Programme Human Resources Development 2007-2013 of the Romanian Ministry of Labour, Family and Social Protection through the Financial Agreement POSDRU/88/1.5/S/61178.

TABLE OF CONTENT

ACKNOWLEDGMENTS....2

INTRODUCTION....7

I.1. GENERAL ASPECTS ON BONE....11

I.1.1 Definitions....11

I.1.2. Tissue engineering of bone....12

I.1.3 Bone morphology and composition....13

a. Mineral matrix....17

b. Organic matrix....18

c. Bone cells....18

I.1.4. Bone mineralization....20

a. Local inhibitors of mineralization....20

b. Local stimulators of mineralization....21

c. Hydroxylapatite as stimulator biomaterial for bone mineralization....21

I.2. GENERAL ASPECTS REGARDING BIOMATERIALS....23

I.2.1. Definitions....24

I.2.2. Biomaterials-based scaffolds....26

The biocompatibility of polymers....28

I.2.3. Synthetic biodegradable polymers as biomaterials....28

I.2.4. Natural biodegradable polymers as biomaterials....29

I.3. STRUCTURE AND PROPRIETIES OF POLYHYDROXYALKANOATES....30

3 Poly(3-hydroxybutyrate) and Poly(3-hydroxybutyrate-co-3-hydroxyvalerate)....33

I.3.1 Mechanical Properties....34

I.3.1. Polyhydroxyalkanoates based biomaterials....37

Biocompatibility....37

Toxicity Testing....37

Cell Culture Studies....37

In vivo Studies....43

I.3.2. Biocompatibility and biodegradability of polyhydroxyalkanoates....45

In Vitro Degradation....45

In vivo Degradation....47

I.3.3. Applications of polyhydroxyalkanoates in tissue engineering....48

Patches....48

Nerve Conduits....49

Bone and Cartilage Repair....50

I.3.4. Other applications of polyhydroxyalkanoates....51

I.4. STRUCTURE AND PROPRIETIES OF SILK FIBROIN....52

I.4.1. Fibrous proteins with potential in biomedical applications....60

a. Silk fibroin fibers....61

b. Silk fibroin scaffolds....61

c. Silk fibroin particles....62

I.4.2. Applications of silk fibroin in tissue engineering....63

I.5. STRUCTURE AND PROPRIETIES OF POLY(HYDROXYETHYL METHACRYLATE)....64

CHAPTER II - PREPARATION, PHYSICO-CHEMICAL AND MECHANICAL ASSESSMENTS OF THE BIOPOLYMER BASED STRUCTURES....67

II.1 MICROPARTICLES PREPARATION 68
Materials 68
Methods 68
Solution preparation 68
Microparticles preparation 69
Optical microscopy (OM) analysis 69
SEM analysis 69
Results 70
Conclusions 72
II.2 BIODEGRADABLE POLYHYDROXYALKANOATES BASED STRUCTURES WITH MEDICAL APPLICATIONS 72
Materials and methods 72
Films preparation 73
Tubes preparation 73
Differential scanning calorimetry analysis (DSC) 73
In vitro test 73
SEM analysis 74
Contact Angle Measurement 74
Results 75
Contact angle 75
Conclusion: 77
II.3 FUNCTIONALIZATION OF NATURAL POLYESTER FILMS BY LOW-PRESSURE OXYGEN PLASMA DISCHARGE AND THEIR MEDICAL USES 77
Materials 78
Conclusions 80
II.4 BIODEGRADABLES BLENDS OF POLY(3-HYDROXYBUTYRATE) WITH NATURAL FIBERS 81
Experimental part 83
Materials 83
Methods 84
Characterization 85
Results and discussion 85
Conclusions 95
II.5 DETERMINATION OF MICROPOROSITY USING MICROCT TECHNIQUE 96
Material and methods 97
Image analysis 102
Measurements of lacunarity and succolarity 103
Results and discussion 105
Conclusion 110
CHAPTER III - EVALUATION OF BIOPOLYMER-BASED STRUCTURES FOR APPLICATION IN TISSUE ENGINEERING 112
III.1 INFLUENCE OF POROSITY UPON CELL ADHESION ON POLYHYDROXYALKANOATES FILMS 113
Experimental 113
Materials 113
Methods 114

Biocompatibility tests 114
Results and Discussion 115
Conclusions 119
III.2 *IN VITRO* AND *IN VIVO* BEHAVIOR OF POLY(HYDROXYBUTYRATE-CO-HYDROXYVALERATE) FIBERS ..... ERROR! BOOKMARK NOT DEFINED. 119
Material and method ..... Error! Bookmark not defined. 121
Fibers preparation ..... **Error! Bookmark not defined.** 121
Fibers scaffolds preparation ..... **Error! Bookmark not defined.** 122
Cell culture ..... **Error! Bookmark not defined.** 123
Cell viability assay ..... **Error! Bookmark not defined.** 124
Scanning electron microscopy (SEM) ..... **Error! Bookmark not defined.** 124
Transmission electron microscopy (TEM) ..... **Error! Bookmark not defined.** 124
Animals and surgical procedure ..... **Error! Bookmark not defined.** 125
X-ray microcomputed tomography (microCT) ..... **Error! Bookmark not defined.** 127
Histological analysis ..... **Error! Bookmark not defined.** 128
Results ..... Error! Bookmark not defined. 128
Cell viability assay ..... **Error! Bookmark not defined.** 128
Scanning electron microscopy (SEM) ..... **Error! Bookmark not defined.** 130
Transmission electron microscopy (TEM) ..... **Error! Bookmark not defined.** 133
MicroCT ..... **Error! Bookmark not defined.** 133
Histological examination ..... **Error! Bookmark not defined.** 136
Discussion ..... Error! Bookmark not defined. 136
Conclusion ..... Error! Bookmark not defined. 137
III.3 MINERALIZATION OF GRAFTED SILK FIBROIN ' 120
Experimental 122
Materials 122
Methods 124
IA-HEMA grafting onto cellulose and silk fibroin fibers 124
Grafting AMPSA, HEMA-AMPSA onto fibroin fiber 126
Biomineralization assay 130
Biomineralization assay of grafted cellulose and fibroin fibers with IA-HEMA 130
Biomineralization assay of grafted fibroin fibers with AMPSA, HEMA-AMPSA 131
Physico-chemical characterization 131
Physico-chemical characterization of grafted cellulose and fibroin fibers with IA-HEMA 131
a. SEM analysis 131
b. Ca and P dosage 131
Physico-chemical characterization of grafted fibroin fibers with AMPSA, HEMA-AMPSA 131
a) FTIR-ATR characterization 131
b) XPS characterization 132
c) SEM analysis 132
Grafting yield 132
Results and discussions 132
Grafting yield of grafted cellulose and fibroin fibers with IA-HEMA 132
Grafting yield of grafted fibroin fibers with AMPSA, HEMA-AMPSA 133
Ca and P dosage grafted cellulose and fibroin fibers with IA-HEMA 133
FTIR-ATR measurements 134
XPS characterization 136
Biomineralization assay and SEM analysis 139
Biomineralization assay and SEM analysis of grafted cellulose and fibroin fibers with IA-HEMA 139

Biomineralization assay and SEM analysis of grafted fibroin with grafted fibroin fibers with AMPSA, HEMA-AMPSA 141
Conclusions **147**
CHAPTER IV - INFLUENCE OF ALUMINUM ON BONE MINERALIZATION **148**
INTRODUCTION **149**
MATERIAL AND METHOD **150**
The monomer **150**
Preparation of polymer pellets **151**
Incubation of pellets in synthetic body fluids **153**
Chemical analysis **154**
Scanning electron microscopy (SEM) and energy-dispersive X-ray analysis (EDX) **154**
Statistical analysis **154**
RESULTS **155**
Chemical analysis **155**
Scanning electron microscopy **158**
DISCUSSION **162**
CONCLUSIONS. **163**
CONCLUDING REMARKS AND PERSPECTIVES **165**
BIBLIOGRAPHY **169**
LIST OF PUBLISHED PAPERS AND CONFERENCE PARTICIPATIONS **184**

INTRODUCTION

Tissue engineering, as a strategy for the repair or replacement of damaged tissues or organs, involves the use of materials and cells *in v*itro on a synthetic structure, in order to understand the effects on tissue proliferation, and the subsequent implantation of the construct into patients.

The far-reaching goal of tissue engineering is to enable virtually any tissue or organ of the body to be made *de novo* [1]. To achieve this very ambitious endeavor, multidisciplinary research is needed, with considerable biological input to gain insight into the behavior of cells during *in vitro* culture and *in vivo* implantation. It also requires extensive engineering knowledge to fabricate and process materials that are suitable for guiding tissue development [2].

In the past decades there has been extensive research on various biopolymers with the aim of assessing the most suitable materials for repairing bone defects and promoting osteoconductivity. Polyhydroxyalkanoates (PHA), along with natural fibers, have emerged as one of the most promising materials for bone reconstruction/tissue engineering.

AIM AND STRUCTURE OF THE RESEARCH PROGRAMME

My research aimed to assess the biological effects of polymers, especially on biopolymers, used as supports for osteoconduction and interactions phospho-calcium ions and metals. To achieve this aim, the following specific objectives were defined:

1. Obtaining structures based on PHA and natural fibers, for medical purposes - films; fibers; blocks or other types of compact and/or porous structures – from solutions;
2. Physical or chemical modification of the obtained structures to improve their biocompatibility properties;
3. Biological characterization of the materials *in vitro* and *in vivo*;
4. Study the influence of metals on the mineralization of bone tissue.

In order to combine the engineering and medical approaches for meaningful results, the research was conducted at two departments with complementary approaches: the Faculty of Applied Chemistry and Material Sciences at the Politehnica University of Bucharest and the Faculty of Medicine of the University of Angers, France.

The initial part of the work was conducted in Bucharest and included analyses on the following lines:

- Considering the polyhydroxyalkanoates as natural polymers to be good candidates to make grafts *in vivo*, there was the need to extensively purify them to obtain suitable materials for implantation; The processing of polymers used a variety of techniques allowing them to be molded and shaped (films, filaments, 3D networks ...).

- The obtained structures were characterized by employing mechanical and physical chemical methods (Raman, FTIR, profiling ...). A chemical and physical modeling of surfaces of the material was used to improve their biocompatibility.

The research conducted at the University of Angers included:

- Optimization of processing methods for the biopolymers, to adjust them to *in vitro* environment. New functionalization techniques were carried out in order to obtain controlled and reproducible biomaterials with physical and mechanical properties that are compatible with osteoconductive and mineralization surface (carboxymethylation).

- Determination of certain biological characteristics of the obtained materials, such as cytotoxicity, mineralization ability and cytocompatibility;

- Examine biomaterials/polymers *in vitro* and *in vivo* to determine their physical properties (size, shape) and mechanical specifications required for the use as bone graft;

- Implantation of the biopolymer grafts in animal critical bone defects in order to quantify the osteoconduction *in vivo*.

STRUCTURE OF THE THESIS

This thesis is divided into four chapters as given below:

Chapter I is based on literature review and gives an overview of the biomaterials used in tissue engineering. My study included review of the properties and applications of the following biomaterials: polyhydroxyalkanoates; silk fibroin and poly(hydroxyethyl methacrylate). Special emphasis is put on biopolymers, namely PHA and silk fibroin.

The chapter also gives an overview of the work done by others and of the current limits and perspectives in the use of biopolymers.

Chapter II presents the various biopolymer-based structures: films; microparticles; fibers; tubes and microporous structures which have been prepared in the inception phase of my research. It also includes the assessment of physical, chemical and mechanical properties of

PHA and natural fibers, including the results of a study on microporosity assessment using microCT technique.

Chapter III discusses the evaluation of biopolymers structures on cell proliferation, in order to assess their potential for application in tissue engineering. The first part discusses the influence of porosity on cell adhesion of polyhydroxyalkanoates films. The second part of this chapter is a study on *in-vitro* and *in-vivo* behavior of poly(hydroxybutyrate-co-hydroxyvalerate) (PHBV) fibers.

The final part includes the results of a study concerning the modification of fibroin fibers with synthetic polymers, with the aim to enhance mineralization on silk fibroin.

Chapter IV discusses the influence of aluminum on bone mineralization. While this may come across as a separate direction within my research programme, this study was motivated by the alarming findings on the harmful effects of aluminum on bone mineralization, which can influence the success of bone regeneration using biopolymers.

The thesis ends with concluding remarks and perspectives for the use of results and further research.

Chapter I - Literature review

I.1. General aspects on bone

Bone is not an inert tissue but dynamically metabolized connective tissue throughout life [3, 4]. It is very clearly that old bone matrices are always replaced by newly formed matrices. This process occurs continuously (named bone remodeling) and is important for maintaining bone volume and strength. Bone volume is maintained by the balance of bone resorption and bone formation due to the cells which compose it . Bone cells consist of osteoblast-lineage cells [5, 6] and osteoclast-lineage cells [7]. Their differentiation and function are regulated by osteotropic hormones and cytokines. Recent research are showing that osteoblast cells are not only involved in bone formation but also in bone resorption via supporting differentiation and activation of osteoclasts [8].

I.1.1 Definitions

Bone is a complex regenerative tissue which can be described by any of one of the following definitions, depends of how exact or precise it should be the definition:

The hard, rigid form of connective tissue constituting most of the skeleton of vertebrates, composed chiefly of calcium salts embedded in collagen fibers (this definition refers to bone as a material) [9].

Any distinct piece of the skeleton of the body (a simple and pointed definition) [9].

Any of numerous anatomically distinct structures making up the skeleton of a vertebrate animal. There are more than 200 different bones in the human body (this is based on previously with more words) [1].

The dense, semirigid, porous, calcified connective tissue forming the major portion of the skeleton of most vertebrates. It consists of a dense organic matrix and an inorganic, mineral component [2].

Hard tissue consisting of a calcified matrix (mainly calcium phosphate) and fibres of protein. It is living tissue with its own blood supply. Bones have a number of functions: they support

[1] http://www.thefreedictionary.com/Bones

[2] Ibidem

and protect soft tissues; they act as levers for muscle movement; and the central cavities of long bones store minerals and produce blood cells[3].

I.1.2. Tissue engineering of bone

Tissue engineering defined *as an interdisciplinary field that applies the principles of engineering and life sciences toward the development of biological substitutes that restore maintain or improve tissue or organ function [10]* provides new opportunities for bone regeneration and substitution based on an implant composed of a biocompatible, biodegradable scaffold, which modulates the cells to form new tissue.

Bone defects represent a major problem medicine field. Bone transplantation may be a solution, but has many disadvantages, including additional patient pain and rehabilitation time. Bone grafts are the second most transplanted material into the body.

Due to their strength and resistance to fracture fatigue, metals are the current material of choice for load-bearing implants (fracture fixation), but not the ideal because they are not naturally absorbed by the body.

Other strategies for surgical intervention and subsequent bone repair are represented by natural bone-grafts (xenografts, autografts and allografts), but each possesses several limitations. Also synthetic bone-graft substitutes are developed to exceed the inherent limitations of these. These synthetic graft substitutes, formed from a variety of materials (natural and synthetic polymers, ceramics, and composites) are designed to mimic the three-dimensional characteristics of autografts tissue and in the same time maintaining viable cell populations [11].

An ideal bone graft material should supports or stimulates: osteointegration, osteoconduction, osteoinduction, and osteogenesis [12].

Mechanical and geometrical requirements still remain problems for tissue engineering, and are considered the causes of many unsuccessful implants, such as those based on collagen. In this respect, it is essential to use basic building materials that retain mechanical and structural requirements found in bone. Ideally, the implanted tissue must be functional in terms of mechanical and biological, and restore when it is introduced, all biological and biomechanical functions [13].

This biological activity has received much attention in developing new materials for bone repair and regeneration.

[3] http://www.answers.com/topic/bone

Bone is an organic-inorganic hybrid, with a characteristic structure leading to specific mechanical properties such as high fracture strength and flexibility. In order to obtain new materials for bone repair, a good strategy would be mimicking the bone structure. From this point of view, the production of hybrid materials consisting of apatite and natural organic polymer may be a good strategy to get the materials for bone repair, which have the ability to bind to bone and mechanical properties similar to those of natural bone.

Bioactive ceramics, like hydroxyapatite and organic glass are widely used as bone substitute materials because it can bond to the living bone.

Also it was proposed a biomimetic process using a reaction between bioactive glass and plasma simulating fluids, called SBF (Simulated Body Fluid). This has attracted increased attention because bone apatite layer can be deposited on organic substrates. In this method, an organic substrate is initially placed near the glass bioactive in SBF, which has an ion concentration almost equal to that of human extracellular fluid [14].

I.1.3 Bone morphology and composition

Bone is a superb engineering construction with an outer compact sheath and a inner trabecular scaffold allowing optimal mechanical properties with minimal weight [15].

From a biological perspective, bone is a remarkable living tissue whose functions in the body are to support loads imposed on the body, provide a rigid frame that permits locomotion, protect internal organs against injury, act as a reservoir for mineral elements and actively participate in calcium homeostasis of the body, and also to produce blood cells within the marrow [16].

Bone contains different structures on different levels due to its hierarchical structure. Macroscopically, bone may be classified as either compact bone or trabecular bone (Figure I.1).

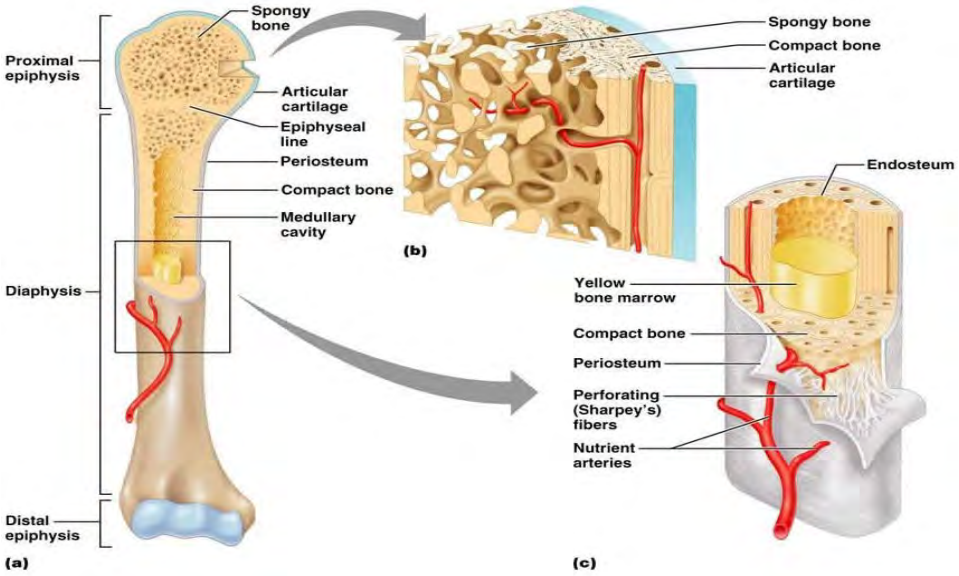

Figure I. 1: Structure of a Typical Long Bone [4]

In the adult skeleton, compact bone represents 80 % of the total bone mass. The compact bone, also called cortical bone, is a "composite" material in the true sense of the word, and is characterized by its dense compact structure, with 5-10 % porosity thus containing minimal amounts of cells and blood vessels [17].

It is rigid, anisotropic and plays a major role in mechanical stability and protection to vital organs. Cortical bone porosity consists of the Haversian canals (aligned with the long axis of the bone) and Volkmann's canals (oriented approximately perpendicular to the long axis of the bone, transverse canals connecting Haversian canals) with capillaries and nerves. Other porosities are associated with lacunae (cavities connected through small canals known as canaliculi) and with the space between collagen and hydroxyapatite.

Cortical bone consists of cylindrical structures known as osteons or Haversian systems, which represent its basic structural building blocks. The osteon diameter is always about 200 μm, formed by cylindrical lamellae surrounding the Haversian canal.

[4] http://classes.midlandstech.edu/carterp/Courses/bio210/chap06/Slide3.JPG

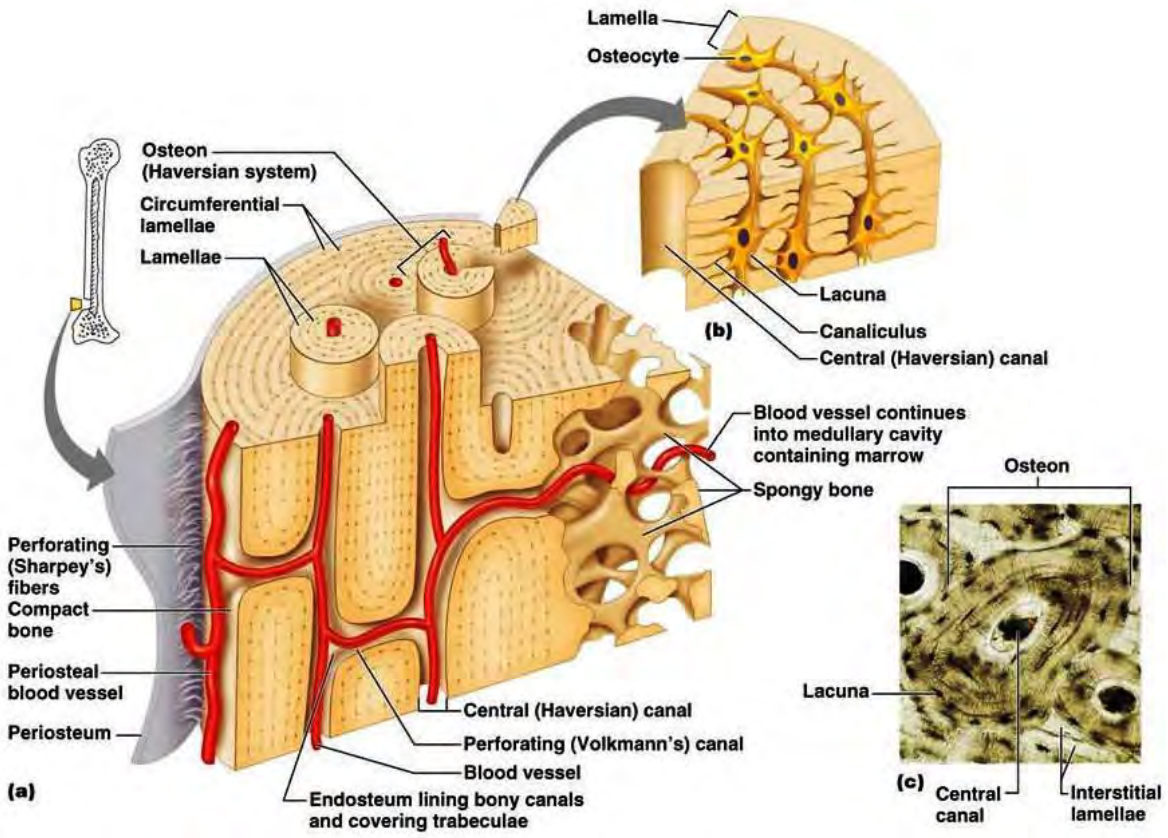

Figure I. 2: Microscopically structure of cortical bone. a) 3D sketch of cortical bone; b) Cut of a Haversian system; c) photomicrograph of a Haversian system [5].

Blood vessels run within these canals and are the primary source of nutrients to osteocytes embedded in the concentric lamellae. The boundary between the osteon and the surrounding bone is known as the cement line. Cortical bone is usually found in long bones (femur and tibia), short bones (wrist and ankle) and flat bones (skull vault and irregular bones). Cortical bone acts as an "envelope" for trabecular bone, together providing resistance to bending, tensional, and compressive forces [18].

The trabecular bone named cancellous (Figure I. 3) is less dense than cortical bone but it is metabolically more active. It is commonly found in the interior part of the bones, especially in the vertebral bodies, pelvic bones, and in the epiphyses and methaphysis of long bones.

The structure of the trabecular bone is a latticework of struts (trabeculae), that have a lamellar structure and shaped as plates and rods 100–150 μm thick [19]. Trabecular bone is a highly porous form of bone which has a porosity ranging between 50–95 % with the trabeculae

[5] Ibidem

aligned in the direction of stress application, thus varying between different bones. Three dimensional structure of trabecular bone consists of interconnected pores.

The pores are interconnected and filled with marrow (a tissue composed of blood vessels, nerves and various types of cells, whose main function is to produce the basic blood cells) [20].

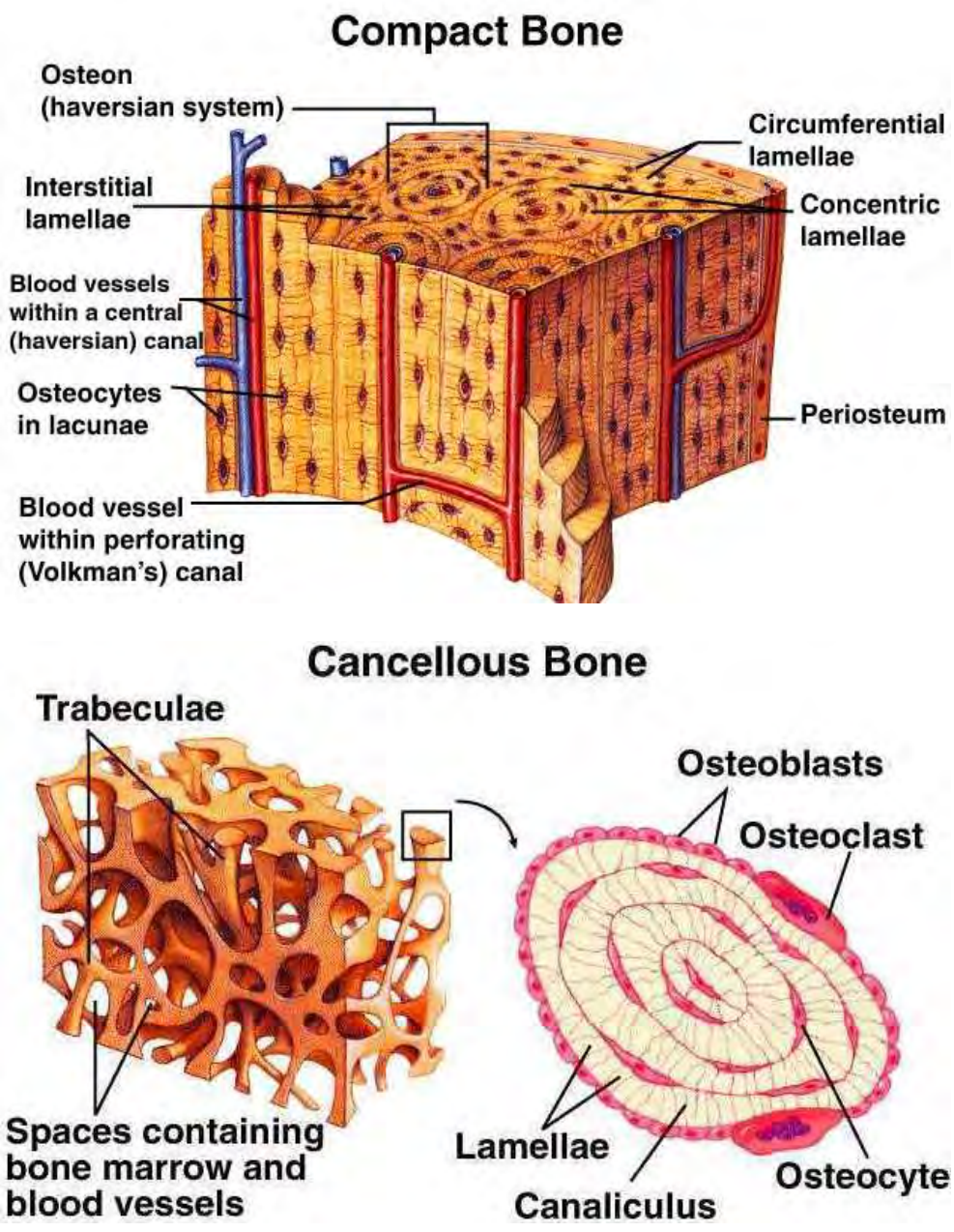

Figure I. 3: Microscopically structure of compact and cancellous bone [6]

[6] http://fau.pearlashes.com/anatomy/Chapter%209/Chapter%209.htm

This combination of cortical and trabecular bone a *sandwich-type* structure, well known in engineering for its optimal structural properties [18]. Although both cortical and trabecular bone have the same material properties, the difference in mineral distribution and micro architecture within and between the texture of these two compartments, explains the differences in the mechanical properties of specific bones and parts of bones.

Microscopically, *woven* and *lamellar bone* can be distinguished. Woven bone is characterized by a random orientation of collagen fibrils and is formed initially in the embryo and during growth. In the adult, it is replaced by the lamellar bone, so it is practically no longer present in the adult skeleton, except in pathological conditions of rapid bone formation.

Lamellar bone, as the name suggests, is characterized by layers of parallel collagen fibrils. In contrast, lamellar bone is the form present in the adult, both in cortical and trabecular bone [21].

Bone tissue is a natural composite material, composed mainly of mineral, organic matrix, cells and water. In general, the mineral part accounts for approximately 65 % (hydroxyapatite), the organic matrix 35 % which consists mainly of 90 % collagen fibres and other non-collagenous proteins and lipids in decreasing proportion (depending on age, species and site). The rest are the cells (osteoblasts, osteocytes, osteoclasts and lining cells).

a. Mineral matrix

The mineral or inorganic composition of bone is formed of small crystals mostly from carbonated hydroxyapatite [22, 23] ($Ca_{10}(PO_4)_6(OH)_2$) with lower crystallinity [22]. Hydroxyapatite constitutes at last 90 % of total mineral weight, is impure, containing many structural substitutions, such as carbonate, magnesium, sodium, fluoride, citrate, strontium and acid phosphate. These are either incorporated into the crystal lattice or adsorbed onto the crystal surface.

The matrix is initially laid down as unmineralised osteoid (manufactured by osteoblasts). Mineralisation involves osteoblasts secreting vesicles containing alkaline phosphatase. This cleaves the phosphate groups and acts as the foci for calcium and phosphate deposition. The vesicles then rupture and act as a centre for crystals to grow on. More particularly, bone mineral is formed from globular and plate structures [24, 25], distributed within and between the collagen fibrils of bone and forming yet larger structure.

Table I. 1: Bone element composition [26]

Element	Weight %
Ca	34
P	16
Na	1–10
Fe, Mg, K, Al, Cu, Sr	< 1
Ag, Ba, Cr, Pb, Sn, Mb, Si, Ni	< 0.1

The functions of the mineral are to strengthen the collagen composite, providing more mechanical resistance to the tissue, and also to serve as a source of calcium, phosphate and other ions for mineral homeostasis [27].

b. Organic matrix

The organic matter is concentrated in the bone matrix, which consists mainly of 90 % collagen fibers, and is the most abundant protein in the body. Its complex three-dimensional structure gives bone its elasticity and tensile strength. The non-collagenous proteins in bone play an important role in bone remodeling and in ontogenesis and include: osteonectin, osteocalcin (OCN), also called bone gla-protein (BGP), osteopontin, bone sialoprotein (BSP) [28].

c. Bone cells

Bone is constantly built, resorbed and then rebuilt through a physiological process called remodeling that is carried out and carefully controlled by a variety of cell types.

Osteoblasts

The osteoblasts are defined as a sophisticated fibroblast; therefore they are difficult to distinguish in cell culture. Osteoblasts are small cells of mesenchymal origin, which

synthesize the extracellular bone matrix. They form an epithelial-like structure at the surface of the bone where they secrete unidirectional the osseous matrix.

In a second step, the mineral salts are precipitated within the matrix from the ions in the extracellular fluid. Osteoblasts secrete a large variety of macromolecules such as: collagens, alkaline phosphatase, osteonectin, osteopontin, fibronectin, and bone sialoprotein.

Osteoblasts are thought to influence matrix organization even after protein secretion, although the exact mechanism is not fully understood. Several hormones and cytokines influence osteoblasts *in vitro*, among them the insulin-like growth factors (IGFs), transforming growth factor β (TGFβ), acidic and basic fibroblast growth factor (FGFs) and bone morphogenetic proteins (BMPs), their individual roles *in vivo* are not yet clear [15].

Osteocytes

Osteocytes are mature, no dividing osteoblasts that have stopped synthesizing matrix and lie in lacunae within the bone. Despite the fact that the osteocytes are the most numerous cells in the bone, make up 95 % of all bone cells, but their function is still relatively poorly known [29]. The osteocytes are actively involved in maintaining the bone matrix, playing a role in the regulation of plasma minerals, especially calcium. They may also serve as a mechanical or damage sensor, hence initiate bone remodeling or repair.

Osteoclasts

Osteoclasts are highly specialized, multinucleated cells, sometimes mononucleated cells, responsible for the resorption of old or damaged bone. They originates from the hematopoietic compartment, more precisely from the granulocyte-macrophage colony-forming unit (GM-CFU), and are situated either on the surface of the cortical or trabecular bone or within the cortical bone [15]. The bone resorption is performed in a specialized compartment, located between the cell and the bone, delimited by a peripheral ring of tight adherence between the cell and the bone matrix. Osteoclasts secrete acids and proteolytic enzymes, which dissolve mineral salts, and digest the organic matrix of bone [26].

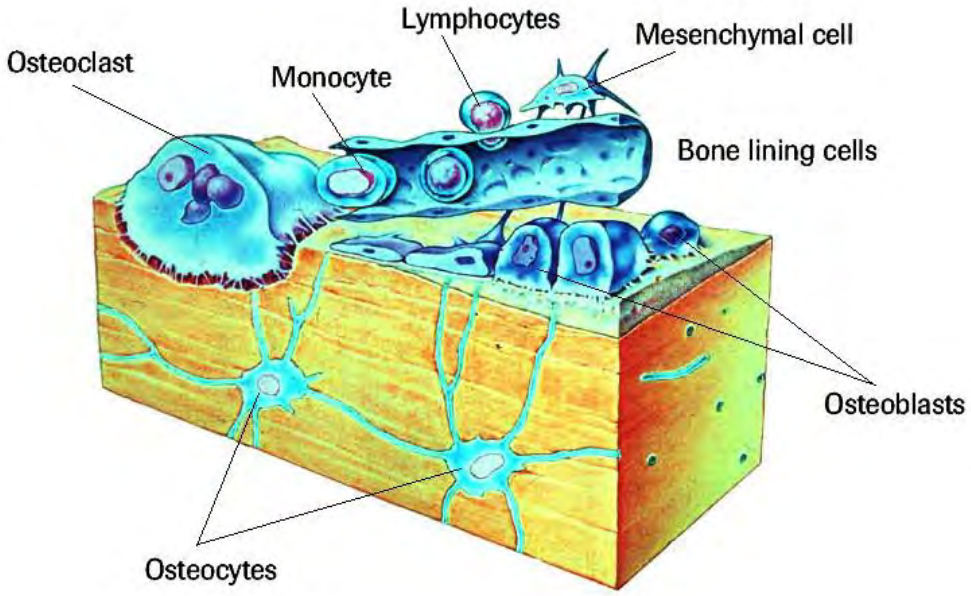

Figure I. 4: Diagram of bone cells[7]

Lining cells

Bone lining cells (BLC's) are thinly extended over bone surfaces and they have flat or slightly ovoid nuclei, heaving role in the regulation of bone remodeling [30].

I.1.4. Bone mineralization

The mineralization phenomenon involves a well orchestrated process in which crystals of calcium phosphate are produced by bone-forming cells and laid down in precise amounts within the bone fibrous matrix. The normal (non-pathologic) mineralization (calcification) process that occurs in the body is controlled by physicochemical and cellular regulation of substances that promote and inhibit HA formation [31].

a. Local inhibitors of mineralization

Inorganic Pyrophosphates (PP(i))

Inorganic pyrophosphates, present in plasma, saliva, bones and teeth, which are eliminated in part by urinary excretion, are inorganic molecules of the pyrophosphates family (P-O-P) that inhibit the ability of inorganic phosphate ions (Pi) to promote mineralization [32].

[7] http://www.roche.com/pages/facets/11/ostedefe.htm

Proteoglycans and glycosaminoglycans

Proteoglycans are large molecules synthesized in connective tissue and found in matrices of calcifying or non-calcifying tissue, which contain glycosaminoglycans (acidic polysaccharide side chains) covalently attached. They also serve as an inhibitor of growth and nucleation of HA crystals [26].

Also, serum proteins slow the transformation of amorphous calcium phosphate (ACP) of forming HA by adsorbing on the ACP surface, which decreases its dissolution rate, aluminum ions concentration-induced osteomalacia in renal bone diseases, magnesium ions has a great inhibitory effect of growth and nucleation of HA crystals, and metal-citrate complexes can inhibit HA formation and growth even at low concentration [32].

b. Local stimulators of mineralization

Collagen

Many research suggested the idea that collagen type I may induce heterogeneous nucleation [33], and also type X-collagen, a component of bone matrix was considered potential nucleation site.

Acidic molecules

Acidic molecules, a special class of macromolecules, proteins of glycoproteins rich in amino acids with high content of serine and aspartate, also promote mineralization acting as a protein. Phospholipids and proteolipids are examples of this class of macromolecules that activated nucleation and crystals growth [34].

c. Hydroxylapatite as stimulator biomaterial for bone mineralization

Hydroxyapatite, $Ca_{10}(PO4)_6(OH)_2$ is a calcium orthophosphate hexagonally crystallized. Figure I.5 represent the elementary cell of HA crystals. The calcium orthophosphates are conventionally classified according to their Ca/P molar ratio, which varies from 0.5 to 2.

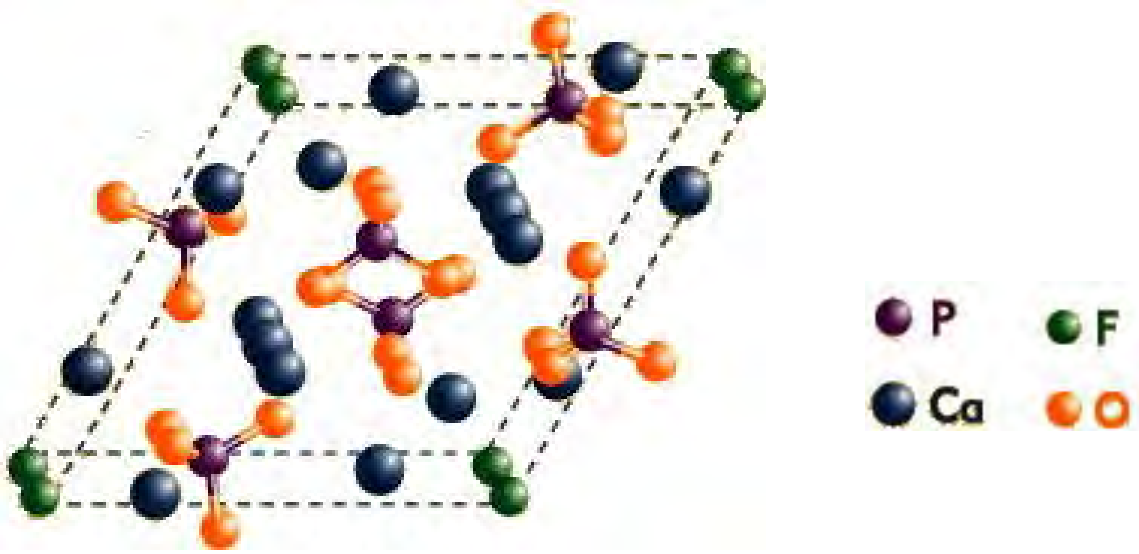

Figure I. 5: Elementary cell of HA crystals –3D projection

Stoichiometric hydroxyapatite has a Ca/P molar ratio of 1.67, while hydroxyapatite with a Ca/P molar ratio lowers than 1.67 is named *calcium–deficient hydroxyapatite* [35].

The most important inorganic constituent of hard tissue, hydroxyapatite, has been used as bone substitute material due to its non-toxic nature, biocompatibility, and osteoconductivity.

According to the literatures, the calcification of bone matrix is influenced to the presence of numerous anionic (some hydrophilic polar groups such as carboxyl, hydroxyl and phosphate) sites representing promoters of nucleation.

The affinity of calcium ions for these organic structures is essential for the development of a biomaterial-associated calcification. The mechanism of HA formation is initiated by attracting Ca^{2+} from the physiologic fluids by the anionic centers of the biomaterial. Once bound, these ions attract PO_4^{3-} ions assuring the nucleation of calcium phosphate, and inducing the formation of HA deposits [36].

In vivo and *in vitro* studies indicated that SF/HA composite materials have improved biocompatibility and bioactivity to induce and support bone regeneration [37].

Table I. 2: Calcium orthophosphates types [38]

Ca/P ionic ratio	Compound	Chemical formula
0.5	Monocalcium phosphate monohydrate (MCPM)	$Ca(H_2PO_4)_2 \cdot H_2O$
0.5	Monocalcium phosphate anhydrous (MCPA)	$Ca(H_2PO_4)_2$
1	Dicalcium phosphate dihydrate (DCPD), mineral brushite	$CaHPO_4 \cdot H_2O$
1	Dicalcium phosphate anhydrous (DCPA), mineral monetite	$CaHPO_4$
1.33	Octacalcium phosphate (OCP)	$Ca_8(HPO_4)_2(PO_4)_4 \cdot 5H_2O$
1.5	α-Tricalcium phosphate (α-TCP)	α-$Ca_3(PO_4)2$
1.5	β-Tricalcium phosphate (α-TCP)	β-$Ca_3(PO_4)2$
1.2-1.22	Amorphous calcium phosphate (ACP)	$CaxHy(PO_4)z \cdot nH_2O$, n = 3-4.5; 15-20 % H_2O
1.5 – 1.67	Calcium-deficient hydroxyapatite (CDHA)	$Ca_{10-x}(HPO_4)_x(PO_4)_6$-x$(OH)_2$-x (0 < x < 1)
1.67	Hydroxyapatite (HA)	$Ca_{10}(PO_4) \cdot 6(OH)_2$
1.67	Fluorapatite (FA)	$Ca_{10}(PO_4) \cdot 6F_2$
2.0	Tetracalcium phosphate (TTCP), mineral hilgenstockite	$Ca_4(PO_4) \cdot 2O_2$

I.2. General aspects regarding biomaterials

At the present time, numerous biomaterials are available as bone substitutes. They are used either in orthopedic surgery (fillings of bone defects, hip prostheses, osteotomy…), in neurosurgery (vertebral fusion), in reconstructive surgery, in dental surgery (and especially in parodontology and implantology). If one excepts the use of bone autograft, (whose volume is

necessarily limited, with additional problems of harvesting), none of the biomaterials available have true osseoinduction capacities (i.e., the capacity to induce locally the differentiation of mesenchymal stem cells into actively bone-forming osteoblasts). Moreover, only purified bone allografts and bone xenografts have a sufficient mechanical resistance that allow them to be used in load-bearing areas. These materials are osteoconductive and allow a guided bone regeneration supported by the material architecture and the physicochemical states of bone surfaces. According to their biochemical nature, these materials are more or less resorbable. Nowadays, it appears clearly that an improvement of bone substitutes should be done to induce:

1. an increased adherence of osteoblasts onto the material surface,
2. an *in situ* differentiation of osteoblast progenitor cells into active osteoblasts,
3. an increased capacity for osteoblasts to produce larger amounts of bone matrix.

There is an increasing demand for the development of new synthetic biomaterials. Polymers can represent a very good answer to this challenge.

The continuous and rapid evolution of knowledge and practical achievements in the field of biomaterials implies permanent adaptation and actualization.

The definition of biomaterials refers to materials both natural and synthetic used in contact with biological system [39]. The prefix *bio* does not therefore refer to the nature of the materials included in this class, but the applications they are intended.

I.2.1. Definitions

A biomaterial can have one of the following definitions:

1. Non-viable material used in a medical device, intended to interact with biological systems.

2. Material intended to interface with biological systems to evaluate, treat, augment or replace any tissue, organ or function of the body (ESB Consensus Conference II) [9].

This definition was formulated for to remove reference to non-viability and to make more explicit the intended functions of biomaterials [9].

3. Synthetic, natural or modified natural material intended to be in contact and interact with the biological system (ISO) [9].

Notes: the use of this definition is not recommended to be used, although forming part of an ISO Technical Report, since it implies that living natural materials (i.e. tissues) are

biomaterials, which they are not, and also because of the ambiguity of the term 'in contact' [9].

4. Any substance (other than a drug), synthetic or natural, that can be used as a system or part of a system that treats, augments, or replaces any tissue, organ, or function of the body (Dorland Medical) [9].

Since it does not contain reference to an interface with tissues this definition is not recommended; this definition would encompass the power supply or any microelectronic component of a pacemaker, which would not normally be considered to be biomaterials.

First definition emphasizes the non-viable character of the biomaterial; other definitions were necessary when biomaterials have been used as support grafts or living cell cultures; an example is formulated as follows:

A biomaterial is a systemically and pharmacologically inert substance designed for implantation within or incorporation with living systems [40].

The implementation of biomaterials must take into account the chemical nature of raw materials, the morphology, the mechanical (such as strength and fatigue properties) and physical (durability and stability) properties, the environmental conditions required and possible biological interactions between it and the materials [41]. Also, an ideal biomaterial should be: *biocompatible [42]*; non-toxic, non-carcinogenic [43]; sterilizable, accessible and easily processed [44].

Biomaterials can be classified into three major groups: *bioinert/biotolerant* materials, *bioactive* and *bioresorbable* materials [45].

Bioinert materials are biocompatible materials, but cannot induce any interfacial biological bond between implants and bone[45].

Examples of such materials are: alumina (Al_2O_3), zirconia (ZrO_2) and titanium [46].

Tissue adhesion on the inert material can be made by: tissue growth into surface irregularities, using bone cement or by introducing the pressure inside the defect. A bioinert material is not useful for long−term application, because it affects the long−term stability, often causing problems in orthopedic and dental applications.

Bioactive materials are a group of biocompatible materials that can attach directly with body tissues and form chemical and biological bonds during early stages of the post implantation period [45].

A few examples of bioactive materials are hydroxyapatite [47], Bioglass [48] and glass ceramic [49].

Bioresorbable materials are the type of biocompatible materials that are gradually resorbed before they finally disappear and are totally replaced by new tissues in vivo [45].

Tricalcium phosphate [$Ca_3(PO_4)_2$] [50], poly(glycolic acid), poly(lactic acid) and their copolymers [51] are examples of bioresorbable materials.

Bioresorption is a concept that reflects the total elimination of a stranger material by cellular activity and/dissolution in a biological environment [9], without side effects. Bioresorption term is used for solid polymeric materials or pieces that can dissolve in body fluids without the scission of the polymer chain or molecular weight decreased.

I.2.2. Biomaterials-based scaffolds

Polymer matrices need to provide a number of key functions in order for them to be successful in tissue-engineering applications. To enable scaffold conduits to be successful in recruiting reparative cells in an organized manner, a number of key characteristics need to be achieved. Scaffolds ideally need to provide the following:

- A biocompatible and biodegradable matrix with controllable degradation kinetics.
- Suitable surface chemistry for cell attachment, proliferation and differentiation.
- An interconnected and permeable pore network to promote nutrient and waste exchange.
- A three-dimensional and highly porous structure to support cell attachment, proliferation and ECM production.
- Appropriate mechanical properties to match those at the site of implantation.
- An architecture which promotes formation of native anisotropic tissue.
- A reproducible architecture of clinically relevant size and shape [52, 53].

Polymers can replace diseased organ function by acting as a cellular nucleus for tissue regeneration or as a source of molecular signals to control host cell growth and tissue regeneration [54]. The formation of tissue produced by implanted cells is influenced greatly by the scaffold on to which they are seeded [55]. The choice of polymer is therefore vitally important in determining the success of the TEC.

Polymers comprise the most diverse class of biomaterials. The uses of polymers in medical field are quite known since their discovery or synthesis because medical applications were imposed immediately after using this material in general areas of activity. The original use of polymers was primarily in experimental surgical studies for replacement or augmentation of various tissues. The use of nylon fibers for surgical sutures is reported since the 1940s [56]. Around the same time have been tailored for medical and dental applications, other polymers such as: poly(methyl methacrylate) (PMMA) [57], Dacron polyester, polyvinyl chloride, and

modify polymers polytetrafluoroethylene (Teflon), polyurethanes and high density polypropylene (HDPE) [58]. These polymers still remain as major components in biomedical applications: contact lens, intraocular lens, joint replacements (hip, knee), breast implants, artificial hearts, heart valves, vascular grafts, blood vessel prosthesis, pacemakers, and catheters.

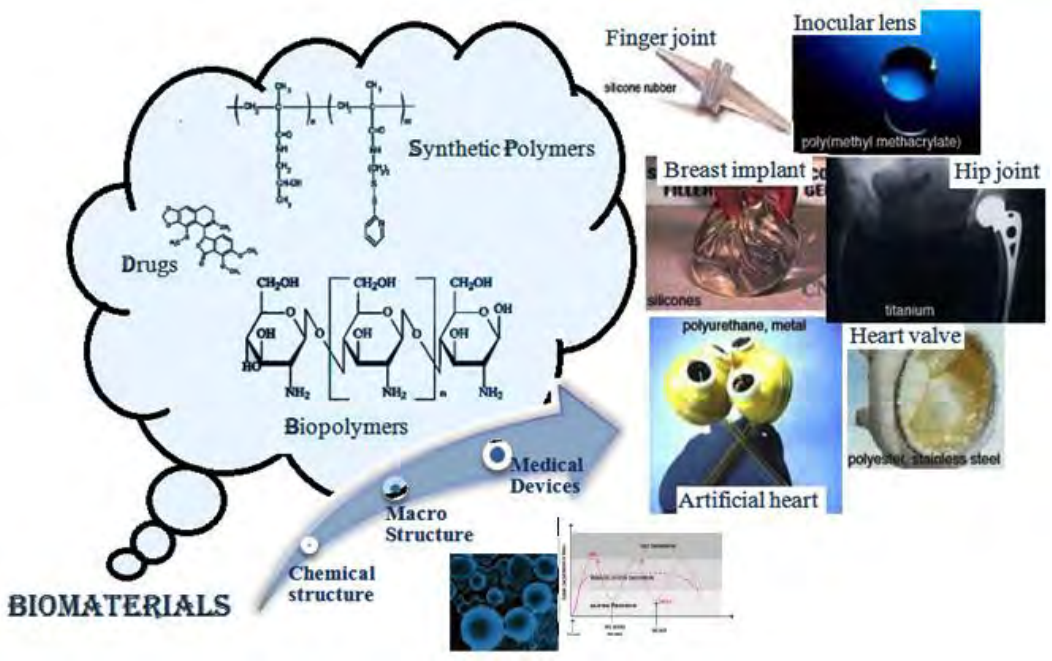

Figure I. 6: Body reconstruction based on biomaterials[8, 9, 10]

Research continuously optimizes the stability and performance of these materials *in vivo*, due to their versatility and their composition, properties and different forms that can be manipulated: foams, gels, films, fibers and solids [59].

In the last years, surgery and dentistry research has added new areas of biomedical uses of polymers: controlled release of pharmaceutical active principles (including drugs), their use as active principles, to assist regeneration of three-dimensional tissue and organ structures, gene therapy, polymeric biocides and bioregulators, materials for highly efficient biocatalysts, membrane and sorption materials for separating and purifying biologically active substances and products of biotechnological and food productions, and materials for bioanalysis [60].

[8] http://www.uweb.engr.washington.edu/research/tutorials/introbiomat.html

[9] imagini google

[10] imagini google

By their biological nature, natural polymers are often similar species to biomacromolecules of biological environment that can recognize and to deal with metabolically [39, 61]. They offer the potential to be biodegradable and biocompatible in the majority of cases. However, the biological nature of these materials may cause immunogenic reactions, leading to complications or risk of rejection [39]. Moreover, their use usually requires the transformation of a raw material to extract the biopolymer or biomacromolecules. This process of extraction and purification must be well controlled to maintain the integrity of biological molecules in order to subsequently generate them materials into functional materials. In this respect, biomaterials, including polymers must have a certain feature called *biocompatibility [62]*.

The biocompatibility of polymers

The biocompatibility of a material is its ability to fulfill a role in the biological system in which it is applied, while producing little or no adverse reactions. By Williams, the biocompatibility was defined as:

Biocompatibility is the ability of a material to perform with an appropriate host response in a specific application [9].

The biocompatibility of biomaterials is linked to their nature and to the ability of biological system to accept or reject the material. The possible adverse reactions may be of various origins and natures of such chronic inflammation [63], thrombotic reactions [64], tissue responses including injury and fibrous encapsulation of the biomaterial [65]. A polymeric material can be biocompatible for a specific use, in a place of implantation, and non-biocompatible in relation to another place of implantation.

The assessment of the implant on the body, involves knowledge of polymer toxicity, its products degradation, the mechanical properties, processing and sterilization possibilities, estimating his antigenic, mutagenic, thrombogenic and carcinogenic potential [66].

The influence on the living body refers to the estimation of polymer degradation, erosion, hydration, protein absorption onto the surface, oxidation, surrounded with tissue and calcification [67].

I.2.3. Synthetic biodegradable polymers as biomaterials

Synthetic polymers have been used in tissue engineering because of their advantages such as ease of use, strength, durability, resistance to chemical and biological corrosion, and low production cost. They can be made into the required shape, surface area, wettability and

porosity by controlling mechanical and physical properties. They can also be made easily into complex shapes and structures. However, they may produce undesirable biological responses such as poor cell attachment and growth. In addition, their degradation products may be toxic to the host. For instance, poly(α-hydroxy acids), specifically poly(lactic acid) (PLA), poly(glycolic acid) (PGA) and their copolymer (PLGA) were the most widely used synthetic aliphatic polyesters in medical applications since the 1970s. They were used clinically due to their high purity, convenient processing and good mechanical properties. In addition, their biodegradability can be controlled by changing their molecular weight and copolymer compositions.

I.2.4. Natural biodegradable polymers as biomaterials

To overcome the lack of intrinsic biological activity of synthetic polymers, natural biodegradable polymers were used. They possess specific biological property such as good biocompatibility. Another advantage is that the degradation products are non-toxic which are then transformed into carbon dioxide and water over a period of time. They are normally enzymatically degradable, possessing various degradation rates. On the other hand, limited control over molecular weight, the potential for unfavorable immunological responses and poor mechanical properties are the disadvantages of natural based polymers. Some examples of natural polymers used for tissue engineering scaffolds are collagen, polysaccharides, alginate, chitosan, glycosaminoglycan, hyaluronic acid etc.

Collagen scaffolds have been produced in the forms of sponges, woven and non-woven meshes, gels and porous composites. They have been successfully utilized as skin, cartilage and nerve regeneration.

Another type of natural polymer is polysaccharides, which are polymers of five-carbon (pentose) or six-carbon (hexose) sugar molecules. They have been widely used in tissue engineering because most of them are biodegradable, hydrophilic and non-toxic. They possess high molecular weights and extended chain configurations that enhances highly viscous gel formation. An example is chitosan, a partially or fully deacetylated derivative of chitin. The primary source of chitosan is shells from crab, shrimp, and lobster. It is the most promising polysaccharide because of its excellent ability to be processed into porous structure. It is hydrolyzed enzymatically *in vivo*. Glycosaminoglycan is also a polysaccharide that occurs within the extracellular matrix (ECM) of most animals. Chitosans have been also investigated as woven and non-woven fiber-based structural materials.

The last example given here is microbial polyester, natural aliphatic polyester such as PHB and PHBV which have been attractive for a wide range of environmental industries, such as

agriculture, marine and packaging. More recently, they have been attractive for medical applications because of their biodegradability, biocompatibility and non-cytotoxicity.

I.3. Structure and proprieties of polyhydroxyalkanoates

Polyhydroxyalkanoates (PHAs) are naturally derived polyesters that accumulate as a carbon storage material in a wide variety of bacteria, usually under conditions of limiting nutrients (such as ammonium, sulfate, and phosphate) in the presence of an excess carbon source [68-72]. An imbalanced nutrient supply leads to intracellular storage of excess nutrients. By polymerizing soluble intermediates into insoluble molecules, cells do not undergo alterations of their osmotic state and leakage of nutrients is prevented. Accumulated PHAs form discrete granules that can account for up to 90% of the cell's dry weight [72]. Up to date, more than 150 hydroxyalkanoate units with different R-pendant groups have been isolated from bacteria [72] (Figure I.7).

Poly(3-hydroxybutyrate) (P3HB) is the simplest and most common member of the group of PHAs. It was discovered by Lemoigne in the 1920s, but its commercial evaluation did not start until the late 1950s. The potential of P3HB for biomedical applications was first suggested by Baptist J.N. and Ziegler J.B. (1965) in their patent. The patent presented the idea of using the P3HB as biodegradable surgical sutures or films to support tissue healing of injured arteries and blood vessels. They have described a method for producing, prosthetic devices such as tubes support for healing of a severed blood vessel or ureter, as well as devices support for hernia repair [73].

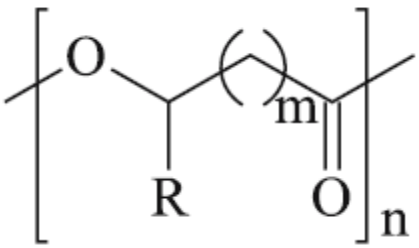

Figure I. 7: Chemical structure of PHA homopolymers

It the 1980s P3HB became again of interest for biomedical research when a study on P3HB tablets for sustained drug delivery was done [72]. Since then, an increasing number of investigations on potential use of P3HB have been reported, including here: implants for bone repair [74], anastomoses tubes and separating films [75] or cardiovascular patches [72].

The first reported clinical study of P3HB implants was when pericardial patches have been tested in humans [75]. P3HB conduits and scaffolds have been introduced for the repair of peripheral nerves and spinal cord [76-78], and P3HB patches have been developed for covering damaged tissue of the gastrointestinal tract [70, 79]. Summarizing just these studies, P3HB can be considered to be a polymer with high potential as a degradable implant biomaterial [13, 16, 17].

The majority of research on medical applications of PHAs refers mostly to P3HB and its copolymer poly(3-hydroxybutyrate-*co*-3-hydroxyvalerate), P3HB-3HV. However, due to their broad range of mechanical and biodegradation properties, other PHAs have been studied for their biomedical applications, particularly in cardiovascular tissue engineering. Firstly, elastomeric poly(3-hydroxyoctanoate-*co*-3-hydroxyhexanoate), P3HO-3HH, was used to develop scaffolds for repair of blood vessels [80] and heart valves [81]. Poly(4-hydroxybutyrate), P4HB, was introduced subsequently as a faster degrading biopolymer and was tested as vascular patches [82], heart valves [83, 84], and vascular grafts [83]. Based on results from these studies, P4HB is regarded as a particularly promising biopolymer for clinical applications when elastomeric properties are required [85]. Furthermore, copolymers such as poly(3-hydroxybutyrate-*co*-4-hydroxybutyrate), P3HB-4HB, and poly(3-hydroxybutyrate-*co*-3-hydroxyhexanoate), P3HB-3HH, have been introduced as scaffolds for tissue engineering, including the repair of cartilage and bone [86, 87]. An example of an unsaturated PHA is poly(3-hydroxyundecenoate) (P3HU), containing 3-hydroxynonenoate and other unsaturated and saturated side-chains of medium length, which has been suggested as a suitable material for applications in blood contact [88]. The chemical structures of the most extensively studied PHAs are shown in Figure I. 8.

A summarize of the range of properties provided by PHAs is exemplified in Figure I. 9 [70, 89-91]. The stiffness and brittleness, as well as slow hydrolysis *in vitro* and *in vivo* of the isotactic P3HB can be put on the high crystallinity degree. P4HB films due to the elastomeric properties of the polymer are characterized by low stiffness and high elongation at break. The low degree of crystallinity accelerates the rate of the degradation *in vitro*. A surface erosion mechanism is involved in the degradation *in vivo* of P4HB. Probably, due to the same elastomeric properties and low crystallinity of P3HO-3HH make this to be degraded faster *in vitro* than P3HB despite the increased hydrophobicity resulting from the longer alkyl side-chains. However, the degradation of P3HO-3HH under *in vivo* conditions appears to be slower than under *in vitro*.

The advantage of the elastomeric properties was shown by P3HB copolymers containing more than 20% of 4-hydroxybutyrate [85] or medium chain-length (C6-18) 3-hydroxyalkanoate units, as well as medium chain-length PHA homopolymers (e.g., P3HO-3HH or crosslinked P3HU [88]). This is of particular interest in tissue engineering applications since many tissues in the body have elastomeric properties. For example,

cardiovascular tissue engineering requires a scaffold that can sustain and recover from cyclic deformations without irritation of the surrounding tissue. The development of an elastomeric scaffold is therefore highly desirable. Moreover, mechanical stimuli promote the formation of functional tissue, for example in cardiovascular or cartilage tissue engineering, and allow for gradual stress transfer from the degrading synthetic matrix to the newly formed tissue. Most of the biodegradable polyesters currently used in tissue engineering (such as PGA, PDLLA, and their copolymers) undergo plastic deformation and fail when exposed to long-termcyclic strain, thereby limiting their efficacy in engineering elastomeric tissue [92].

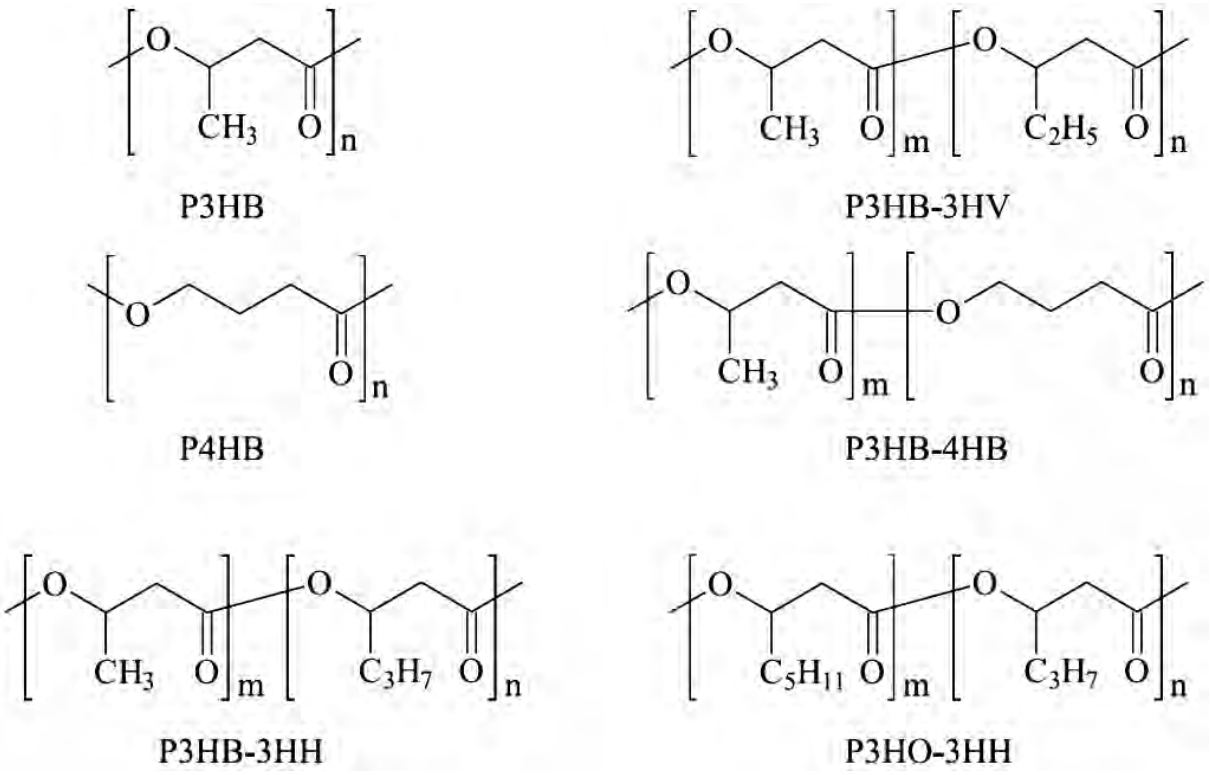

Figure I. 8: PHAs tested in tissue engineering applications

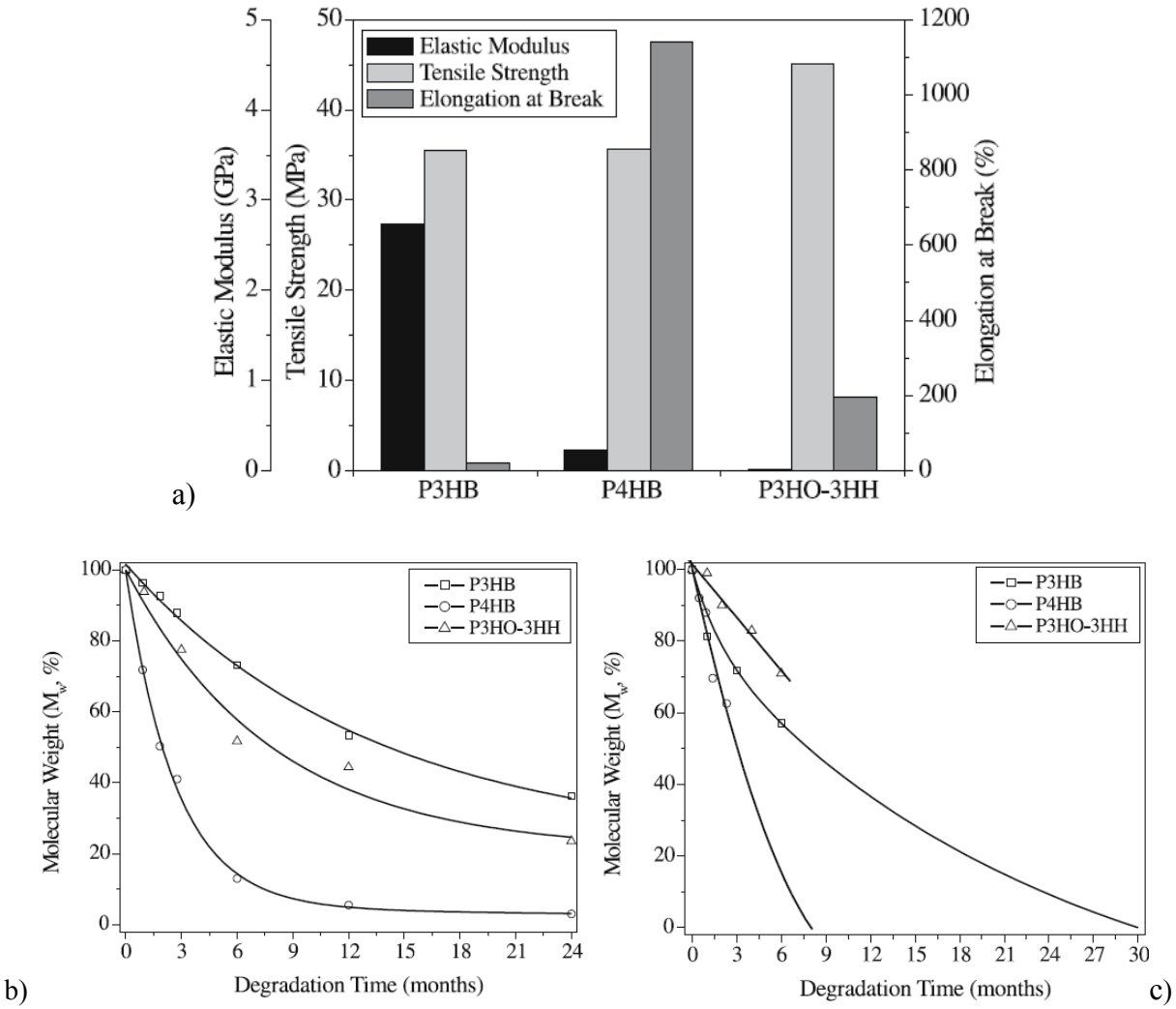

Figure I. 9: Comparison of P3HB, P4HB and P3HO-3HH films: a) mechanical properties [38, 51, 52]; b) *in vitro* degradation (*p*H 7.4, 37 °C) [38, 51, 53, 54] and c) *in vivo* degradation (s.c., mice or rats) [53, 55, 56]

3 Poly(3-hydroxybutyrate) and Poly(3-hydroxybutyrate-co-3-hydroxyvalerate)

P3HB is the classic, most extensively studied and characterized PHA as it was already shown. It is produced by a large number of microorganisms, including Gram-negative and Gram-positive aerobic and photosynthetic species, lithotrophs or organotrophs [93]. A glucose-utilizing mutant of *Alcaligenes eutrophus* can accumulate up to 80% of P3HB with glucose as carbon source. By addition of propionic acid to the medium, P3HB-3HV is produced as a random copolymer, with the comonomer ratio dependant on the ratio of propionic acid to glucose. This technology has been scaled-up, and industrial processes have been developed for the synthesis of large quantities of P3HB-3HV under commercial name of BIOPOL.

However, one of the major drawbacks for the broad utilization of P3HB or P3HB-3HV in medicine is the limited supply of these polymers of medical grade. Furthermore, there is currently no Drug Master File submitted to the FDA, and a medical device made of P3HB or P3HB-3HV has not yet been clinically approved.

I.3.1 Mechanical Properties

P3HB as a natural thermoplastic polyester has mechanical properties comparable with those of synthetically produced degradable polyesters such as the polylactides [94]. The relatively high brittleness of the crystalline natural isotactic P3HB is of disadvantage in tissue engineering applications but can be overcome by copolymerization and incorporation of PHA components such as 3-hydroxyvalerate (3HV), 4-hydroxybutyrate (4HB), or 3-hydroxyhexanoate (3HH) [68, 69].

The effect of increasing 3HV content on the properties of P3HB-3HV is summarized in Table 1 [95]. Crystallinities of P3HB-3HV copolymers are high over the whole composition range due to isodimorphism, i.e., cocrystallization of the two monomer units in either of the homopolymer crystal lattices [96]. Molecular weight is one of the major factors governing the mechanical properties of a polymer. Thus, the tensile strength of P3HB-3HV has been reported to rapidly decrease below molecular weights of about 100 000 [97] or 150 000 [98].

The mechanical properties of P3HB can also be improved by addition of plasticizers [99-101] (Figure I. 10a). For example, citric acid esters, which are considered to be nontoxic [102], were demonstrated to be effective plasticizers for P3HB-3HV [103, 104]. However, triethyl citrate, which is commonly used for plasticization, is highly water soluble resulting in fast leaching out of the polymer matrix under physiological conditions leading to embrittlement of initially plasticized polymer films [70, 104]. Recently, it has been shown that esters of anti-inflammatory drugs such as salicylic acid, acetylsalicylic acid, and ketoprofen have plasticizing effects on P3HB films comparable to those of citric acid esters [104].

Blending with other degradable polyesters, such as atactic P3HB (at-PHB) [105-107] syndiotactic P3HB (st-PHB) [108], poly(ε-caprolactone) (PCL) [109, 110], poly(6-hydroxyhexanoate) [111], P3HB-3HH [112], and P3HO-3HH [89], has been shown to increase the flexibility and elongation at break of P3HB or P3HB-3HV. Some examples of P3HB blends are given in Figure I. 10b. In contrast, addition of polyesters commonly used in medical applications,

such as PDLLA, PLLA, poly(d,l-lactide-*co*-glycolide) (PLGA), or poly(*p*-dioxanone), does not improve the mechanical properties of P3HB due to lack of miscibility.

Table I. 3: Thermal and mechanical properties of P3HB and P3HB-3HV [95]

Polymer	T_g, °C	T_m,°C	Elastic modulus, GPa	Tensile strength, MPa	Elongation at break, %
P3HB	9	175	3.8	45	4
P3HB-11%3HV	2	157	3.7	38	5
P3HB-20%3HV	-5	114	1.9	26	27
P3HB-28%3HV	-8	102	1.5	21	700
P3HB-34%3HV	-9	97	1.2	18	970

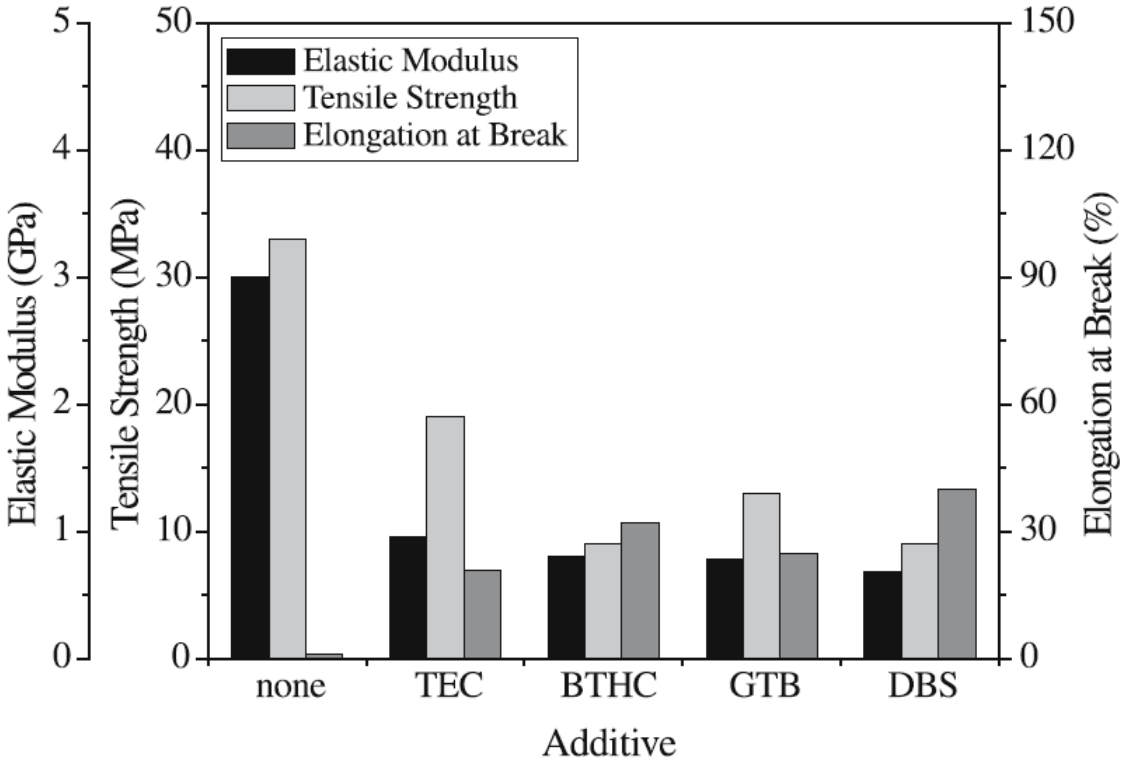

a)

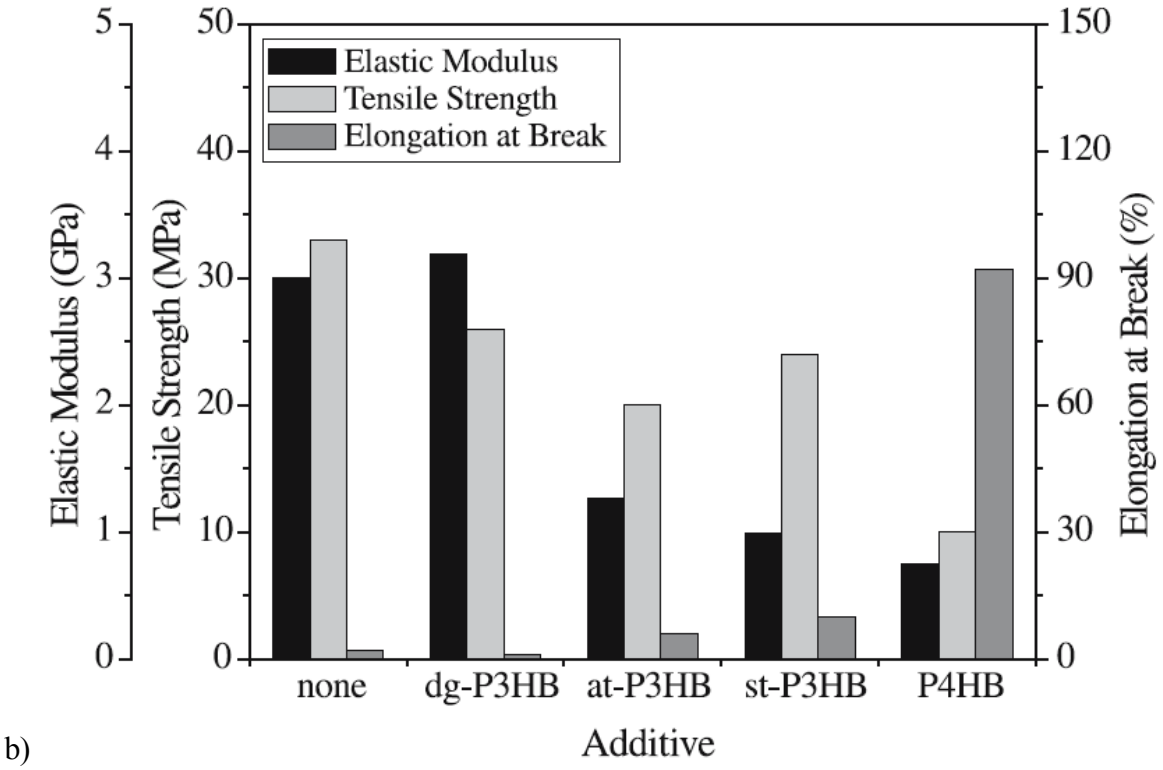

b)

Figure I. 10: a) Mechanical properties of solution-cast P3HB films plasticized with 30% each of triethyl citrate (TEC), butyryltrihexyl citrate (BTHC), glycerin tributyrate (GTB), and dibutyl sebacate (DBS) [71, 72]. b) Mechanical properties of solution-cast P3HB films blended with 30% each of degraded P3HB (dg-P3HB, *M*w = 3000), at-P3HB, st-P3HB, and P4HB [38, 72]

Polymer films with improved mechanical properties can also be obtained by hot-drawing of ultrahigh molecular weight P3HB [113] or P3HB/PLLA blends [114]. If unmodified, filmsmade from ultrahighmolecular weight P3HB (*M*w 11 million) have comparable mechanical properties with those of common high molecular weight P3HB (*M*w 500 000 to 1 million). Low molecular weight P3HB shows increasing brittleness with decreasing molecular weight, and mechanically stable films cannot be prepared below a molecular weight of 50000. Films can still be prepared from mixtures of high and low molecular weight P3HB showing mechanical properties comparable with those of unmodified high molecular weight P3HB (Figure I. 10b).

P3HB-based composites, which are of interest in bone tissue engineering, were found to have an increasing stiffness with an increasing content of hydroxyapatite (HA) [115, 116] or tricalcium phosphate (TCP) [117].

I.3.1. Polyhydroxyalkanoates based biomaterials

Biocompatibility

Material–tissue interactions are best described by the term biocompatibility. This implies that any material placed into a body will not be inert but will interact with the tissue. The biological response of a material is basically dependent on three factors: the material properties, the host characteristics, and the functional demands on the material. Therefore, the biocompatibility of a material can only be assessed on the basis of its specific host function and has to be uniquely defined for each application.

Toxicity Testing

P3HB has been found to be an ubiquitous component of the cellular membranes of animals. The resulting presence of relatively large amounts of low molecular weight P3HB in the human blood, as well as the fact that the degradation product, 3-hydroxybutyric acid (3HB), is a common metabolite of all higher living beings, serve as evidence for the nontoxicity of P3HB [71].

Toxicity testing according to USP XXII and ISO 10993 revealed that P3HB is suited for use as an implant material. The subcutaneous, intraperitoneal, and intravenous eluate testing did not result in any significant reactions in rabbits, mice, or guinea pigs, and no febrile reactions were observed during the pyrogen test. Histocompatibility was demonstrated in the implantation study in rabbits (Schmitz KP, personal communication).

P3HB did not cause any inflammation in the chorioallantoic membrane of the developing egg [118]. P3HB-5%3HV was nontoxic in the bacterial bioluminescence test over a period of 16 weeks [119]. P3HB-3HV (7%, 14%, 22% 3HV) films were found to elicit only a mild toxic response in the direct contact or agar diffusion tests. However, P3HB-22%3HV extracts in saline provoked a noticeable hemolytic reaction [72].

Cell Culture Studies

Mouse fibroblast cell-lines are relatively unaffected by small changes in cell culture conditions and are therefore commonly used to assess and compare the cell compatibility of biomaterials *in vitro*. For example, it was reported that NIH 3T3 mouse fibroblasts remained highly viable on P3HB and P3HB-3HV (15%, 28% 3HV) films [120]. In another study, L929 mouse fibroblasts showed a better viability on P3HB surfaces than on PLLA. A good cell compatibility of P3HB films has also been concluded from experiments using Chinese hamster lung (CHL) fibroblasts [121]. Typical results from cell compatibility tests of P3HB films using L929 mouse fibroblasts are shown in Figure I. 11 and Figure I. 12 [72]. Melt-spun P3HB fibers [122] also support L929 mouse fibroblast adhesion, as shown in Figure I. 12c.

Canine anterior cruciate ligament fibroblasts cultured in highly porous P3HB-9%3HV scaffolds sustained a cell growth similar to that observed in collagen sponges [123]. On the other hand, human scoliotic fibroblasts isolated from spinal ligaments exhibited low proliferation rates on P3HB-3HV (7%, 14%, 22% 3HV) surfaces, independent of the copolymer composition. P3HB-8%3HV was found to be slightly more compatible than P3HB-12%3HV in terms of L929 fibroblast proliferation, cytotoxic effect, and cytokine production [72].

A limited cell compatibility of plasticized P3HB-3HV was observed in a study using NIH 3T3 mouse fibroblasts, and was attributed to leaching of plasticizers. Thus, the potential toxicity of leachable such as plasticizers or other additives has to be considered when conducting cell culture experiments. Additionally, removal of remaining solvent is crucial if polymer films are prepared by solution-casting, which is the most widely used method for sample fabrication in cell culture studies. It has been shown that storage of solution-cast polymer films even under vacuum does not allow for complete chloroform removal (Figure I. 13), so that solvent may be released from the polymer film during cell culture experiments.

The relatively low surface wettability of P3HB solution-cast film surfaces has been discussed as a limiting factor for cell attachment and growth. Strategies to improve cell compatibility of P3HB include methods to increase the surface wettability (decreasing water contact angle) such as carboxyl ion implantation [124] or oxygen plasma treatment. Introduction of oxygen-based functionalities on the surface of P3HB-15%3HV films, either by corona-discharge treatment or treatment with a mixture of perchloric acid and potassium chlorate, resulted in decreasing water contact angles and increasing mouse NIH 3T3 fibroblasts adhesion and proliferation [71]. A limited adherence of L929 mouse fibroblasts on unmodified P3HB films has been reported in another study. However, a strong improvement of cell adherence and growth could be observed on UV-irradiated films and after fibronectin coating, as well as after surface modification by ammonia plasma treatment [125].

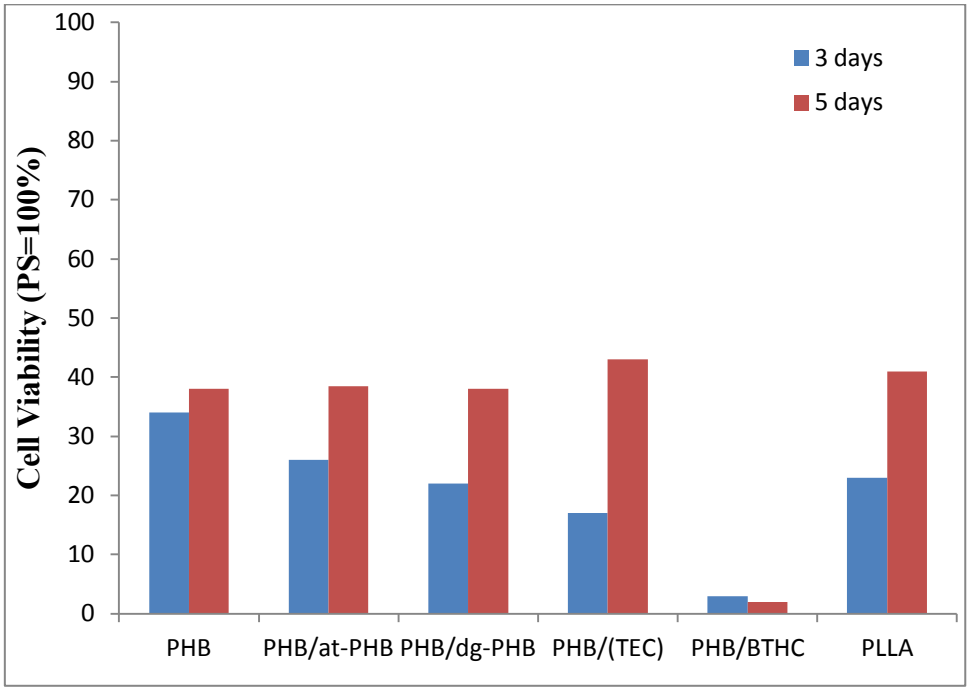

Figure I. 11: Cell viability of L929 mouse fibroblasts after 3 and 5 days of culture on solution cast P3HB films, compared to that of P3HB films modified with 30% at-P3HB, dg-P3HB, TEC (leached), and BTHC; PLLA films for comparison [72]

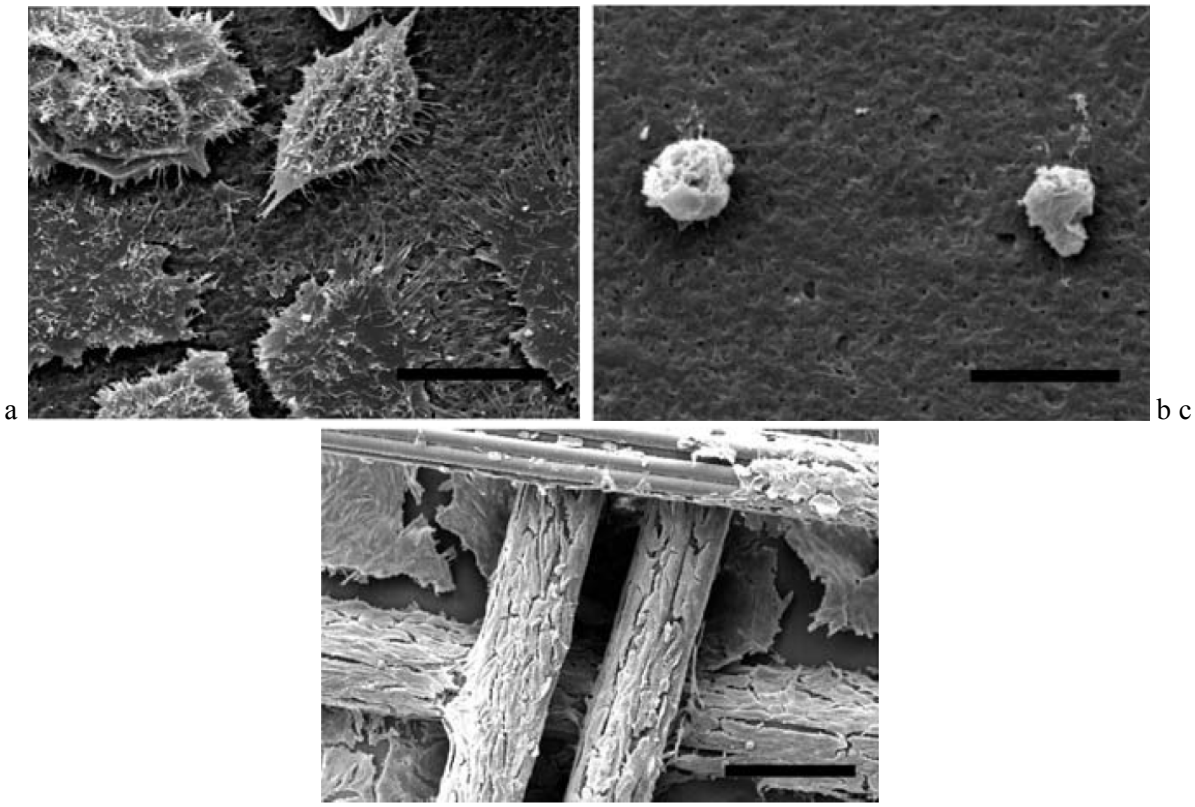

Figure I. 12: SEM images of L929 mouse fibroblast attachment to: a) P3HB films; b) P3HB films plasticized with 30% BTHC after 5 days of culture (*Scale bar* 20 µm.) and c) L929 mouse fibroblast attachment to P3HB fibers after 9 days of culture. *Scale bar* 200 µm [72]

P3HB/BTHC films show limited cell adhesion, and cells exhibit a spherical, nonviable morphology. The low cell viability of these films was also confirmed by the quantitative analysis (Figure I. 11).

Low viability of L929 fibroblasts on unmodified P3HB films, but strongly improved viabilities after surface hydrolysis using lipases or alkaline solution, have been reported [112, 126, 127]. In experiments with P3HB porous scaffolds, an increasing growth of L929 cells could be observed after surface treatment with lipase but a decreasing cell growth was found after coating with hyaluronic acid despite significantly decreased water contact angles. It was concluded that an appropriate balance of hydrophilic and hydrophobic surface properties is required for appropriate protein adsorption and cell attachment [117]. Surface modification of P3HB-5%3HV films with hyaluronic acid or chitosan after ozone treatment and acrylic acid grafting has also been examined. Enhanced cell attachment and proliferation of L929 fibroblasts have been observed after immobilization of hyaluronic acid. Chitosan grafting leads to more cell attachment to the film surfaces but less proliferation in comparison to hyaluronic acid. It was shown that fibroblast attachment increases but proliferation decreases with increasing surface density of amine groups [128].

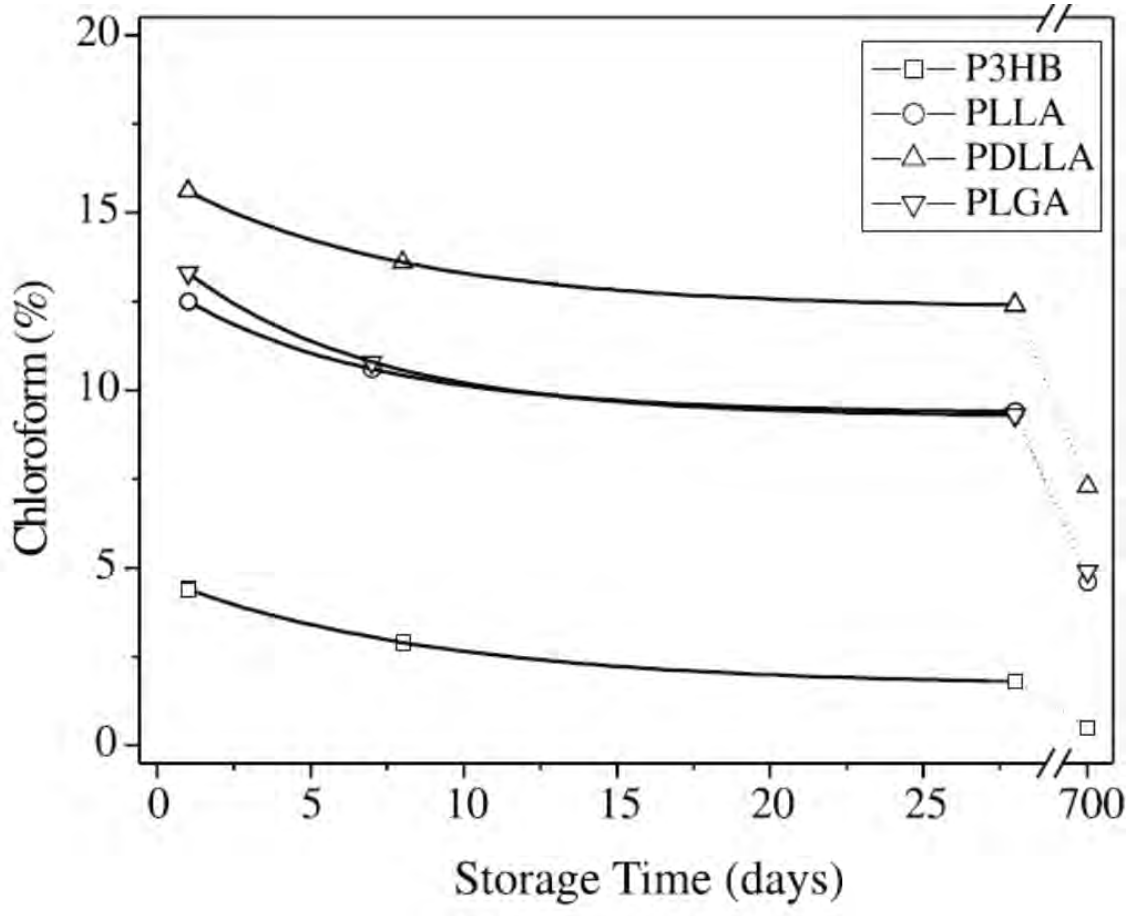

a)

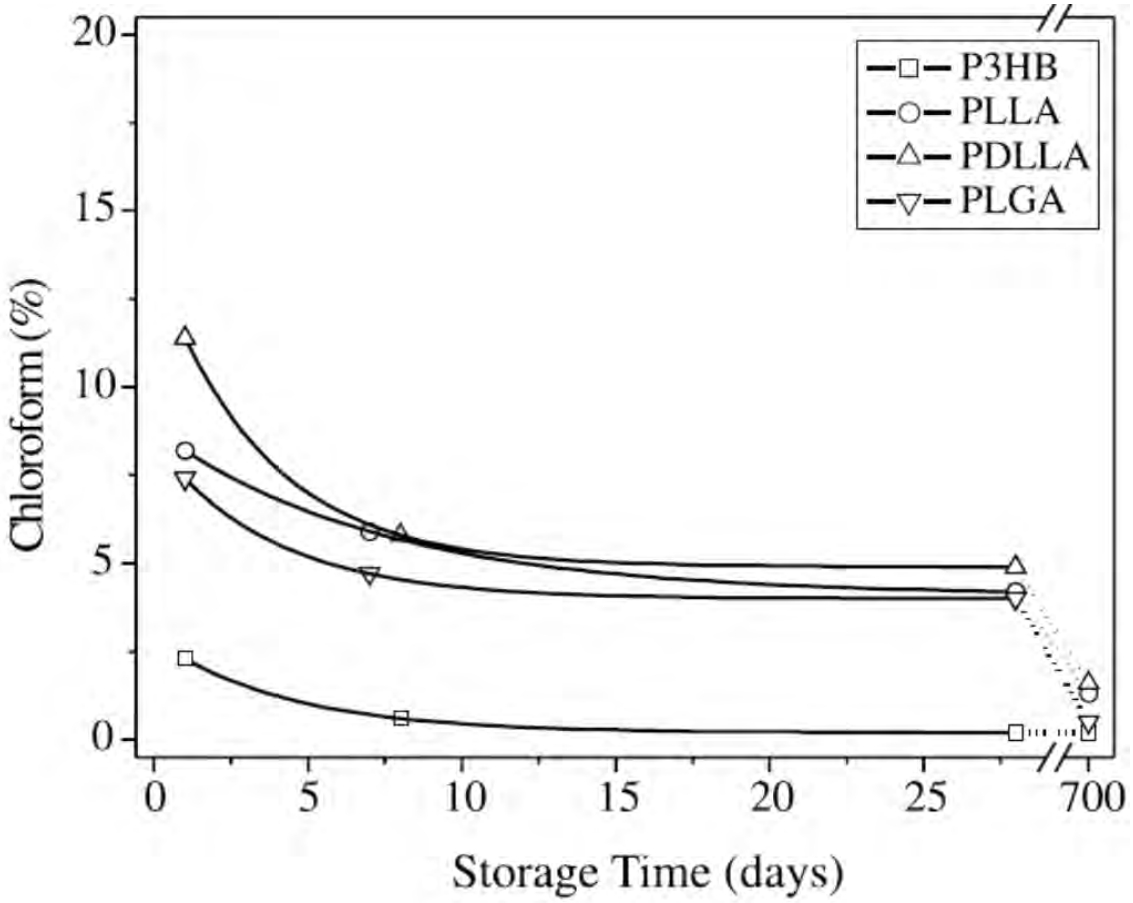

b)

Figure I. 13: Chloroform content of solution-cast polyester films after storage: a) at normal pressure (23°C) and b) under vacuum (40 ◦C) [79]

In order to assess the biocompatibility of degradable polymers, it is necessary to study not only the polymer properties but also those of the low molecular weight degradation products. 3HB, the ultimate degradation product of P3HB, has been found to be biocompatible in tests with CHO-K1 fibroblasts. Other studies included short-chain P3HB oligomers. For example, the incubation of P3HB oligomers with hamster V79 fibroblasts and marine melanoma B16(F10) cells did not affect the cell viability [129]. Furthermore, particles of short-chain P3HB were found to cause dose-dependent cell damage in macrophages but not in fibroblasts. Therefore, controlling the degradation rate and thus concentration of degradation products was concluded to be important for controlling the biocompatibility. Cocultures of liver cells (Kupffer cells and hepatocytes) were not affected by treatment with this material [130].

A murine monocytes-macrophages cell line was used as a model to study foreign-body response and phagocytosis capability. The adhesion and proliferation of these cells increased after alkaline surface hydrolysis of P3HB-8%3HV films. Pretreatment of the unmodified polymer with collagen had a repulsive effect on the cells, which disappeared on the

hydrolyzed polymer, while fibronectin promoted cell adhesion on both surfaces. Despite these screening studies to assess the cell compatibility of P3HB based materials in general (including suitable methods for processing, modification, purification, and sterilization), a number of studies have been conducted to study the potential and biocompatibility of P3HB in tissue engineering applications using different tissue-specific cell types, such as osteoblasts, chondrocytes, and vascular cells.

For example, the biocompatibility of P3HB has been assessed by studying the structural organization of cellular molecules involved in adhesion using osteoblastic and epithelial cell lines. Both cell lines exhibited a rounded cell shape due to reduced spreading on the polymer surface. The interactions between matrix proteins and the actin cytoskeleton mediated by integrins were found to be impaired, including the colocalization of fibronectin fibrils with actin filaments. Moreover, the cell morphology was modified showing larger lateral extensions in the cell–cell contacts [131]. Osteoblast compatibility has also been tested after seeding of rabbit bone marrow cells on P3HB films and more cells could be found on P3HB than on PLLA surfaces [94]. P3HB porous scaffolds showed slightly higher osteoblast viability, but comparable alkaline phosphatase production to that of PLLA samples [87]. P3HB-3HH copolymer matrices showed superior cell compatibility in both studies (see Sect. 5.2). Addition of hydroxyapatite to the P3HB scaffolds resulted in enhanced viability and alkaline phosphatase activity. Cell culture studies with primary human osteoblasts showed very limited cell attachment and proliferation on P3HB-7%3HV in comparison to P3HB surfaces [132]. Surface modification of P3HB-8%3HV porous scaffolds by oxygen plasma treatment resulted in more viable rat bone marrow osteoblasts and increased alkaline phosphatase activity in comparison to unmodified materials [133, 134].

Covalent immobilization of collagen I onto the surface of P3HB-8%3HV films after ozone treatment and methacrylic acid grafting also enhanced bone cell growth, as tested with mouse osteoblastic and rat osteosarcoma cells [135].

Chondrocytes derived from rabbit articular cartilage were seeded on P3HB films [136][129] and porous scaffolds [137, 138]. Cells attached to P3HB films secreted both collagen II and collagen X, which are major cartilagespecific ECM proteins, indicating maturational differentiation of chondrocytes into cartilage [136]. However, collagen II expression was low on P3HB in comparison to PLLA scaffolds [138]. Enhanced cell adhesion and growth, as well as more collagen II synthesis, could be obtained after addition of P3HB-3HH to the P3HB matrices [136, 138]. In another study, P3HB-9%3HV porous matrices incubated with ovine chondrocytes showed lower cell densities in comparison with collagen sponges [123]. However, electrospun P3HB-5%3HV nanofibrous mats promoted chondrocyte attachment when compared with polymer films [71]. Other cell types tested included mammalian or human epithelial cells, which showed little or no cell adhesion on P3HB fiber-based “wool”.

However, surface treatment with acidic or alkaline solutions promoted cell proliferation on these fibers [139].

Cells of the human respiratory mucosa (fibroblasts and epithelial cells) have been incubated with P3HB films as a potential replacement matrix of respiratory mucosa after surgical resections. However, while PLLA and collagen supported cell growth, P3HB showed cell growth only after surface modification by intense ammonia plasma treatment. No differentiation of epithelial cells with beating cilia could be found on all materials during the 6-week study [140].

The attachment rate of human retinal pigment epithelium cells was higher on P3HB-8%3HV films modified by oxygen plasma than on unmodified films due to increasing hydrophilicity and decreasing surface roughness. The cells were grown to confluency as an organized monolayer suggesting P3HB-8%3HV as a potential temporary substrate for subretinal transplantation to replace diseased or damaged retinal pigment epithelium [141].

Cell culture experiments using mouse liver cells (endothelial cells and hepatocytes) grown on P3HB and P3HB-3HV films (15%, 28% 3HV) suggested lack of cytotoxicity of the highly purified materials tested [120]. The adhesion of human endothelial cells on P3HB films could be controlled by plasma treatment introducing positive (NH_3 plasma) or negative (H_2O plasma) surface charge, which was explained by modulated anchorage and conformational changes of adsorbed fibronectin [141].

In vivo Studies

A number of *in vivo* studies have shown very mild tissue reactions after implantation of P3HB, which were comparable to those of other polymers in medical use. For example, an excellent *in vivo* biocompatibility of P3HB has been reported after s.c. implantation in mice [72]. Nonwoven P3HB patches tested as pericardial substitutes in sheep appeared to be slowly phagocytosed by polynucleated macrophages without any other kind of inflammatory cells, except for a small number of lymphocytes. The number of macrophages surrounding the polymer particles decreased with the absorption of the polymer [142]. Histologically, a dense collagen layer similar to that in native pericardium was found on the epicardial side of the patch. A thin fibrotic layer surrounding the patch disappeared along with the macrophages when the patch was absorbed but the regenerated pericardial tissue remained [142].

A mild inflammatory response to the nonwoven P3HB patch material similar to that reported for the pericardial substitutes appeared after closure of an atrial septal defect and enlargement of the right ventricular outflow tract in sheep [142].

P3HB and P3HB-3HV (5.5%, 9%, 19%, 22% 3HV) films manifested good tissue tolerance when implanted s.c. in mice for up to 6 months. No acute inflammation, abscess formation, or tissue necrosis was observed. At 1 month after implantation, implants were surrounded by a fibrous, vascularized capsule consisting primarily of connective tissue cells. A mild inflammatory reaction was manifested by the presence of mononuclear macrophages, foreignbody cells, and lymphocytes. The number of inflammatory cells increased with increasing valerate content in the copolymer. Thus, inflammation was most pronounced for P3HB-22%3HV. Three months after implantation, the fibrous capsule had thickened due to an increase in the amount of connective tissue and a few collagen fiber deposits. A substantial decrease in inflammatory cells was observed at this time, but inflammation still remained more pronounced for P3HB-3HV with a higher content of valerate units. After 6 months of implantation, the number of inflammatory cells had further decreased and the fibrous capsule, consisting mainly of collagen fibers, had thinned. Within 3 months of implantation a slightly stronger tissue reaction to P3HB than to PDLLA or PLLA was observed in this study and attributed to low molecular weight components and impurities leaching out of the polymer samples. At 6 months, the tissue response to the implants was similar for all these types of polymers [91].

An increasing inflammatory response with increasing 3HV content was also observed for P3HB-3HV (8%, 12% HV) films s.c. implanted in rats for up to 12 weeks. Few differences between P3HB-3HV copolymers in terms of tissue response have been found after i.m. implantation of P3HB-3HV (7%, 14%, 22% HV) in sheep for up to 90 weeks. Acute inflammatory reactions significantly decreased with time and no abscess formation or tissue necrosis were reported in this study [72]. The tissue response to P3HB and P3HB-3HV (15% HV) fibers implanted i.m. in rats was characterized by a short acute inflammation period (up to 2 weeks) followed by the formation of a fibrous capsule of less than 200 μm thickness during weeks 4 to 8, which was reduced to 40–60 μm after 4–6 months. Forty eight weeks after surgery, the fibrous capsule surrounding the implants was minimal. Mono and polynuclear macrophages were still abundant at this time. The tissue response to P3HB and P3HB-3HV fibers was similar in terms of inflammatory reaction and fibrous capsule formation. There were no adverse reactions, such as suppurative inflammation, necrosis, calcification, and malignant tumor formation for up to 48 weeks after implantation [143, 144].

P3HB discs implanted for 3 months in the peritoneum of rats showed the presence of a thin and poorly adherent fibrous capsule that contained no inflammatory cells. P3HB was assessed to be biocompatible because the formed capsule was porous and ensured communication between the polymer and the biological fluids. Perfluorohexane plasma-modified P3HB discs were surrounded by a nonporous capsule indicating a slight decrease in the surface biocompatibility. P3HB samples implanted s.c. and i.p. in rats were found to be tissue compatible without inflammation reaction or tumor formation. After 1 year of implantation the fibrous capsule surrounding the s.c. implant was about 30% thicker than that surrounding

the i.p. implant. A small number of phagocytes indicated the polymer resorption process at that time [72]. No inflammatory reactions resulted from the i.m. injection of P3HB or 3HB in rats, indicating a good *in vivo* biocompatibility. P3HB patches implanted onto the rat stomach showed no significant inflammatory response as confirmed by analysis of cytokine production. A group of mRNAs encoding pancreatic enzymes was transiently present in tissue surrounding the patch material [145] 1–2 weeks after implantation. The amount of mRNA of the inflammation marker C-reactive protein (CRP) was also found to transiently increase [146].

P3HB in bone contact causes a strong initial cellular reaction with slight or no inflammation [147]. P3HB bone screws showed an optimal tissue compatibility. Osteosynthesis plates and screws made of P3HB were highly compatible without induction of immunologic or inflammatory reactions [72].

A very fast healing and formation of new bone substance could be achieved with P3HB/HA composites [115]. The interface between the composite and bone was physically and biochemically active over a 6-month period of implantation into the condyles of rabbits. Bone bonding to these composites occurred by degradation of the P3HB matrix, which led to the formation of new crystallites between the parent HA particles in the P3HB/HA composite, as well as at the surface of the parent HA particles [148]. With respect to the mechanical properties and the tissue response, P3HB-20%HV films were more suitable than PLLA, PDLLA, and PCL to separate mucoperiostum and bone in a dog model for closure of palatal defects [149]. In contrast, P3HB-3HV reinforced with polyglactin was not useful as an occlusive barrier over dental implants in dogs, since the material prevented bone healing due to an increased inflammatory reaction [150]. P3HB-22%3HV coated onto a tantalum stent implanted for 4 weeks in the porcine coronary artery induced a marked inflammatory and foreign body response, thrombosis as well as extensive fibromuscular proliferation leading to eccentric stenosis. Intense inflammatory reactions and proliferations, thrombosis, and in-stent lumen narrowing have also been reported after implantation of P3HB stents (plasticized with 30% TEC) into the rabbit iliac artery for up to 30 weeks. The polymer degradation process was suggested to be the main reason for the significant chronic inflammation induced by these stents [151]. Another explanation might be the fast leaching of the watersoluble plasticizer [104], together with polymer crystallization induced by the laser-cutting in the stent manufacturing process [152] leading to polymer stiffness and brittleness, which may cause the tissue irritation and early stent rupture observed in the study.

I.3.2. Biocompatibility and biodegradability of polyhydroxyalkanoates

In Vitro Degradation

In addition to suitable mechanical and biocompatibility properties, a temporary implant material needs to degrade within clinically reasonable time periods. *In vitro* degradation

studies on P3HB films in buffer solution (*p*H 7.4, 37 °C) showed no mass loss after 180 days, but a decrease in molecular weight starting after an induction period of about 80 days [153].

This induction period was attributed to the time required for water to penetrate the polymer matrix. The degradation mechanism was examined in an accelerated test at 70 °C. It was concluded that the hydrolysis of microbial polyesters proceeds in two steps. First, there is a random chain scission both in the amorphous and crystalline regions of the polymer matrix associated with a decrease in the molecular weight with unimodal distribution and relatively narrow polydispersity. Simultaneously, an increase in crystallinity occurs that is attributed to the crystallization of chain fragments in the hydrolyzed amorphous regions. When the molecular weight of the degrading polymer reaches a critical low *M*n of about 13 000, mass loss starts as the second step [154].

This *in vitro* degradation profile is typical for a bulk-degrading polymer and can also be found in synthetic polyesters in medical use, such as PGA, PLGA, PDLLA, and PLLA. Thus, significant mass loss of P3HB will be observed only after the prolonged period of time necessary for the molecular weight to reach the critical lower limit. Therefore, the degradation profile can hardly be predicted solely by determination of mass loss but should preferably be based on the molecular weight analysis.

The occurrence of low molecular weight P3HB in the human body may suggest that specific enzymes are involved in the polymer synthesis and its depolymerization *in vivo*. Moreover, it is worth noting that a Ser..His..Asp triad constitutes the active center of the catalytic domain of both P3HB depolymerase [155] and pancreatic lipase [156]. The serine is part of the pentapeptide Gly-X1-Ser-X2-Gly, which is located in all known P3HB depolymerases as well as lipases, esterases, and serine proteases [155]. However, the occurrence of P3HB-specific enzymes in the human body and their contribution to the hydrolysis of implanted P3HB needs still further clarification.

The hydrolytic degradation of P3HB-3HV copolymers with low hydroxyvalerate content (up to 20%) has been extensively studied. A comparison with the P3HB homopolymer is possible because the low 3HV content has only little influence on the hydrolysis rate while the molecular weight, crystallinity, porosity, and any additives are of significant importance. P3HB-3HV samples showed an increased degradation rate with decreased initial molecular weights [157, 158].

Porous scaffolds made from P3HB-3%3HV and P3HB-3%3HV/wollastonite composites showed a continuous fast decrease in their mass and molecular weight when stored for up to 15 weeks in buffer solution (*p*H 7.4, 37 °C). For example, unmodified P3HB-3HV scaffolds lost about 12% of their initial mass and about 90% of their initial molecular weight at the end of the incubation period. Increasing the amount of wollastonite in the composite resulted in increased mass loss due to wollastonite dissolution but delayed polymer hydrolysis, which

was explained by the buffering effect of acidic hydrolysis products by alkaline ions dissolved from the wollastonite. This was confirmed by *p*H measurements showing a drop during the incubation of unmodified P3HB-3HV, but almost constant values when testing the composites [159]. Porous P3HB scaffolds tested in another study showed a mass loss of only 3% after 50 days of incubation in buffer solution (*p*H 7.4, 37 °C) [116]. Mass loss of P3HB-8%3HV porous scaffolds started after an induction period of 120 days and reached about 40% after 180 days *in vitro* (*p*H 7.4, 37 °C) [133, 134].

The degradation behavior of P3HB was also studied for the selection of suitable sterilization methods. It was found that with steam sterilization and with gamma-irradiation in particular a molecular weight reduction and deterioration of mechanical properties takes place, while sterilization with ethylene oxide or formaldehyde gas has no affect on the polymer properties [152].

Significant loss in the molecular weight together with embrittlement have been observed for P3HB films, but not P3HB-3HV films, in a screening study testing a variety of sterilization methods [120]. The irradiation-induced degradation of P3HB or P3HB-3HV was studied and confirmed also by other authors [97, 160-163]. However, it was also reported that P3HB-3HV can be sterilized by steam, gamma-irradiation, and ethylene oxide/carbon dioxide without losing stress and stiffness [164].

In vivo Degradation

The *in vivo* degradation (decrease of molecular weight) or resorption (mass loss) of P3HB has long been a controversial subject in the literature. Main reasons for the controversy were the use of samples made by various processing technologies (e.g., solution-casting, melt-processing, drawing/orientation) in different shapes and designs (e.g., films, fibers, porous scaffolds) and the incomparability of different implantation sites (e.g., blood contact, “soft” tissue, “hard” tissue). However, there is now a significant body of research data available confirming that P3HB is a completely resorbable polymer, with a degradation rate comparable to that of slowly degrading synthetic polyesters such as high molecular weight PLLA. Most valuable for an estimate of the *in vivo* resorption time of P3HB are studies conducted in sheep which demonstrated the resorption of arterial implants (blood contact) after approximately 12–24 months and pericardial implants (“soft” tissue contact) after approximately 30 months.

For example, various P3HB samples implanted for 1 year s.c. in rats showed a decrease in the molecular weight to about 70–85% of the initial value [192]. Systematic degradation studies of polyesters, among them P3HB, were carried out s.c. in mice [91]. The 2%mass loss of P3HB after 6months of implantation was ascribed to low molecular weight impurities. The molecular weight was reduced to 57% of the initial value. The *in vivo* degradation rate had the

order PDLLA > PLLA > P3HB. It was concluded that P3HB degrades *in vivo*, although at a much slower rate than the poly(lactide)s. Additionally, the *in vivo* degradation of P3HB was systematically compared with that of P3HB-3HV. P3HB-3HV copolymers show a slower degradation than P3HB if the 3HV content is less than 10%. However, the hydrolysis rates become comparable when the 3HV content reaches about 20%. This might be explained by a slightly decreased polymer crystallinity with increasing amount of 3HV, which overshadows the decelerating effect caused by the increasing hydrophobicity. However, crystallinities of P3HB-3HV copolymers are generally high and in the order of magnitude of that of the P3HB homopolymer [65, 200] so that degradation rates can be expected that are similar for both types of polymers.

Bioresorbable intravascular stents made of P3HB plasticized with TEC were nearly completely dissolved 16–26 weeks after implantation into the iliac arteries of rabbits [151, 165]. P3HB conduits for nerve regeneration showed softening [77] or fragmentation and size reduction [76] after a 12-month implantation in cats. In another study, the canine urethra was replaced by a polyglactin mesh coated with P3HB. The complete resorption of the graft was observed 8–12 months postoperatively [166].

I.3.3. Applications of polyhydroxyalkanoates in tissue engineering

Medical and pharmaceutical uses such as gauzes, sutures, filaments, implants, drug carriers, and coatings for drugs because Biopol is biocompatible, biodegradable and non-toxic.

Patches

P3HB patches have shown potential for guided tissue regeneration in a number of animal studies and in patients. Nonwoven P3HB patches made from solution-spun fibers have been extensively studied for defect repair in heart surgery, such as for pericardial substitution [75, 167, 168].

Resorbable P3HB patches for the gastrointestinal tract have been developed to cover large open lesions if closure by conventional surgical techniques with sutures or clips is impossible. These asymmetric patches were designed to have a porous surface facing the bowel defect to support tissue regeneration, and a smooth surface to prevent adhesions to the surrounding gut (Figure I. 14). Tests have been made on patches made either from P3HB films [145], P3HB films blended with at-P3HB in order to reduce stiffness and enhance hydrolysis [70].

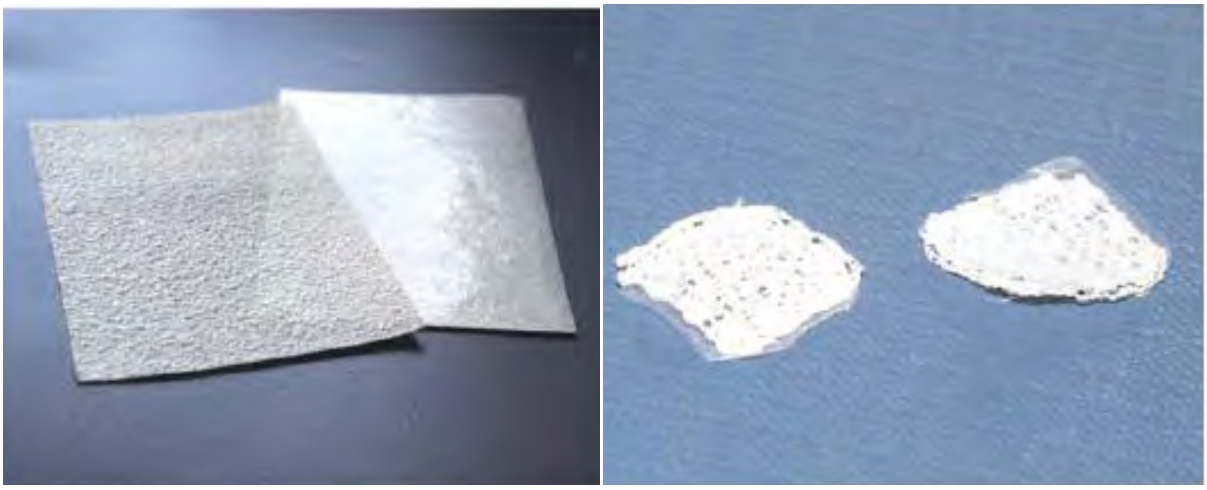

Figure I. 14: a) P3HB/at-P3HB asymmetric patches [17] (reprinted by permission of Wiley) and b) P3HB film/textile composite patches (Institute of Polymer Research, Dresden, Germany) with porous surface to support tissue regeneration and smooth surface to prevent adherence to surrounding organs

Nerve Conduits

Conduits for peripheral nerve regeneration were formed from nonwoven P3HB sheets having polymer fibers oriented in one direction. These sheets were wrapped around a 2–3mm gap of the transected superficial radial nerve in cats, and were sealed with fibrin glue [76, 77][34, 36]. The fibers were oriented longitudinally in order to provide contact guidance and mechanical support for

growing axons. The slow degradation of P3HB was considered to be of advantage, supporting the nerve during a period long enough for regeneration to take place and reducing the risk of accumulation of large amounts of acidic degradation products. Axonal regeneration was found to be similar to that observed with epineural repair, which was used as a control.

P3HB tubes with unidirectional fiber orientation were prepared by rolling a sheet of nonwoven P3HB around a cannula and sealing it with cyanoacrylate glue. These tubes were successfully used to bridge a 10mm gap in the sciatic nerve of rats. An increased axonal regeneration was found by filling the tubes with transplanted Schwann cells [169]. Allogenic Schwann cells, embedded in an alginate/fibronectin matrix inside the P3HB conduit, were shown to enhance axonal regeneration of the transected rat sciatic nerve without eliciting a deleterious immune response [170]. Additionally, P3HB conduits filled with leukemia inhibitory factor in an alginate/fibronectin matrix enhanced the repair of the rat sciatic nerve in comparison to conduits without growth factor, but still did not perform as well as autografts [171].

Tubes made from P3HB sheets were also tested as conduits for long-gap peripheral nerve repair. P3HB tubes used to bridge up to 40 mm-long gaps in the transected peroneal nerve in rabbits supported nerve regeneration, although not as well as autografts. The authors concluded that empty P3HB conduits may not be optimal for long-gap repair, and improvements might be considered by using exogenous growth factors or cultured cells [172].

Bone and Cartilage Repair

The long-term degradation profile of P3HB is considered to be of advantage in orthopedic applications [147, 173]. Additionally, the piezoelectric potential of P3HB has been considered as a special feature, because it is comparable with that of natural bone [174]. It is well-known that bone can be strengthened and repaired by electrical stimulation. Therefore, P3HB composites may stimulate bone growth and healing [175].

P3HB implants have been tested for connecting osteotomies in the tibia of rabbits. The defect was healed after 12 weeks in most cases and the implant was completely resorbed after 24 weeks [176]. P3HB was also successfully tested as an occlusive membrane for guided bone regeneration in the mandibula of rats [177]. Osteosynthesis plates made of P3HB and anchored with two P3HB bolts were examined for repair of a cut through zygomatic arches of rabbits. The polymer was assessed to be suitable for covering defects of the osseus skull and as an osteosynthesis material for fractures of the visceral cranium [178].

P3HB composites were extensively examined for bone repair, such as composites made of P3HB and HA. HA is a stimulator in the formation of new bone, while P3HB is considered as potentially bioactive due to its degradability and piezoelectricity. P3HB/HA composites were found to closely match the mechanical properties of cortical bone, but had insufficient strength and ductility for the construction of major load-bearing components [115]. To improve mechanical strength, phosphate glass was added to this composite. It was observed that also bone-forming osteoblasts proliferation was increased [147]. Among composites made from P3HB or P3HB-3HV (8%, 12%, 24% 3HV) and HA, the P3HB-8%3HV/HA (30/70) composite had a compressive strength similar that of human bone, making it a candidate for fracture fixation [179]. Composites made from P3HB-7%3HV and HA were used also as cortico-cancellous bone grafts [180].

In vitro studies have shown the formation of bone-like apatite on the surface of P3HB-12%HV/TCP composites [181] similar to P3HB/HA [182]. Recently, the fabrication and properties of a composite scaffolds based on P3HB-3%3HV copolymer and wollastonite have been reported [159]. The potential of P3HB and P3HB-8%3HV as matrices for bone tissue engineering was assessed *in vitro* when bone marrow cells were used. A chemically synthesized degradable polyesterurethane foam containing crystalline domains of short-chain

P3HB and amorphous domains of PCL exhibits good osteoblast compatibility and is being considered as scaffold biomaterial for bone repair [183].

I.3.4. Other applications of polyhydroxyalkanoates

Due to the thermoplastic and biodegradable character of the polyhydroxyalkanoates class polymers they are used in the production of bioplastics. Below there are presented a few examples of commercial PHAs used in industrial packaging production.

Biomer (Biomer, Germany) thermoplasts are polyesters obtained from renewable resources. The products are waterproof, heat resistant, have appealing surfaces, and are fully biodegradable [11].

This polyhydroxybutyrate is produced by Alcaligenes Latus. Pellets are commercialised for classical plastic transformation processes. The low viscosity of the melted polymers allows the injection of objects with thin walls. This product is very hard and can be used from -30-120 °C. composting duration is about two months.

The pellets are processed on standard machines. The melt behaves like liquid crystalline polymers (LCP's). This property allows to mold thin walled or complex structures even on small machines.

Nodax™ polymers are a series of PHA copolyesters consisting of short-chain-length HB and mcl HA currently in development by Procter & Gamble (P&G, USA), with efforts focused on achieving low cost fermentation production and targeted polymer specifications. The development is being conducted on a global basis, combining P&G's resources with the support of several companies and research institutes. The global combination of resources provides the best available technology, scientists and engineers, as well as continuous localized feedback [12].

Nodax™, polyhydroxybutyrate-hexanoate (PHB-H), is a biorenewable polymer, or plastic material. Nodax™ is made from corn, sugar beet and/or vegetable oils and is often referred to as a biopolymer, since it is derived from plants. Sugar and/or oil are extracted from the plant(s) and, through a fermentation process, can create a variety of plastic materials and/or products including packaging, laminates and coatings, and nonwoven fibers.

P&G is working with converters and end users. This aspect of the value chain includes conversion of the formulated resins into initial forms, like films, fibers or molded articles, as

[11] http://www.biomer.de/IndexE.html

[12] http://www.pgchemicals.com/case-studies/plastic-made-from-nature-nodax/

well as secondary conversion into nonwovens, laminated packages and papers. End users then use these to make or package consumer or industrial products, like diapers, hamburgers or computers. Finally, the products are used and then eventually disposed of in one of several ways (composting, landfill, digestion, incineration) where the biocycle is completed [13].

The biodegradablility of blends of poly(3-hydroxybutyrate) with a copolymer of poly(3-hydroxybutyrate) and poly(3-hydroxyvalerate) is better than that of each component taken separately. This is an advantage found in many other blends of biodegradable plastics. The same fact is observed for blends of poly(3-hydroxy-butyrate) and polyethylene glycol.

Biopol is the trade name of one of the most common synthetic biopolymers produced today. This biopolymer is a polyhydroxyalkanoate (PHA) and it is a co-polymer (2 different monomers joined), consisting of the monomers polyhydroxybutyrate (PHB) and polyhydroxyvalerate (PHV). Biopol is produced industrially, using the fermentation of sugars by the bacterium *Alcaligenes eutrophus* which grow in tanks with a carbon-based food source. The polymer is then separated and purified [14].

Disposable products used in the food industry such as utensils, cups and plates because Biopol is strong, insoluble in water, non-toxic and biodegradable.

Application of Biopol include: plastic wrap for packaging, coatings for paper and cardboard, moisture barrier films for hygienic products, disposable containers for shampoo and cosmetics, and disposable items such as razors, rubbish bags and disposable nappies because Biopol has high tensile strength, it is insoluble in water, non-toxic and biodegradable [15].

I.4. Structure and proprieties of silk fibroin

Silk is a natural protein fiber produced by some *Lepidoptera larvae* such as silkworm, spiders, scorpions, files and mites. The most studied silk is the domesticated silkworm, *Bombyx mori (Lepidoptera: Bombycidae family)* [184].

Bombyx mori silk is a natural macromolecular protein composed of two major proteins: fibroin and sericine [185], which constitute ~75% and ~25% of the cocoon, but also consist of fat and wax (1.5%) and mineral salts (0.5%) [186]. These proteins consist of the same 18 amino acids such as Glycine, Alanine, Serine and Tyrosine [187].

[13] http://www.pgchemicals.com/case-studies/plastic-made-from-nature-nodax/

[14] http://hscchem.wikispaces.com/file/view/biopol.pdf

[15] http://hscchem.wikispaces.com/file/view/biopol.pdf

Table I. 4: Composition of *Bombyx mori* silk [188]

Component	%
Fibroin	**70−80**
Sericine	**20−30**
Wax matter	**0.4−0.8**
Carbohydrates	**1.2−1.6**
Inorganic matter	**0.7**
Pigment	**0.2**

Silk sericine (10-300 kDa) [189], a hydrophilic protein is the glue-like, globular protein that surrounds the fibroin fibers to cement them together [190]. Sericine also provides oxidation and UV resistance, antibacterial and moisture properties, and property to absorb and remove water. After the degumming process, the water-soluble sericine is removed, a structure consisting of fibroin remains.

Silk fibroin consists of a heavy (~350 kDa) and a light (~25 kDa) chain [191], which are present in a 1:1 ratio, linked by a disulfide bond [192]. The silk fibroin also contains a glycoprotein, named P25, with a molecular mass of about 30 kDa [193].

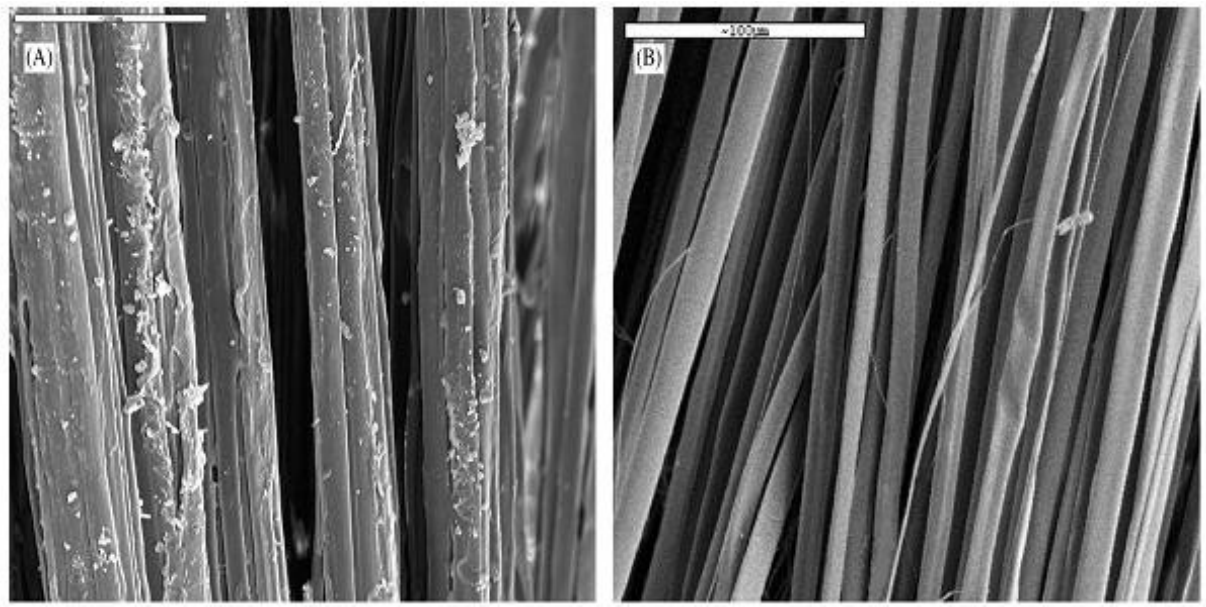

Figure I. 15: SEM images of *Bombyx mori* silk fibers A-before and B-after degumming process [194]

Therefore silk fibroin is considered as a block copolymer composed of crystalline (hydrophobic chains) and amorphous states (hydrophilic chains) [195]. The fibroin structure contains repeating basic unit of Gly-Ser-Gly-Ala-Gly-Ala amino acid sequence.

The crystalline nature of silk fibers is due to the high content of repetitive Gly-Ala-Gly-Ala-Gly-Ser sequence [196], and the amorphous domain is represented by amino acid sequence Thr-Gly-Ser-Ser-Gly-Phe-Gly-Pro-Tyr-Val-Ala-Asp-Gly-Gly-Tyr-Ser-Arg-Arg-Glu-Gly-Tyr-Glu-Tyr-Ala-Trp-Ser-Ser-Lys-Ser-Asp-Phe-Glu-Thr [197].

The highly repetitive sections is characterized by the presence of Glycine (45%), Alanine (30%), and Serine (12%) [198], totalling approximately 85 mol % of the total amino acids [199], in a rough 3:2:1 ratio [200], and the amino acid sequences are expressed as $[Gly\text{-}Ala\text{-}Gly\text{-}Ala\text{-}Gly\text{-}Ser]_n$ [201].

Also, it is reported that silk fibroin has many hydroxyl residues based its amino acid composition: Ser (10.6 mol %), Tyr (5.0 mol %) and Thr (0.9 mol %), by comparison with the carboxyl and amino group content which was low (3.9 mol %) [202]. The macromolecular polypeptide chain of silk fibroin has a zigzag shape, similar to β-keratin [203].

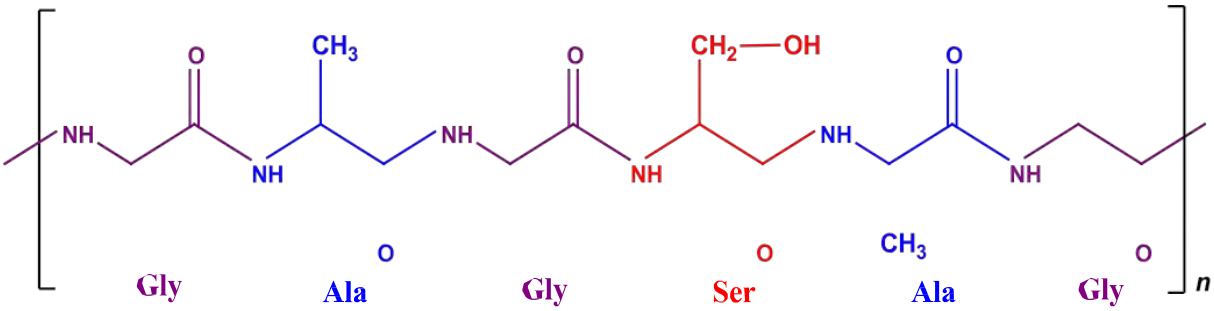

Figure I. 16: Primary structure of silk fibroin: [Gly-Ala-Gly-Ser-Ala-Gly]*n*

Table I. 5: Amino acid composition of *Bombyx mori* silk fibroin [204]

Amino acids	Composition, mol %		
	Total	Heavy areas	Light areas
Glycine	42.9	49.4	10.0
Alanine	30.0	29.8	16.9

Serine	12.2	29.8	7.9
Tyrosine	4.8	4.6	3.4
Valine	2.5	2.0	7.4
Aspartic acid	1.9	0.65	15.4
Glutamic acid	1.4	0.70	8.4
Threonine	0.92	0.45	2.8
Phenylalanine	0.67	0.39	2.7
Methionine	0.37	-	0.37
Isoleucine	0.64	0.14	7.3
Leucine	0.55	0.09	7.2
Proline	0.45	0.31	3.0
Arginine	0.51	0.18	3.8
Histidine	0.19	0.09	1.6
Lysine	0.38	0.06	1.5

For *Bombyx mori* silk fibroin, in crystalline areas, can be distinguished two secondary structures: silk I (α-helix) and silk II (β-sheet) [205]. The silk I structure in formed by intra-molecular hydrogen bonds, is water soluble and, upon exposure to organic solvents converts

to silk II structure [206]. The silk II structure is water insoluble and also in various solvents, and is well understood [207].

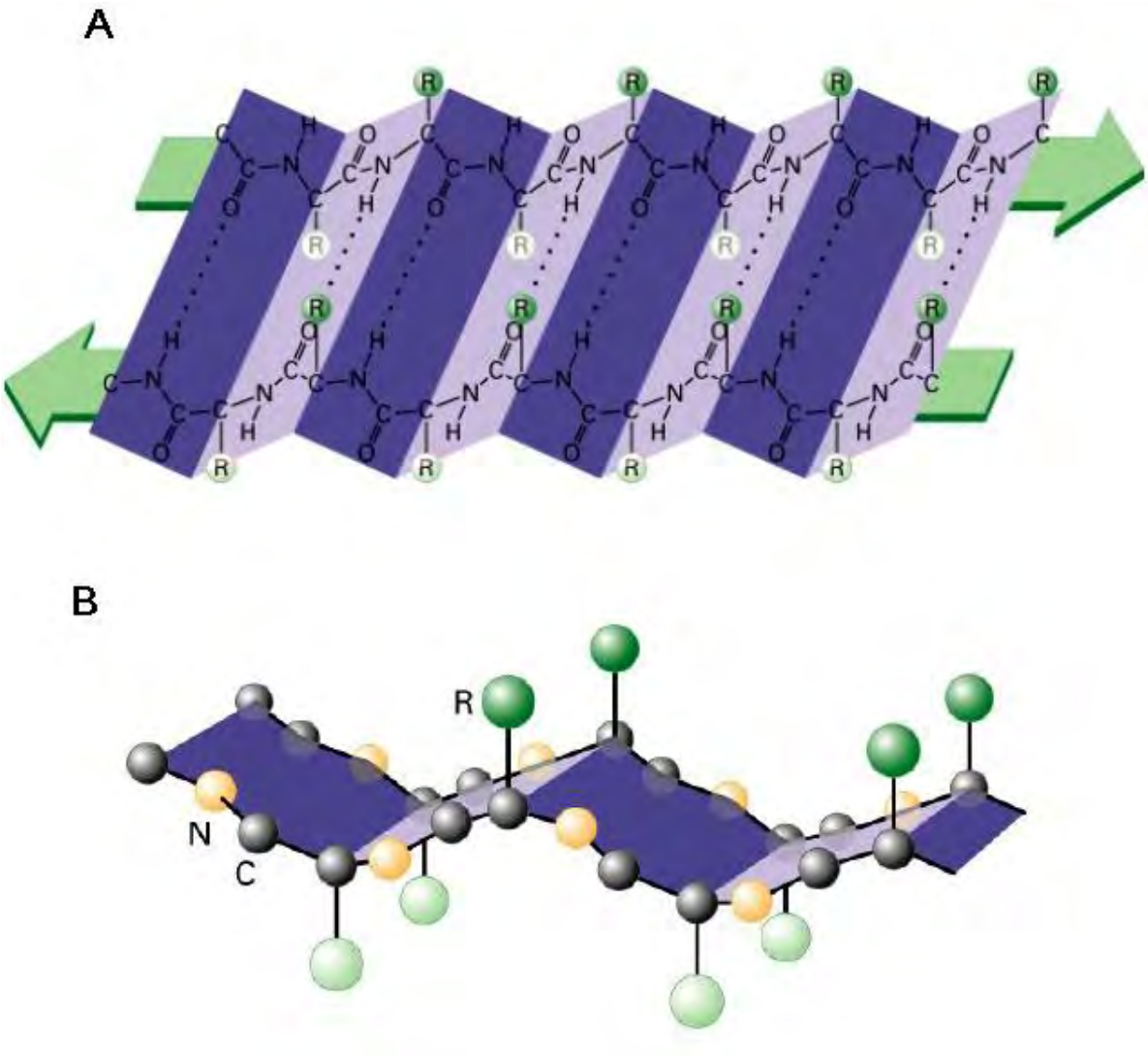

Figure I. 17: β-pleated structures of silk fibroin macromolecules: A-face view, B-side view [208].

Table I. 6: Composition of *Bombyx mori* silk [188]

Component	%
Fibroin	**70−80**
Sericine	**20−30**
Wax matter	**0.4−0.8**
Carbohydrates	**1.2−1.6**

Inorganic matter	**0.7**
Pigment	**0.2**

Silk sericine (10-300 kDa) [189], a hydrophilic protein is the glue-like, globular protein that surrounds the fibroin fibers to cement them together [190]. Sericine also provides oxidation and UV resistance, antibacterial and moisture properties, and property to absorb and remove water. After the degumming process, the water-soluble sericine is removed, a structure consisting of fibroin remains.

Silk fibroin consists of a heavy (~350 kDa) and a light (~25 kDa) chain [191], which are present in a 1:1 ratio, linked by a disulfide bond [192]. The silk fibroin also contains a glycoprotein, named P25, with a molecular mass of about 30 kDa [193].

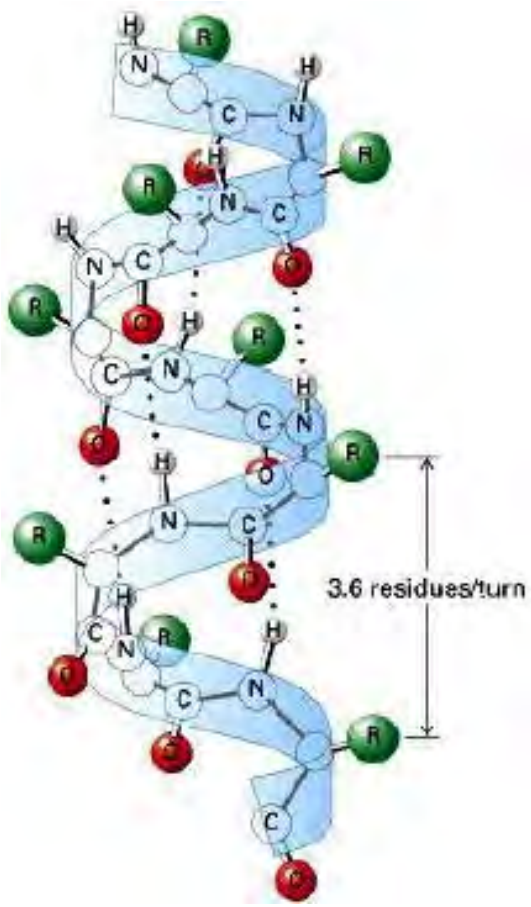

Figure I. 18: α-Helical structures of silk fibroin macromolecules [208]

In the crystalline areas of silk fibroin, the side-chain protein marked the R-group (H-glycine, CH3-alanine and CH2-OH-serine) are almost fully extended in β-sheet structure, allowing the formation of hydrogen bonds.

The β-sheet interacts with each other only through hydrogen bonds (inter-chain and intra-chain) and Van-der-Waals interactions, generating a flexible structure [209].

The remarkable properties of natural silk may competing with the most advanced synthetic polymers, yet unlike these, are obtained in less harsh conditions, from renewable raw materials and are biodegradable [188]. Silk fibers are long, thin, light and soft.

The outstanding mechanical properties of silk fibroin characterized by high strength combined with high extensibility, and good compressibility, is due to the extensive hydrogen bonding, hydrophobic nature and to the crystalline domains orientations [210].

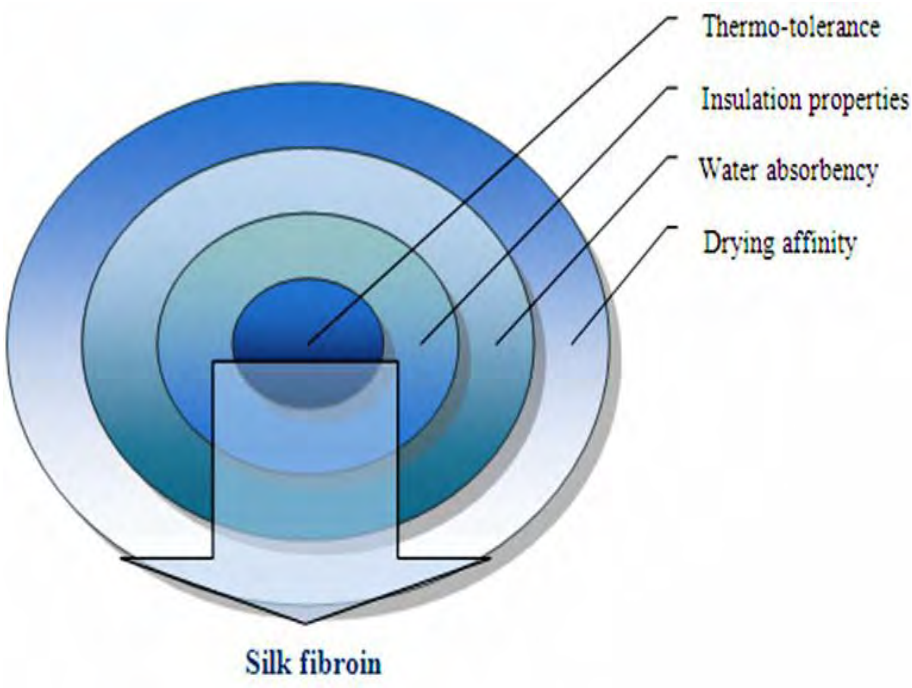

Figure I. 19: Representation of silk fibroin attributes

A few mechanical properties of silk fiber and its components, and some other biomaterials are presented in Table I. 7.

Table I. 8: Comparison of mechanical properties of several types of biomaterials and silk [194]

Material	Ultimate tensile strength (UTS) (MPa)	Modulus of elasticity (GPa)	Elongation at break (%)
Bombyx mori silk sericin	500	5-12	19
Bombyx mori silk fibroin	610-690	15-17	4-16
Bombyx mori silk	740	10	20

Spider silk	875-972	11-13	17-18
Collagen	0.9-7.4	0.0018-0.046	24-68
Tendon	150	1.5	12
Bone	160	20	3
Kevlar	3600	130	2.7
Synthetic rubber	50	0.001	850

Due to the lack of covalent linkages in the polymer system, the thermal stability of silk fibers is excellent up to 110 °C, starting with 200 °C, the chemical reactions involve the degradation of amino acid side groups with the formation of gases (CO, CO_2, NH_3) [211].

Silk fibers present hygroscopic nature. Under normal conditions (20 °C, 65 % RH), silks absorb approximately 11 wt. % of its weight in water. Water absorption causes swelling of fiber, to a value of 1.6 % in longitudinal direction and 18.6 % in transverse direction. The specific gravity of raw silk, range between 1.33 and 1.40 $g \cdot cm^{-3}$ [212].

The dry silk fibroin has a glass transition [213] at 178 °C (Tg = 451.15 K) [214], but decreases considerably in the presence of water [215].

The chemical reactivity of silk fibers is high due to the amino acids side groups. This property is used for chemical modification and grafting of some monomers on the chain protein, to modify its properties [216].

Silk presents an amphoteric character, containing both cationic and anionic groups, which interacts according to the *p*H. In reaction with mineral acids forms salts or, if acids are weak, they can attach to the protein through hydrogen bonds. In an acid environment peptide bonds are hydrolysed [203].

Natural silk fibers dissolve only in a limited number of solvents due to its crystalline nature and to the intra- and intermolecular hydrogen bonds. Silk fibroin dissolves in aqueous-organic solution of salts NaSCN (sodium thiocyanate), LiSCN (lithium thiocyanate), 9.0-9.5M LiBr (lithium bromide), mixtures of aqueous calcium chloride and ethanol $CaCl_2$-Et-OH-H_2O, calcium nitrate in methanol $Ca(NO_3)_2$-Me-OH or aqueous lithium bromide and ethanol LiBr-EtOH-H_2O [217], hexafluoroisopropanol (HFIP) [218], hexafluoroacetone [219] and formic acid [220].

I.4.1. Fibrous proteins with potential in biomedical applications

Fibrous proteins, due to their connecting special properties, are a class of biomacromolecules with applicability in biomaterials production.

The nature and the orientation of the amino acids in their primary sequence leads to the formation of secondary structures relatively homogeneous [221]. This organization has significant repercussions on the macroscopic and functional properties of these proteins.

They possess the ability to self-assembling into various physical states, with exceptional mechanical properties, for the development of new biomaterials [222].

Fibrous proteins such as silk fibroin, collagen, elastin and keratin, practically insoluble in water, characterized by high mechanical strength represent different architectural function in nature. The use of fibrous proteins in the design of biomaterials requires strict control methods of extraction and purification process. Moreover, the materials must support sterilization process after their synthesis, or be prepared in sterile medium. This aspect represents a challenge with the size of protein systems that can degrade, denature and/or change conformation under the action of certain solvents and heat [61].

B. mori silk fibroin, a naturally occurring protein polymer [223], has been used in textiles production for centuries and for sutures in biomedical applications for decades [194].

Also, due to its processing versatility, biocompatibility [224], good mechanical properties, controlled degradability [225], microbial resistance and good oxygen permeability [226], silk is became an attractive biomaterial for biomedical applications.

Due to its high processing versatility, silk fibroin can be used as biomaterial in diverse forms [227], such as films, foams [201], fibers, gels [228], membranes, powders, sponges, and scaffolds [229].

Silk fibroin is a worldwide used material, with applications in the cosmetic field, biomedical research and also in the art craft industry and automotive [230].

In regenerated forms, silk fibroin has been used in drug delivery systems [231], wound protection, burn-wound dressing [232] (wound healing bandages-to facilitate re-modelling, re-epithelisation of connective tissue) [233], ophthalmic applications [234] (ocular treatments-preparation of soft contact lens), enzyme immobilization matrices, vascular grafts, nerve grafts [235], structural implants, nets, and ligament tissue engineering (anterior cruciate ligament for knee joints) [236].

Also silk fibroin have been blended with alginate [237], collagen, cellulose, chitosan, gelatin, hyaluronic acid [238], PVA, PEG, polyurethane , keratin [232] and CNTs [239], as tissue engineering scaffolds with different biomedical applications.

a. Silk fibroin fibers

In the last years, the modification of silk fibroin fibers with tailored surface properties has been widely considered as a new powerful method to substantially improve some intrinsic fibers properties [240].

There are three classes of methods regarding the surface modification and functionalization of SFFs: surface modification by physical techniques (UV treatment, plasma treatment, and gas treatment), surface modification through chemical approaches (grafting copolymerization techniques, surface modification using chemical agents) and surface functionalization with nanomaterials. As for applications the surface modification and functionalization of SFFs can be divided into two classes: surface modification for biomaterials applications and surface pretreatment for improvement of dyeing and finishing performance [241].

Silk fibers obtained by winding from cocoons, can be used directly or in regenerated form in applications as ligaments engineering or sutures [216]. The SFFs 3D scaffolds have suitable mechanical strength properties for human ACL regeneration using (MSCs) [242].

The reasons for using this kind of fibrous material are related to its mechanical properties, aqueous processability and slow degradation profile [243-245].

Silk fibroin fibers modified with immobilized Arg-Gly-Asp (RGD) peptide allow the human tenocyte adhesion, proliferation, and differentiation. Silk fibroins sutures have been used for tendon-bone healing and tendon reconstruction surgery [246]. SFFs grafted with different acidic and amino groups was used as a template for the HA crystal growth [247].

Various methods including post spinning treatment with methanol and stretching [239], incorporation of MWCNTs, and gelatin-coated SF fiber were employed to improve the properties and biocompatibility of scaffolds [248-250].

b. Silk fibroin scaffolds

During the last decade, the synthesis of fibroin sponges used as templates to perform 3D cell culture, promoting the adhesion, proliferation and differentiation of human dermal fibroblasts [251], has been greatly studied.

SF sponges can be obtained using lyophilization [252], gas-foaming [253], porogens (e.g., NaCl) [254], and freeze-drying in presence of various organic solvents (methanol, ethanol,

propanol, butanol, DMSO, and acetone) [255]. Also e-spinning has been one of the important methods to obtain SF porous scaffolds [256].

Lyophilization method is used to modify the final morphology of the matrices. This is possible by varying the freezing temperature, the freezing rate, and the initial concentration of fibroin before freezing prior to lyophilization. Furthermore, the scaffolds prepared by lyophilization can be solubilized in an organic solvent such as HFIP [257].

Then, by controlling the concentration of fibroin solutions, other types of sponges with morphological characteristics (porosity, pore size, material density) vary according to the porogenic added to these solutions can be formed. Aqueous based porous silk sponges can be prepared using NaCl crystals as porogens with control of pore size from 490-940 μm [258].

Higher porosity and better mechanical strength is obtained from aqueous-based SF sponges with a faster enzymatic degradation [197].

Porous 3D silk scaffolds had been successfully used for healing critical size femur defect in rats [13], insulin growth factor I (IGF-I) from silk scaffolds promoted chondrogenic differentiation of human bone marrow mesenchymal stem cells [259], in tissue engineering for cartilage and meniscus regeneration [260].

SF-based scaffolds have shown to promote the adhesion, proliferation and differentiation of chondrocyte cells [261] and human cervical cells [262]. SF scaffolds have also been used for the immobilization of Horseradish peroxide (HRP) enzyme gradients, using water-soluble carbodiimide [263].

The properties of SF scaffolds had also been exploited by loading with adenosine, in antiepileptic effects [264], and heparin (cytocompatibility and blood compatibility) [265].

Recently, a green process avoiding organic solvents and harsh chemical processes was developing to obtain SF/Gelatin biomaterial scaffolds [266].

c. Silk fibroin particles

As a fibrous protein, SF fibres from *B. mori* have been explored as a versatile protein biomaterial for the formation of particles for drug delivery due to its aqueous processability, biocompatibility, and biodegradability [267].

Silk fibroin protein based micro- and nanoparticles provide new options for drug delivery due to their unique combination of self-assembly, controllable structure and morphology, their tunable drug loading and release properties.

Silk fibroin micro- and nanoparticles can be obtained using several techniques such as phase separation, solvent displacement, self-assembly, spray drying, emulsion-solvent evaporation/extraction, and rapid expansion of supercritical fluid solution [268].

Each method has advantages and disadvantages; therefore the selection of the right method is very important in fabricating micro- and nanospheres for drug delivery applications.

HRP was used as a model drug for silk fibroin microspheres to aim encapsulation and release [269], silk fibroin particles including rhodamine B (RhB), rhodamine B isothiocyanate-dextran (RITC-Dextran) and fluorescein isothiocyanate labelled bovine serum albumin (FITC - BSA) as model drugs had also been exploited [225].

I.4.2. Applications of silk fibroin in tissue engineering

Silk fibroin fiber scaffolds prepared via e-spinning for inclusion of BMP-2 and/or hydroxyapatite nano-particles (nHAP) were used *in vitro* to enhance bone-like tissue formation for human mesenchymal stem cells (hMSCs) [270].

SF hydrogels also were used as implant for the reconstruction of critical size calvarial defects [13], as scaffold both *in vitro* and *in vivo* for bone tissue growth in rabbits bone defects without inflammatory reactions contributing to the bone remodelling and maturity [271].

Apatite-coated porous biomaterial based on SF scaffolds have also been reported, to repair inferior mandible border defects in a canine model, the results suggesting an increased osteoconductive environment for bone marrow stromal cells (bMSCs) to regenerate sufficient new bone tissue [272].

Also the mineralization ability of RSF/PAAm hydrogels in SBF was further investigated, as a substrate for deposition of bone-like apatite crystals [273].

Due to their unique properties, SF hydrogels are potentially useful as bone replacement/reconstruction material in reconstructive orthopaedic surgery, and also as a substrate for deposition of bone-like apatite crystals.

In order to improve the mechanical properties of hydrogels several techniques have been developed such as fibre-reinforced hydrogels [274], nano-composite hydrogels [275], double network hydrogels (DN) [276], and interpenetrating polymer network [277].

IUPAC defined an Interpenetrating Polymer Network (IPN) as "*A polymer comprising two or more networks which are at least partially interlaced on a molecular scale but not covalently bonded to each other and cannot be separated unless chemical bonds are broken*", while *"A polymer comprising one or more polymer networks and one or more linear or branched*

polymers characterized by the penetration on a molecular scale of at least one of the networks by at least some of the linear or branched chains" is referred to a Semi IPN.

The reason for the development of these structures is to combine the favourable properties of each constituent polymer within well designed and tailored hydrogel and/or to modulate the mechanical and biological properties of each constituent polymer, suitable for biomedical applications.

It is very important to have a compromise between mechanical strength and flexibility in order to properly use these materials. Another property is the elasticity of the hydrogel, this is very important to give flexibility to the cross-linked chains, and also to facilitate the movement of incorporated bioactive agent.

I.5. Structure and proprieties of poly(hydroxyethyl methacrylate)

(2-hydroxyethyl) methacrylate (HEMA) is an hydrosoluble monomer, which can polymerize even at low temperatures (starting from -20 °C) and form one of the most used synthetic polymer in biomedical applications poly(hydroxyethyl methacrylate) (PHEMA) [67]. Polymer can be used to prepare various hydrogels, to immobilize proteins or cells.

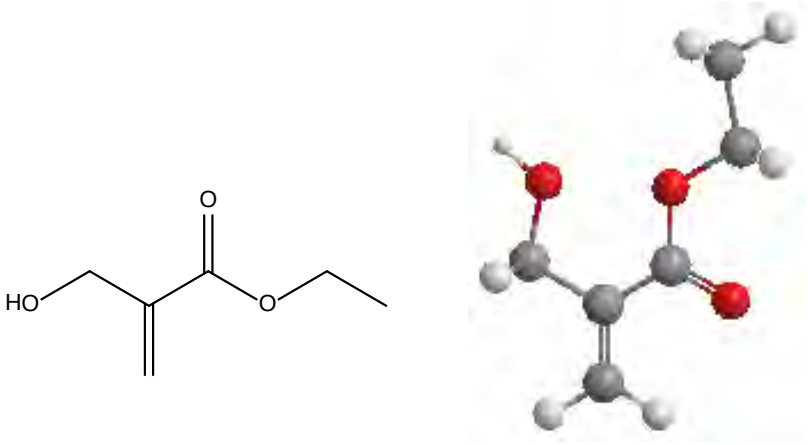

Figure I. 20: Linear and 3D model of (2-hydroxyethyl) methacrylate structure

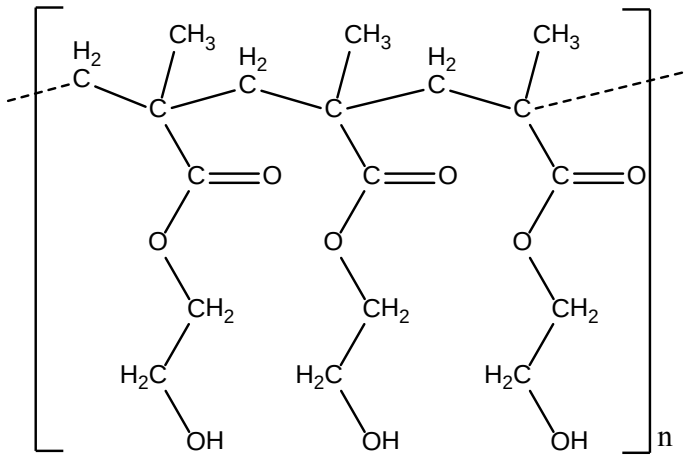

Figure I. 21: Linear model of poly(2-hydroxyethyl methacrylate) structure

Quite a variety of techniques are employed in forming polymer medical devices. The technique depends on several factors such as whether the material is thermosetting or thermoplastic, and if thermoplastic, the temperature at which it softens. Thermosetting polymers must be prepared as a liquid linear polymer and then cured in a mold. They cannot be molded after this step. Thermoplastic polymers can be molded repeatedly (by compression, injection, extrusion, etc.), cast, and formed into fibers or films by extrusion followed by drawing or rolling to improve properties such as strength. Precipitation after being dissolved in a solvent by introduction of a nonsolvent is a way to form porous polymer scaffolds for tissue engineering. Large pores suitable for cellular infiltration can be created by adding particulates with the desired pore size to the polymer/solvent mixtures. Pores are created when the particulates are washed out after solvent removal.

These issues are strong arguments for the existence of a large number of researches on the monomer, homopolymer and copolymer.

Although the first synthesis of HEMA and corresponding to the homopolymer PHEMA was made from 1936, until 1955 Wichterle and Lim identifies exceptional optical qualities of the polymer, and in 1961 Wichterle discovers a method of obtaining the PHEMA lens. PHEMA and its copolymers have many applications: as material for immobilization of cells and enzymes of medicines, contact lenses and ophthalmic many applications in dentistry, such as implants and hemocompatibile materials in tissue engineering.

PHEMA is used in many orthopedic applications because it is biocompatible and has a hardness comparable to bone mass when it is in the dried state.

HEMA is a commercial product with a relatively low cost. May be synthesized by transesterification of MMA and ethylene glycol, which results in the formation of ethylene

glycol dimethacrylate (EDMA), but is also obtained and a rate of hydrolysis of methacrylic acid HEMA.

Many applications require pure HEMA, so purification of the monomer based on the water solubility or insolubility in diethyl ether and petroleum ether or hexane (EDMA is soluble in hexane).
HEMA can be polymerized by free radical initiation as well as derivatives of methacrylic acid. Anionic initiators are used to make isotactic PHEMA. The radical polymerization is very exothermic and may be carried out in an environment that retains the heat of reaction. We studied the polymerization of HEMA containing small amounts of methacrylic acid and EDMA. For example, using benzoyl peroxide as a polymerization initiator was made HEMA block. HEMA polymerization was further carried out with the redox system (ammonium persulfate and sodium metabisulfite) to give a hydrogel.

PHEMA hydrophilic gel formation was achieved by polymerization of HEMA in organic solvents with very low concentrations of EDMA in the presence of AIBN as initiator. There have been numerous studies on the physical properties of PHEMA. Since we are interested in biomedical applications PHEMA crosslinked been studied less soluble PHEMA which is obtained from pure HEMA or PHEMA containing a small percentage of EDMA. Crosslinked polymers are insoluble in water but is soluble in dimethylsulfoxide, dimethylformamide, alcohols, and diethylene glycol.

Crosslinked polymers swell in water but swells more polar organic solvents, such as alcohol or ethylene glycol. In order to remove residual monomers and oligomers of PHEMA gels, they are washed with distilled water.

Chapter II - Preparation, physico-chemical and mechanical assessments of the biopolymer based structures

II.1 Microparticles preparation

Micro- and nanoparticles have gained great research interest in the field of drug delivery due to their ability to deliver many types of drugs to targeted areas of the body for sustained periods of time. Also, nanoparticles and nanoformulations have already been applied as drug delivery systems with great success; and nanoparticulate drug delivery systems have still greater potential for many applications, including anti-tumour therapy, gene therapy, and AIDS therapy, radiotherapy, in the delivery of proteins, antibiotics, virostatics, vaccines and as vesicles to pass the blood - brain barrier [278].

Micro- and nanoparticles can be made from a number of synthetic and natural biodegradable polymers. Synthetic polymers used for micro- and nanoparticles preparation include poly (lactic acid) (PLA), poly (lactic-co-glycolic acid) (PLGA) whilst natural polymers include gelatin, chitosan, collagen, albumin, whey protein and silk fibroin.

Materials

For preparation of the microparticles poly(3-hydroxybutyrate-co-2%-3-hydroxyvalerate) (PHBV) was employed (structure is presented in Figure II. 1). The polymer powder was purchased from Goodfelow Ltd. UK and used without any purification. Polyvinyl alcohol (PVA) was provided by Acros Organics (MW 88.000 Da, 88 % hydrolyzed). Sodium dodecyl sulfate (DDS) ($CH_3(CH_2)_{11}OSO_3Na$) was provided by Alfa Aesar GmbH&Co KG, Germany and chloroform by Sigma-Aldrich.

Methods

Solution preparation

PHBV 5% (w/v) chloroform solution was prepared as follows: 1 g of PHBV powder was dissolved in 20 mL chloroform at 65 °C, under magnetical stirring and reflux until it was not observed any polymer particles.

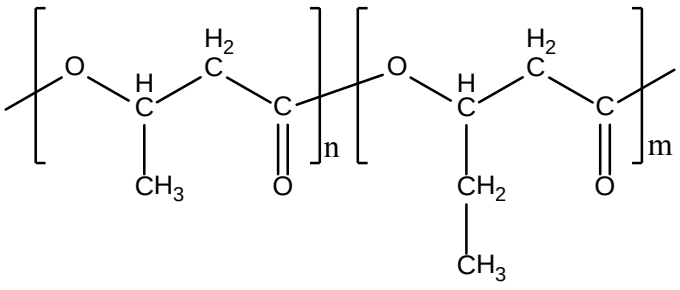

Figure II. 1: Chemical structure poly[*R*-3-hydroxybutyrate-*co*-*R*-3-hydroxyvalerate]

DDS 5% (w/v) water solution was prepared by dissolving 5 g of surfactant in 100 ml of distilled water under magnetical stirring.

PVA 3% water solution was prepared at 50 °C under magnetical stirring by mixing 3 g of PVA crystals in 100 ml of distilled water.

Microparticles preparation

The PHBV microparticles were prepared using an inverse oil-in-water (o/w) emulsion solvent evaporation technique. 10 mL of polymer solution was emulsified with 100 mL of DDS solution or PVA solution. The emulsion was put under mechanical stirring at 300 rpm for 2h or if needed until the hole solvent was evaporated. To complete the chloroform evaporation the mixture was heated at 50 °C. After that the surfactant solution containing formed microparticles was filtrated. The filtrate (microparticles) was washed with large amount of distilled water in order to rinse any surfactant. The resulting particles were collected into a glass vial and kept away from sunrise and air until characterization or further use. The preparation process of the microparticle is shown schematically in Figure II. 2.

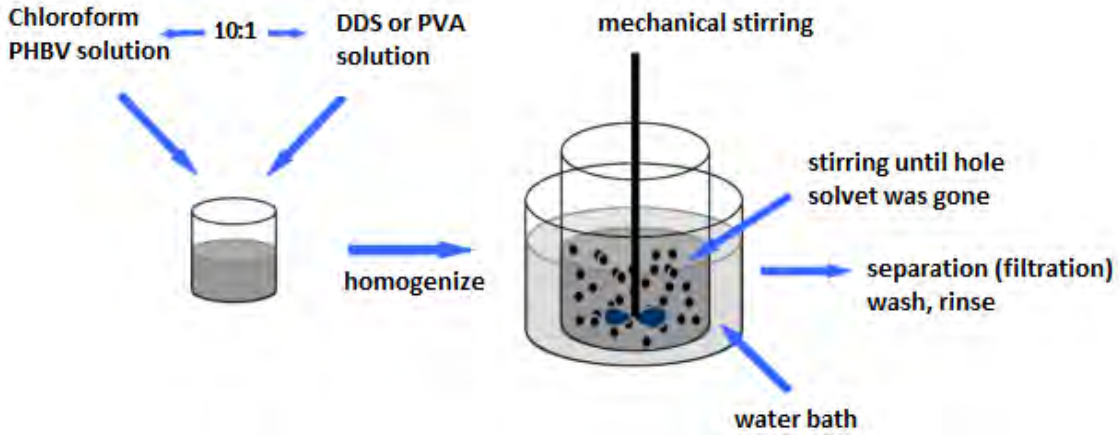

Figure II. 2: Schematically preparation of the microparticles

Optical microscopy (OM) analysis

Information of shape and size were collected by using an optical microscope BX 41 Olympus Live view digital SLR camera E-330 (7.5 Mpxl) with special software Quick Photo Micro 2.3 – capture of static or sequential images and video, morphometric functions, automatic analysis of 4 simultaneous images.

SEM analysis

Morphological information including shape and size of the PHBV particles were obtained through the scanning electron microscopy (SEM) analysis of the gold-coated samples. The analysis has been performed using a QUANTA INSPECT F SEM device equipped with a field emission gun (FEG) with a resolution of 1.2 nm.

Results

Analysis on OM and SEM images revealed that the obtained particles, with both surfactants presented a spherical shape and micrometric size. In OM images (Figure II. 3) it can be observed the polydispersity and for any specific application a sieving operation must be employed.

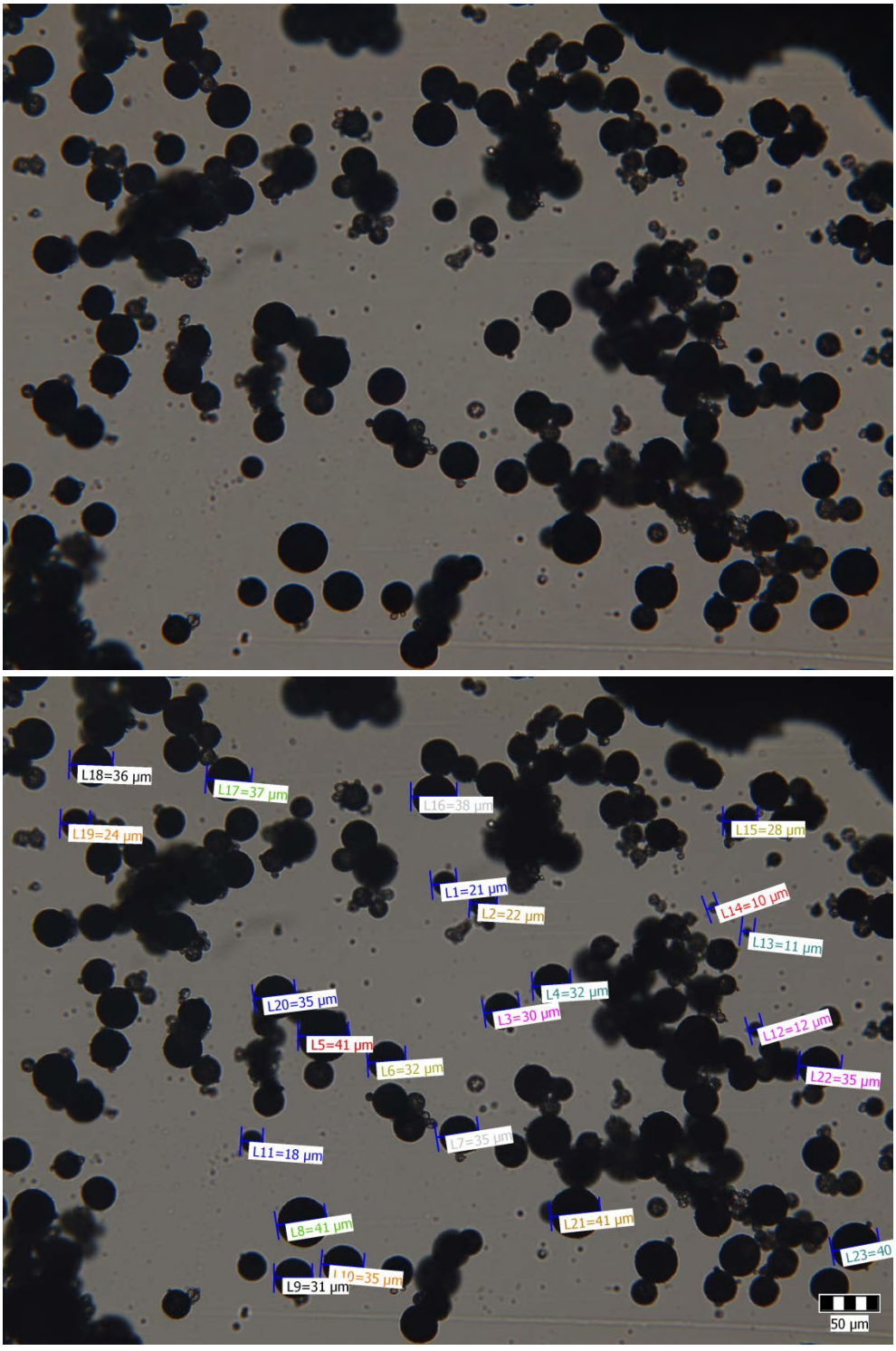

Figure II. 3: Optical images of PHBV microspheres

SEM images indicate that the obtained particle are empty inside (Figure II. 4) and the morphology of the external surface presents a nanoarchitecture (Figure II. 4).

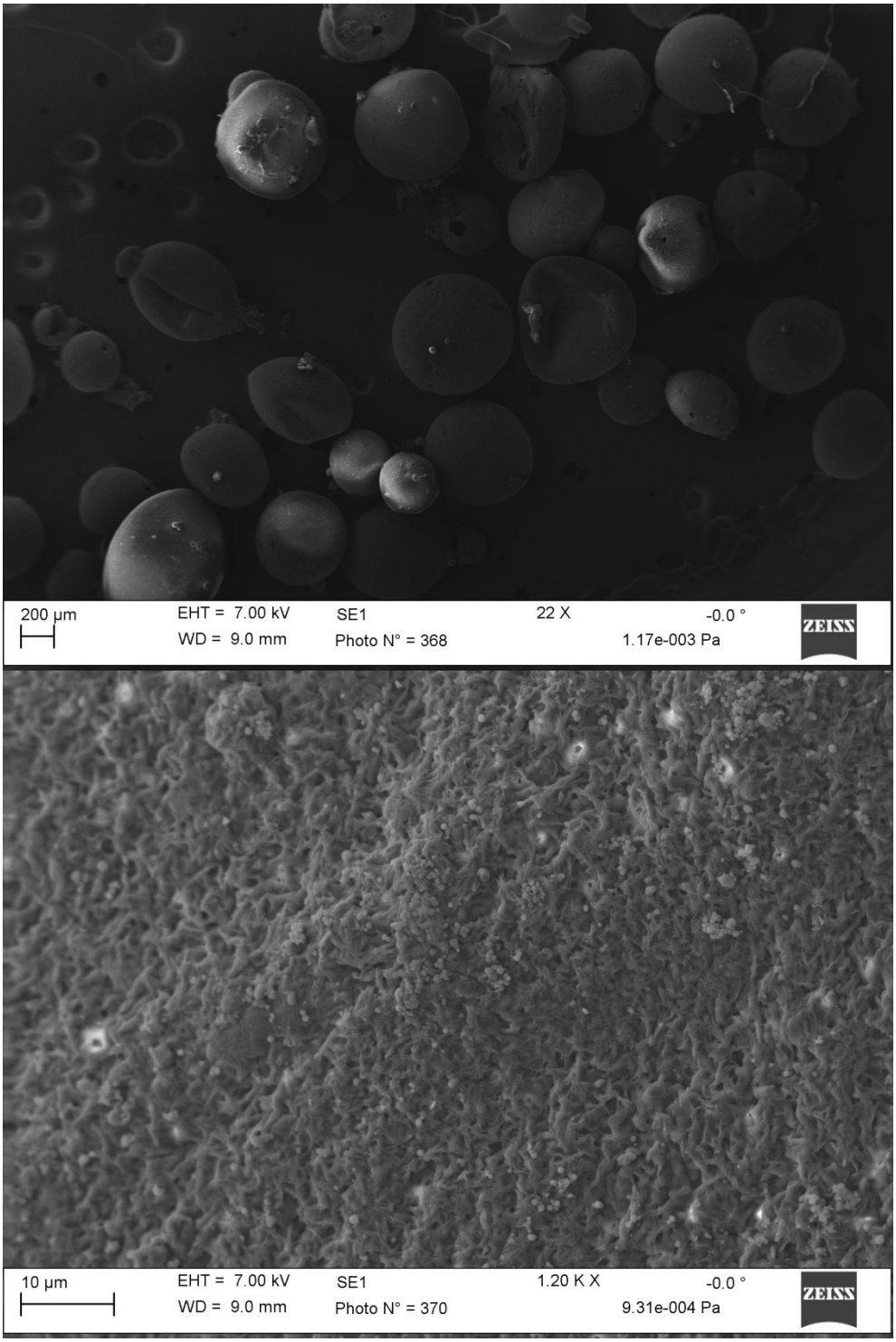

Figure II. 4: SEM images of PHBV particles: up image - general view; down image - detailed particle surface

Conclusions

PHBV microspheres can be obtained very easily in any size range by vary the concentration of the polymer solution concentration or/and stirring speed or/and surfactant solution concentration.

Obtained microparticles would be used as drug delivery system based on polymer biodegradability. For such an application there is an issue regarding the polymer solvent which is chloroform and the substance which must be delivered should dissolve in this or to form a surfactant-like solution to play the role of PVA or DDS.

If necessary a sieving operation can be employed in order to reduce polydispersity of the microspheres and to obtain a certain diameter size range.

II.2 Biodegradable polyhydroxyalkanoates based structures with medical applications

Natural materials exhibit a lower incidence of toxicity and inflammation as compared to synthetic materials; however, it is often expensive to produce or isolate natural materials. There is also variability between lots of natural materials, which makes it difficult to maintain consistency and sometimes prevents widespread commercial use. The isolation or purification steps typically involve the use of solvents to extract the desired component from the rest of the tissue or the use of solvents to remove the undesired components from the tissue and leave the desired natural material intact.

The realization of new biodegradable structures based on polyhydroxyalkanoates with applications in: bone pathology, biodegradable patches for tissues, surgical drains etc. seems to be a good idea due to their properties.

Polyhydroxyalkanoates (PHA) is the term given to a family of polyesters produced by microorganisms. The most well known among them is the thermoplastic poly[R-3-hydroxybutyrate] (P[3HB]). Microbial polyester is a crystalline thermoplastic with properties comparable to that of polypropylene [67]. They also present a very good biocompatibility and a well determined biodegradability.

Materials and methods

Poly(3-hydroxybutyrate) (PHB) in powder form was kindly supplied by **ICCF Bucuresti** and used without any purification. Chloroform and other chemicals were purchased from Sigma-Aldrich Company.

Films preparation

Polymer thin films were prepared by spin coating method to examine hydrophilicity and mineralization ability by biomimetic method. PHBV 5% (w/v) chloroform solution was prepared by dissolving 1 g of PHBV powder in 20 mL chloroform at 65 °C, under magnetical stirring and reflux for 2h.

Tubes preparation

Tubes from PHB were prepared by dry spinning of polymer solution using lab technique. A glass tube was attached to a mechanical stirrer. The stirrer was positioned perfectly horizontally and let spin. An appropriate amount, so that it do not leak, of polymer solution was introduced in the spinning tube and let spinning for 4 h. After the hole amount of solvent have been evaporated a PHB tube was formed into the glass tube. The polymeric tube was removed using distilled water and hydrofilic characteristic of the glass against the hydrofobic characteristic of the PHB material.

Differential scanning calorimetry analysis (DSC)

DSC measurements were performed on a TA Instruments DSC Q10, under a nitrogen atmosphere heating from 25 to 200 °C at 10 °C·min^{-1}. Two successive heating cycles were programmed into the analysis of each DSC sample.

In vitro test

In vitro tests were performed by two methods:

- The classical incubation method (biomimetic) in 1x and 1.25x synthetic body fluid (SBF) having the composition similar to that of human plasma, for 14 days at *p*H=7.42 and 37 °C, see Table II. 1.
- The incubation method based on alternating cycles in two solutions: $CaCl_2$ 200mM/Tris-HCl at *p*H=7.42 (Ca solution) and Na_2HPO_4 150mM (P solution).

The samples were weighed and then immersed in 25 ml Ca solution at 37 °C for 2 hours. After this procedure the samples were washed with distilled water and immersed in P solution at 37°C for 2 hours. This procedure was repeated three times.

Table II. 1: Synthetic body fluid (SBF) and human blood plasma compositions

Ion	SBF 1x (mM)	Human plasma (mM)
Na^+	142.19	142.0
K^+	4.85	5.0
Mg^{2+}	1.5	1.50
Ca^{2+}	2.49	2.5
Cl^-	141.54	103.0
$\mathbf{HCO_3^-}$	4.2	27.0
$\mathbf{HPO_4^{2-}}$	0.9	1.0
$\mathbf{SO_4^{2-}}$	0.5	0.5

SEM analysis

SEM analysis of the morphology of the films was achieved with an electronic microscope SMPE XL 30 Philips.

Contact Angle Measurement

KSV CAM 200 apparatus was used for static contact angle measurements performed on dried films. Ultrapure water droplets were used with a drop volume of 20 µl. The measurement of each contact angle was made within 10 s after each drop to ensure that the droplet did not soak into the compact. The contact angles reported were the mean of 10 determinations. Smaller contact angles correspond to increased wettability.

Results

Contact angle

The contact angle measurements were assessed by pure distilled water and ethylene glycol. The mean value of contact angle was: for water θ_1=91.82 and for ethylene glycol θ_2=50.99.

Based on the values above and Young-Dupré-Fowkes equations (II.1) there were calculated the free energies: γ_S^P=0,42 mN/m; γ_S^D=42,9 mN/m.

$$\begin{aligned} \gamma_{L_1} + \gamma_{L_1}\cos\theta_1 &= 2(\sqrt{\gamma_s^D \gamma_{L_1}^D} + \sqrt{\gamma_s^P \gamma_{L_1}^P}) \\ \gamma_{L_2} + \gamma_{L_2}\cos\theta_2 &= 2(\sqrt{\gamma_s^D \gamma_{L_2}^D} + \sqrt{\gamma_s^P \gamma_{L_2}^P}) \end{aligned} \quad \text{(II.1)}$$

The DSC curve was assessed on samples and the result is presented in Figure II. 5.

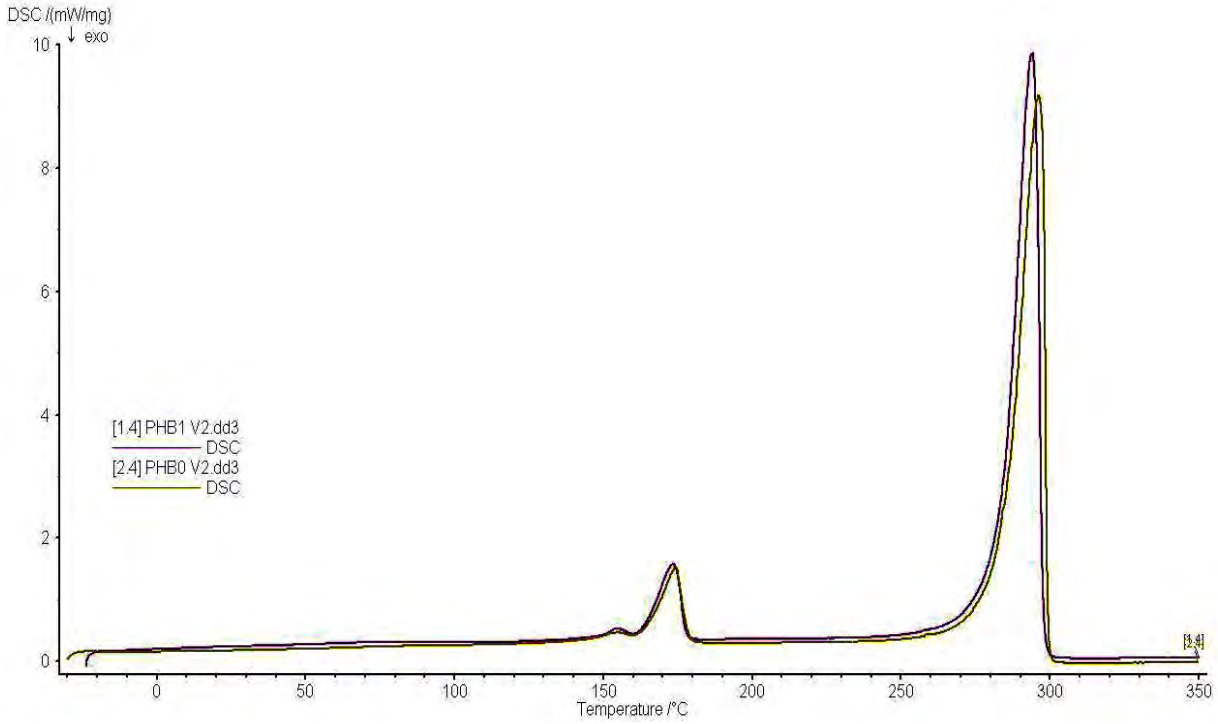

Figure II. 5: DSC curve for PHB

SEM assessment on mineralized PHB films was performed in order to observe any mineral crystalline form deposit. As can be observed in microphotographs shown in Figure II. 6 the amount of mineral deposit is emphasized and is very poor, because of strongly hydrofobic character of the PHB film.

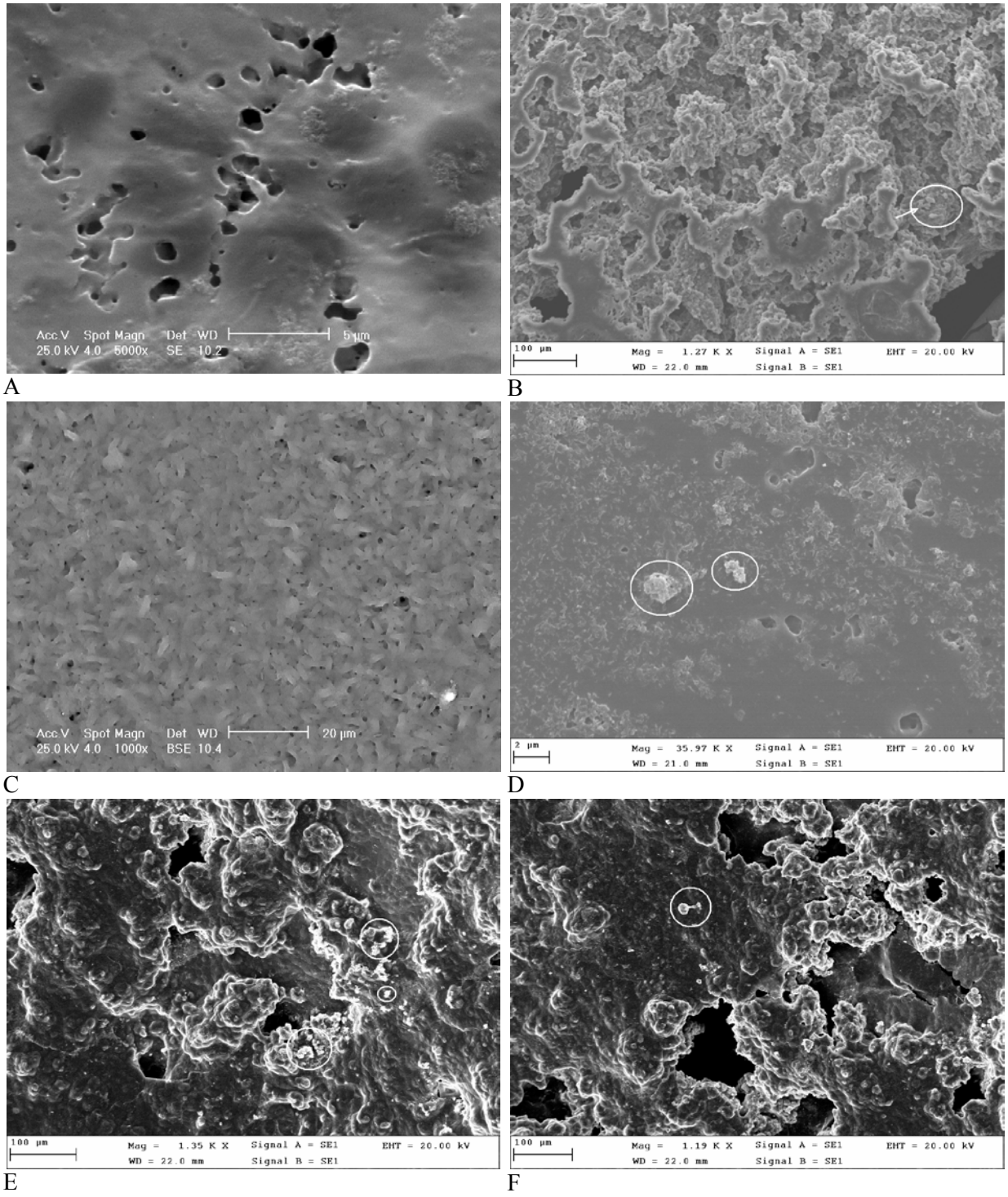

Figure II. 6: SEM images: A, B - porous film of PHB-Taguchi; C - compact film of PHB-Taguchi; D - compact film of PHB-Taguchi; E, F - porous film of PHB-Kokubo

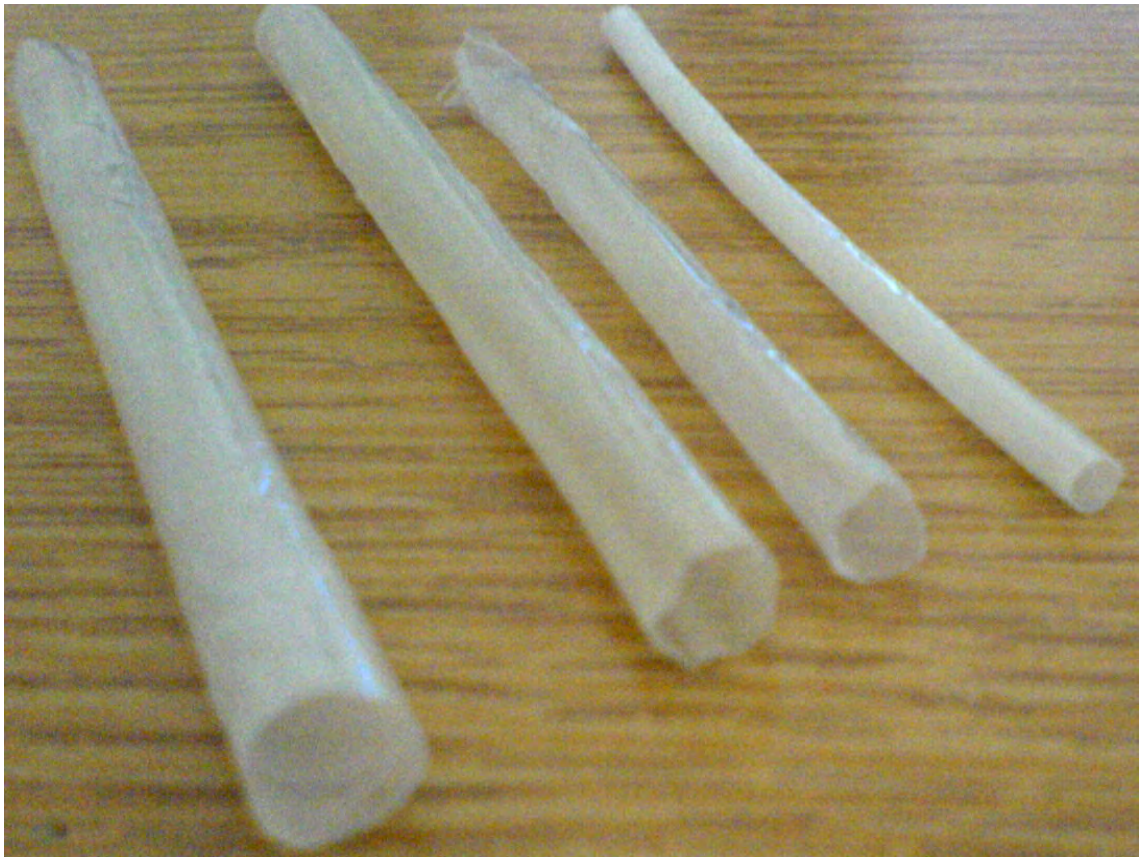

Figure II. 7: Image of four different diameter PHB tubes obtained by dry spinning method

Conclusion:

The obtained PHB films were studied as potential scaffolds for bone reconstruction implants. The mineralization results (using SEM images) have shown a poor amount of mineral deposit on PHB films surface.

We investigated and set up a laboratory technique for the manufacture of PHB tubes. Further studies, in cooperation with Emergency Floreasca Hospital will be necessary to establish if this tubes can be used successfully as surgical drains in Romanian hospitals.

II.3 Functionalization of natural polyester films by low-pressure oxygen plasma discharge and their medical uses

Plasma treatment is very important for biomaterials to enhance their biocompatibility and adhesion properties. The surface of the plasma-treated polymers can be designed to become more or less wettable to satisfy a variety of biomedical applications. In this respect, poly[(3-

hydroxybutyric acid)-co-(3-hydroxyvaleric acid)] (PBHV) films were subjected to low-pressure oxygen plasma treatment in different conditions of power, pressure and time. The polyester film surfaces were then characterized by FTIR-ATR and XPS spectroscopy to confirm the functionalization. Contact angle measurements were also performed and surface free energies were computed by Young-Dupré and Fowkes equations.

Functionalization of polyesters by oxygen plasma treatment leads to increased wettability and better properties for biomedical applications

The present study focuses on the functionalization of the surface of natural poly[(3-hydroxybutyric acid)-co-(3-hydroxyvaleric acid)] (PHBV) films by low-pressure oxygen plasma treatment in various conditions of power, pressure and time

Materials

PHBV films were prepared by casting from chloroform solution (5% w/v) and then dried a room temperature to allow solvent evaporation. The obtained film thickness was between 40-50 µm.

Low-pressure oxygen plasma treatment conditions were: pressure 0.5 mbar, power 75W, time of treatment 1, 10 and 30 minutes.

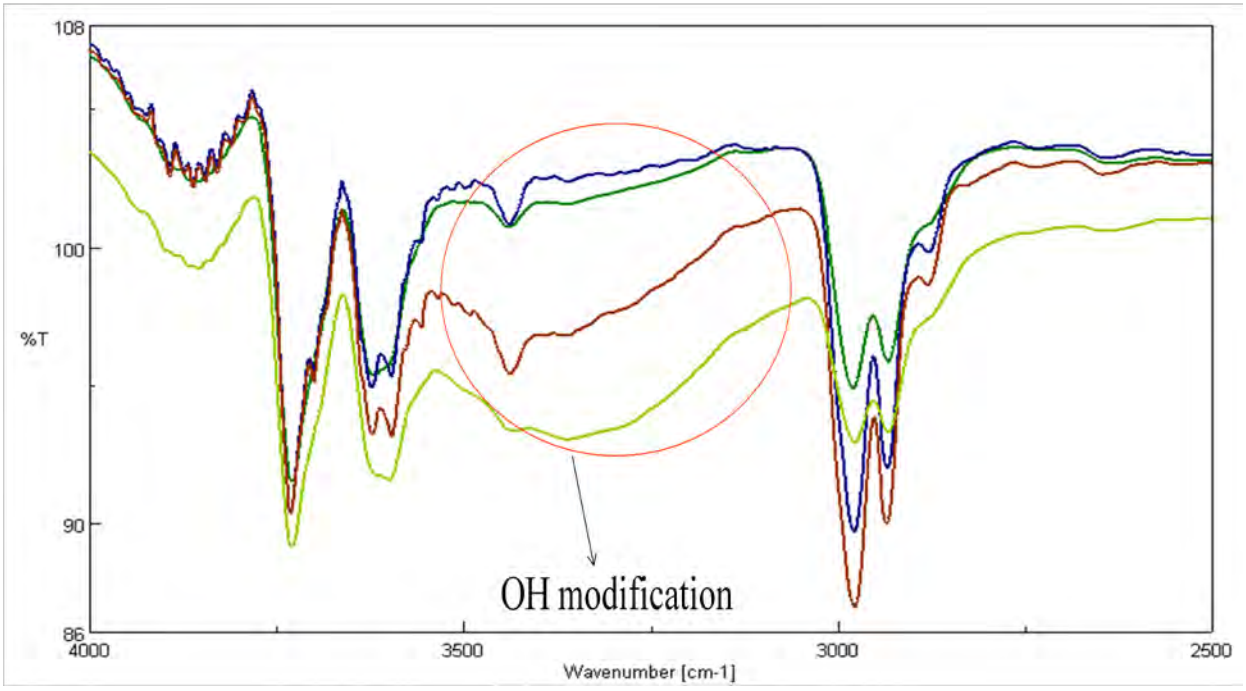

Figure II. 8: FTIR-ATR spectra of PHBV films functionalized by plasma treatment: dark green-blind; blue-1 min; brown-10 min; light green-30 min)

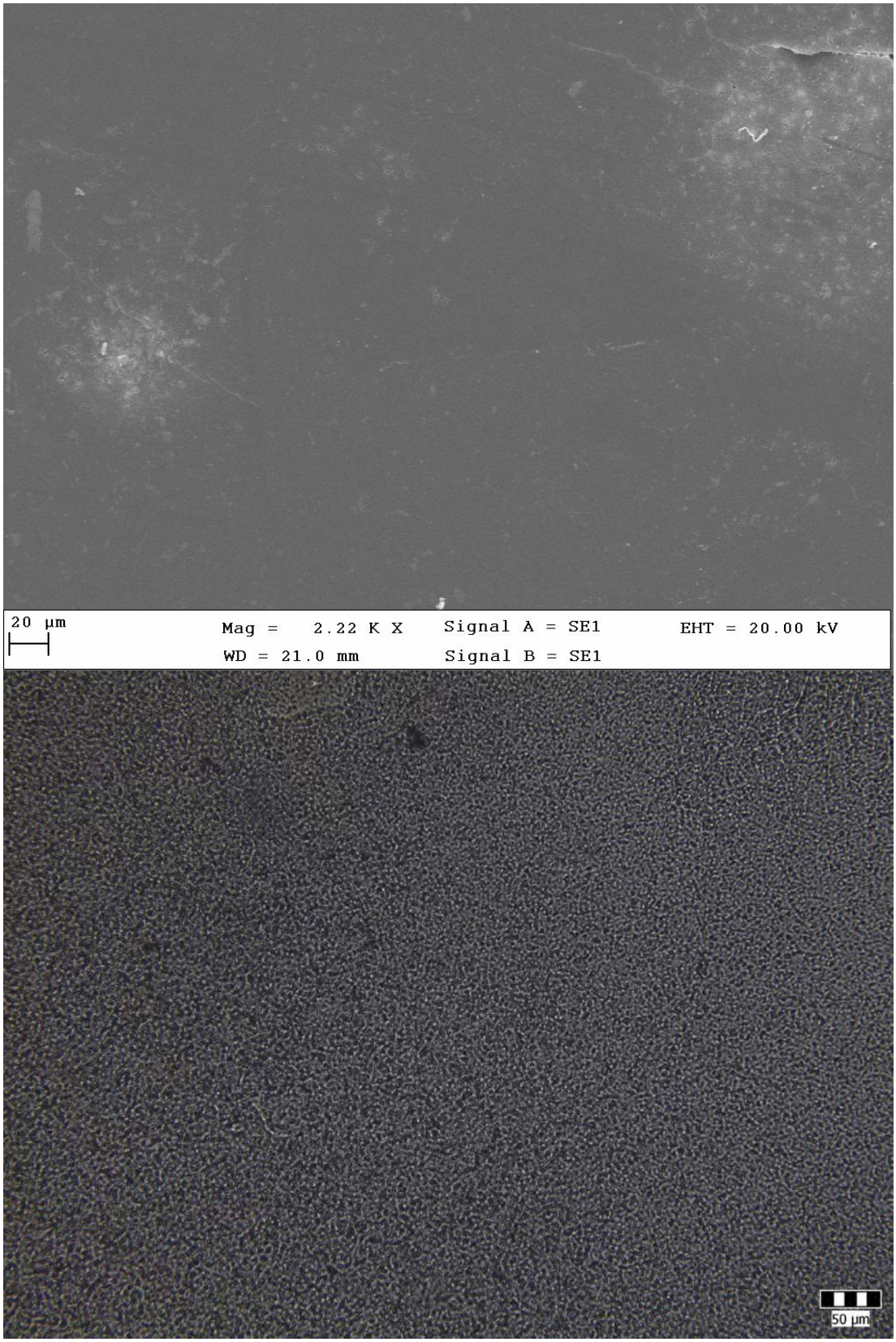

Figure II. 9: SEM microphotograph and optical microscopy image (20x objective) of PHBV films

Contact angle and free surface energy for polyester films

Young-Dupré-Fowkes equations:

$$\gamma_{L_1} + \gamma_{L_1} \cos\theta_1 = 2(\sqrt{\gamma_s^D \gamma_{L_1}^D} + \sqrt{\gamma_s^P \gamma_{L_1}^P})$$

$$\gamma_{L_2} + \gamma_{L_2} \cos\theta_2 = 2(\sqrt{\gamma_s^D \gamma_{L_2}^D} + \sqrt{\gamma_s^P \gamma_{L_2}^P})$$

Table II. 2: Summarize of all data computed based on contact angle measurements and Young-Dupré-Fowkes equations: γ_s – free surface energy; X_{sp} – polarity; W_{sp} – mechanical work of adhesion ; γ_{sl} – solid-liquid free energy; F – Good parameter and θ – *contact angle*

						θ, degree	
Oxidation time, min	**γ_s, mN/m**	**X_{sp}**	**W_a, mN/m**	**γ_{sl}, mN/m**	**F**	water	methylene iodide
0	37.18	0.018	44.73	65.45	0.429	112.78	45.98
1	58.91	0.358	123.29	8.62	0.940	46.45	43.48
10	64.53	0.310	126.49	7.61	0.921	42.87	29.29
30	70.41	0.489	140.10	-2.57	0.977	23.18	47.00

Conclusions

A preliminary study allowed the determination of the experimental procedure of plasma treatment leading to the best wettability of the polymer film surface.

The values of the contact angles increase with the storage time and the value of the free surface energy decrease with the same storage time. Nevertheless, they do not equalize the initial values before treatment, even not after 3 months.

This study offer an excellent possibility of functionalization of PHAs films by low pressure plasma treatment and our studies are now oriented towards biocompatibility and biodegradability, which are two important properties of these copolymers.

II.4 Biodegradables blends of poly(3-hydroxybutyrate) with natural fibers[16]

The new researches are focused on producing of biodegradable plastics/materials. Poly-3-hydroxybutyrate (PHB) is 100% biodegradable (after a few weeks in soil and other environments) and can be produced from renewable resources. PHB is highly crystalline, brittle and the price is very high. To reduce the quantities of polymeric material required, incorporating filler or fibers with biopolymers is an effective method of reducing effective end-product costs. The biopolymeric matrix is also ecofriendly.

In recent years, the use of natural fibers as filler in the manufacture of fiber-biopolymers composites has been of great interest to many researchers. Natural fibers are biodegradable and so can be suitably blended with PHB without losing their biodegradable properties. PHB biocomposites with wood fiber, flax, recycled cellulose fiber, pineapple fiber and other natural fibers have been reported. These fibers have many advantages, such as low density, high specific strength and modulus, ease of fiber surface modification and wide availability. The main disadvantages of natural fibers in blends are the lower processing temperatures allowable, incompatibility between hydrophilic natural fibers and hydrophobic polymers and potential moisture absorption of the fibers. This also leads to a weak interfacial bonding with the polymer matrix leading to the segregation of the two materials during polymerisation, affecting the mechanical properties.

The leak of interfacial interactions leads to porosity, internal strains and environment degradation. Therefore, modification of the fiber and/or polymer matrix is a main area for obtaining good composite properties. Evidences showed tensile and flexural strength were increased by improving interfacial adhesion through fiber surfaces modification, fiber surfaces treatment by plasticizer and silane. The modification of wood fiber surfaces has been the subject of a number of reviews and texts. In order to improve the affinity and adhesion between wood fibers and thermoplastic matrices in production, chemical coupling agents have been employed. Coupling agents are substances that are used in small quantities to treat a surface so that bonding occurs between it and other surfaces, e.g., wood and thermoplastics.

[16] M. Rapa, E. Grosu, **C. Degeratu**, A. Scheau, C. Stanescu, *Biodegradable Blends Prepared from Poly(3-hydroxybutyrate) and Wood/Cellulose Fibers,* Materiale Plastice 47 (4), pp. 503-508, 2010

Coupling agents in wood fiber composite normally have bi- or multifunctional groups in their molecular structure.

These functional groups, such as urethane structure (-N=C=O) of isocyanates, [-(CO)2O-] of maleic anhydrides (MA), respectively succinic anhydrides (SA) and (Cl-) of dichlorotriazine derivatives, interact with the polar groups [mainly hydroxyl groups (-OH)] of cellulose and lignin to form covalent or hydrogen bonding.

Anhydrides such as MA and SA are popular coupling agents in wood fiber composite. SA and PHB have two functional groups, i.e., carboxylate groups (-COO-), which can link wood fiber through sterification or hydrogen bonding. But MA is an α, β-unsaturated carbonyl compound, containing one carbon-carbon double bond (C=C) and two carboxylate groups (-COO-). This conjugated structure greatly increases the graft reactivity of the carbon-carbon double bond on the heterocyclic ring with the polymer matrix through the conjugate addition under a radical initiator resulting in crosslinking or strong adhesion at the interface. However the molecular chain of MA is much shorter than that of PHB matrix and wood fibers.

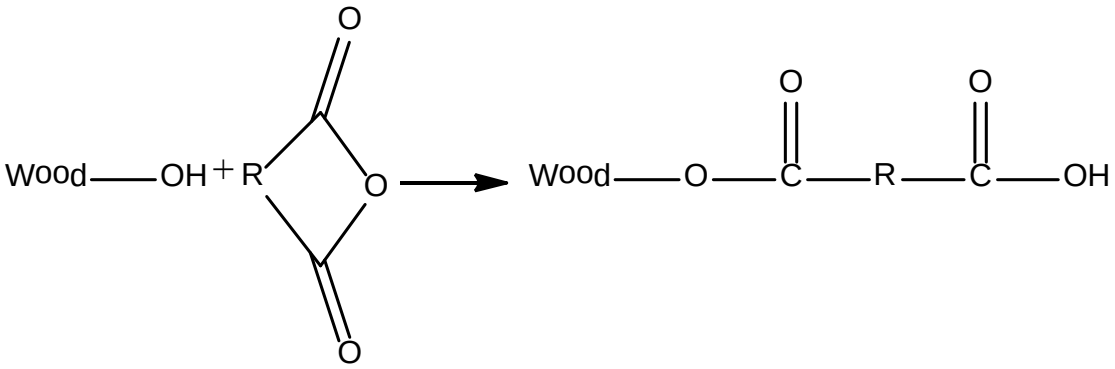

Figure II. 10: Esterification reactions for wood fiber reacted with maleic anhydride (R = HC=CH) or succinic anhydride (R = CH_2– CH_2–)

The esterification reactions of MA and SA with wood are shown in Figure II. 10. The hydroxyl groups of wood are most often the reactive sites. The MA-modified natural fiber showed much lower reactivity than the natural fiber SA modified. This was probably due to the higher activation energy for reaction of MA compared to SA.

The aims of this section was to obtain blends based on PHB and wood/cellulose fibers and to determine the effect of filler type on mechanical, thermal and rheological characteristics of each formulations performed. Improving compatibility between fiber and PHB was studied using coupling agents like maleic anhydride (MA) and succinic anhydride (SA). The effect of fiber content on properties of blends was also studied.

Experimental part

Materials

Poly(3-hydroxybutyrate)(PHB), type P226 was used as the polymer matrix. The material has a density of 1.17 g/cm3 and melting point of 173 °C. Prior blending, PHB was dried in the oven at 80 °C, for 2 h.

Cellulose fibers, type EFC 1000, were supplied by CARTIF, Spain. The properties of the fibers are: water content = 4.5 ± 0.1(%); wax = 0.9 %; lignin = 28.7 ± 0.1%; holocellulose = 87.3 ± 1.3 %; free –OH content on the surface = 322 ± 14 mg KOH/g and aspect ratio = 6.7.

Wood fibers type LSL 200/150, were supplied by CARTIF, Spain. These show the following properties: water content = 8.7 ± 0.1 %; free –OH content on the surface = 230 ± 15 mg KOH/g and aspect ratio = 5.4. The fibers were used as the discontinuous phase in the mixtures. All fibers with sizes of 200 µm, were untreated. Coupling agents as maleic anhydride (MA) and succinic anhydride (SA)had both purity ≥ 99%. The fibers were treated with 7 % (weight) of MA, respectively SA. Prior to surface modified and blending, the fibers were dried in the oven for at least 4 h at 105 °C to ensure that moisture content was below 0.5 %. The fibers treated were then oven-dried at 105 °C for 6 h.

PHB and wood/cellulose fibers treated were initially weighed and melted according to the various fiber contents indicated in Table II. 3. The composition of each formulation is also shown.

Table II. 3: Composition of evaluated formulations (% vol.): *B = pure PHB; R = Cellulose Fiber; L = Wood Fiber; MA = maleic anhydride; SA = succinic anhydride*

Mixture	Formulation	Filler content, %	Resin content, %
PHB	B	0	100
PHB-Cellulose fiber 5%-MA	BRMA-5	5	94
PHB-Cellulose fiber 10%-MA	BRMA-10	10	89
PHB-Cellulose fiber 20%-MA	BRMA-20	20	79
PHB-Cellulose fiber 5%-SA	BRSA-5	5	94

PHB-Cellulose fiber 10%-SA	BRSA-10	10	89
PHB-Cellulose fiber 20%-SA	BRSA-20	20	79
PHB-Wood fiber 5%-MA	BLMA-5	5	94
PHB-Wood fiber 10%-MA	BLMA-10	10	89
PHB-Wood fiber 20%-MA	BLMA-20	20	79
PHB-Wood fiber 5%-SA	BLSA-5	5	94
PHB-Wood fiber 10%-SA	BLSA-10	10	89
PHB-Wood fiber 20%-SA	BLSA-20	20	79

Methods

The formulations were prepared using a BRABENDER Plastograph, under a mixing temperature of 180 °C for 10 min and a rotation speed of screws of 40/70 rpm.

Preparation of test specimens

After blending, the samples were pressed into thin plates by a laboratory press type POLYSTAT 200 at the following conditions: temperature: 160 °C, pressing time: 5 min and pressure of 200 bar. Plates with the thickness of 1 mm were obtained.

Conditioning

Prior to performing mechanical measurements, the specimens were conditioned at (50 ±5) % relative humidity for at least 40 h at (23 ±1) °C, in a humidity-controlled room type BTH80/-20 according to ISO 291.

Characterization

Blend morphology

Specimens were analyzed with optical microscope (BX 41 OLYMPUS Live view digital SLR camera E-330 with special software Quick Photo Micro 2.3). The micrographs of samples were taken at X20 magnification to identify the dispersion of fibers in polymer matrix.

Melting temperatures

Melting temperatures were determined using a differential scanning calorimeter (METTLER TOLEDO, DSC 823e). The sample sizes were approx. 5-7 mg, and the samples were sealed in 40µL aluminum crucibles. The measurement was done in a range from 20-200 °C with a 10 °C/min temperature rate.

Density

The density was calculated from the resulting volume (length x width x thickness) and the sample mass.

Tensile strength

Measurements of tensile strength were performed on a DINAMOMETER FP 10, according to ISO 527-3. A minimum of five samples was tested and the results were averaged. The tensile strength is the maximum load divided by the original cross sectional area. The specimens of the previous conditioned samples were used and the measurements were conducted at a 500 mm/min crosshead speed.

Contact angle measurements

Contact angle measurements were carried out at room temperature using the sessile drop technique, with the equipment type CAM 101 with a high-speed digital video camera type C200-HS KSV Finlanda to record the drop image. Water at room temperature was used for this purpose. Sessile drops were deposited using a Hamilton syringe of 5 µL directly on the surface films.

Results and discussion

Blend morphology

The micrographs of blends with different fibers volume percentage are shown in Figure II. 11. Morphology of the polymer blends plays an important role in the properties of the final product, especially their mechanical properties depend on it.

The results showed that the fillers were found to be well distributed in BRSA-5 (b), BRSA-10 (c), BRSA-20 (d), BRMA-10 (f), BRMA-20 (g), BLSA-5 (h), BLSA-10 (i), BLSA (j), BLMA-5 (k), BLMA-10 (l), BLMA-20 (m) blends. BRMA-5 (e) is evidence to see an uneven distribution of Retenmaier cellulose fibers because of poor melt homogeneity.

In PHB/Cellulose fibers blends, the maximum size of filler is 200 μm, whereas in the PHB/Wood fibers blends it became 130 μm.

a)

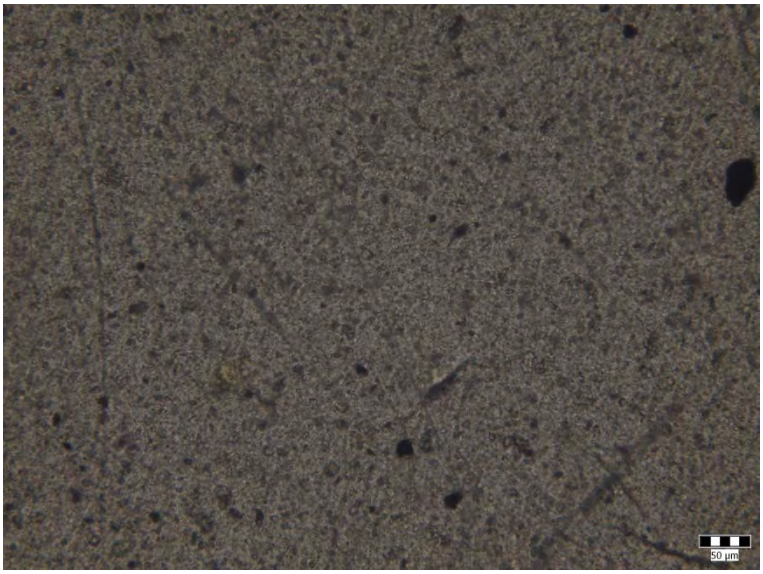

b)

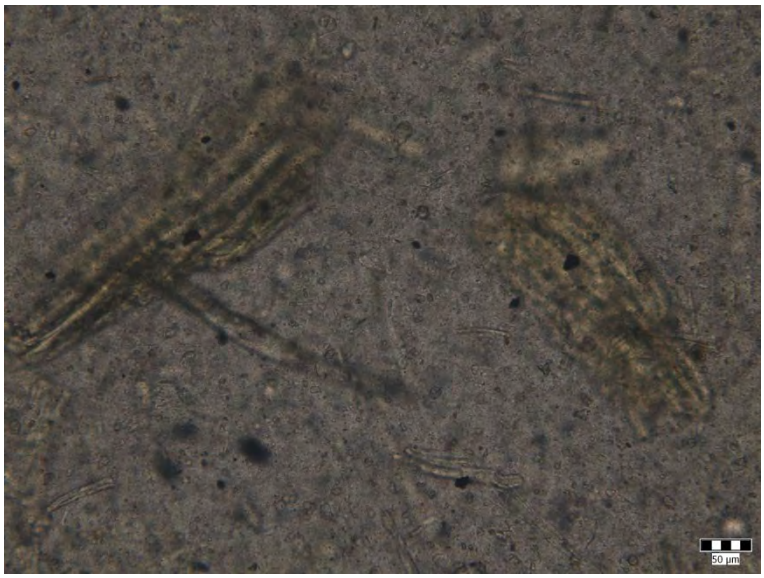

c)

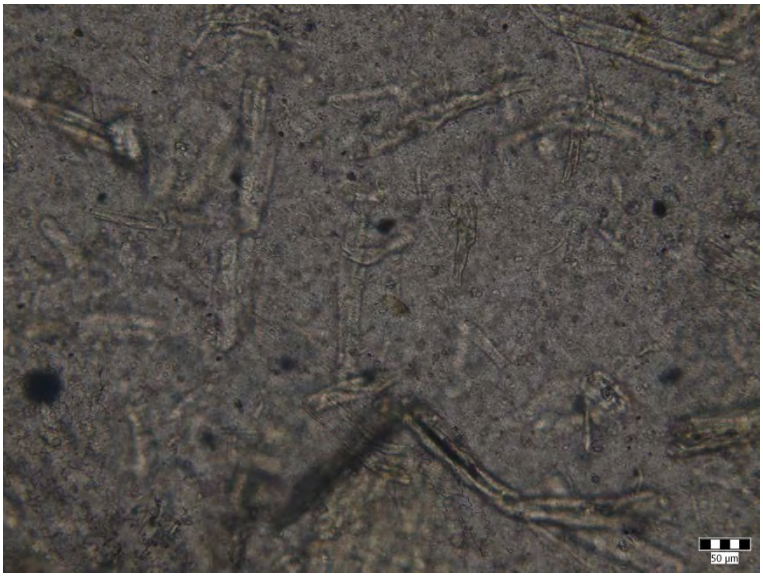

d)

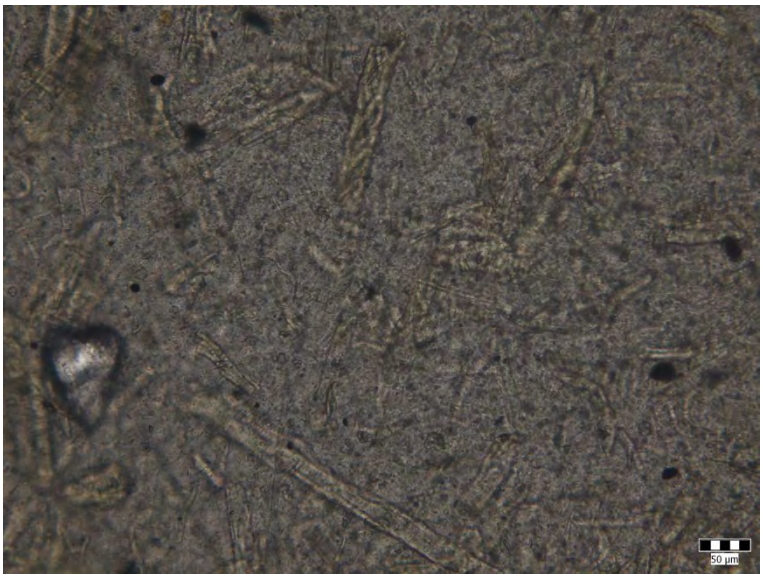

e)

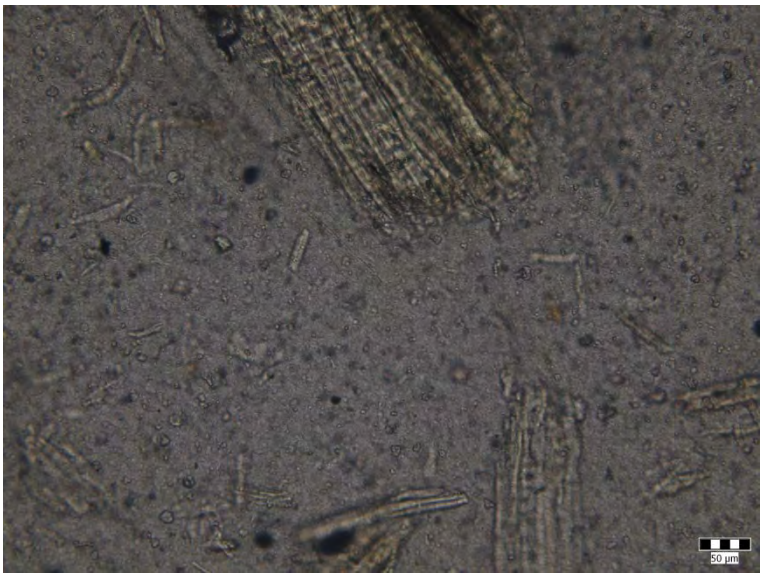

f)

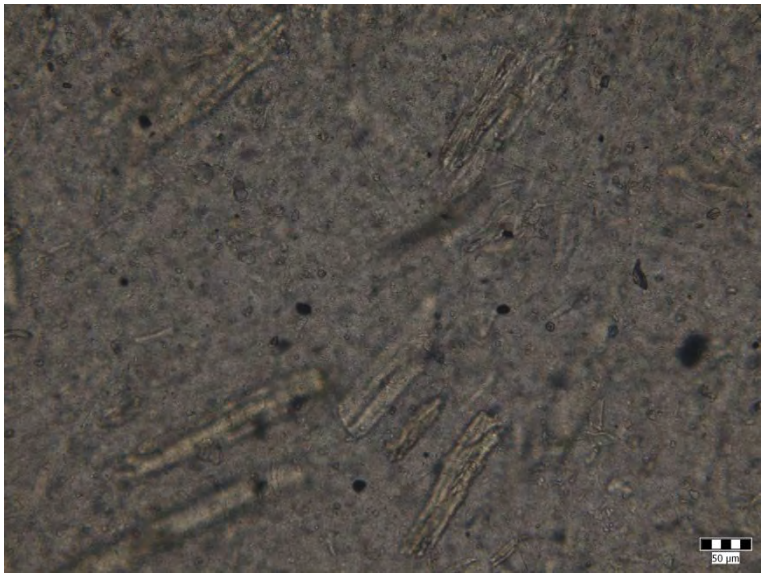

g)

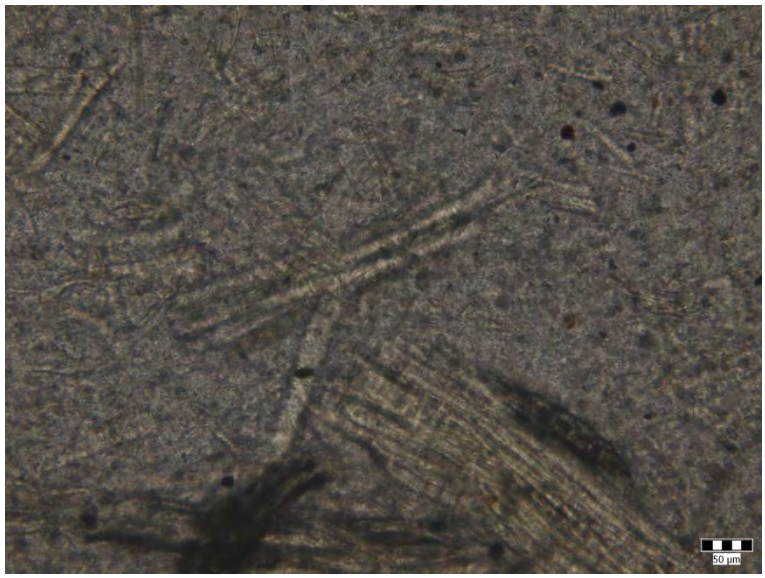

h)

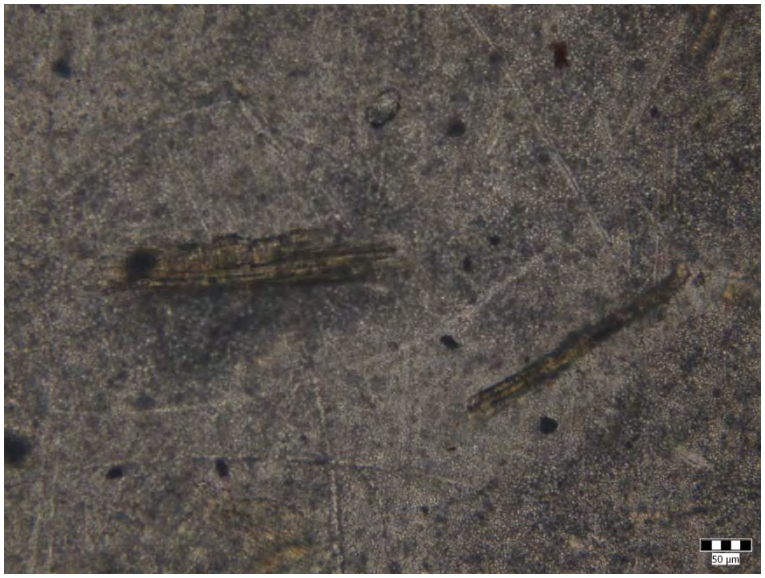

i)

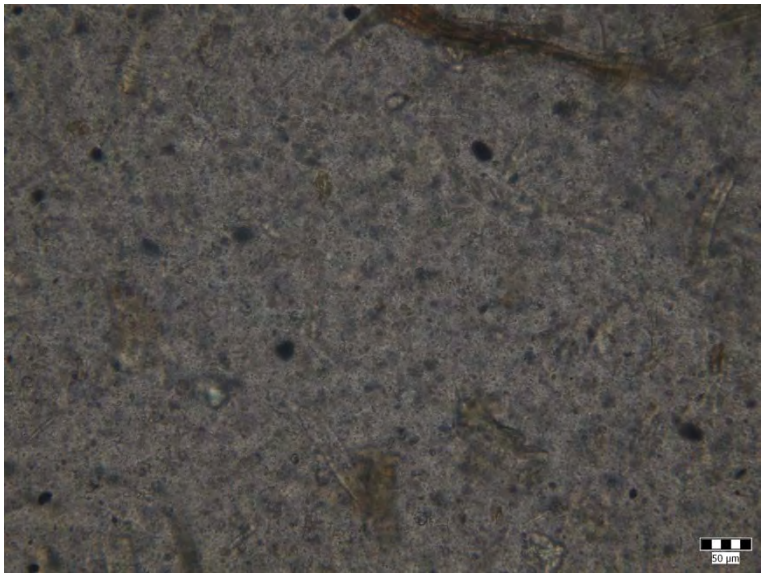

j)

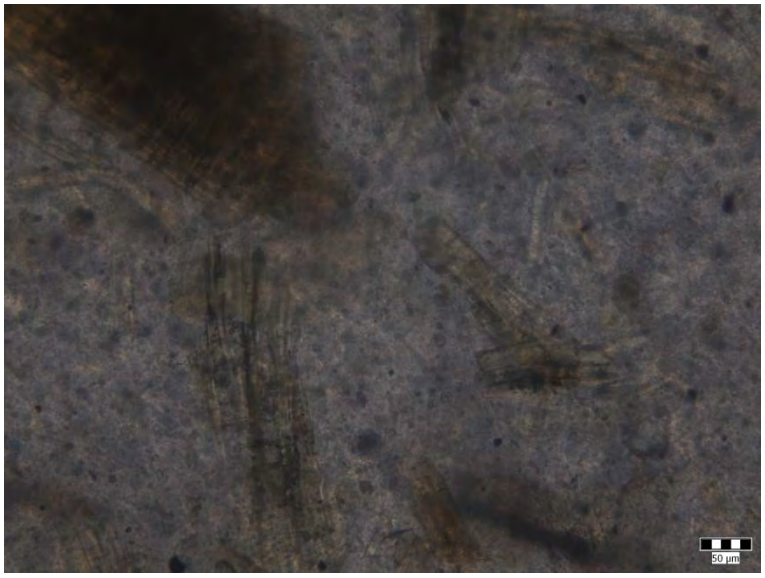

k)

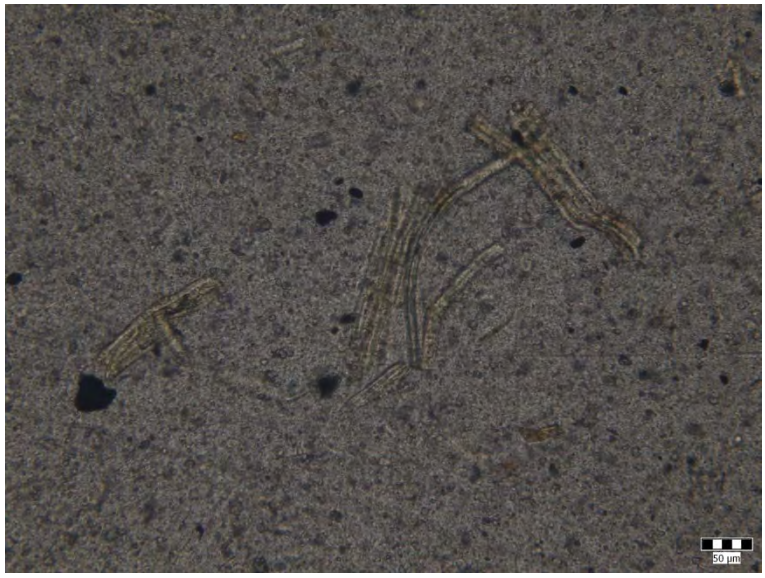

l)

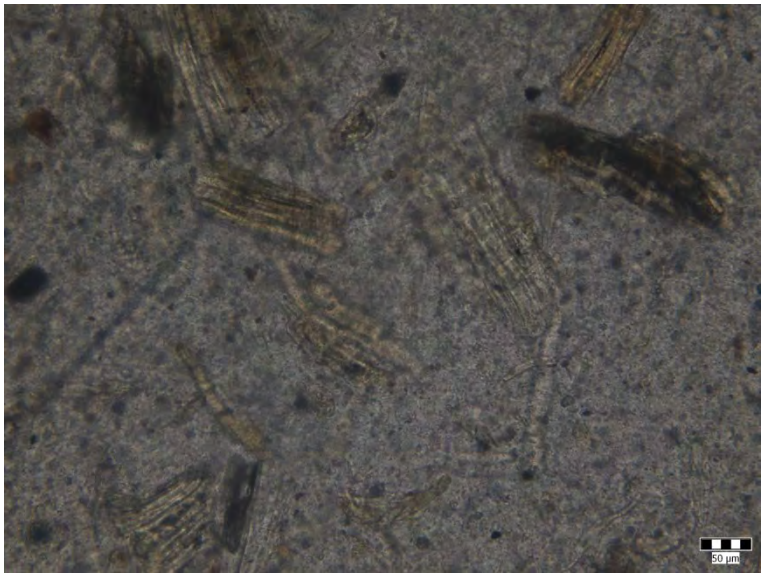

m)

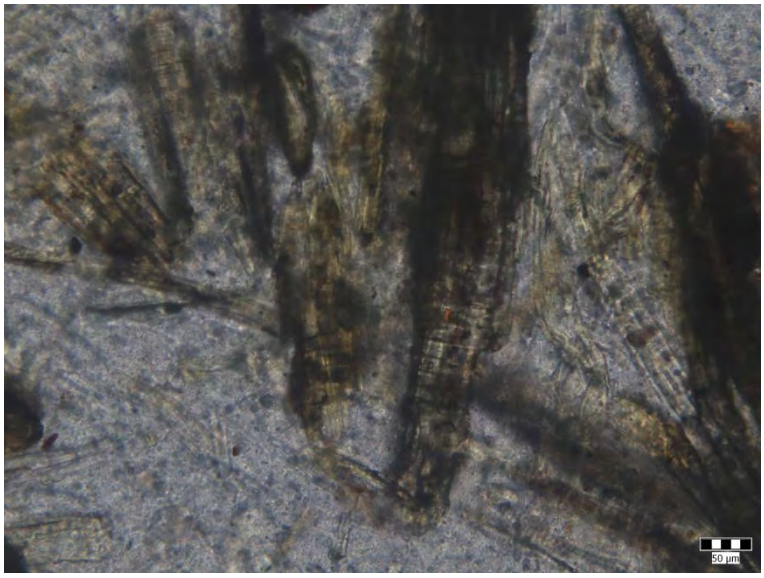

Figure II. 11: OM images on film: a)-PHB; b)-BRSA5; c)-BRSA10; d)-BRSA20; e)-BRMA5; f)-BRMA10; g)-BRMA20; h)-BLSA5; i)-BLSA10; j)-BLSA20; k)-BLMA5; l)-BLMA10; m)-BLMA20

Torque measurements

All the blends showed lower torque than PHB (sample code B). Torque value of blends decreased with increasing filler content and mixing time, and approached a stable value when the mixing time was greater than 8 min, suggesting that good mixing had occurred after this time. Initially, the torque responses of BLMA and BRMA blends were significantly lower than those of BLSA and BRSA blends at the same filler content (5, 10 and 20 %). Then, after 4 min, the improved rheological behavior of BLSA and BRSA blends is attributed to the conformational change of the wood fiber and cellulose fiber molecules caused by formation It was reported that the melt viscosity of treated wood fibers also decreased with increasing molecular weight of the ester group. Another possible cause is that wood fibers/cellulose fibers behave as filler within the molten PHB matrix.

The main contribution for the torque value is from the molten PHB. When the content of wood fibers and cellulose fibers increases, expansion and stretch of BLMA and BRMA matrices also increases, making movement of molten PHB easier at higher wood fibers contents, and resulting in the decrease in torque. Final torque decreased with increasing filler content for BLSA and BRSA blends because the viscosity of molten wood fiber/cellulose fiber is lower than that of molten PHB.

Measurement of melting temperature (Tm)

We found that for all blends performed, the BRSA blend shows the smallest Tm. For BRMA-5, BRMA-10, BLMA-5, BLMA-10, BLMA-20, BRSA-5, BRSA-10, BRSA-20, BLSA-10 and BLSA-20 blends, a decrease in the melting temperature (by about 1-5 °C) was observed with increasing filler content. This is due to the lower melt viscosity of wood fibers/cellulose fibers compared to that of PHB. These results were in accordance with the corresponding torque measurements, which showed that these blends had a lower melt torque than PHB.

The melting temperatures obtained by differential scanning calorimetry (DSC) for PHB/Wood fiber and PHB/Cellulose fiber blends at different fiber contents (0, 5, 10 and 20 %) are presented in Figure II. 12.

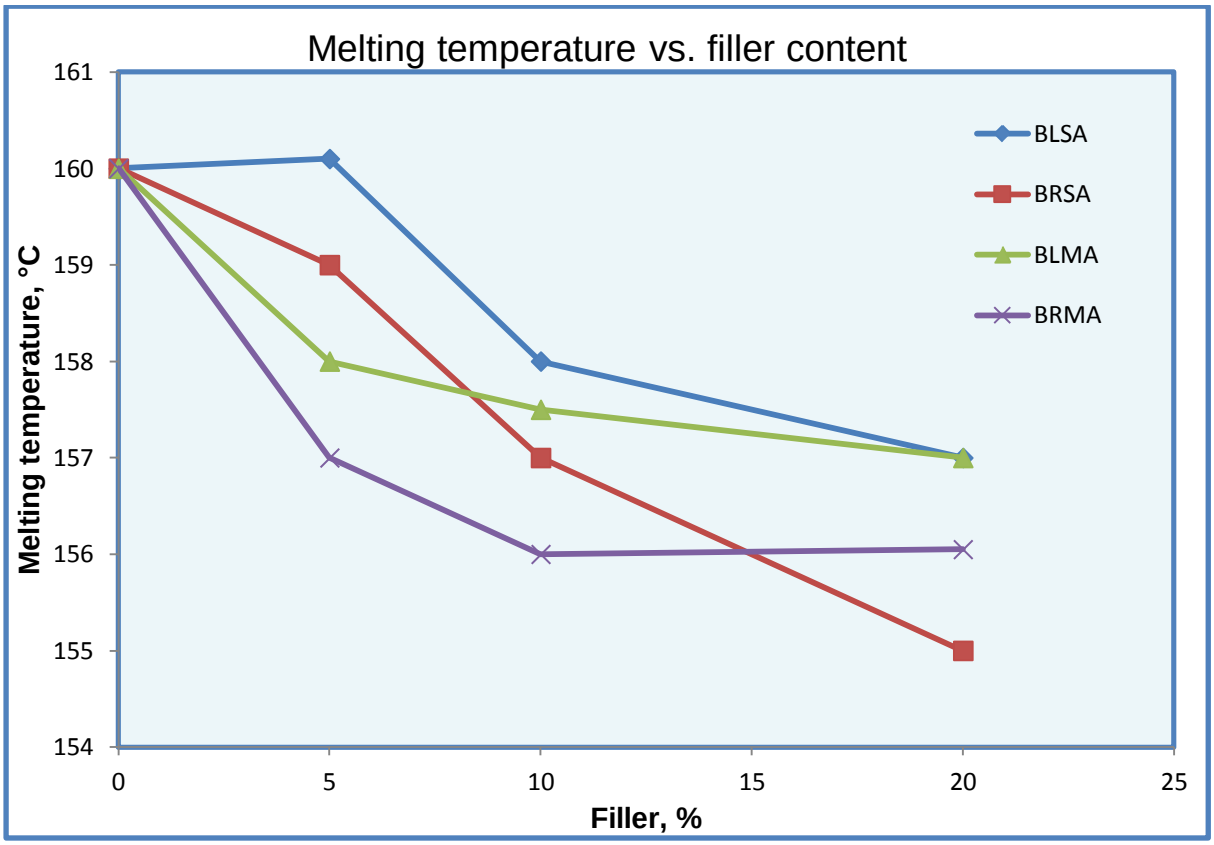

Figure II. 12: Graph showing temperature evolution with the percentage of filler content

Studying the behaviour of cellulose fibers blends with different coupling agents at melt is showing that the blends based on PHB, Rettenmeier fibers and SA present the lower melt temperature. This means that BRSA blends are processed more easily than BRMA blends. Also, between the blends based on PHB, wood fibers and different coupling agents, is no important difference of the melting temperature, only at 5% wood fiber content the BLMA mixture shows a decrease with 2 °C than BLSA-5 mixture. For BLSA-5 blend it is obvious the same Tm as pure PHB. This was probably caused by the hydrophilic character of wood fiber which would lead to poor adhesion with the hydrophobic PHB or homogeneity of fiber with matrix.

Therefore, difficulty in arranging the polymer chain, increases due to fibers prohibiting movement of the polymer segments. The researchers who studied the properties of wood fibers blended with polyethylene-octene elastomer, reported similar phenomena.

Densities of blends

The density values are important in order to know the weight of the blends to be produced as a design parameter. It is obvious that density for all blends performed increased with increased fiber content. The higher density is observed for BLSA and BRSA blends. BLMA and BRMA blends show a decrease in density than BRSA and BLSA blends, for the same fiber content. The effect of fiber content upon the densities for PHB/wood fiber and PHB/cellulose fiber blends is shown in Figure II.13.The increase in density of the PHB/fiber blends with the addition of fiber indicates a good dispersion of the polymer based matrix material within the wood fibers.

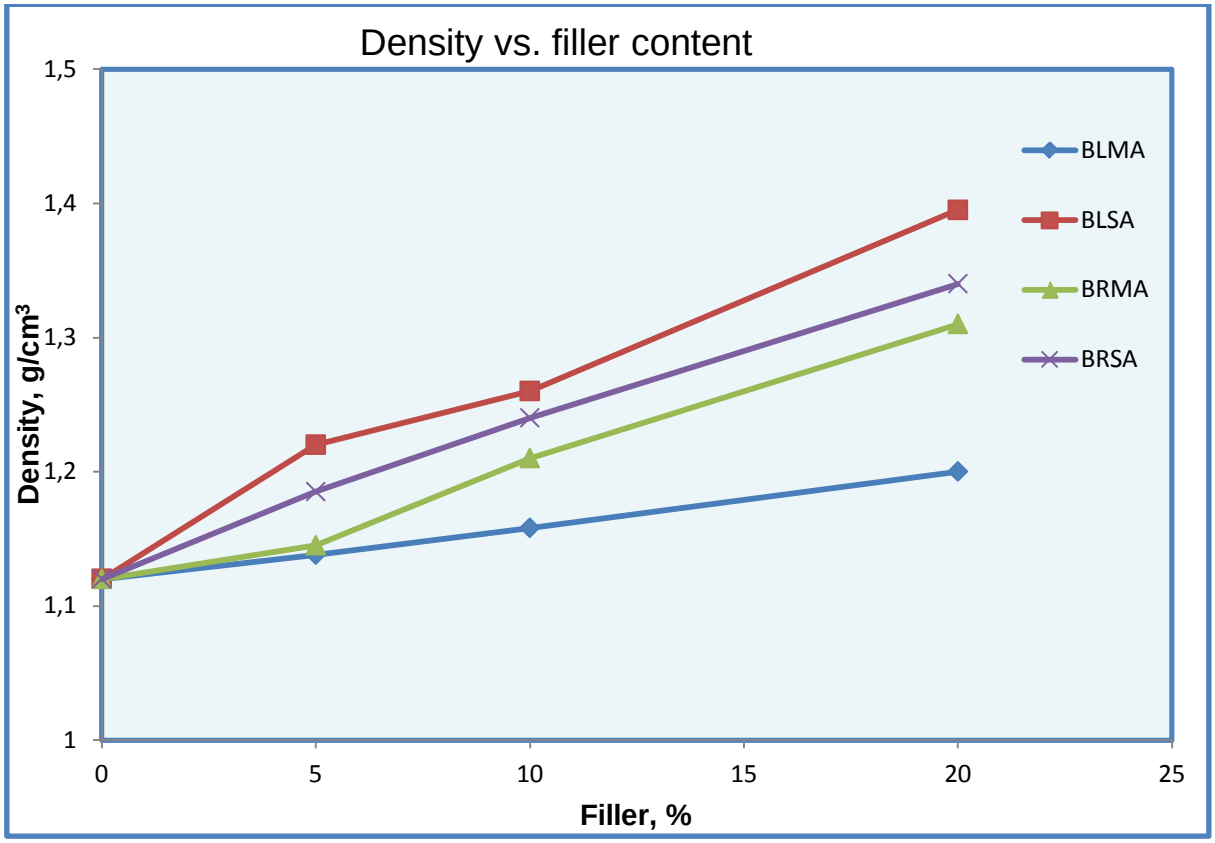

Figure II. 13: Graph showing density modification with percentage of filler content

Tensile strength

The tensile strength indicates improvement of this property when cellulose fibers or wood fibers are incorporated. This property depends on the easenes of stress transfer between the phases present in the blend, higher stress transfer leading to higher strength. In all blends performed, tensile strength increase has been observed with increase of fiber content. This might be attributed to the decrease in melting temperature of mixtures with incorporation of cellulose/wood fibers. The stress transfer is more evident between PHB and cellulose fibers than between PHB and wood fibers. It was reported that the acetic anhydride grafted PHB and blended with wood fibers improved the tensile strength of PHB/wood fibers. The increased bonding between fiber and matrix effectively transfers the applied load to the fiber through the matrix, resulting high tensile strength. The effect of filler content on the tensile strength for PHB/wood fiber and PHB/cellulose fiber blends is presented in Figure II. 14.

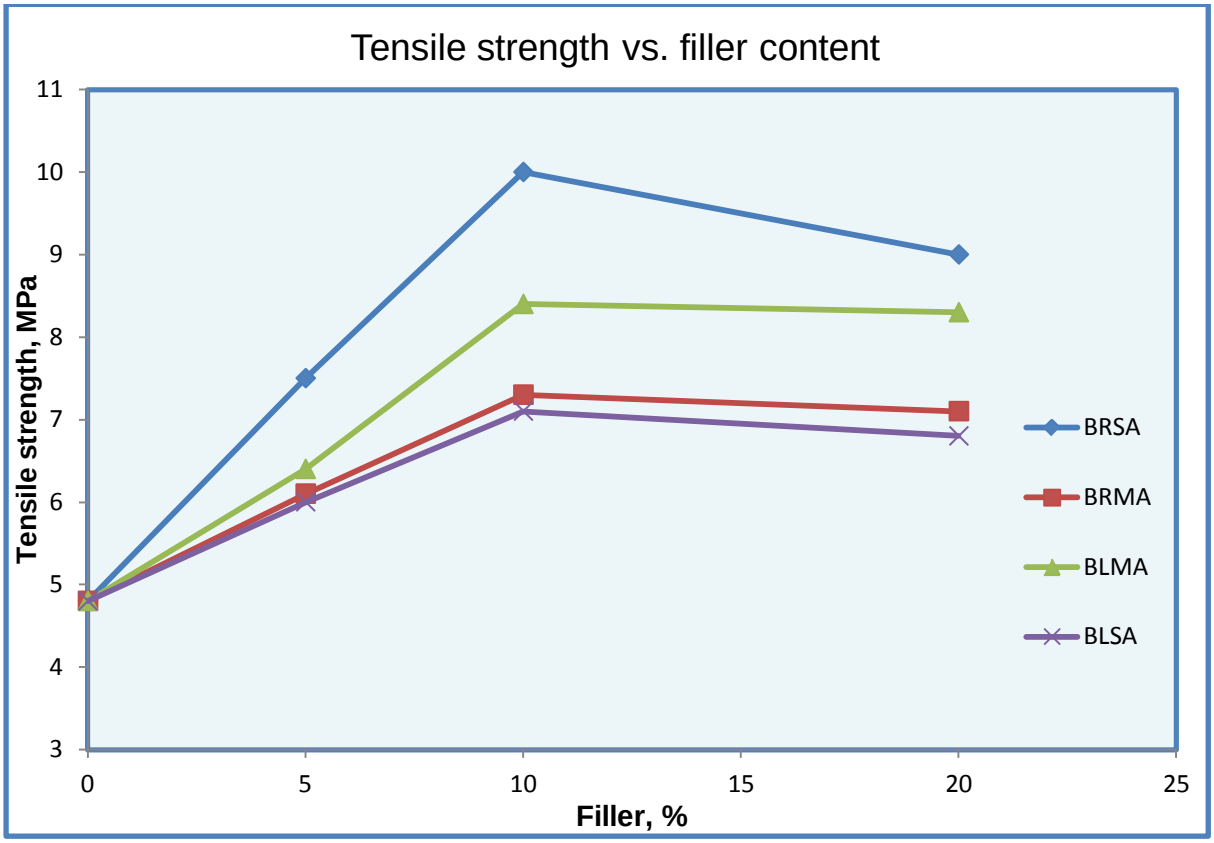

Figure II. 14: Graph showing the variation of tensile strength with the filler content

For BRSA, BRMA, BLSA and BLMA blends, the tensile strength increased continuously and markedly as fiber content increased to a content of 10 %. The blends containing 20 vol. % wood fibers and cellulose fibers gave the lowest tensile strength at break because the higher filler content increased the phase size. The decline in tensile strength is observed to a content of 20 % filler. This effect is due to the amount of glassy material present in the blends and this make them more brittle. It is evident that the mechanical properties strongly depend on the dispersion and phase size of fiber in the polymer matrix.

Contact angle measurements

The variation of contact angle for blend compositions was given in the Figure II. 15. It can be observed that the blends possess smaller contact angle compared to neat PHB due to hydrophilic nature of fibers. The decrease of contact angle of water is prominent to BLSA-5, BLSA-10, BLSA-20, BRSA-5, BRSA-20, BLMA-5, BLMA-10, BLMA-20, BRMA-5, BRMA-10, BRMA-20 blends. Lowest contact angle shows BRSA-20 blends probably due to the ratio aspect of the cellulose fibers which is too lower than the wood fibers. The less affinity of the blends indicates the reduction in the hydrophilic nature of the blends due to the sizes of fibers.

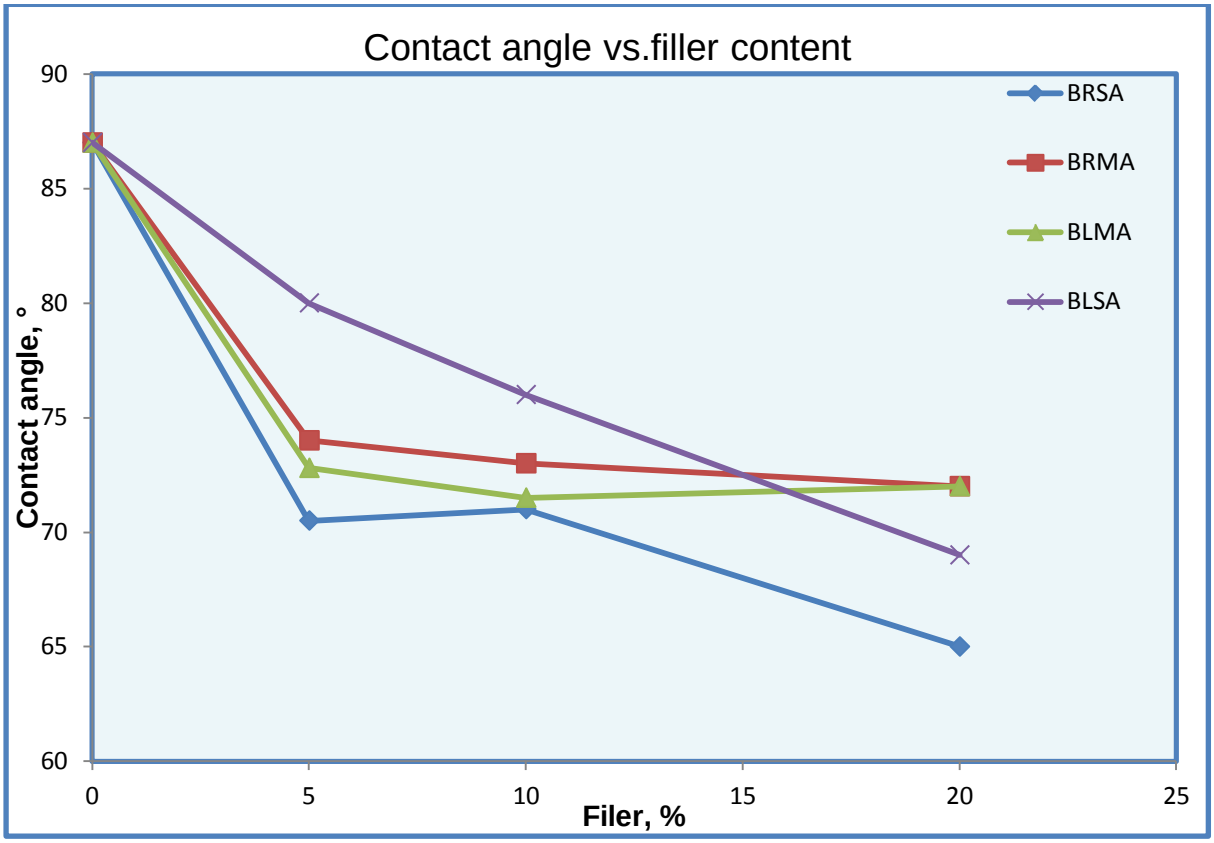

Figure II. 15: Contact angle against filler content for PHB/wood fiber and PHB/cellulose fiber blends

For mixtures made in the laboratory there are observed two phenomena: the decrease of contact angle for BLSA, BLMA, BRMA, BRSA-5, BRSA-20 samples that is due to high hydrophilic character of fillers and on the other hand, the slowly increase of contact angle value for BRSA-10 may be due to homogeneity and to increase in surface roughness mixtures. Grundke and colab. reported similar phenomena.

Conclusions

The properties of blends made from PHB reinforced with treated cellulose/wood fibers have been studied. The results indicate that the cellulose fibers or wood fibers enhance the mechanical properties when these fillers are blended with PHB.

The torque measurements for all blends performed have shown that the viscosity of molten wood fiber/cellulose fiber is lower than that of molten PHB. The melting temperature decreased with increasing filler content for all blends. The blends containing PHB and cellulose fibers exhibit enhanced mechanical properties compared with those containing PHB and wood fibers, especially regarding tensile strength.

The results presented in this study suggest that cellulose fibers are superior to wood fibers in terms of physico-mechanical properties. The fineness and large aspect ratio cellulose fiber were probably the major reasons. Due to large size of the cellulose fibers is observed lower values of contact angle compared with wood fibers. Moreover, the increasing in surface roughness of polymer surface has influence the contact angle. This research has investigated only a few important issues of PHB polymers and natural fillers. The findings from this study will provide a framework for the future development of trials at laboratory and pilot scale in order to obtain items such as tomato yarn, packaging for agriculture by extrusion and molding injection technologies.

II.5 Determination of microporosity using microCT technique[17]

Biomaterials are used in orthopedic, maxillo-facial and odontology surgeries to fill localized bone loss. They are the support of osteo-conduction which allows osteoblasts (bone forming cells) to synthesize new bone on their surface[279]. Biomaterials come in direct contact with cells and biological fluids. They are exposed to biochemical attacks but biomechanical strains can also influence their behavior when placed in weight-bearing sites. The tissue bioreaction of a material depends not only on its chemical composition but also on other factors such as its 3D arrangement, i.e. its shape or microarchitecture. For a given bone biomaterial, its amount, microarchitecture, degree of anisotropy, porosity (connected or not), are significant factors to be considered. Porosity is a property which depicts the amount of void cavities in a given material. The parameter is known to correlate with mechanical properties. There are numerous methods to determine porosity based on physical methods (e.g. mercury injection porosity, Archimedes' principle, Helium pycnometry). However, these methodologies are often destructive, require techniques which are not at disposal in biological laboratories and do not provide information on the spatial distribution of the pores. X-ray microcomputed tomography (microCT) was recently described as an interesting technique when applied to porous biomaterials. Most microCT allow the quantitative analysis of the material volume and also provide some 2D and 3D microarchitectural descriptors. However, the complexity and uniformity of the material distribution within the volume of interest are poorly investigated. MicroCT offers the advantage of been nondestructive for samples. However, it provides a limited number of parameters concerned with porosity and algorithms used by the different systems on the market are not fully validated. The use of other methods for determining

[17] M. N'Diaye, **C. Degeratu**, J.M. Bouler, D. Chappard, *Biomaterials porosity determined by fractal dimensions, succolarity and lacunarity on microcomputed tomographic images.* Materials Science and Engineering: C. 2013;33(4):2025-30

microarchitectural descriptors of porosity can be obtained on 2D sections obtained after re-slicing the 3D models.

Fractal geometry is well adapted to describe complexity and powerful parameters can quantify and discriminate the irregularity of material samples. Several methods for determining fractal dimension exist: box counting dimension, mass radius, Hausdorff dimension… These fractal dimensions are measurements of the irregularity of a given material but do not take into account its uniformity of repartition in the referent space. Recently, new fractal parameters (lacunarity and succolarity) have been reported to improve the description of a fractal porous object. Lacunarity is influenced by the variation of the pores in a given structure; a low lacunarity reflects homogeneity while a high lacunarity is an indicator of heterogeneity. Lacunarity was used as a measure of the complexity of objects: microcalcifications on mammograms, lung texture neuronal complexity cutaneous nevi or trabecular bone.

Succolarity was defined by Mandelbrot as a parameter which informs about connectivity and inter communication. Succolarity can be represented as the degree of penetration of a liquid inside an object according to the direction of entry of the liquid. Porosity, fractal dimension, lacunarity and succolarity are likely to be complementary parameters because objects having same porosity and/or fractal dimension can differ by the connectedness of their pores or the presence of connecting channels. Succolarity was found useful to evaluate the blood flow in atheromatous carotids and the complexity of DNA olfactory receptors.

In this section there are presented the evaluation of different types of porous biomaterials in order to get a more precise description of their microarchitecture. Biomaterials were analyzed using microCT which allowed the measurement of the 3D volume and basic parameters linked with porosity. Fractal dimensions, lacunarity and succolarity were also determined in order to characterize the ability of biological fluids to invade the biomaterial. Other classical descriptors of 2D connectivity and pore size available in Euclidean geometry were used in parallel.

Material and methods

Sample preparation

Eight types of porous biomaterials were prepared with an interconnected or non-connected porosity. For each series, 3 samples were prepared.

Porous blocks of methacrylic polymer

Several porogens were used to prepare porous blocks of poly (2-hydroxethyl methacrylate) (PHEMA) as previously described. “Angel's hairs”, (i.e. filamentous fibers of glucose +

sucrose) were prepared from sucrose/glucose as previously described. Urea beads were obtained from Merck (France) and used as received. Polystyrene beads were prepared by the emulsion method as previously described. Polystyrene beads were sieved to obtain homogeneous populations of 500, 800, 1100 and 1500 μm in diameter.

Briefly, porous blocks of PHEMA were prepared by pouring the accelerated and initiated monomer into polyethylene molds (Peel-a-Way embedding systems, Polysciences, Warrington, PA, USA) containing the porogen. The different types of porous blocks were prepared by placing 1 g of porogen in the mold and filling up the mold with 25 mL of HEMA. The accelerated and initiated HEMA contained 0.125% (w/v) of benzoyl peroxide and N,N-dimethyl paratoluidine at a final concentration of 0.3‰. The polymerization process was carefully checked until the gelling phase was obtained at room temperature. During this step, the porogens were gently homogenized and special care was taken to avoid the entrapment of air bubbles. Polymerization was achieved at 4 °C in a flat-bottomed flask that had been previously purged with nitrogen. Blocks of polymer containing "angel's hairs" or urea were transferred in screw-capped bottles containing distilled water and placed on a continuous rotating agitator. Blocks containing the polystyrene beads were similarly transferred to dichloromethane (a solvent for polystyrene and a non-solvent for PHEMA). When all the porogen had dissolved (as checked by trans-illumination), the blocks were dried in an oven at 40 °C for 3 days.

Filamentous polymer

Polyhydroxybutyrate-98%/polyhydroxyvalerate-2% (PHBV) - biopolymer powder was purchased from Goodfellow SARL (France) and used without any purification. PHBV fibers were prepared by a coagulation-precipitation in a coagulation non-solvent bath method (the wet-spinning method) using a 20% (w/v) chloroform solution. Briefly, the PHBV chloroform solution was obtained by dissolving 4g of polymer powder in 20 mL chloroform, under stirring at 70 °C. 5 mL of polymer solution was cooled at room temperature and extruded from a 10 mL commercial syringe into a 1 L ethanol bath (the diameter of the bath was much lower than its height), resulting in the formation of individual PHBV fibers. The extrusion rate was 0.2 mL/min. After 5 minutes every single obtained fiber was collected and let dry - if not used immediately - for 48 h in the air at room temperature. Others substances used for fiber preparation were bought from Sigma-Aldrich Chemicals and used without any purification.

Calcium–phosphate porous material (CaP)

The synthesis of a calcium deficient apatite (Ca/P = 1.60) was completed by alkaline hydrolysis of dicalcium phosphate dehydrated (DCPD, Merck, France). Crystalline sucrose

and ammonium carbonate (Merck) were used as porogen and mechanically sieved (503 502 Sieve, Fristch Laborgerätebau, Germany) on 710 and 450 μm sievers for 20 min to collect the intermediate granular fraction. The apatite powder (31.6 g) was mixed with (NH4)2CO3 particles (12.6 g) and sucrose crystals (13.3 g) and introduced in an elastomer mold under vacuum, then the mold was transferred into a high-pressure chamber containing water and subjected to isostatic compression under 150 MPa during 2 min. The resulting compressed blocks were sintered in a controlled-temperature furnace (Vecstar, Eurotherm, Switzerland) according to the following process: the temperature was first raised to 60 °C (2 °C min^{-1}) for 240 min, then to 560 °C (2 °C min^{-1}) for 300 min and then to 1050 °C (5 °C min^{-1}) for 300 min. Then, the resulting blocks were cooled down to room temperature (5 °C min^{-1}).

X-ray microcomputed tomography (microCT)

The blocks were fixed on brass stubs and analyzed with a Skyscan 1172 X-ray computed microtomograph (Bruker MicroCT, Kontich, Belgium). They were examined at a magnification of × 15.36 (a pixel corresponding to 20 μm) with the cone beam mode at 80 kV, 100 μA with no aluminum filter and a 0.25° rotation angle was applied at each step. Briefly, serial section images of the block were acquired and stored in the *.bmp format. After interactive segmentation, the 3D models were constructed from the stack with a surface-rendering program (Ant, release 2.5.0.2, Skyscan). The fractional amount of the porosity (Po.V/V, in %) and the mean thickness of the biomaterial profiles between the pores (Mat.Th, in μm) were determined by the CTAn software (release 1.11.10.0, Skyscan).

For applying the image analysis software, 2D sections were re-sliced from the 3D models: 2 sagittal images (separated by 200 μm) were obtained, and 2 other section images were done in orthogonal plans. So, for each block, 4 images of size 270 × 270 pixels were obtained and binarized. Images were transferred to a Leica Quantimet Q550 (Leica, Nanterre, France) to be analyzed by lab-made software for the determination of the porosity characteristics. Then the images were transferred to a lab-made software written in Matlab (Math Works, Natick, Ma) release 7.10. The different types of materials used in this study appear in Figure II. 16 and binarized images of the sections in Figure II. 17.

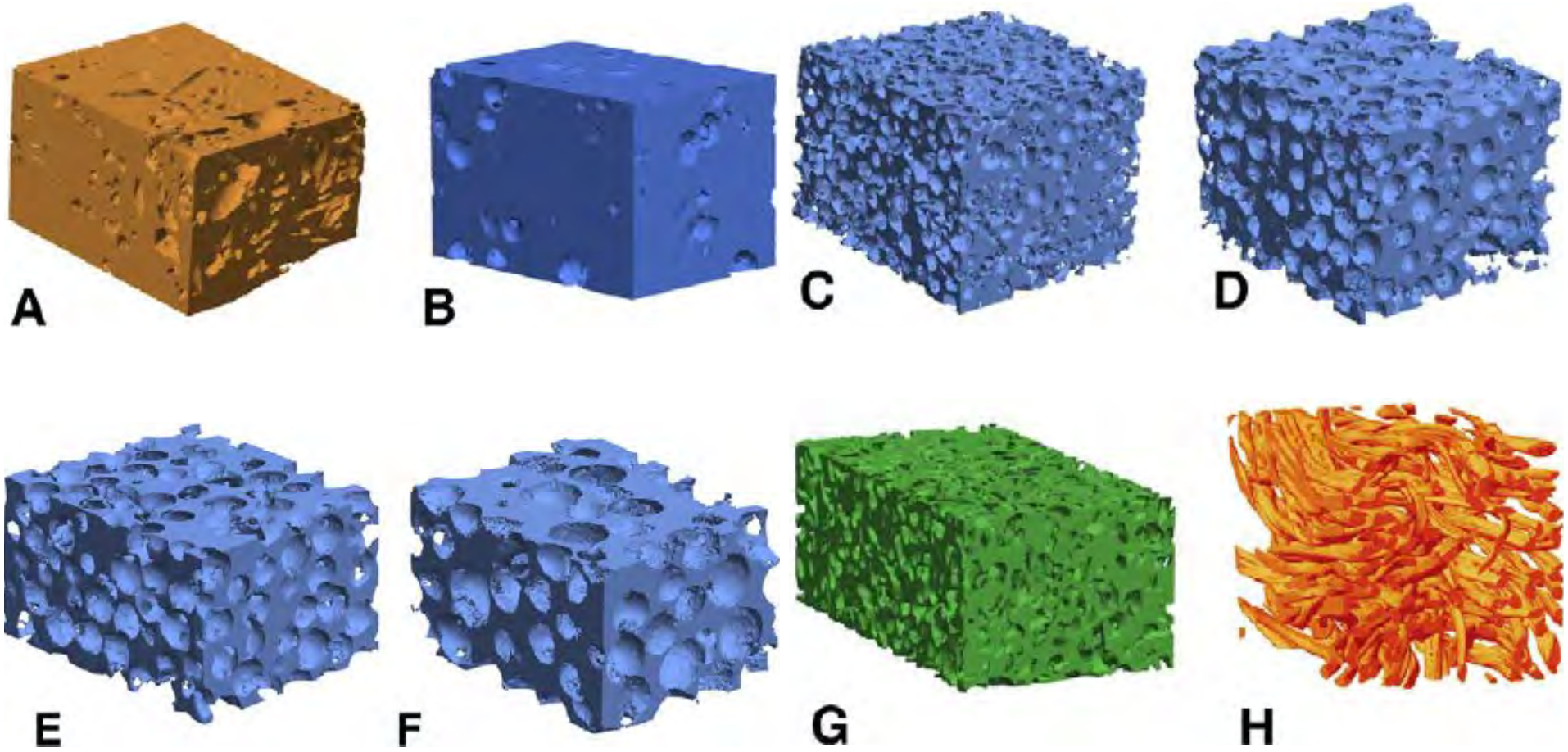

Figure II. 16: 3D microCT analysis of different biomaterials used. A="Angel's hairs" in PHEMA; B=PHEMA with urea beads; C to F: PHEMA with polystyrene beads with a 500, 800, 1100 and 1500 µm diameter; G: CaP material; H: PHBV fibers. All 3D models are figured in pseudo-colors which are also used in graphs of figure. 4

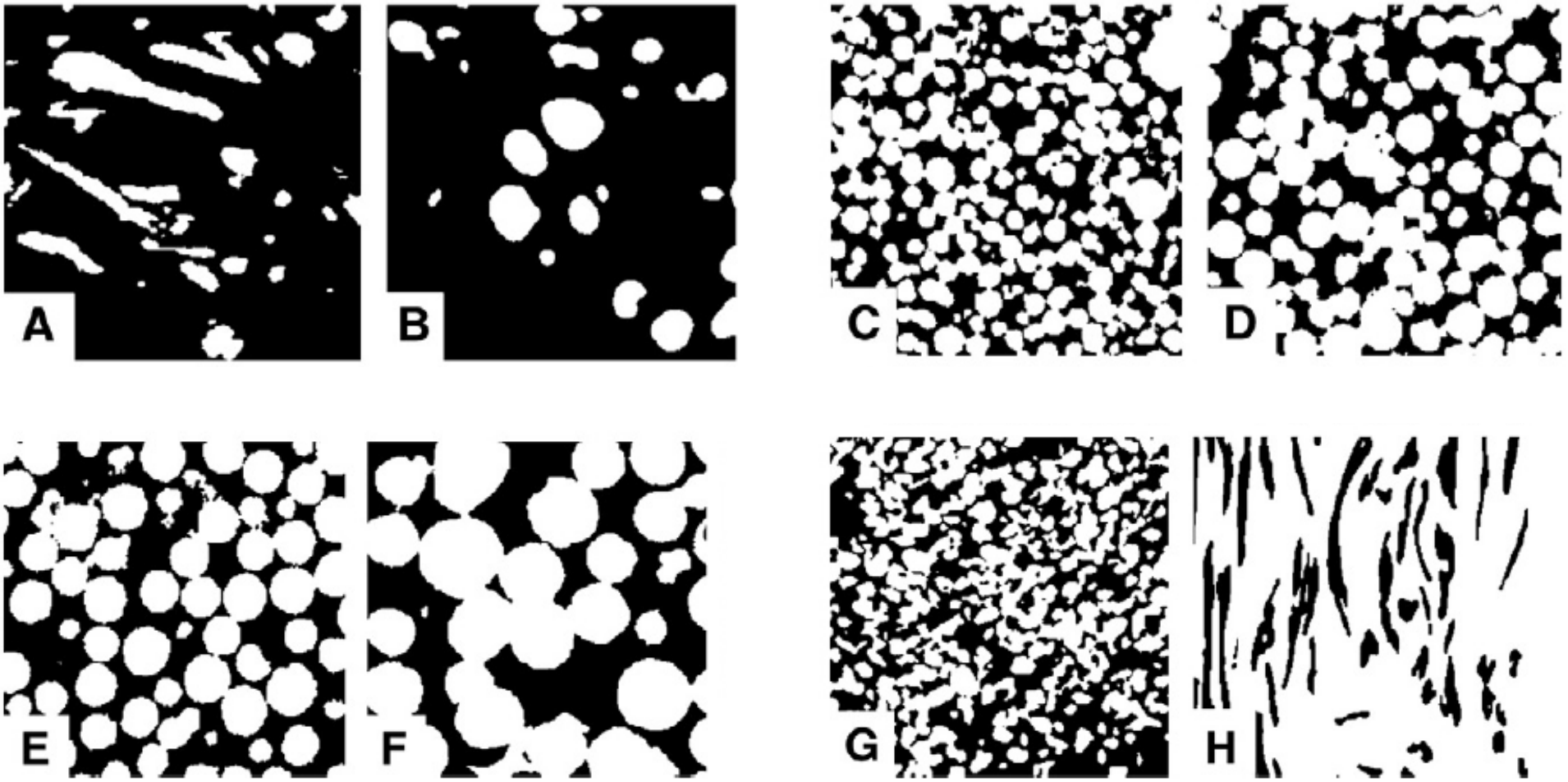

Figure II. 17: The corresponding binarized 2D sections of biomaterials appearing in figure. 1. The material appears as black pixels and porosity as white pixels.

Image analysis

The following parameters were measured using the Q550 Quantimet:

a) The Kolmogorov fractal dimension (D_K) by the box-counting and the Minkowski–Bouligand (D_{MB}) dilatation methods were used as previously described. Briefly DK was computed by overimposing grids of square boxes (with ε pixels as side length) on the material's boundary and intersecting boxes were counted. The total number of boxes required to completely fill the boundaries reflected the perimeter with a scale ratio of ε. this step was repeated with ε varying from 2 to 100 pixels and a log-log graph (i.e. log[N] against log[ε]) was used to determine D_K from the slope of the regression line. D_{MB} was obtained by using a series of dilatations of the material's boundary and was repeated from 1 to 10 times; after each new dilatation φ, the material's border thickened and the surface area of the dilated image A was measured. D_{KM} was determined on the log–log graph from the slope of φ/A(φ).

b) The interconnectivity index of the porosity (ICI) was determined by skeletonization of the pores X (i.e., finding the centroids of by skeletonization of the pores X (i.e., finding the centroids of maximal open discs included in the pore profiles). On the reconstructed skeleton S(X), the total number of nodes N, nodeto-node branches (NN), and node-to-free-end branches NF were determined. The number of 'trees' (T) was also obtained, a 'tree' being the structure composed of interconnected node(s) with node-to-node and/or node-to-free-end branch. ICI of the porosity was then defined as:

$$\mathrm{ICI} = \frac{(\mathrm{N} \times \mathrm{NN})}{\mathrm{T} \times (\mathrm{NF} + 1)}$$

c) The star volumes

The star volume of pores and materials was determined. Starting from a randomly placed seed in the porosity, one can project rays in all the directions of space. The rays stop as soon as they meet a material boundary or edges of the block. This constitutes a kind of star and the measurement of the length of each ray of star is done. One sees that the more disconnected will be the material, the more the length of the rays will be important. If a great number of stars are generated, small perforations are evidenced inside the material network. However, this method is very time consuming and the grid technique is preferred: a series of grids was computed with parallel lines running with various angles running from 0 to 2π. Each grid was intersected with the image of the marrow cavities. This provided linear segments (called chords) superimposed on the pores. The cubed length of each chord l3 was then computed with each grid, so that all directions from 0 to 360° are explored very rapidly. The star volume was determined on the pores V^*_{Pore} (a high star volume indicates a highly fragmented material or the presence of larges pores). The other star volume (V^*_{Mat}) was determined by placing the seeds on the material itself to know the mean width separating the pores.

Measurements of lacunarity and succolarity

a) Lacunarity

We have used the "gliding box" method described by Allain and Cloitre. A square box of side ε was glided along all possible direction of the image. The total number of flooded pixels counted during this process was calculated. This procedure was repeated by gradually increasing the size of boxes. The total number of flooded pixels was defined by a mass distribution n(M, ε). By dividing this number by the total number of boxes of size ε:

$$N(\varepsilon) = (S - \varepsilon + 1)^2$$

we obtained the probability distribution of Q(M, ε), corresponding to the frequency of the number of occupation of a box of mass M and size ε:

$$Q(M, \varepsilon) = \frac{n(M, \varepsilon)}{N(\varepsilon)}$$

To analyze the properties of such a distribution, a common method is to study its statistical moments. Local lacunarity (δ) for a box side ε is defined by the ratio between the second moment and the square of the first moment:

$$\delta = \frac{\sum M^2 \times Q(M, \varepsilon)}{\sum M \times Q(M, \varepsilon)^2}$$

A log–log graph of log(δ) and log (ε) was used to determine D_δ from the slop of the regression line.

b) Succolarity

The approach for calculating succolarity (σ) was provided by Melo and Conci using a box counting approach on a square image of side n pixels. Succolarity is calculated in one direction and then in the opposite direction: e.g. from left to right, from right to left, from top to bottom and from bottom to top (Figure II. 18). Briefly, in the first step, the image is flooded in a given direction ensuring that all black pixels of the first column are detected (the black pixels corresponding to the material, the white pixels to the pores). Then all the four connected black pixels are selected until an impenetrable mass of white pixels is encountered.

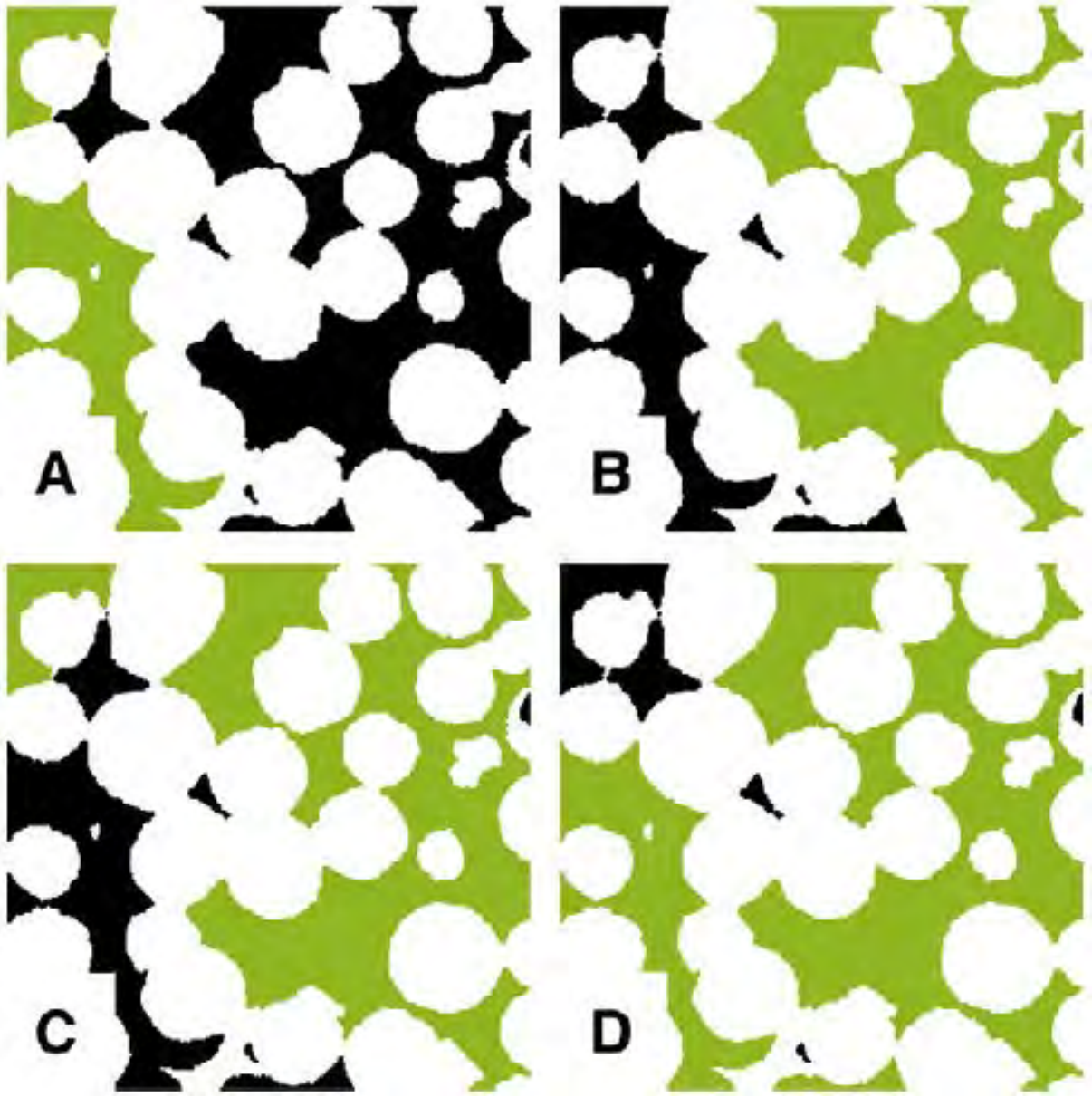

Figure II. 18: Principle of succolarity σ measurement by the flooding algorithm in the 4 directions. The black pixels of materials are flooded. A: from left to right; B: from right to left; C: from top to bottom; D: from bottom to top. The flooded pixels are in green.

In the second step, the flooded image was analyzed using the sliding box method with the size of the box t ranged from 2 to n − 1 where n is the size of the image. The number of flooded pixels in the box $B(N_{pixel(B)})$ is determined as follows:

$$\mathrm{N_{pixel(B)}} = \frac{\sum \text{gray pixel(B)}}{\text{Value of pixels(B)}}$$

In the third step, the occupation percentage of the box PO(B) was calculated as the ratio of the number of flooded pixels and the square size of the box:

$$PO_{(B)} = \frac{\sum N_{pixel(B)}}{t^2}$$

In the fourth step, the "pressure" (PR) exerted on the boxes (by analogy to the liquid which has flooded the image) is stored in an array of pressures. The pressure increases from line to line (or column to column) along the direction of the flood.

On the first row or column : $PR_{(B)} = \frac{1}{2} \times t_{(B)}$

On the other rows or columns : $PR_{(B)} = (\frac{1}{2} + l) \times t_{(B)}$

in which l stands for the number of row or column. Finally, succolarity for a given direction was calculated as:

$$\sigma_{(direction,B)} = \frac{\sum_{t=1}^{n} PO_{(B)} \times PR_{(B)}}{\sum_{t=1}^{n} PR_{(B)}}$$

Values were similarly computed in each direction and were averaged to calculate the global σ of the image.

2.5. Statistical analysis

Statistical analysis was performed using the Systat statistical software release 13.0 (Systat Software Inc., San José, CA). All data were expressed as mean ± standard error of the mean (SEM). Differences between groups were analyzed by a non-parametric ANOVA test (Kruskall–Wallis) with the Conover–Iman post-hoc test. Differences were considered significant when p b 0.05.

Results and discussion

The 3D models of the different biomaterials appear in Figure II. 16, they are represented in pseudocolors which are also used in the graphs to improve clarity. The morphometric parameters of each type of biomaterial are reported in Table II. 4.

Table II. 4: MicroCT and image analysis parameters of the porous materials. Po.V/V: fractional amount of the porosity; Mat.Th: mean thickness of the biomaterial profiles between the pores; ICI: interconnectivity index of the porosity; V^*_{Pore} : star volume of the pores; V^*_{Mat} : star volume of the material; D_K: Kolmogorov fractal dimension; D_{MB} Minkowski–Bouligand fractal dimension; δ: local lacunarity; σ: succolarity.

Parameter	Unit	PHEMA angel's hairs	PHEMA urea	PHEMA beads 500	PHEMA beads 800	PHEMA beads 1100	PHEMA beads 1500	CaP	PHBV
Po.V/V	%	20.9±2.9	14.0±1	38.6±4.5	33.8±0.5	38.3±5.0	40.8±2.6	55.1±0.5	79.7±3.3
Mat.Th	µm	222±56	77±6	94±8	54±11	95±29	181±13	322±26	139±10
ICI		7.42±2.4	23.84±13.8	30.58±9.6	23.31±8.3	10.50±2.1	9.96±0.1	6.15±0.2	192.73±18.4
$\mathbf{V^*_{Pore}}$	mm^3	12.4 ± 9.6	15.5 ± 2.2	36.6 ± 7.1	96.3 ± 40.7	170 ± 103	226 ± 22.6	8.3 ± 1.9	1830 ± 585
$\mathbf{V^*_{Mat}}$	mm^3	1210±880	1634±205	15±3	40±5	74±28	147±27	22±2	33±3
$\mathbf{D_K}$		1.294±0.13	1.204±0.02	1.746±0.01	1.673±0.03	1.638±0.02	1.540±0.01	1.801±0.01	1.567±0.04
$\mathbf{D_{MB}}$		1.212±0.06	1.137±0.01	1.679±0.01	1.514±0.06	1.461±0.02	1.316±0.01	1.828±0.02	1.423±0.04
δ		1.39±0.09	1.55±0.02	1.75±0.02	1.65±0.02	1.75±0.02	1.82±0.01	1.81±0.01	1.50±0.03
σ		0.85±.0.04	0.88±0.01	0.19±0.04	0.28±0.06	0.44±0.05	0.51±0.05	0.51±0.02	0.75.±0.03

MicroCT is a suitable method for measuring porosity. When compared to more classical methods such as Archimedes' principle or mercury intrusion porosimetry, linear correlations have been reported with a 7% error. These techniques were not used in the present study because PHEMA swell in water; furthermore, they are not applicable in case of non-connected porosity. We have chosen to illustrate the method on a series of different samples and comparing the results with morphometry with a 5% error. However, in all these materials, micro-porosity (which is observed in some types of materials prepared by sintering elementary particles) was not considered although it is known to strongly influence biomechanical properties.

Micro-porosity is typically in the range of 1–10 μm, and the mean size of the pixel used in this study was 20 μm. Because the present algorithms have been developed on 2D images, they could be applied to other images obtained by more precise devices such as nanotomograph or synchrotron which can image nanometric details.

The “angel's hairs” method provided an interconnected porosity in PHEMA as previously reported and evidenced on the 3D models (Figure II. 16A). On the 2D sections, the profiles of the pores appeared either as separated filaments when cut longitudinally or as round/ellipsoidal profiles when sectioned transversally. The interconnectivity was observed occasionally when the profiles of two channels came in direct contact (Figure II. 17A). However, porosity occupied only ~ 20% of the material's volume.

PHEMA materials prepared with beads of different diameters provided more or less connected porosities (Figures II. 16B–F and II. 17B–F). The pores appeared spherical and interconnectivity occurred only when the beads were in contact tangentially. Urea beads gave a non-connected porosity and the pores appeared scarcely distributed within the polymer (Figures II. 16B and II. 17B).

The polystyrene beads provided highly porous blocks (Figures II. 16C–F and II. 17C–F) but, surprisingly, the mean porosity Po.V/V did not differ significantly between the four types of materials. However, V^*_{Pore} reflected well the mean size of the beads used as porogen. Reciprocally Mat.Th (reflecting the thickness of the material between the pores) increased as a function of the bead size used to prepare the blocks and interconnectivity, measured by ICI, decreased inversely to the porogen beads. Conversely, σ and V^*_{Mat} at increased as a function of the bead diameter and the complexity of the porosity network decreased as evidenced by D_K and D_{MB} which decreased in parallel.

The CaP material presented the highest porosity among the block materials with numerous very small pores (Figures II. 16G and II. 17G). However, ICI was low and evidenced a poor interconnectivity of the pores. In this last material, the pores appeared to provide a very complex pattern with the highest fractal dimensions δ, D_K and D_{MB}.

The PHBV fibers were well separated (Figures II. 16H and II. 17H) and spaces between them were the highest of this series as evidenced by V^*_{Pore}. These long fibers were thin and not connected as evidenced by ICI which reached very high values.

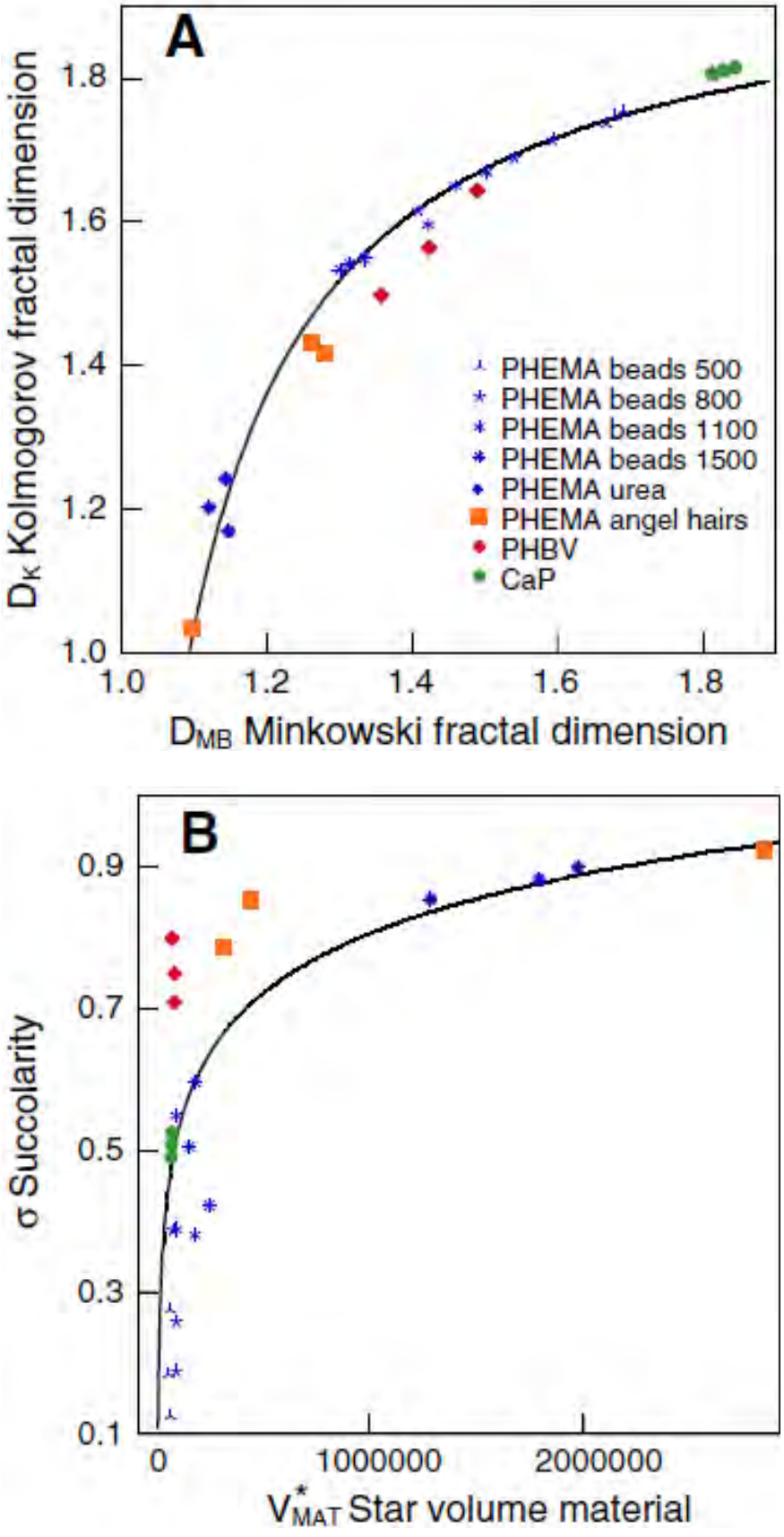
A
1.8
1.6
1.4
1.2
1.0
D_K Kolmogorov fractal dimension
1.0
1.2
1.4
1.6
1.8
D_{MB} Minkowski fractal dimension
PHEMA beads 500
PHEMA beads 800
PHEMA beads 1100
PHEMA beads 1500
PHEMA urea
PHEMA angel hairs
PHBV
CaP
B
0.9
0.7
0.5
0.3
0.1
σ Succolarity
0
1000000
2000000
V^*_{MAT} Star volume material

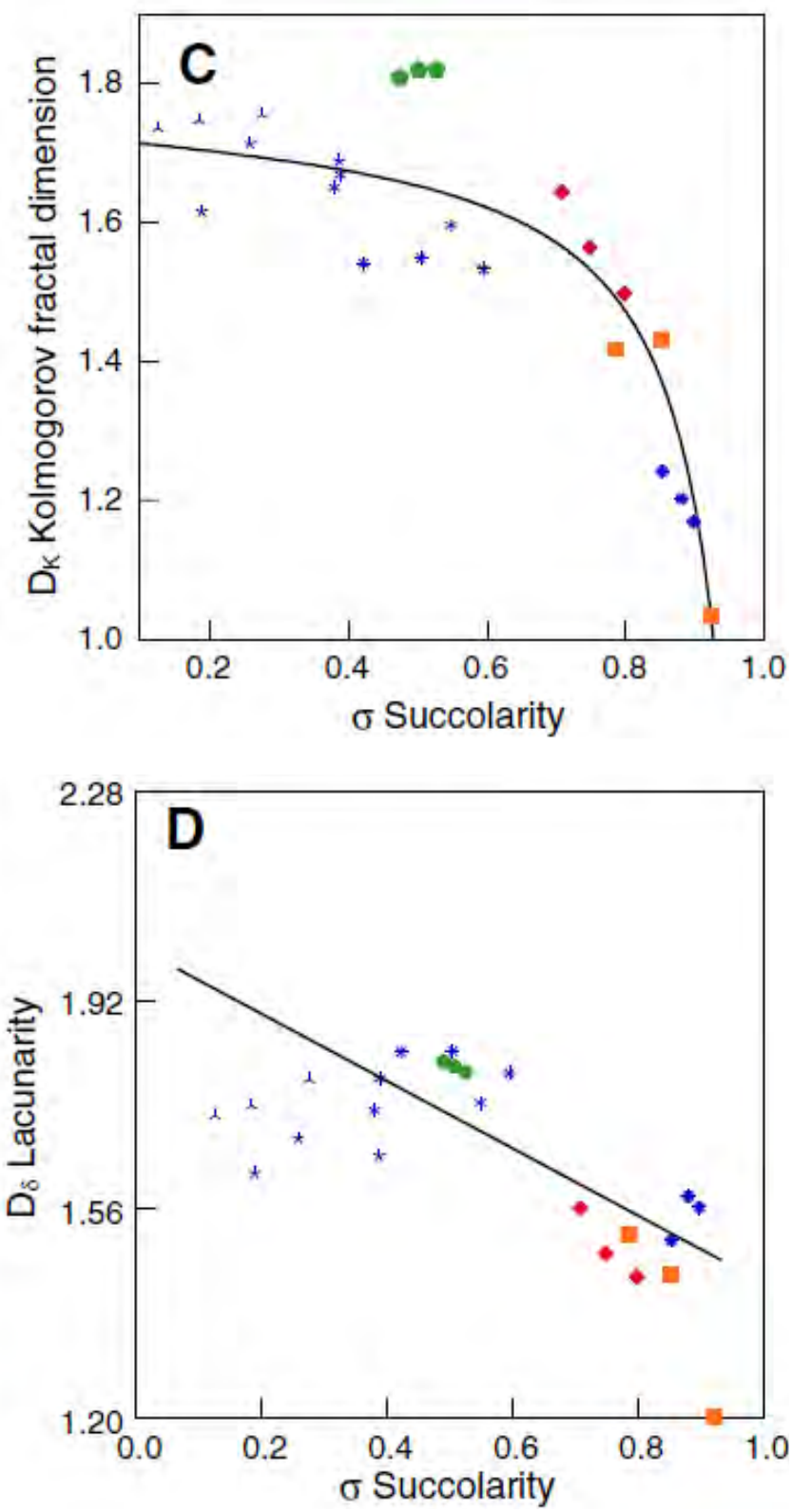

Figure II. 19: Relationships between the different parameters characterizing pores and porosity. Log relationships between **A**: D_{MB} and D_K; **B**: between V^*_{Mat} and σ; **C**: σ and D_K; **D**: linear correlation between succolarity σ and lacunarity δ. On each graph, the different biomaterials are identified by specific symbols and colors which are the same than in Figure II. 16.

Po.V/V was poorly correlated with almost all parameters except D_K and D_{MB} (resp. r=0.53; p=0.08 and r=0.47; p=0.02), but the relationships only explained less than 25% of the variance. ICI and V^*_{Pore} were linearly correlated (r = 0.88; p b 0.0001) confirming the interest of these parameters for the analysis of interconnectivity. D_K and D_{MB} were highly correlated with a logarithmic correlation (y = a + b / log(x)) (r = 0.96; p b 0.0001) (Figure II. 19A). The CaP material having the more complex structure presented the highest D_K and D_{MB} values. Succolarity of the materials (which reflects the degree of penetration of a liquid inside the material; i.e. the black pixels in Figure II. 17) appears at the opposite of D_δ, D_K and D_{MB} fractal dimensions. σ had the highest values in images where large territories of materials were present. When searching for correlations, a logarithmic relationship was observed between σ and V^*_{Mat} (Figure II. 19B). Similarly, σ appeared negatively correlated with D_{MBB} (r = − 0.77; p = 0.0001) and D_K (r = − 0.92; p = 0.00001) (Figure II. 19C). A negative linear correlation was found between σ and δ (r = − 0.68; p = 0.0002) (Figure II. 19D).

Non-linear relationships were observed between porosity Po.V/V and other parameters. This was previously reported for trabecular bone when considering its 3D microarchitecture vs. the bone volume (bone volume been equal to 100-Po.V/V). In this study, the different parameters used appear to provide more information about the porosity of these materials (e.g. on the homogeneity of the pores' size and interconnectivity). In the series of PHEMA blocks prepared with polystyrene beads varying over a wide range of diameters, the evolution of Euclidean (i.e. V^*_{Pore}) and some fractal dimensions (e.g. lacunarity) were similar.

Succolarity represents the percolation of the material itself while the pores constituted the obstacles. In this study, the possibility to investigate σ in a particular direction was not taken into account since the materials (excepted PHBV) had no preferential orientation; so the mean value of the 4 dimensions was used. In the PHEMA series with polystyrene beads, σ regularly increased; it reached its maximum for PHEMA with urea beads that were loosely disposed and did not exhibit interconnectivity. Here again, the relationships of σ with other descriptors were usually nonlinear. σ and D_δ, on the other hand were linearly correlated.

Conclusion

New morphometric methods were used to better characterize the porosity of biomaterials. Connectivity of the pore was measured by computing the interconnectivity index and the star volumes on 2D sections obtained by microCT. These parameters, based on Euclidean geometry, were refined by measuring the complexity of the pore size and their interconnectivity with measurements based on fractal geometry (Kolmogorov and Minkowski–Bouligand fractal dimensions) and the newly described fractal parameters lacunarity and succolarity. Non-linear relationships exist between these descriptors of porosity and the amount of the materials constituting the pore throats. Fractal descriptors constitute a

very promising approach in this field and should be used to better characterize porous materials. These parameters can be applied to non-homogeneous and anisotropic materials. These characteristics may help in designing new types of scaffolds to allow a better invasion of the grafted materials by vascular sprouts and progenitor cells.

Chapter III - Evaluation of biopolymer-based structures for application in tissue engineering

III.1 Influence of porosity upon cell adhesion on polyhydroxyalkanoates films[18]

Along with polyisoprenoids, polypeptides, polysaccharides, and polynucleotides, Nature contains a further group of biopolymers, poly(hydroxya1kanoates). They are polyesters of hydroxyacids synthesized within the cells of microorganisms in the presence of saccharide and oil substrates. Polyhydroxyalkanoates (PHAs) are naturally derived polyesters that accumulate as a carbon storage material in a wide variety of bacteria, usually under conditions of limiting nutrients (such as ammonium, sulphate, and phosphate) in the presence of an excess carbon source. An imbalanced nutrient supply leads to intracellular storage of excess nutrients. By polymerizing soluble intermediates into insoluble molecules, cells do not undergo alterations of their osmotic state and leakage of nutrients is prevented. Accumulated PHAs form discrete granules that can account for up to 90% of the cell's dry weight. Up to date, approximately 150 hydroxyalkanoate units with different R-pendant groups have been isolated from bacteria.

Poly(3-hydroxyalkanoates), which are synthesized by a wide variety of microorganisms, have attracted a great deal of industrial attention because of their potential applications as biodegradable and biocompatible thermoplastic polymers. In particular, much interest has focused on the use of poly(3-hydroxybutyrate) (P3HB) and related copolymers with 3-hydroxyvalerate. Poly(3-hydroxybutyrate), P3HB, is the simplest and most common member of the group of PHAs. Discovered by Lemoigne in the 1920s, its commercial evaluation did not start until the late 1950s. The potential of P3HB for biomedical applications was first suggested in a 1962 patent, which presented the ideas of biodegradable surgical sutures and of films to support tissue healing of injured arteries and blood vessels.

PHAs are biocompatible, so they are potential scaffolds for the growth and proliferation of cells for partial or permanent replacement of living tissues. The present paper work focuses on the obtaining of polyhydroxyalkanoates films based on poly(3-hydroxybutyrate-co-3-hydroxyvalerate) with controlled porosity and the evaluation of physical and biological properties for medical uses.

Experimental

Materials

Natural poly(3-hydroxybutyrate-co-3-hydroxyvalerate) (PHBHV8%) copolymer was kindly provided by INCERPLAST S.A. PHAs films were prepared by casting from chloroform

[18] **C.-N. Degeratu**, C. Zaharia, M.R. Tudora, C. Tucureanu, G. Hubca, A. Salageanu, C. Cincu, *Influence of Porosity Upon Cells Adhesion on Polyhydroxyalkanoates Films,* Chemical Bulletin of "Politehnica" University of Timisoara 55(69), 2, pp. 189-192, 2010

solution (5% w/v) and then dried a room temperature to allow solvent evaporation. The film thickness was between 30-50 μm.

PHAs porous structures were obtained with sodium chloride (Fluka), gelatine B, sodium alginate and sugar. Gelatine B was obtained by the alkaline treatment of porcine collagen was supplied from PB Gelatines GmbH, member of Tessenderlo Group, Germany and it conforms to the requirements of Pharmacopoeia Europea. Gelatine used in this study has an isoelectric point of 4.7-5.6 and Bloom strength of 250. The viscosity of a 6.67% (w/v) solution at 60°C is 4.62 mPas and the *p*H at 45°C is 5.73. Low viscosity sodium alginate (SA) rich in α-L-guluronic residues (approx. 70 % of G-block content) was purchased from Medipol SA (Lausanne, Switzerland).

Methods

The morphology of the specimens was assessed by SEM and optical microscopy. The SEM device was a Zeiss Evo 50 XVP Scanning Electron Microscope. Prior to imaging the samples were sputtered with a thin layer of gold.

The optical images were achieved with an Olympus BX41 Microscope equipped with Live view digital SLR camera E-330 (7.5 Mpxl) and special software Quick Photo Micro 2.3.

KSV CAM 200 apparatus was used for static contact angle measurements performed on dried films. Ultrapure water droplets were used with a drop volume of 20 μl. The measurement of each contact angle was made within 10 s after each drop to ensure that the droplet did not soak into the compact. The contact angles reported were the mean of 10 determinations. Smaller contact angles correspond to increased wettability.

Biocompatibility tests

The biocompatibility of materials was assessed by using L929 mouse fibroblast cells monolayers grown on polymer films covering approximately 90% of the well surfaces in 24-well cell culture plates. Cells were cultured in Dulbecco's Modified Eagle's Medium (DMEM) supplemented with 10% fetal bovine serum and 1% antibiotics (penicillin and streptomycin) at 37ºC in a humidified incubator with 5% CO2. After 24 h incubation, polymer films were removed and the number of cells grown both on their surface and adjacent well bottom were measured using an MTT [3-(4,5-dimethylthiazol-2-yl)-2,5-diphenyltetrazolium bromide]-based cell viability test. This assay is based on the ability of

dehydrogenase enzymes from viable cells to cleave the tetrazolium rings of the pale yellow MTT and form insoluble dark blue formazan crystals. Cell lysis and crystals solubilization was performed according to described method. The absorbance at 540 nm is directly proportional to the number of viable cells. Finally, the cells were microscopically examined for detecting cytotoxicity visible signs, cellular lysis or cellular components dimensions and conformation (optical microscopy, ZEISS - Axiovert 135 Microscope). A cellular viability test (MTT) was also employed and the number of cells grown on polymer films was calculated relative to an equivalent area of cells culture plastic.

Results and Discussion

The non-porous PHBHV films have variable thickness (30-50 μm). Figure III. 1 shows SEM of non porous film and optical images of these polyester film with clear non-porous morphology.

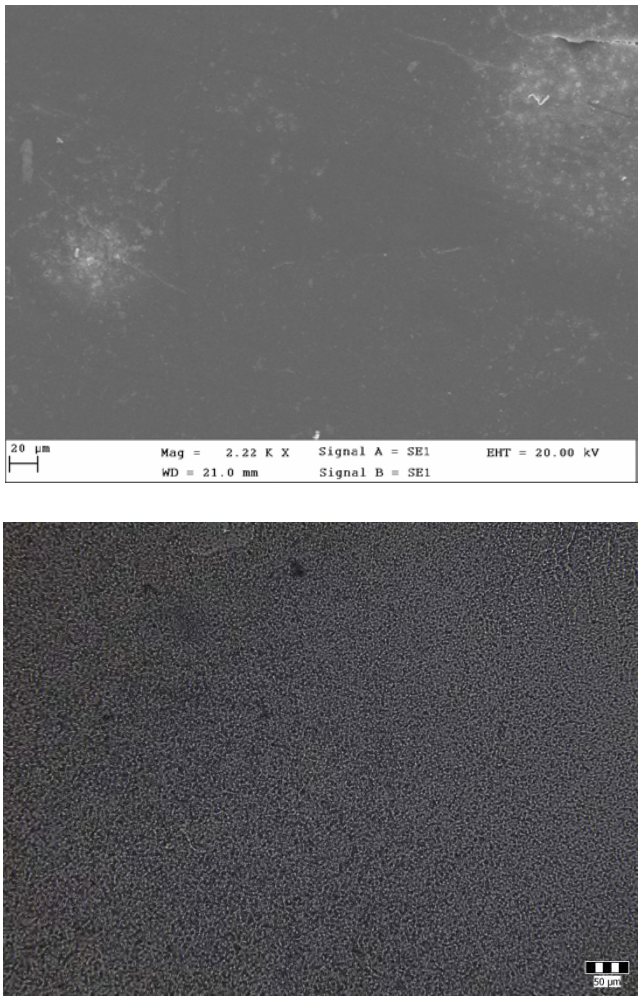

Figure III. 1: SEM microphotograph and optical microphotographs OM (20x objective) image of PHBHV film

The high values of the contact angles of the specimens (~95°) prove the hydrophobic character of these materials. The porosity was induced by various porosity agents for a higher cell adherence of the polyester films according to their nature and granulometry.

Table III. 1: *Pore size measurements*

Porogen agent	Pore diameter range, µm
Distilled water	< 1
Sugar	2 - 50
Sodium chloride	5 - 25
Gelatin	200 - 300
Alginate	3 - 20

The SEM and OM images of some porous structures are presented in Figure III. 2. Pore dimensions lie between 1-50 µm for most of the porogen agents, except gelatine, which induces higher pores (200-300 µm). The pore size distribution is presented in Table III. 1. Lower pore size is obtained with NaCl and alginate.

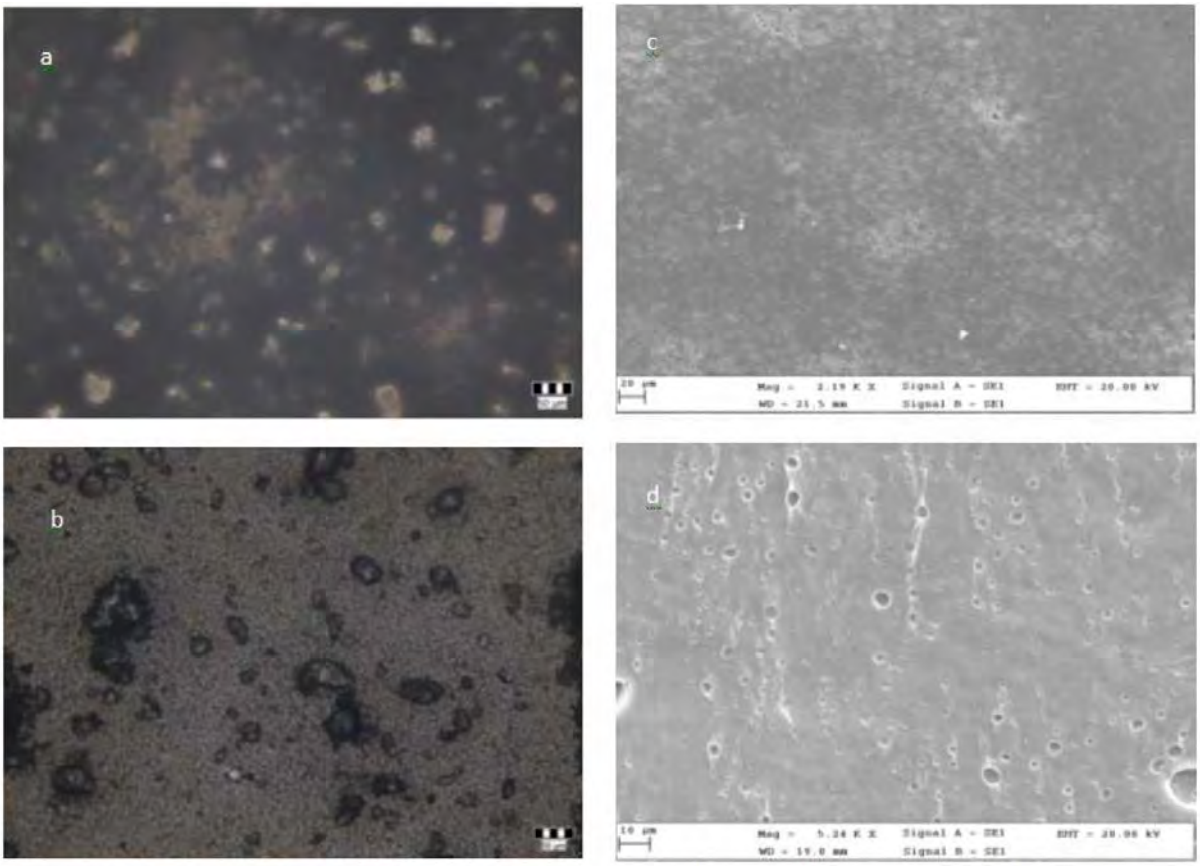

Figure III. 2: OM and SEM microphotograph image of PHBHV porous films: a, c – sodium chloride; b, d – alginate

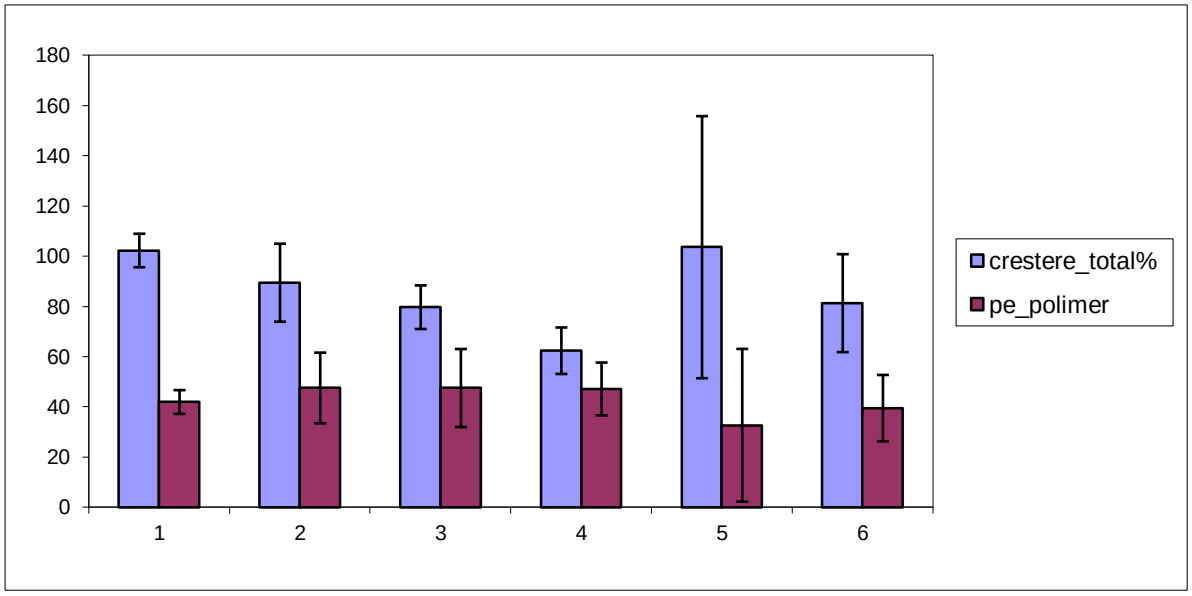

Figure III. 3: Cells growth on polymer porous and nonporous films: 1 - gelatine; 2 - sugar; 3 - PHBHV without porogen agent; 4 - sodium chloride; 5 - distilled water; 6 - alginate

As we have already mentioned the cytotoxicity of the PHBHV films was assessed on L929 murine cell line. It is known that porous structures lead to a better cell adhesion of the polymeric materials. Figure III. 3 shows the adherence of the cells onto the PHBHV films and control sample (polystyrene - cells culture plastic) and the image of cells growth on a blank test, respectively on polymer porous film. The porous PHBHV films do not induce a higher cell adhesion as compared to non-porous films. In most of the cases the cytotoxicity was a little bit increased. The porous materials obtained with NaCl do not have significant cytotoxicity effects.

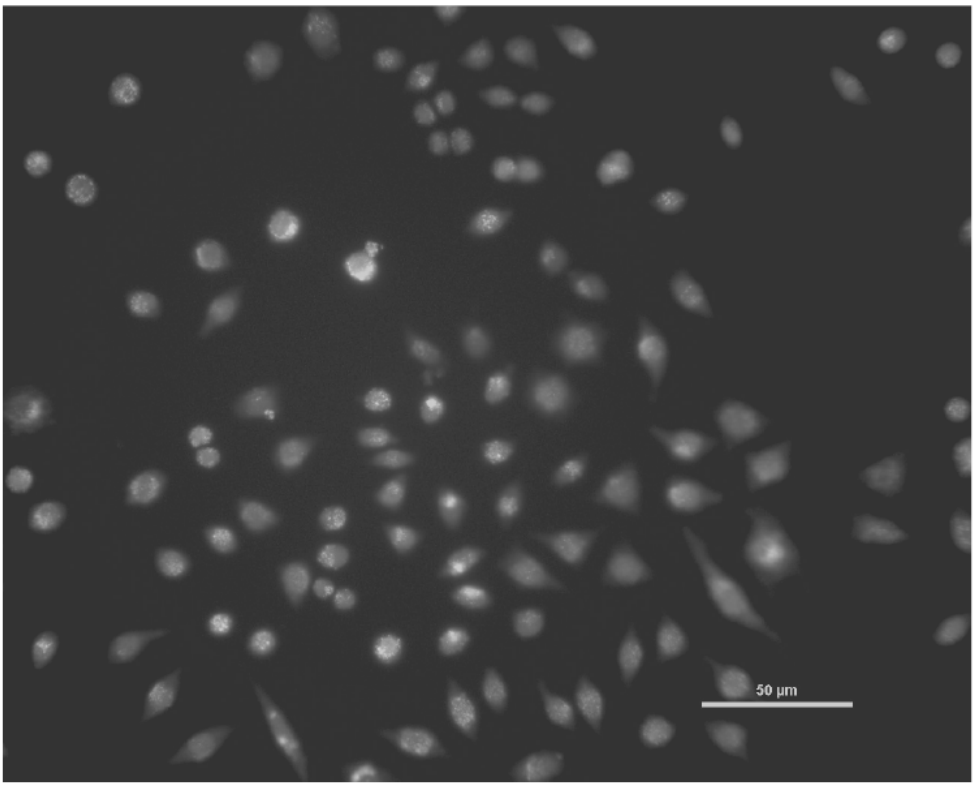

Figure III. 4a: OM microphotographs of cells cultured grown on blank test;

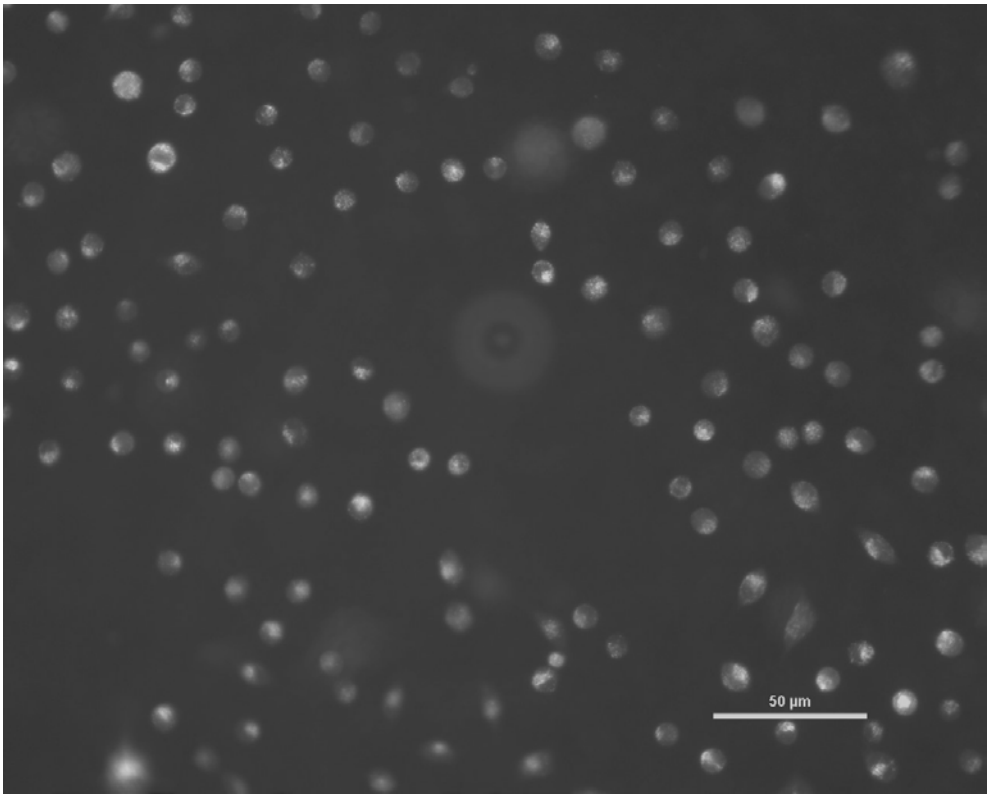

Figure III. 5b: OM microphotographs of cells cultured grown on PHBHV porous films

Conclusions

The PHBHV8% films have a hydrophobic character resulting from the high value of the contact angle. The best porosity was achieved with sodium chloride, but this porous film has an increased cytotoxicity. The idea that the porous structures favour a higher cell adhesion is not sustained by our results with porous polyester films. The optimum cell adhesion was obtained with porous films with gelatine as porogen.

III.3 Mineralization of grafted silk fibroin [19, 20]

The development of osteoconductive biomaterials for bone repair represents a major challenge in the biomedical research. A wide range of materials were used as synthetic bone grafts. The design of osteoconductive behaviour is considered one of the most important characteristics of natural grafts, consisting in apatite-type content and porous interconnected microarchitecture.

Combining these two attributes in a new orthopaedic formulation could ensure the success of the implant via osteoconduction and osteoinduction. The use of polymers, especially the natural polymers, for bone repair allows the synthesis of numerous biomaterials with specific structure and properties. Polymers are used in osseous applications due to their wide chemical composition, to their different mechanical behaviour and because the organic bone matrix are mainly formed by macromolecules.

In order to form apatite deposits in/on the implant, after implantation, polymer must contain negative chemical groups, in order to mimic the activity of bone proteins responsible for mineralization. The respect of the bone porous microarchitecture can be obtained by an innovative solution, using fibrous polymers, forming micro- and macropores by plying.

In the last years there has been an increasing interest in using silk fibroin in biomedical and biological applications. The reasons for using this kind of fibrous material are related to its high mechanical properties combined with flexibility, tissue biocompatibility and good oxygen permeability.

Natural silk fibers have excellent mechanical properties. For example, domesticated *Bombyx mori* silkworm fibers possess a tensile modulus on the order of 5 GPa, strengths of 400 MPa, and tensile elongations of 15 % or more and are able to undergo quite large deformations in compression without kinking.

The mechanical performance of silk is even more remarkable since the fibers are produced under ambient conditions from aqueous solutions. *Bombyx mori* silk fibers consist primarily of two components, fibroin and sericin. Fibroin is the structural protein of the silk fibers while sericin is the water-soluble glue that serves to bond fibres together. The majority of silk

[19] M.R. Tudora, C. Zaharia, A. Diacon, **C.-N. Degeratu**, E. Mircea, C. Andronescu, C. Cincu, N. Preda and I. Enculescu, *Deposition of Bone-Like Hydroxyapatite on Grafted Fibroin Silk Fibers*, Chemical Bulletin of "Politehnica" University of Timisoara 55(69), 1, pp. 82-85, 2010

[20] E. Mircea, C. Zaharia, C. Cincu, F. Miculescu, G. Hubcă, **C.-N. Degeratu**, *Natural fibers modified by chemical methods for application in bone* pathology, Politehnica University of Bucharest. Scientific Bulletin.Series B: Chemistry and Materials Science, 4, 201

fibroin is highly periodic with simple repeating sections broken by more complex regions containing amino acids with bulkier side chains.

The basis, highly repetitive sections are composed of glycine (45 %), alanine (30 %), and serine (12 %) in a roughly 3:2:1 ratio. These three residues contain short side chains and permit close packing of crystals through the stacking of hydrogen-bonded β-sheets. The structure is dominated by [Gly-Ala-Gly-Ala-Gly-Ser]n sequences, with corresponding side groups of H, CH_3, H, CH_3, H, CH_2-OH. The sericin proteins, which comprise approximately 25 wt. % of the silkworm cocoon, contain glycine, serine, and aspartic acid totalling over 60 %.

Hydroxyapatite HA [$Ca_{10}(PO_4)\cdot 6(OH)_2$] is the most commonly used calcium phosphate based biomaterial, which is the major mineral part of natural bones and teeth, due to its excellent biocompatibility, osteoconductivity and bioactivity. To find new ways for the synthesis of improved bone implants materials, combination of HA with other biocompatible polymers of proteins was reported, such as recombinant collagen, chitosan, polylactic acid, and hyaluronic acid.

Bombyx mori silk fibroin is of practical interest because of its excellent intrinsic properties utilizable in the biotechnological and biomedical fields, such as suture, artificial ligament and substrate for cell culture, as well as the importance of silkworm silks in the manufacture of high quality textiles.

The recent researches with biomineralized silk fibroin and silk fibroin/HA composite showed its potential application to be explored as hard tissue replacement materials. However, the mechanism of silk fibroin mediated mineral initiation is far from understood.

In these studies, silk fibroin and cellulose were selected as natural fibres due to their wide use in different biomedical applications. Two types of fibroins were used, secreted by *Bombyx mori* and Phylosamia ricini silk worms.

The focus of this work was on the design of porous materials based on natural fibrous polymers (silk fibroin and cellulose for comparison), modified by grafting with itaconic acid (IA), responsible for the presence of negative groups. IA was chosen because its presumed efficacy, one molecule introducing two acid groups on the fibrous support, this diminishing the level of the grafting agent in the reaction. IA was used in mixture with 2-hydroxyethyl methacrylate (HEMA), a very biocompatible monomer.

After the different treatments, two different protocols to induce the HA deposition were used: in the first method the silk fibroin fiber was immersed into a simulated body fluid (SBF) (Biomimetic method), while the second method involved the pre-treatment with $CaCl_2$ before incubation in SBF1x. The results showed the growth of HA crystal after the mimicking biomineralization.

Experimental

Materials

Cellulose and domesticated silkworm *(Bombyx mori* silk - *Lepidoptera: Bombycidae family)*, cocoons were kindly supplied by Commercial Society SERICAROM SA (Bucharest, Romania). The molecular weight of *Bombyx mori* silk fibroin is approximately 400.000 g/mol.

Sodium bicarbonate (NaHCO3), and sodium dodecyl sulfate (SDS) [$CH_3(CH_2)_{11}OSO_3Na$] were provided by Alfa Aesar GmbH&Co KG, Germany.

2-Acrylamido-2-methylpropane sulfonic acid (AMPSA) reactive monomer with the chemical formula C7H13NO4S, M=207.25 g/mol, m.p.=195 °C was provided by Sigma-Aldrich, St-Quentin Fallavier, France. The AMPSA monomer presented as white crystalline powder or granular particles is used for drug delivery systems, but due of the presence of the acidic sulfonic groups we will try to assess its capacity to initiate the formation of bone mineral phase *in vitro*, by grafting on the silk fibroin support. PAMPSA shows the thermal stability due to the geminal dimethyl group and the sulfomethyl group. It is very soluble in water and dimethylformamide (DMF) and also shows limited solubility in most polar organic solvents.

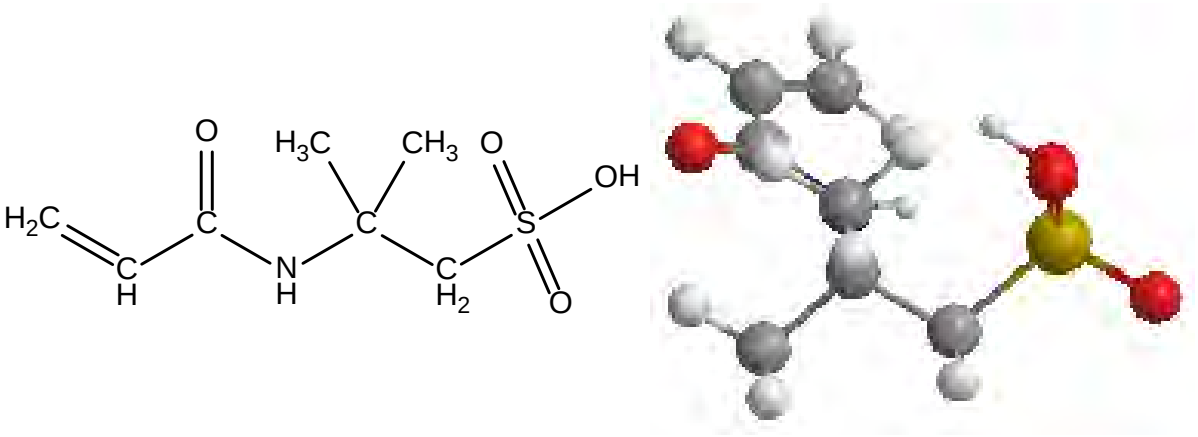

Figure III. 6: Linear and 3D model of 2-Acrylamido-2-methylpropane sulfonic acid (AMPSA) structure

Commercial 2-hydroxyethyl methacrylate (HEMA) was purchased from Aldrich and purified by extraction with 3% (w/v) solution of sodium bicarbonate ($NaHCO_3$) in distilled water, extracted with chloroform ($CHCl_3$) and the solvent was removed by rotary evaporation under vacuum. HEMA was made free of $CHCl_3$ by distillation (b.p. 75 °C at 3 mmHg).

2-Hydroxyethyl methacrylate (HEMA), a liquid monomer with the chemical formula C6H10O3, M=130.14 g/mol, ρ=1.073 g/cm3 was purified by distillation under reduced pressure. The polymer, noted PHEMA, biocompatible, nontoxic, including the most widely used polymers in the biomedical sector. The HEMA polymer presents a similar water content of human tissues, high resistance to degradation and is not absorbed by the body. PHEMA presents various substitutions that lead to the formation of a wide range of its derivatives for multiple medical applications, such as contact lenses, controlled delivery systems of drugs, and artificial membranes.

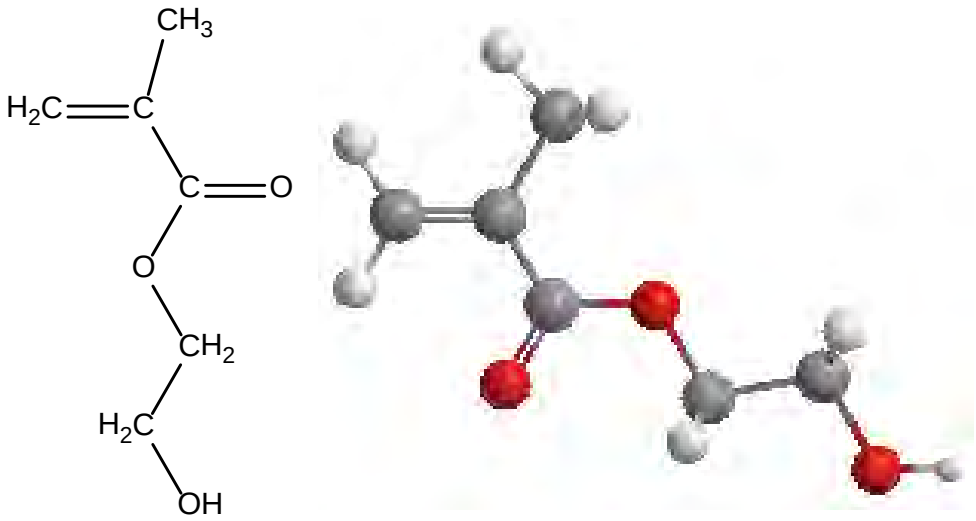

Figure III. 7: Linear and 3D model of 2-Hydroxyethyl methacrylate (HEMA) structure

2-Diethylaminoethyl methacrylate (DEAEMA) with the chemical formula C10H19NO2, M=185.3 g/mol, b.p.=80 °C was purified by distillation under reduced pressure. DEAEMA is a colourless liquid is a monofunctional acrylate monomer with dual methacrylic and amine reactivity.

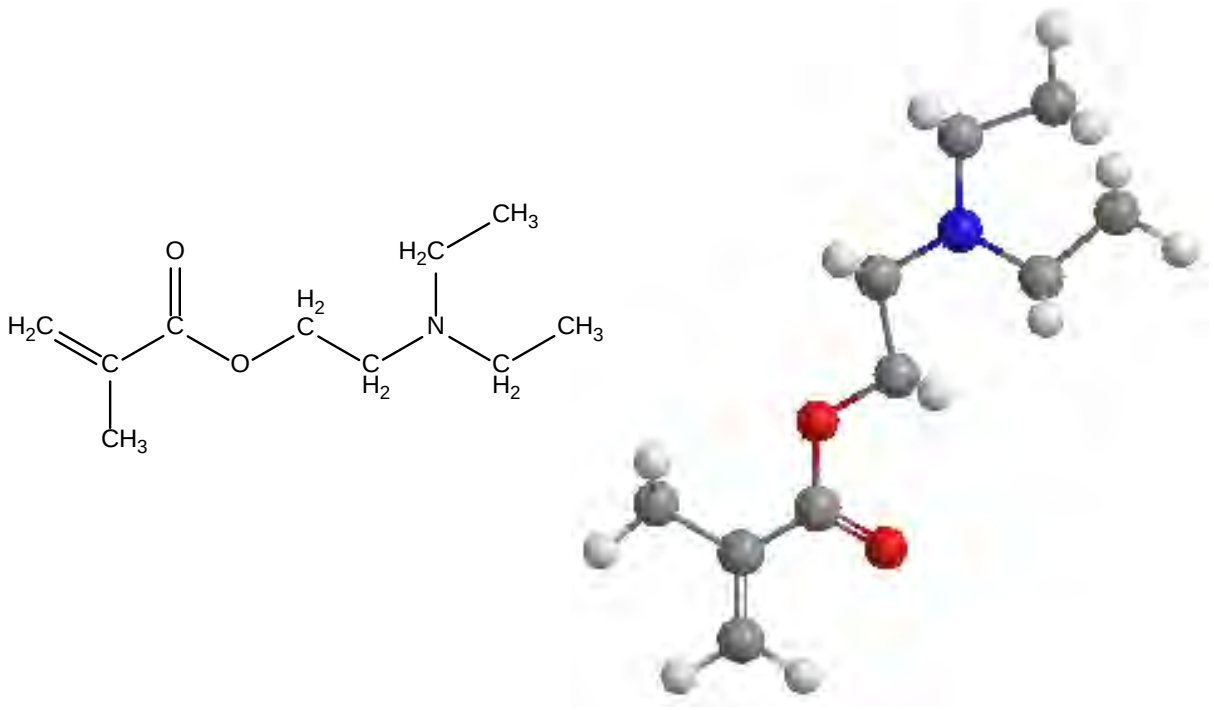

Figure III. 8: Linear and 3D model of 2-Diethylaminoethyl methacrylate (DEAEMA) structure

Itaconic acids (IA) (Aldrich), potassium persulphate (PSK) (Fluka) and ammonium cerium nitrate (ACN) (Merck) were used without any further purification. All other substances were of analytical or pharmaceutical grade and obtained from Sigma-Aldrich.

Methods

The processing of Bombyx mori natural silk in order to obtain pure silk fibroin.In order to ensure complete removal of sericin, the purification method used was adapted according to the literature. *Bombyx mori* silkworm were cut and boiled for 30 min 0.5 % (w/v) NaHCO3 and SDS and then rinsed thoroughly with distilled water to extract the sericin protein. This operation was repeated three times to get the pure silk fibroin. The degummed silk fibroin was dried at 40 °C and atmospheric pressure.

IA-HEMA grafting onto cellulose and silk fibroin fibers

Cellulose was washed three times for 1 hour with boiling demineralised water, followed by drying at 40°C (up to constant mass). The grafting reaction developed in heterogeneous medium because the reaction mixture was liquid and the fibrous support solid. Cellulose was weighted and introduced in an acid solution of ceric salt, with nitrogen bubbling for 10 minutes.

The monomers mixture and sulphuric acid 0.1N was added, followed by nitrogen bubbling for 15 minute. The reaction temperature was 45°C, in inert atmosphere, for 90 minutes. At the end of the reaction, the fibers were washed with demineralised water and extracted in order to completely eliminate the residual monomers.

Several compositions were synthesized, as shown in Table III. 2, using constant IA:HEMA ratios (30:70) and different monomer/substrate ratios. The solution of ACN was used in 0.1N sulphuric acid. All samples were washed with distilled water, extracted to remove residual monomers and dried (up to constant mass).

Table III. 2: Reaction mixture for grafting of IA-HEMA onto cellulose

Reactive	Role	Quantity		
		1	**2**	**3**
Cellulose	Substrate	0.5 g	0.5 g	0.5 g
ACN	Initiator	5.45 mmole	5.45 mmole	5.45 mmole
HEMA	Monomer	1.95 mL	2.54 mL	3,9 mL
IA solution 5%	Monomer	17.94 mL	23.4 mL	35.88 mL
Sulfuric acid 0.1 N	Catalyst	25 mL	25 mL	25 mL

Two types of fibroin were used as fibrous substrates: *Bombyx mori* (FBM) and *Phylosamia ricini (*FPR). Fibroin samples were extensively washed with boiling water solution of Na2CO3 0.5M and NaHCO3 0.5M for 30 minutes in order to eliminate the sericine and then dried at 40°C. Two initiators were used for grafting of IA-HEMA: PSK and ACN. Two copolymers series were synthesized using both FPR and FBM fibres. The ratios initiator fibroin were 1/10 and 1/5 (w/w), Table III. 3.

Table III. 3: Reaction mixture for IA grafting onto fibroin

Reactive	Role	Quantity			
		1/10		**1/5**	
		FPR	FBM	FPR	FBM
FPR or FBM	Substrate	0.5 g	0.5 g	0.5 g	0.5 g
ACN	Initiator	0.31 g	0.31 g	0.61 g	0.61 g

HEMA	Monomer	1.7 mL	1.7 mL	3.4 mL	3.4 mL
IA aqueous solution 5%	Monomer	15 mL	15 mL	11.2 mL	11.2 mL
Sulfuric acid 0.1 N	Catalyst	25 mL	25 mL	25 mL	25 mL
FPR or FBM	Substrate	0.5 g	0.5 g	0.5 g	0.5 g
PSK	Initiator	0.05 g	0.05 g	0.05 g	0.05 g
HEMA	Monomer	1.7 mL	1.7 mL	3.4 mL	3.4 mL
IA aqueous solution 5%	Monomer	15 mL	15 mL	11 mL	11 mL

Fibroin was initially treated with acidic solution of cerium (IV) salt at 45°C under nitrogen bubbling for 10 minutes. The mixture of monomers was added under nitrogen atmosphere for 15 minutes. The reaction developed at 45°C under inert atmosphere for 90 minutes.

The grafting initiated by PSK (1/10 w/w PSK/fibroin) was performed at 70°C, for 90 minutes. All samples were washed with distilled water, extracted to remove residual monomers and dried up to constant mass.

Grafting AMPSA, HEMA-AMPSA onto fibroin fiber

The grafting procedure was adapted from literature and mainly consists in: the fibers are treated with ammonium cerium nitrate (Ce4+) in sulphuric acid solution (0.1N) under inert atmosphere for 30 min. Then the monomer solution of AMPSA, HEMA, HEMA-AMPSA (10 % molar composition of AMPSA), and DEAEMA were added in the reaction medium and the temperature was raised to 45 °C. After 24 hours the grafting reactions were almost complete and the fibers were rinsed with demineralised water to remove the residual cerium salt and dried over night at 37 °C. The recipes are presented in Table III. 4 and the installation of grafting monomers is presented in Figure III. 25.

Table III. 4: Recipes for silk fibroin grafting monomers

System	Mass ratio w/w
Initiator : SF	1/5
AMPSA : SF	1/4
AMPSA : SF	1/7
HEMA-AMSPA* : SF	1/4
HEMA-AMSPA* : SF	1/7
DEAMA : SF	1/4
DEAMA : SF	1/7
*** moral ratio of HEMA : AMSPA = 1 : 9**	

Figure III. 9: Lab installation for silk fibroin grafting monomer

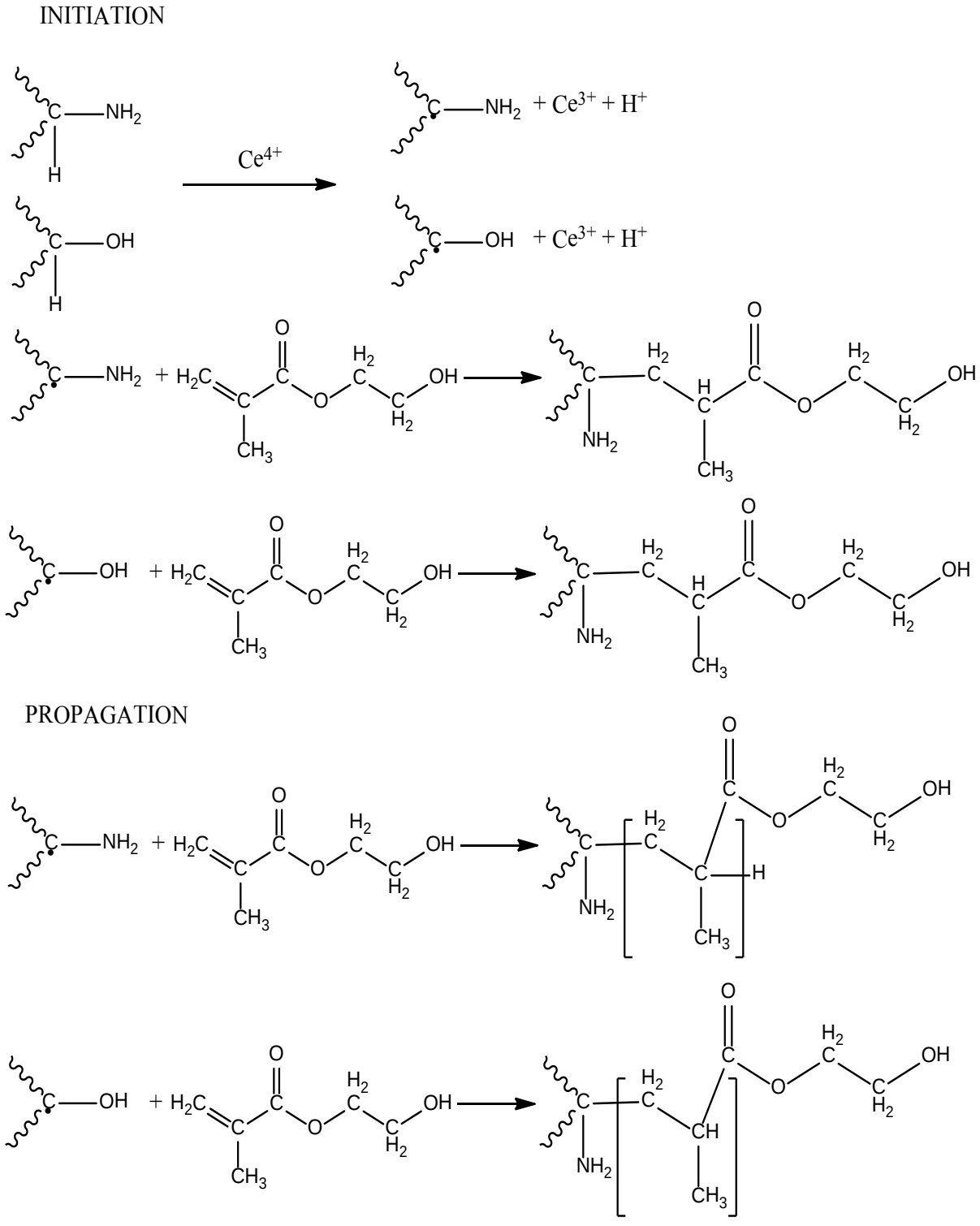

Figure III. 10: HEMA grafting mechanism

Biomineralization assay

Biomineralization assay of grafted cellulose and fibroin fibers with IA-HEMA

In vitro tests were performed by two methods:

- The classical incubation method (biomimetic) in 1x and 1.25x synthetic body fluid (SBF) having the composition similar to that of human plasma, for 14 days at *p*H=7.42 and 37°C, see Table III. 5.
- The incubation method based on alternating cycles in two solutions: $CaCl_2$ 200mM/Tris-HCl at *p*H=7.42 (Ca solution) and Na_2HPO_4 150mM (P solution).

The samples were weighed and then immersed in 25 ml Ca solution at 37 °C for 2 hours. After this procedure the samples were washed with distilled water and immersed in P solution at 37 °C for 2 hours. This procedure was repeated three times.

Table III. 5: Synthetic body fluid (SBF) and human blood plasma compositions

Ion	SBF 1x (mM)	Human plasma (mM)
Na^+	142.19	142.0
K^+	4.85	5.0
Mg^{2+}	1.5	1.50
Ca^{2+}	2.49	2.5
Cl^-	141.54	103.0
HCO_3^-	4.2	27.0
HPO_4^{2-}	0.9	1.0
SO_4^{2-}	0.5	0.5

Biomineralization assay of grafted fibroin fibers with AMPSA, HEMA-AMPSA

To test the ability to induce the hydroxyapatite formation *in vitro*, the surface-modified fibroin fibers were incubated in SBF 1x. Incubation in synthetic body fluid (SBF 1x) at 37 °C, *p*H=7.4, normal pressure for 14 days (BIOMIMETIC METHOD).

The surface-modified silk fibroin fibers and the surface-modified silk fibroin fibers preliminary immersed in $CaCl_2$ solution, were soaked in 45 mL of SBF 1x (mM), in sterile medium to avoid the possible contaminations that may lead to false results, in PE vials, of *p*H 7.4 and ion concentration (Na^+, 142.19; K^+, 4.85; Mg^{2+}, 1.5; Ca^{2+}, 2.49; Cl^-, 141.54; HCO_3^-, 4.2; HPO_4^{2-}, 0.9; SO_4^{2-}, 0.5 mM) approximately equal to those of human blood plasma at 37 °C for 14 days. The SBF 1x was obtained by dissolving the corresponding quantities of salts NaCl, $NaHCO_3$, KCl, K_2HPO_4, $MgCl_2 \cdot 6H_2O$, $CaCl_2$ and Na_2SO_4 in demineralised water. The *p*H of this body synthetic fluid is the physiologic *p*H 7.4, and it is achieved by using a buffer solution of tris (hydroxymethyl) aminomethane (Tris) and hydrochloric acid (HCl). The medium was changed every 2 days. After the soaking period (14 days), the fibrous specimens were removed from the fluid, gently washed with demineralised water, and then dried at room temperature for 24 h.

Physico-chemical characterization

Physico-chemical characterization of grafted cellulose and fibroin fibers with IA-HEMA

a. SEM analysis

SEM analysis of the morphology of the fibrous materials was achieved with an electronic microscope SMPE XL 30 Philips.

b. Ca and P dosage

Calcium and phosphorus dosage was performed by the colorimetric method. For calcium deposits orthocresolphtaleine was used at 570 and 660 nm, and for phosphorus deposits the complex ammonium phosphomolibdate was used at 340 and 375 nm.

Physico-chemical characterization of grafted fibroin fibers with AMPSA, HEMA-AMPSA

a) FTIR-ATR characterization

The FTIR Spectra were recorded on a VERTEX 70 BRUCKER instrument, using 32 scans with a resolution of 4 cm^{-1}, in the 4000-600 cm^{-1} wavenumber region.

b) XPS characterization

XPS analysis was performed on a K-Alpha instrument from Thermo Scientific, using a monochromated Al Kα source (1486.6 eV), at a pressure of $2 \cdot 10^{-9}$ mbar. Charging effects were compensated by a flood gun, and binding energy was calibrated by placing the C 1s peak at 285 eV as internal standard. The survey spectra were registered using pass energy of 200 eV.

c) SEM analysis

The surface morphology of the samples was obtained through the Scanning Electron Microscopy (SEM) analysis. The analysis has been performed using a ZEISS EVO 50 XVP Scanning Electron Microscope.

Grafting yield

The grafting initiated by PSK (1/10 w/w PSK/fibroin) was performed at 70°C, for 90 minutes. All samples were washed with distilled water, extracted to remove residual monomers and dried up to constant mass.

The results of the grafting reactions were gravimetrically evaluated and also by scanning electronic microscopy (SEM).

Gravimetric evaluation represents the "mass gain" compared to the initial weight of the unmodified fibres, offering quantitative information on the copolymer deposited onto the fibres. The grafting yield (η) was calculated using the equation below:

$$\mu = \frac{m_f - m_i}{m_i} \times 100$$

where:

m_i – the weight of the unmodified fibre before grafting, and m_f – represent the final mass.

Results and discussions

Grafting yield of grafted cellulose and fibroin fibers with IA-HEMA

All reactions have significant values of the GR with values ranging from 37% and 302%., these results proving the grafting reactions. When PSK is used as initiator, the values of GR

are higher than 100%, but these values show also the homopolymerisation and copolymerisation reactions that accompany the grafting ones.

The results of the gravimetric analysis are presented in Table III. 6.

Table III. 7: Grafting ratio values

No.	Fibrous support	Grafting with IA-HEMA		GR (%)
1	FBM	Initiator Ce^{4+}		37
2	FBM	Initiator PSK		122
3	FPR	Initiator Ce^{4+}		42
4	FPR	Initiator PSK		302
5	Cellulose	Initiator Ce^{4+}	0.023 moles (IA-HEMA)	79
6	Cellulose	Initiator Ce^{4+}	0.03 moles (IA-HEMA)	60
7	Cellulose	Initiator Ce^{4+}	0.046 moles (IA-HEMA)	61

The presence of the homopolymer PHEMA and copolymer IA-HEMA covering the fibres was also noticed by the SEM analysis.

Grafting yield of grafted fibroin fibers with AMPSA, HEMA-AMPSA

The values for the grafting yields were between 40 and 50 %; η_{AMPSA} = 40%, $\eta_{HEMA\text{-}AMPSA}$ = 50%, and η_{DEAEMA} = 45%.

Ca and P dosage grafted cellulose and fibroin fibers with IA-HEMA

For the fibroin modified with ammonium cerium nitrate and monomer mixture HEMA / IA = 90 / 10 (mole / mole), the mineral deposits resulted after incubation were analysed (Figure III. 27a - d). The Ca/P ratio was estimated at 1.6, value that is very close to that of hydroxyapatite (1.67).

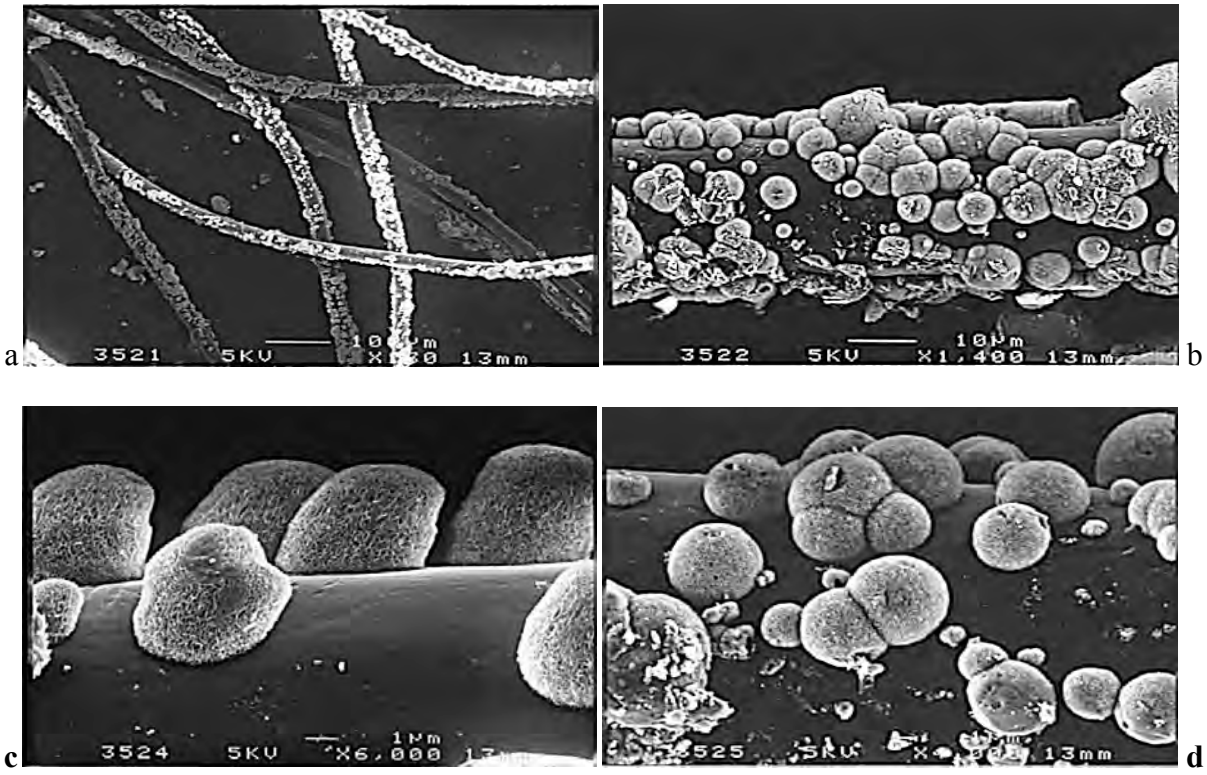

Figure III. 11: SEM of the globular mineral deposits on grafted silk fibroin using (NH4)2Ce(NO3)6 as initiator, incubated in SBF at 37°C: a, b – grafts based on HEMA-IA 10%, monomers/fibroin=2/1; c, d – grafts based on HEMA-IA 10%, monomers/fibroin=4/1

FTIR-ATR measurements

The results of the FTIR-ATR spectra gave us the specific absorbance wavelengths of the specific bonds which appeared in the surface-grafted silk fibroin fibers. The specific absorption band of silk fibroin: amide I (C=O stretching) at 1623 cm^{-1}, amide II (N-H deformation and C-N stretching) at 1512 cm^{-1}, and amide III (C-N stretching and N-H deformation) at 1228 cm^{-1}.

The grafting of AMPSA monomer could not be evidenced by FTIR-ATR analysis (Figure. III. 28). The obtained FTIR-ATR spectra for the HEMA-AMPSA modified silk fibroin contain the characteristic bands of the specific groups carbonyl at 1709 cm^{-1} and hydroxyl at 3384 cm^{-1} (Figure III. 29).

In the case of DEAEMA, for the mass ratio of 1/4 fibroin/monomer does not notice the difference in the FTIR-ATR spectrum, but at a mass ratio of 1/7 fibroin/monomer the FTIR-ATR analysis confirmed the spectral modification through the shifting of the amides I, II, and III (Figure III. 30).

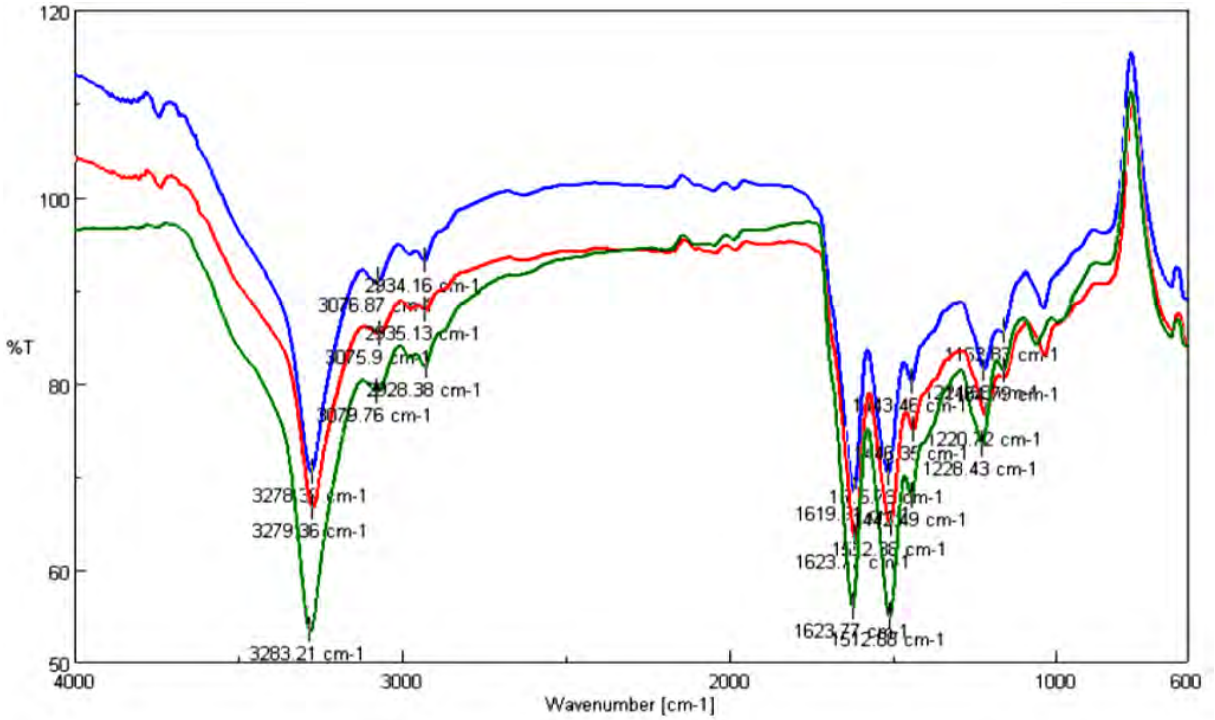

Figure III. 12: FTIR-ATR spectra for (green line) unmodified silk fibroin, (red line) silk fibroin grafted with AMPSA (1/4, w/w); (blue line) silk fibroin grafted with AMPSA (1/7, w/w)

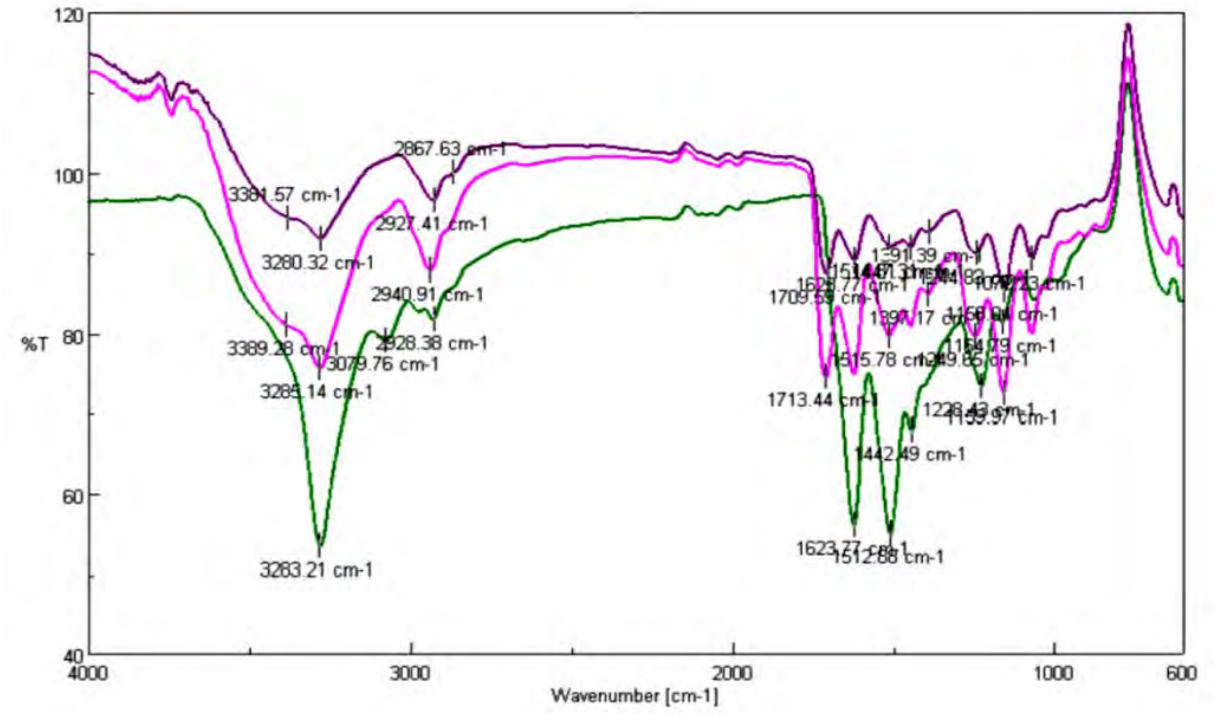

Figure III. 13: FTIR-ATR spectra for (green line) unmodified silk fibroin, (purple line) silk fibroin grafted with AMPSA (1/4, w/w); (pink line) silk fibroin grafted with AMPSA (1/7, w/w)

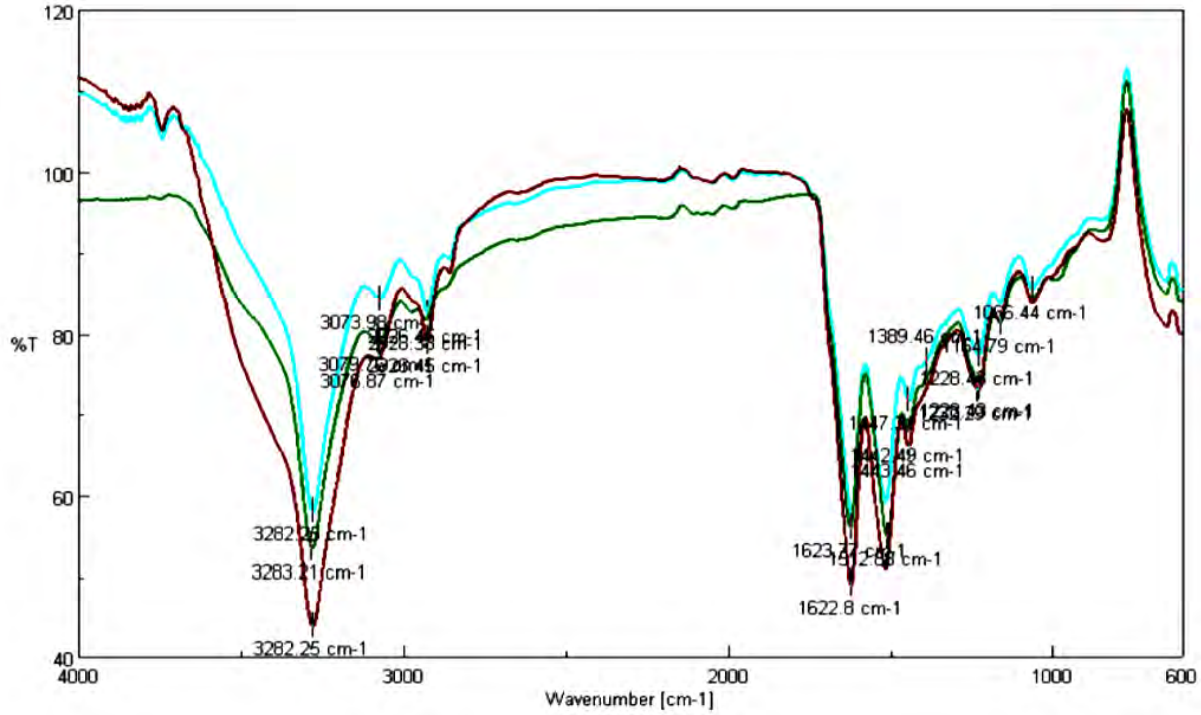

Figure III. 14: FTIR-ATR spectra for (green line) unmodified silk fibroin, (cyan line) silk fibroin grafted with DEAEMA (1/4, w/w); (brown line) silk fibroin grafted with DEAEMA (1/7, w/w)

XPS characterization

XPS spectra of the grafted silk fibroin with HEMA-AMPSA and AMPSA reveal the presence of S peak in these samples (Table III. 8, and Figures III. 32, III. 33), which is not present within the blind fibroin sample.

Table III. 8: Elemental ID and quantification

	Peak BE (eV)				At. %			
	C 1s	O 1s	N 1s	S 2p	C 1s	O 1s	N 1s	S 2p
SF	285.35	532.21	399.92	-	75.62	12.04	11.57	-
SF/AMPSA (1/4, w/w)	284.56	530.55	398.89	167.29	58.89	28.43	10.06	2.61
SF/AMPSA (1/7, w/w)	284.09	530.44	398.69	167.16	72.23	18.90	6.21	2.66
SF/HEMA-AMPSA (1/4, w/w)	285.08	531.82	-	-	62.60	37.40	-	-
SF/HEMA-AMPSA (1/7, w/w)	284.95	531.89	399.18	167.52	64.84	33.94	1.02	0.19

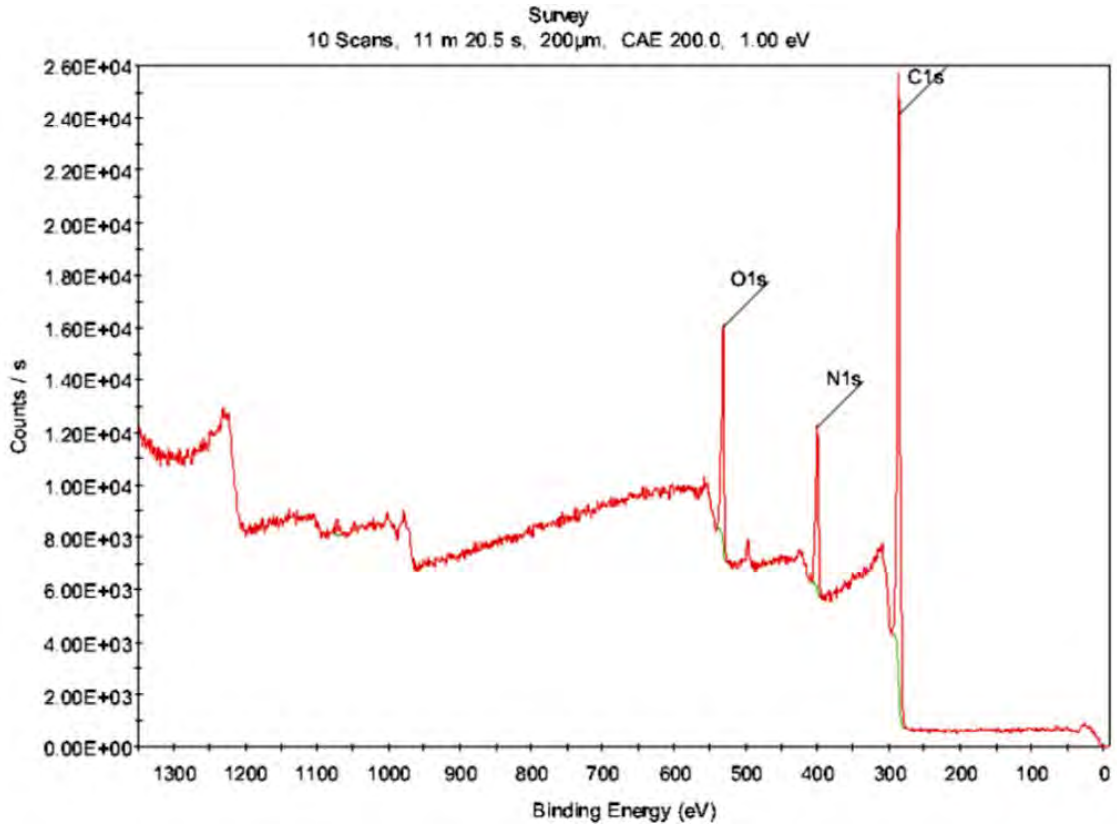

Figure III. 15: XPS spectrum of ungrafted silk fibroin

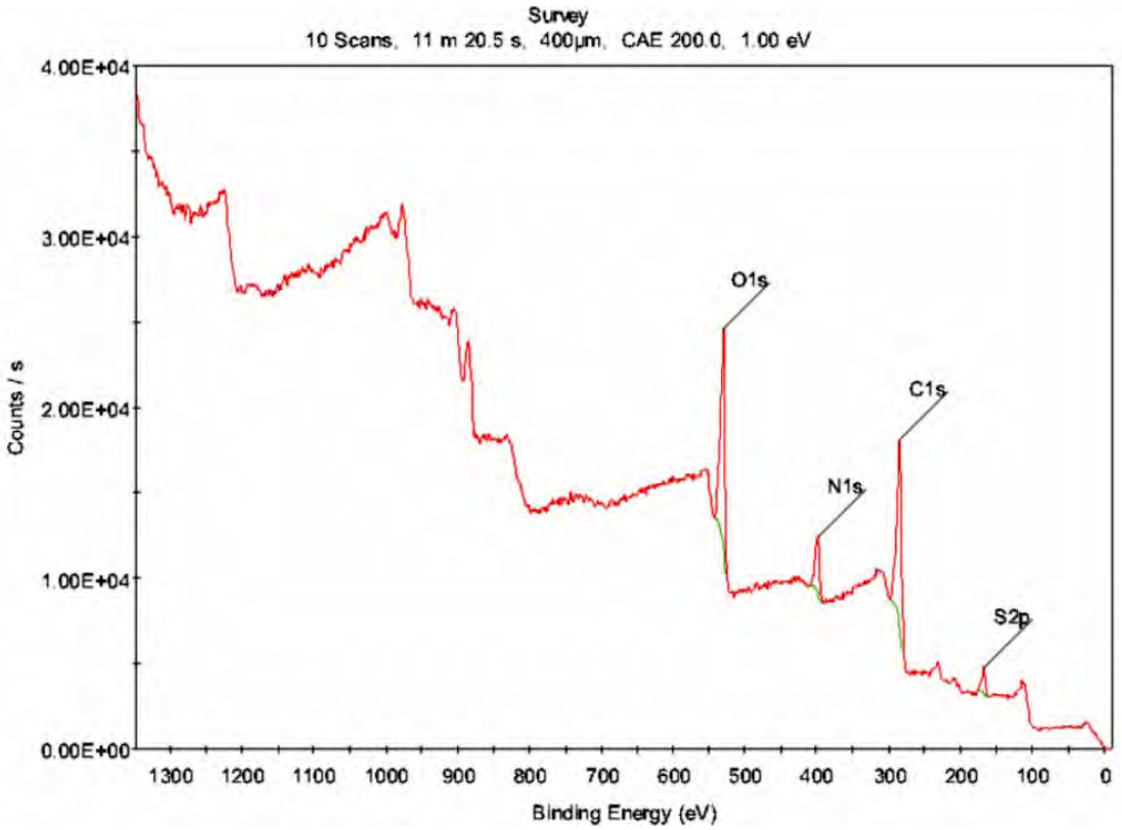

Figure III. 16: XPS spectrum of silk fibroin grafted with AMPSA (1/4, w/w)

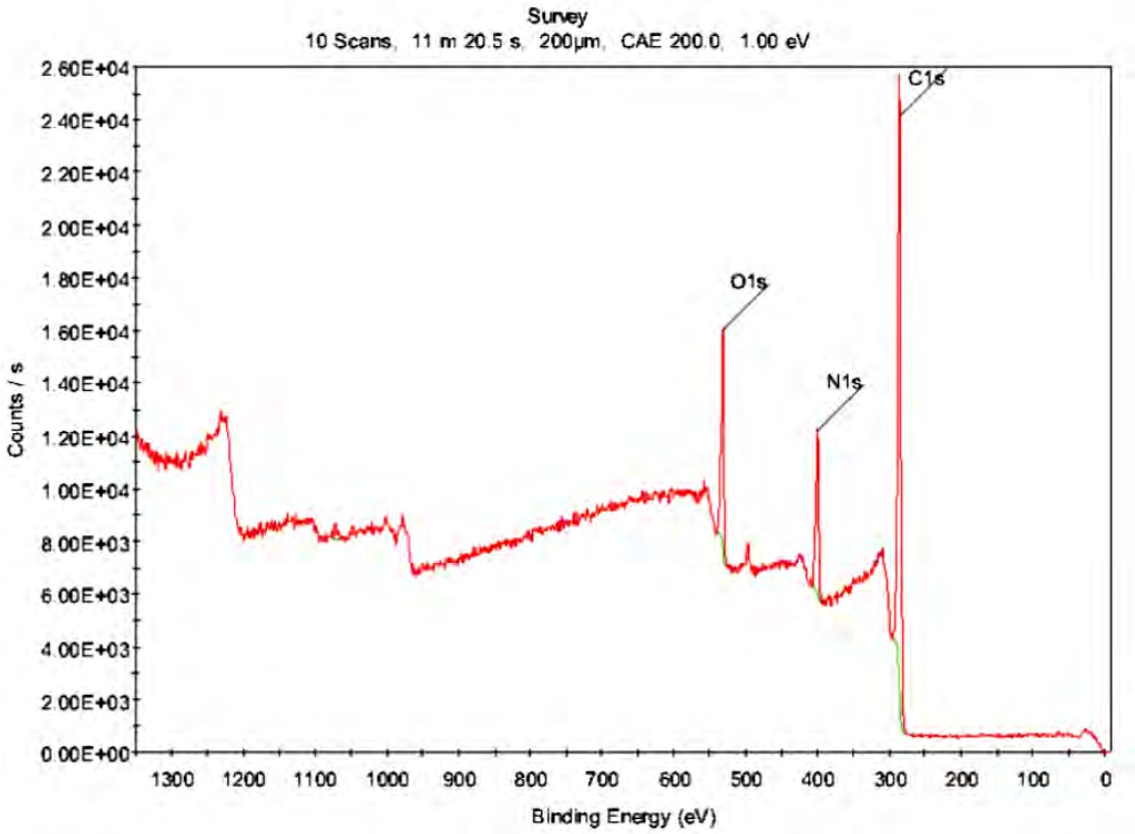

Figure III. 17: XPS spectrum of silk fibroin grafted with AMPSA (1/7, w/w)

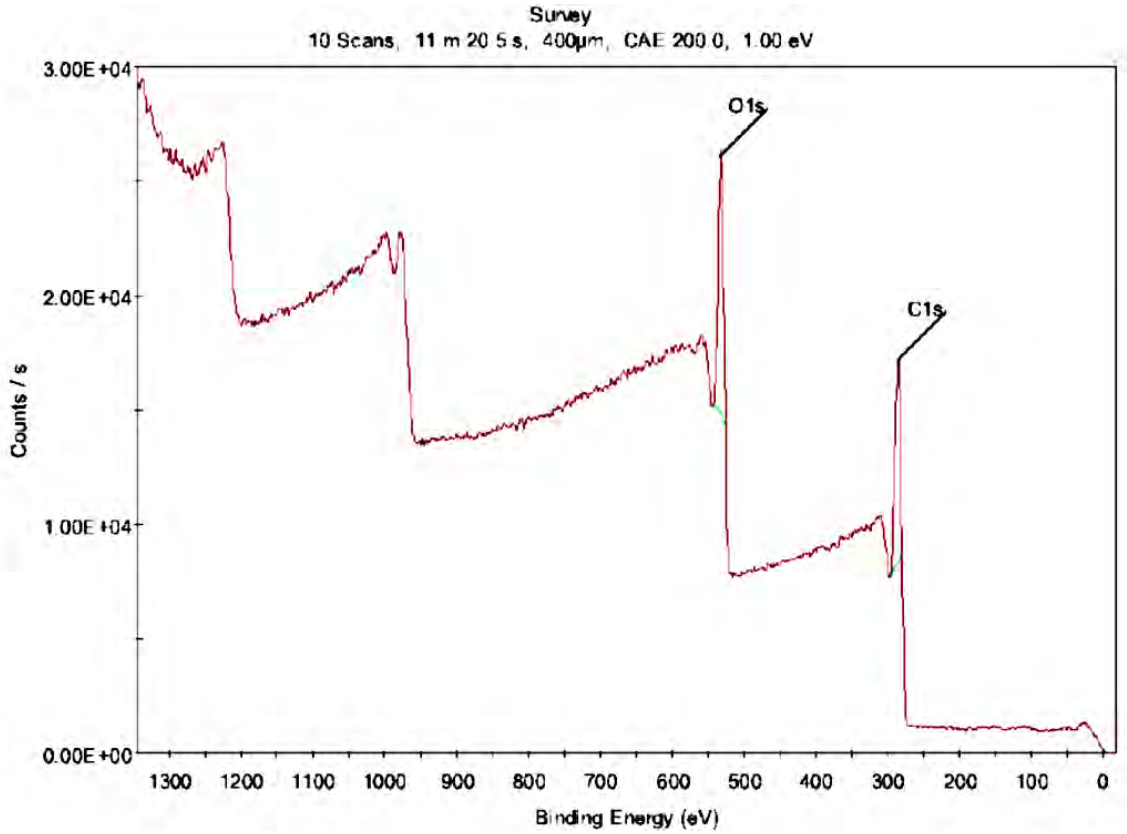

Figure III. 18: XPS spectrum of silk fibroin grafted with HEMA-AMPSA (1/4, w/w)

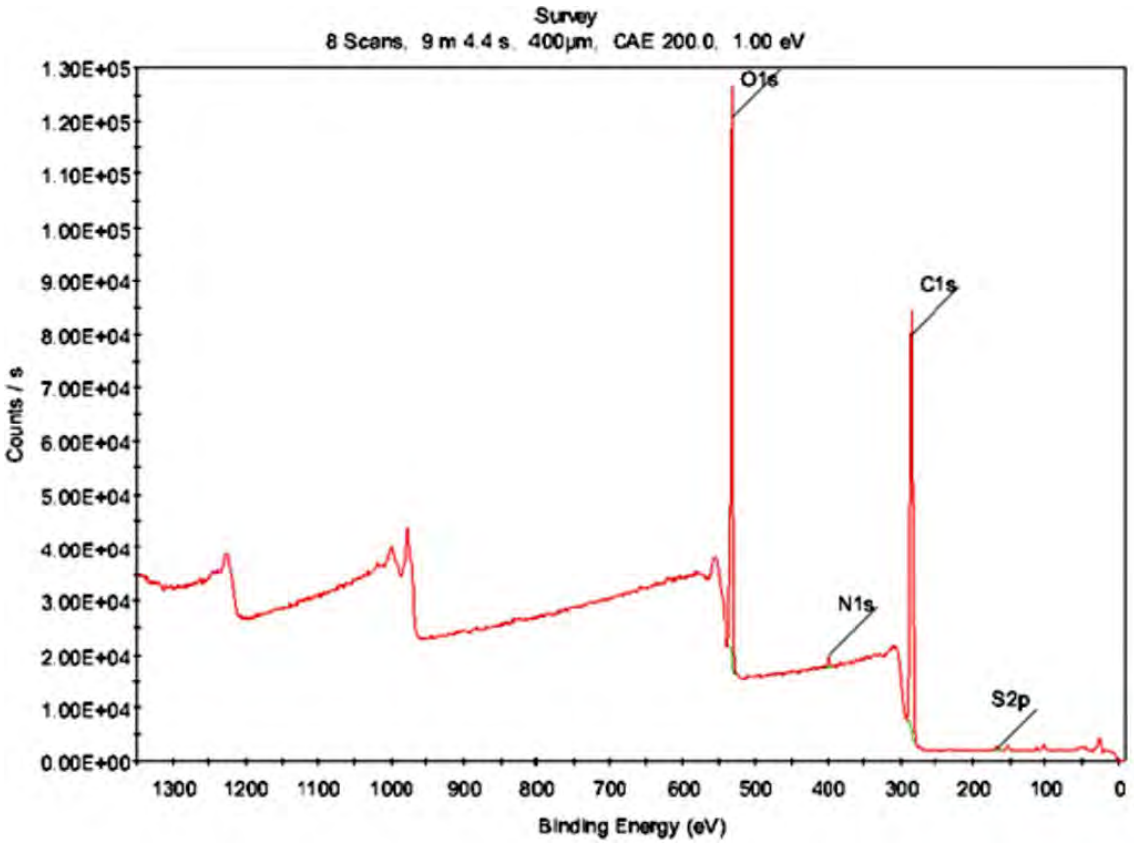

Figure III. 19: XPS spectrum of silk fibroin grafted with HEMA-AMPSA (1/7, w/w)

Biomineralization assay and SEM analysis

Biomineralization assay and SEM analysis of grafted cellulose and fibroin fibers with IA-HEMA

The results of the SEM examination of the fibrous samples are selectively presented in Figures III. 36 - III. 39. The grafted samples were analysed as compared to the original fibres, at different magnification levels (100X, 500X, 2500X, 5000X).

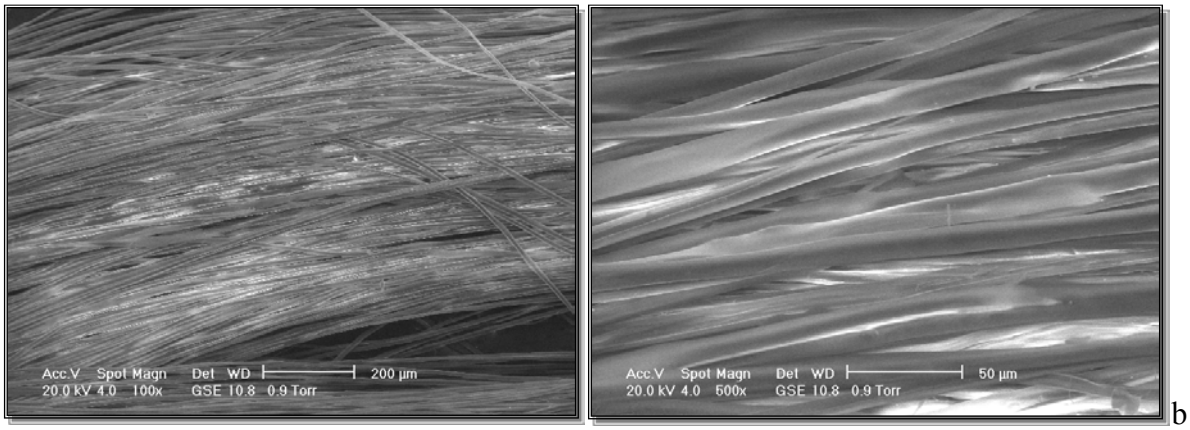

a b

Figure III. 20: SEM morphology of the original *Bombyx mori* silk fibroin general view (a - 100X; b - 500X)

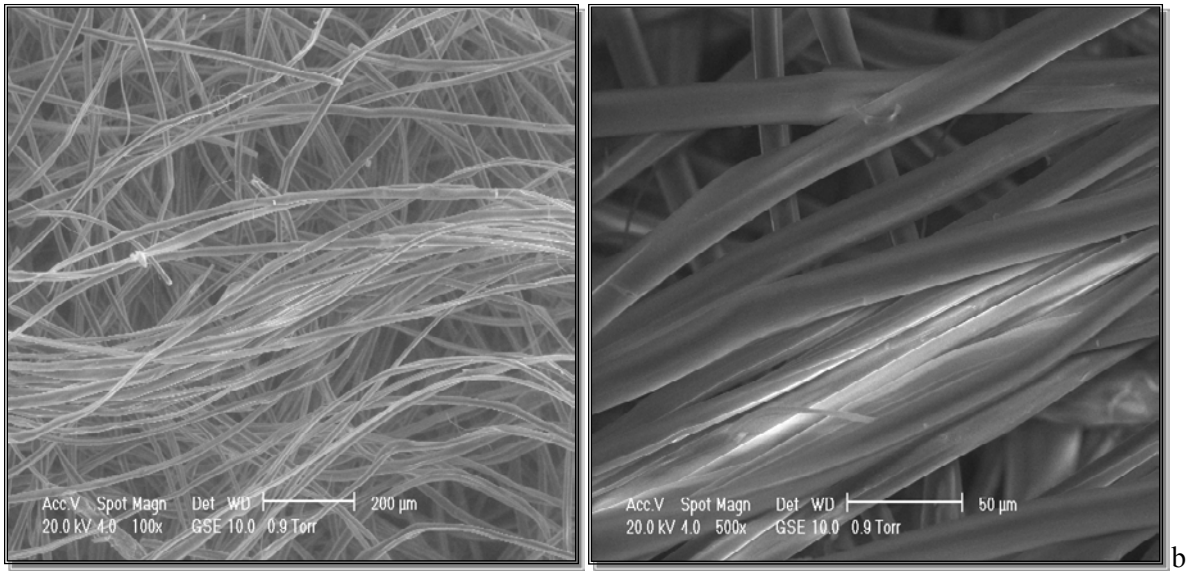

a b

Figure III. 21: SEM morphology of *Bombyx mori* silk fibroin grafted with IA-HEMA (initiator Ce4+) general view (a - 100X; b - 500X)

SEM allows the analysis of the morphology of the fibres following the grafting reaction. This technique offers the possibility to establish the formation of copolymer grafts or/and copolymer deposition on fibrous substrate, without offering specifications about the chemical nature. Some modifications, even if proved by the gravimetric evaluation are not obvious from the point of view of morphological changes. *Bombxy mori* silk fibroin has the same appearance when grafted with IA-HEMA monomers and cerium salt initiator (Figure III. 36 and III. 37). The results obtained for the PSK initiation of silk fibroin grafting are very interesting (Figure III. 38).

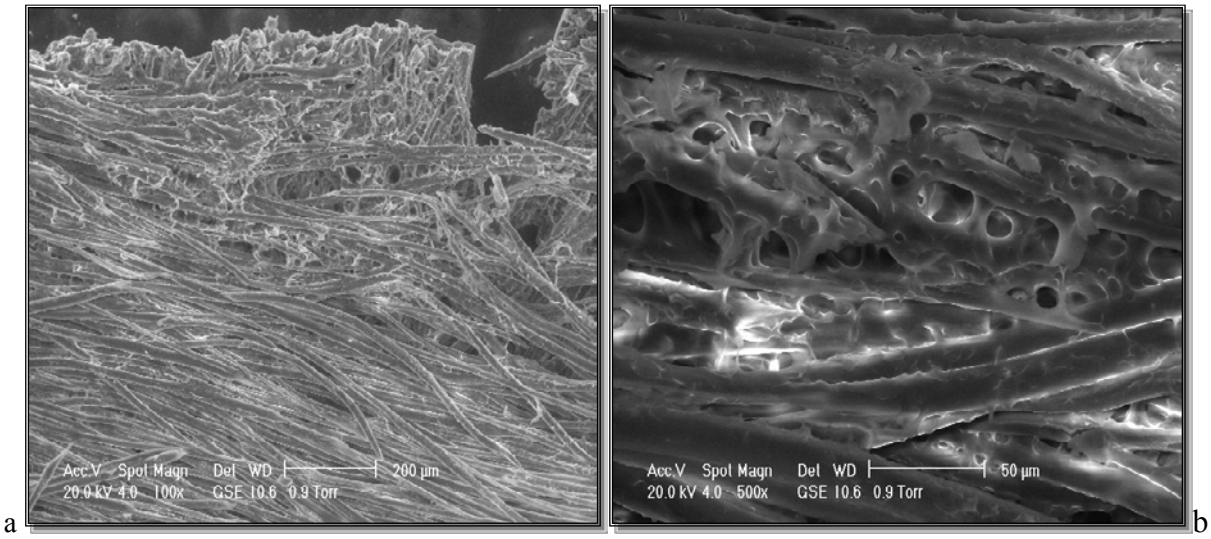

a b

Figure III. 22: SEM morphology of *Bombyx mori* silk fibroin grafted with IA-HEMA (PSK initiator) general view (a - 100X; b - 500X)

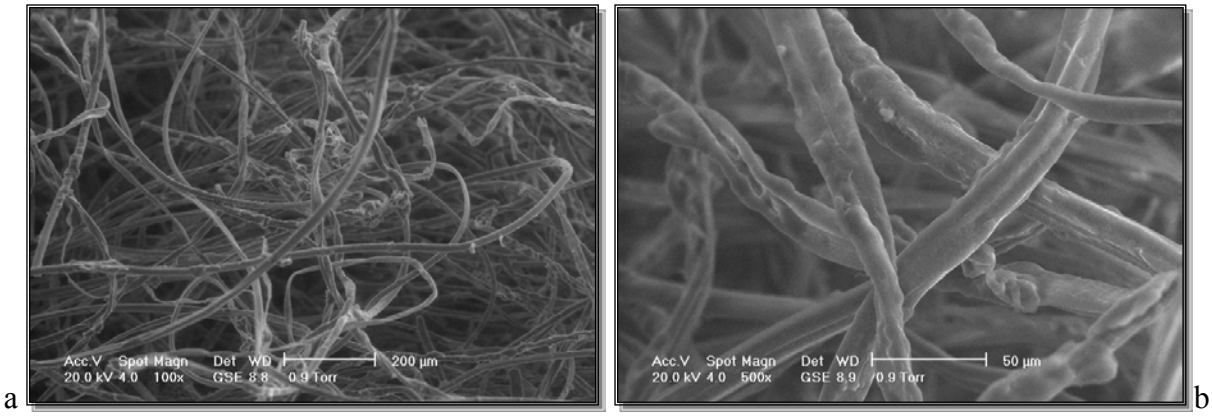

a b

Figure III. 23: SEM morphology of cellulose grafted with 0.03 moles of IA-HEMA general view (a - 100X; b - 500X)

The morphology of the grafted fibers corresponds to interconnected pores, mimicking the trabecular bone architecture. The interconnection is evident (Figure III. 38b), and the copolymer IA-HEMA connection to the fibroin fibers. This behavior is very important by combining the interconnected porosity with the presence of numerous negative groups in the material. The morphology of cellulose fibers after modification is selectively presented in Figure III. 39. Copolymer globular deposits appeared on the cellulose fibers.

Biomineralization assay and SEM analysis of grafted fibroin with grafted fibroin fibers with AMPSA, HEMA-AMPSA

Mineralization potential is a very important property of polymeric biomaterials, which greatly influences their application filed. The Kokubo et al. (1990-2006) method of *in vitro*

evaluation was chosen. The procedure involves samples incubation in simulated body fluid (SBF) in different concentration. The mineralization capacity of the crude silk fibroin and grafted silk fibroin with AMPSA, HEMA-AMPSA, and DEAEMA was assessed through SEM analysis (Figure III. 42, 43, 46, 47, 50, 51).

As we could see from these figures, all the grafted fibroin fibers soaked in SBF 1x, and also pretreated with $CaCl_2$ were covered with a mineral layer whose morphology highlight the apatite forms, tablet type with different sizes. They were clear difference between the incubated, pretreated and incubated crude silk fibroin, and grafted silk fibroin also incubated and pretreated with $CaCl_2$ and incubated in SBF.

The $CaCl_2$ pretreatment induces a significant amount of mineral deposits. The morphology is similar to that of apatite crystals observed on bioactive glasses after heaving soaked in SBF. Smaller forms were obtained for the DEAEMA monomer (Figure III. 48 and III. 49).

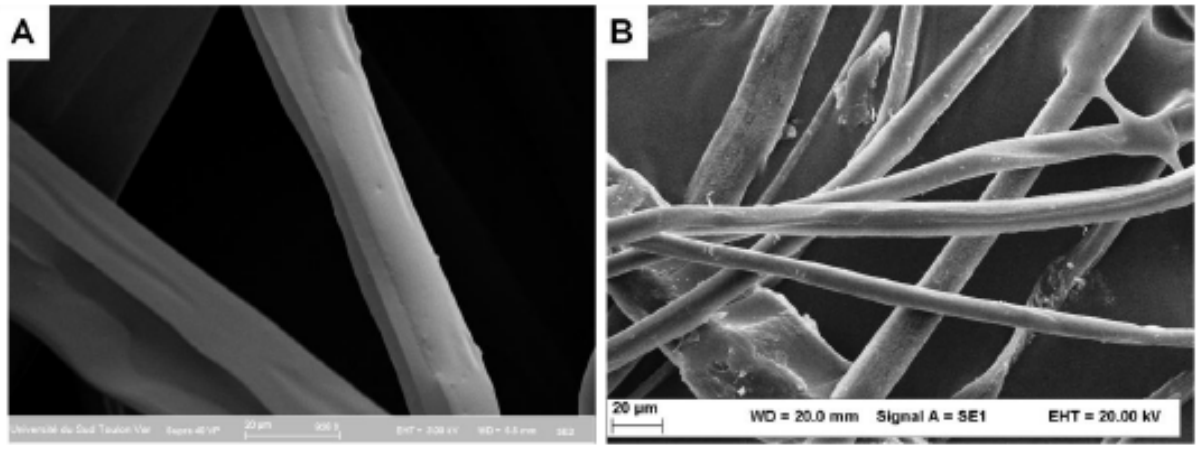

Figure III. 24: SEM images of the A) crude silk fibroin, B) crude silk fibroin incubated in SBF 1x

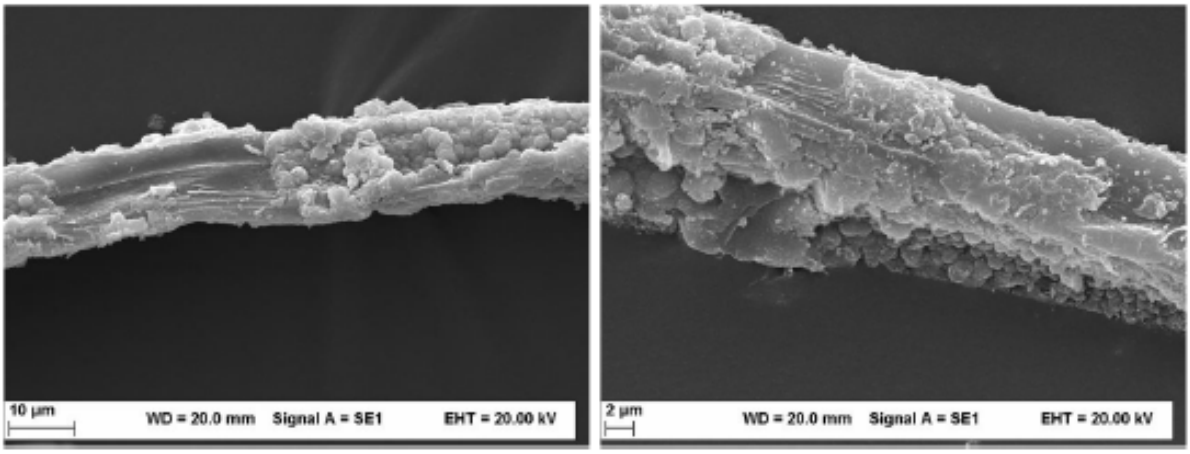

Figure III. 25: SEM images of the crude silk fibroin pretreated with $CaCl_2$, incubated in SBF 1x

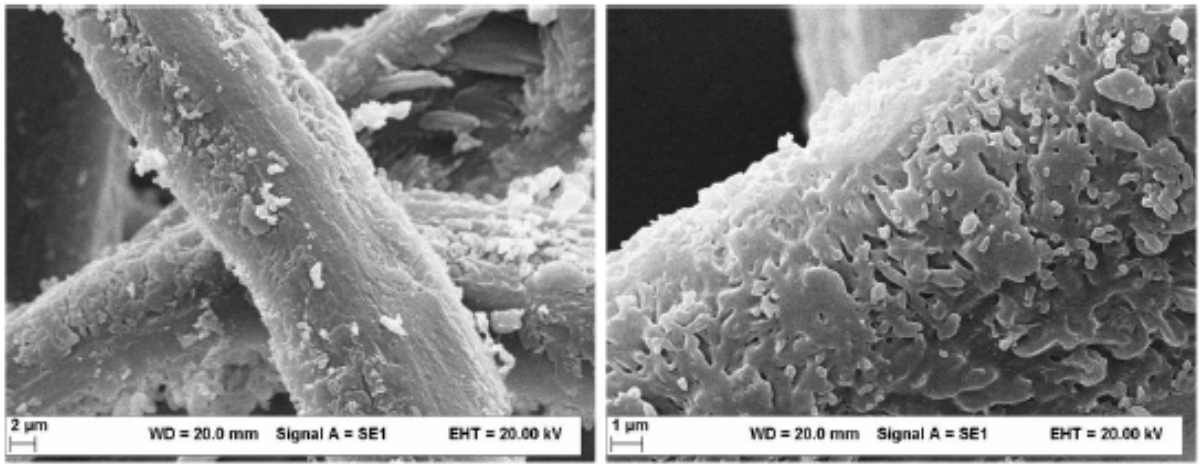

Figure III. 26: SEM images of the silk fibroin grafted with AMPSA (1/4, w/w), incubated in SBF 1x

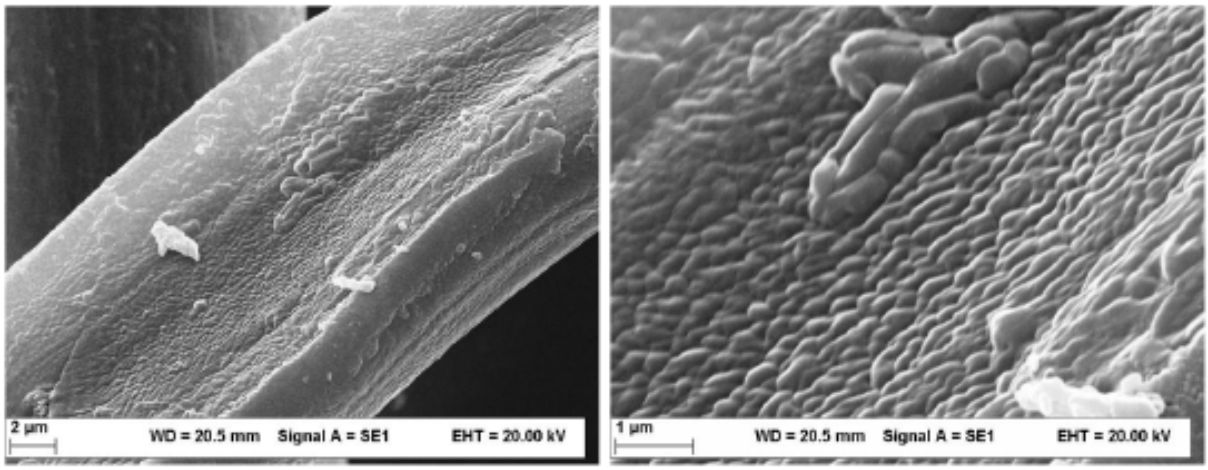

Figure III. 27: SEM images of the silk fibroin grafted with AMPSA (1/7, w/w), incubated in SBF 1x

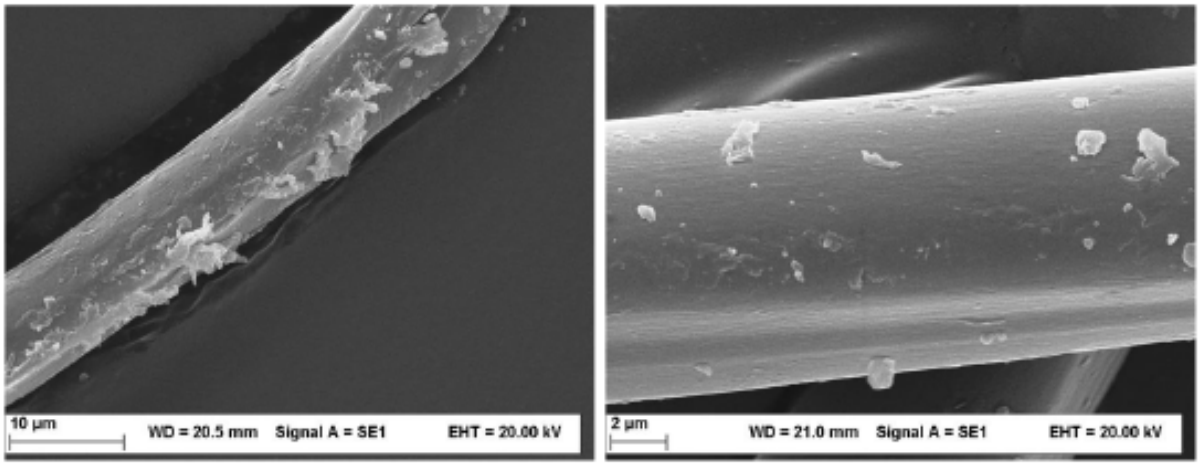

Figure III. 28: SEM images of the silk fibroin grafted with AMPSA (1/4, w/w), pretreated with $CaCl_2$, incubated in SBF 1x

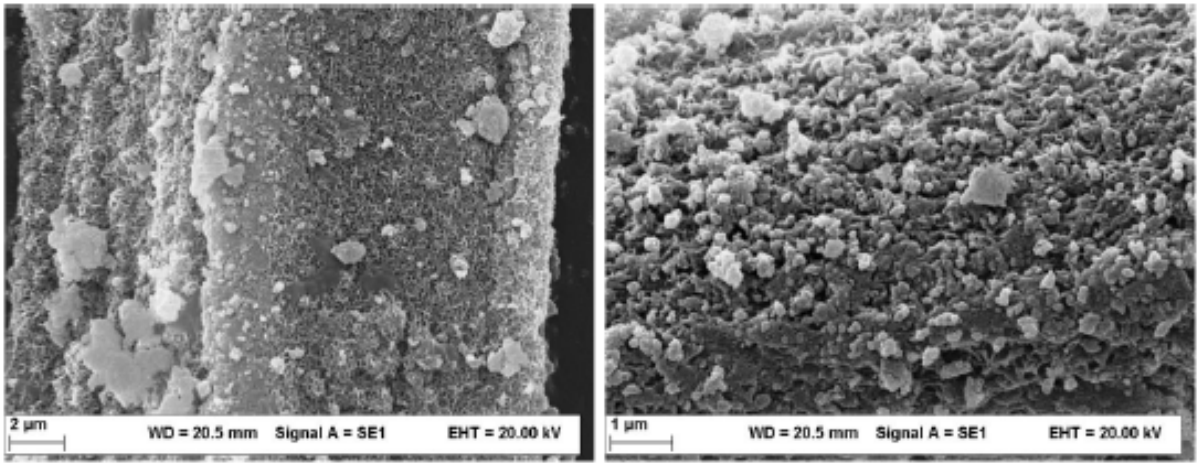

Figure III. 29: SEM images of the silk fibroin grafted with AMPSA (1/7, w/w), pretreated with $CaCl_2$, incubated in SBF 1x

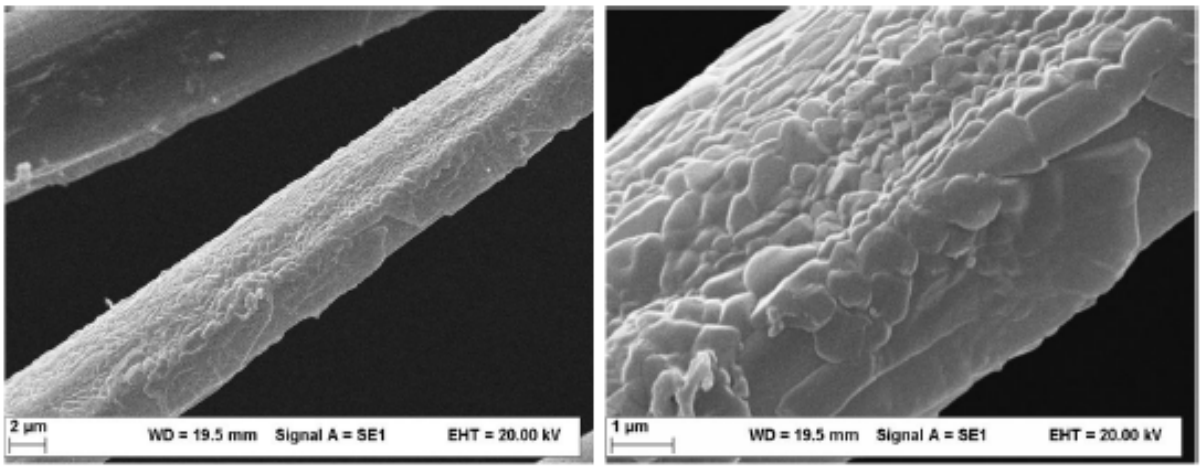

Figure III. 30: SEM images of the silk fibroin grafted with DEAEMA (1/4, w/w), incubated in SBF 1x

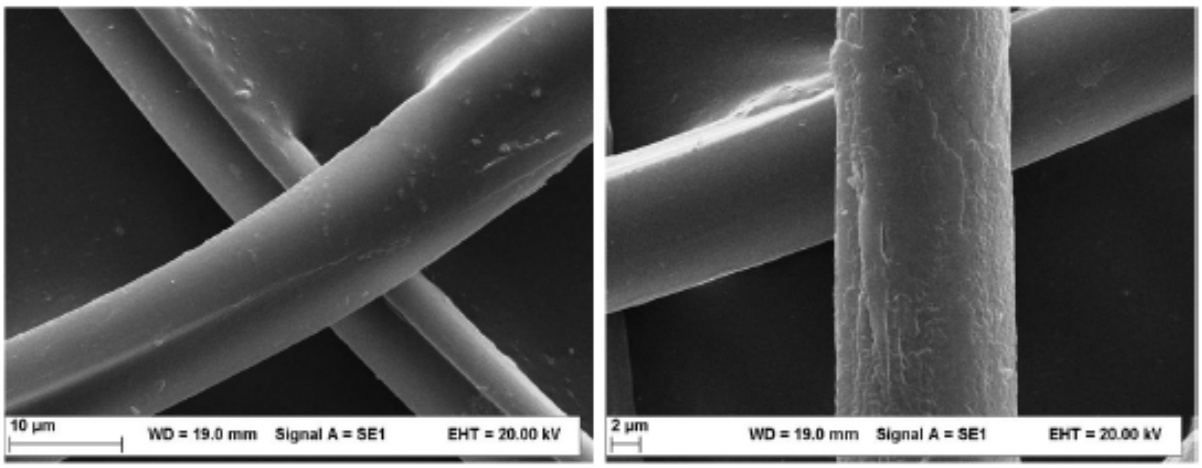

Figure III. 31: SEM images of the silk fibroin grafted with DEAEMA (1/7, w/w), incubated in SBF 1x

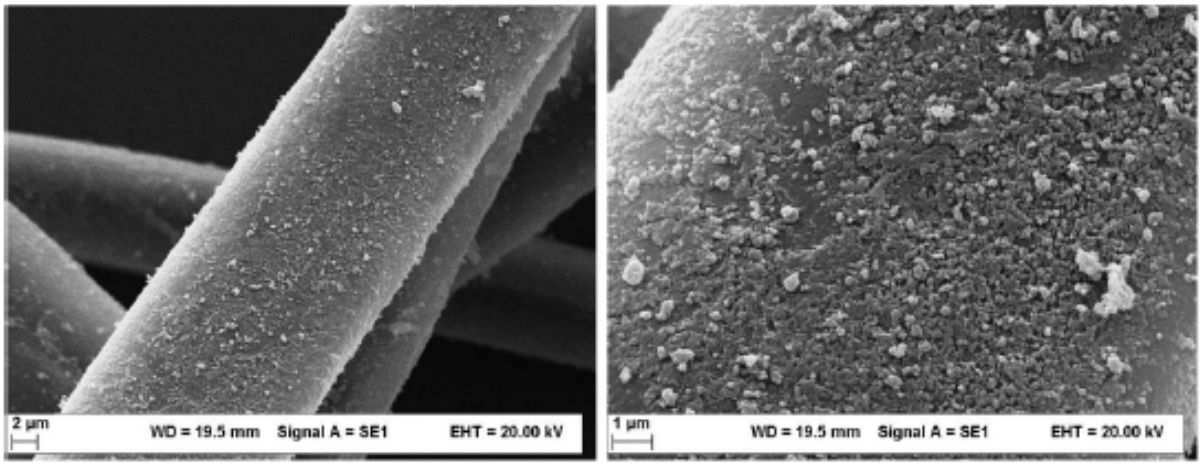

Figure III. 32: SEM images of the silk fibroin grafted with DEAEMA (1/4, w/w), pretreated with $CaCl_2$, incubated in SBF 1x

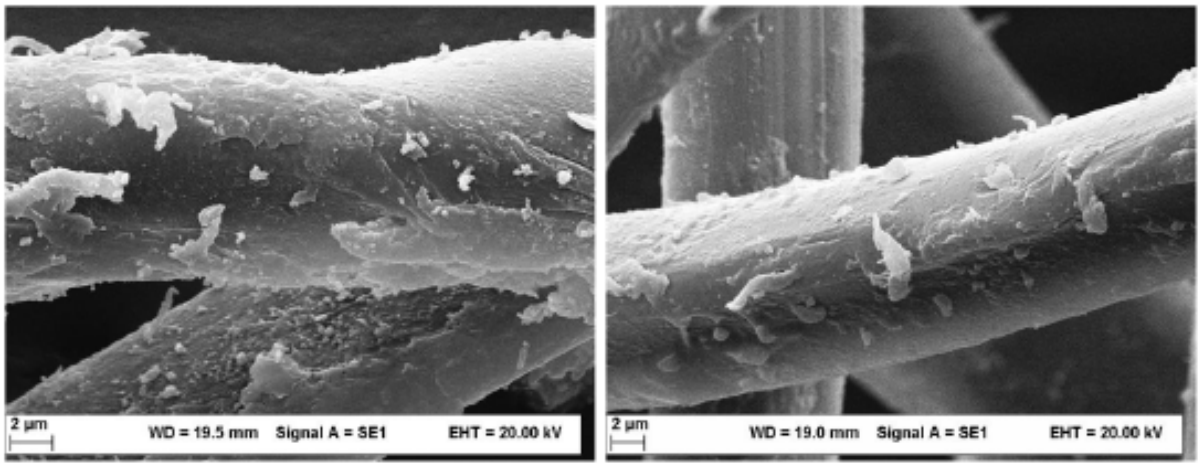

Figure III. 33: SEM images of the silk fibroin grafted with DEAEMA (1/7, w/w), pretreated with $CaCl_2$, incubated in SBF 1x

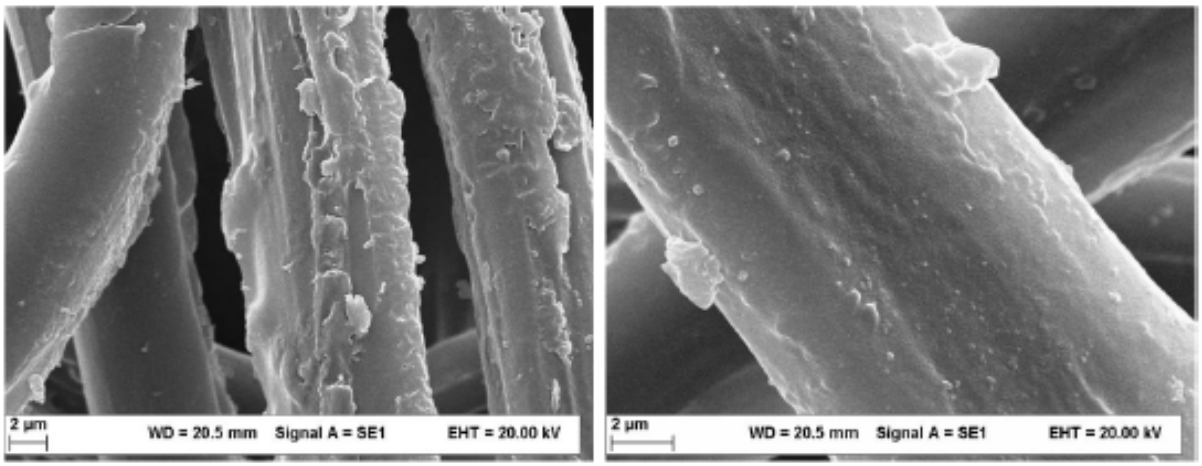

Figure III. 34: SEM images of the silk fibroin grafted with HEMA-AMPSA (1/4, w/w), incubated in SBF 1x

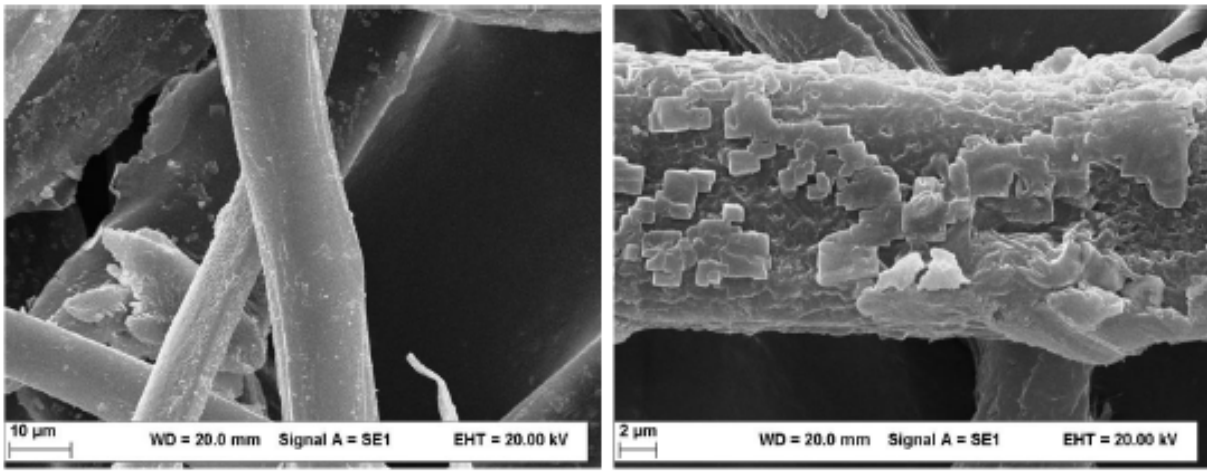

Figure III. 35: SEM images of the silk fibroin grafted with HEMA-AMPSA (1/7, w/w), incubated in SBF 1x

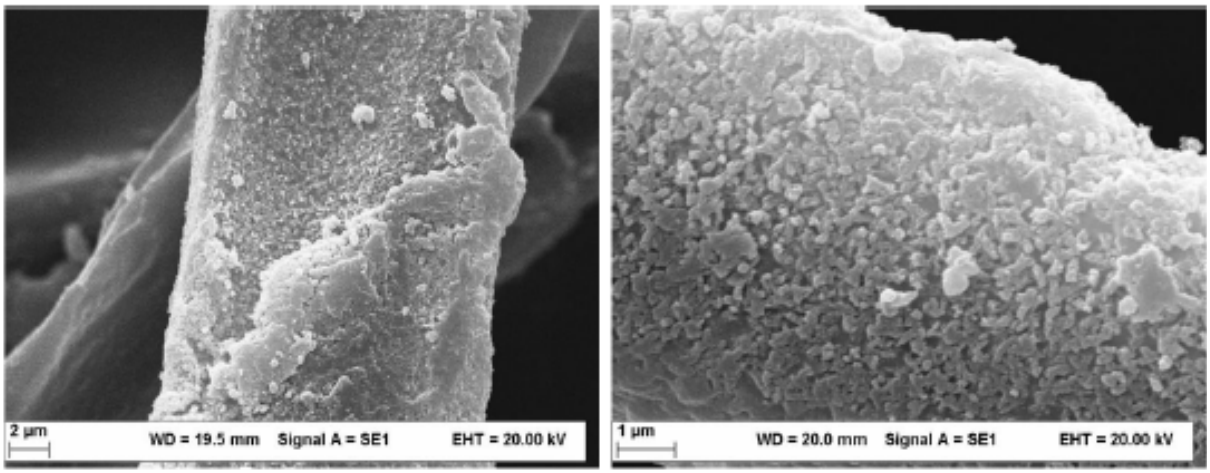

Figure III. 36: SEM images of the silk fibroin grafted with HEMA-AMPSA (1/4, w/w), pretreated with $CaCl_2$, incubated in SBF 1x

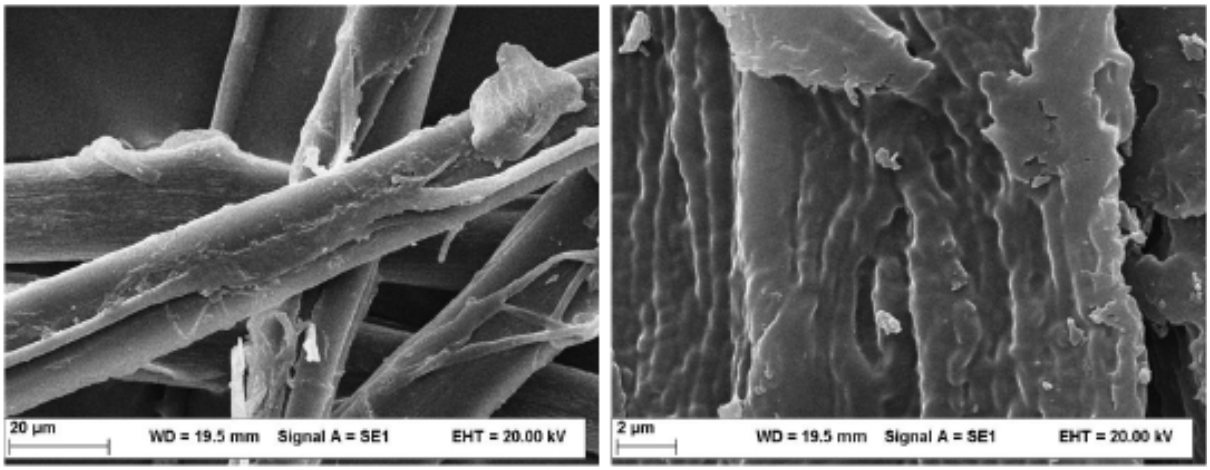

Figure III. 37: SEM images of the silk fibroin grafted with HEMA-AMPSA (1/7, w/w), pretreated with $CaCl_2$, incubated in SBF 1x

It is clear from the results seen Figures III. 40 - III. 53 that grafted fibers have the ability to deposit apatite in SBF 1x and the rate of apatite deposition is enough to cover the entire surface of the fibers after 14 days immersion.

In contrast crude fibroin fiber does not have the ability to deposit apatite under the same conditions. In this way the idea with the functional groups from the surface of the fibers is sustained. The acidic and amine groups present on the surface of the silk fibroin after the grafting procedure induce the mineralization phenomenon.

The EDX results indicated that the mineral layer contain predominantly calcium and phosphorus, and the Ca/P ratio is very close to natural bone hydroxyapatite (1.67). Therefore we are dealing with calcium-deficient hydroxyapatite (CDHA, Ca/P = 1.5–1.67) accompanied by octocalcium phosphate (OCP, Ca/P = 1.33).

Conclusions

The presence of calcospherites was observed on silk samples grafted with HEMA / IA after incubation in synthetic body fluid, respectively Ca and P solutions.

The best results were obtained for the modification of silk fibroin with IA-HEMA mixture following a PSK initiation. Following research will be done in order to completely elucidate the chemical nature of the formed copolymers, the grafting mechanism and the biological behaviour

The results obtained in the present study indicate that grafted fibroin with acidic and amine groups has the potential to induce apatite deposition on its surface in a biomimicking solution, in this case 1xSBF. The presence of calcospherites and the apatite nucleation may be attributed to the existence of acidic and amine groups from the silk fibers.

Hydroxypatite formation on fibroin fiber can be accelerated by prior treatment with an aqueous solution containing calcium ions, such as a $CaCl_2$ solution, having a concentration of 1 kmol/m3 or more. These findings support the use of these hybrid materials based on grafted silk fibers and HA as bone substitutes.

Chapter IV - Influence of aluminum on bone mineralization

Introduction [21]

Aluminum (Al) is the most abundant metal in the terrestrial crust. It is always found combined with other elements such as oxygen, silicon, and fluorine. Aluminum compounds have many different uses, from water-treatment to abrasives and furnace linings. They are also found in consumer products such as antacids, astringents, buffered aspirin, food additives, cosmetics, antiperspirants and medical devices. Although aluminum is commonly encountered in the day-to-day life, little is known about its biological roles. Al can enter the body through ingestion from water or food consumption, especially processed food with food preservatives and/or colorants containing Al. Sodium-Al phosphates are considered as safe emulsifying salts in food industry. Al hydroxide is commonly used to stabilize vaccines and, when injected, can create macrophage myofaciitis. Estimates of Al intakes range from 0.7 mg/day for infants and can reach up to 8-9 mg/day for adults. Al can also be in contact with biological tissues and ions can be released by corrosion from medical implants (e.g. hips prosthesis or dental implants made with the TA6V alloy). Al has been suspected to contribute to the appearance or development of various disorders of the nervous system, as well as of the bone and muscles in humans, namely dementia, anemia, myopathy, bone and joint disease.

Studies have confirmed that Al is absorbed through the gastrointestinal tract in healthy human subjects. However, Al is not an essential trace element in the body and is removed from the body after accumulation in cells of the distal kidney tubule and their desquamation in urine. When kidney functions are altered (renal insufficiency) or when intestinal absorption is increased (e.g. increased intestinal permeability), Al can accumulate in two preferential organs: brain (linked to the phosphoproteins, lipids or phosphate groups of DNA) and bone (linked to the phosphate groups of hydroxyapatite, the major Ca/P salt of the bone matrix). Several decades ago, aluminum encephalopathy associated with osteomalacia have been recognized as the major complications of chronic renal failure in dialyzed patients caused by the contamination of the dialysate by Al and the use of Al-containing phosphate binders. When Al has been completely removed from the dialysate and the use of Al-based phosphate binders reduced, the disease has considerably declined.

Al can accumulate in bones at the mineralization front, where it inhibits mineralization (leading to osteomalacia), as well as osteoblast activity. However, the respective role (or entanglement of these factors) is still a matter of debate since it has been suggested that Al deposition in ostomalacic bone could be a secondary phenomenon that has no influence on mineralization.

[21] **C.-N. Degeratu**, G. Mabilleau, C. Cincu, D. Chappard, *Aluminum inhibits the growth of hydroxyapatite crystals developed on a biomimic methacrylatic polymer,*2013, Article in press Journal of Trace Elements in Medicine and Biology, http://dx.doi.org/10.1016/j.jtemb.2013.05.004

This chapter presents the results of a study about the effect of aluminum on the *in vitro* growth of synthetic hydroxyapatite crystals. We used a modified polymer, carboxymethylated poly (2-hydroxyethyl methacrylate) (pHEMA-CM), which mimics the calcification of woven bone in the complete absence of cells. Pellets of the polymer were incubated in a synthetic body fluid containing either aluminum ion (Al^{3+}) at varying concentrations, or pieces of commercial Al foils. The hydroxyapatite growth in the presence of Al was assessed by chemical analysis, scanning electron microscopy and energy dispersive X-ray analysis.

Material and method

The monomer

Commercial 2-hydroxyethyl methacrylate was purchased from Sigma-Aldrich Chemical (Illkirsh, France) and used after purification. The monomer is known to contain residual methacrylic acid and ethyleneglycoldimethacrylate from the fabrication process.

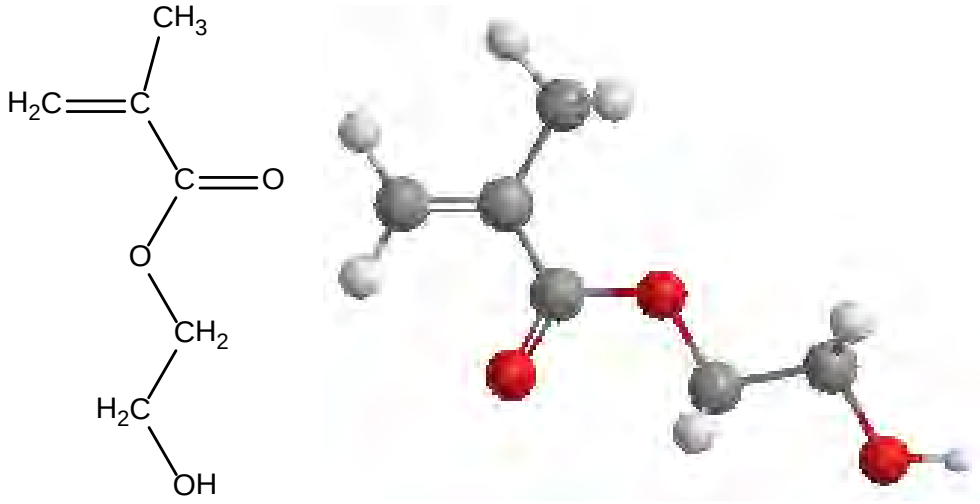

Figure IV. 1: Figure 1: Linear and 3D model of 2-hydroxyethyl methacrylate structure

The polymerization inhibitor 4-methoxyphenol (added by the manufacturer before shipping at a concentration of 350 ppm) was also removed. HEMA was purified by extraction with 3% (w/v) solution of sodium bicarbonate ($NaHCO_3$) in distilled water ($NaHCO_3$ makes water-soluble complexes with methacrylic acid and 4-methoxyphenol). The mixture was extracted with a large amount of $CHCl_3$, and most of the solvent was removed by rotary evaporation under vacuum. HEMA was made free of chloroform by distillation of the main fraction (b.p.

75 °C at 3 mm Hg pressure). Purified HEMA was collected in screw-capped bottles and kept in the dark at -20 °C until use.

Others chemicals, used in this study, were purchased from Sigma-Aldrich Chemical and used without any purification.

Preparation of polymer pellets

The polymer was prepared by bulk polymerization using benzoyl peroxide (BPO) as initiator. A mixture of HEMA (97%) and BPO (3%) was put under nitrogen bubbling for 5 minute in order to remove the oxygen dissolved in any of the components (it is known that oxygen inhibits the polymerization process). Polymerization was carried out at 65 °C for 24 h in polypropylene wells - 3 mm height by 10 mm diameter (Delta Microscopies, Labege, France). In this way, calibrated pellets of pHEMA (140 ± 5 mg) were obtained with a good reproducibility (Figure IV. 2).

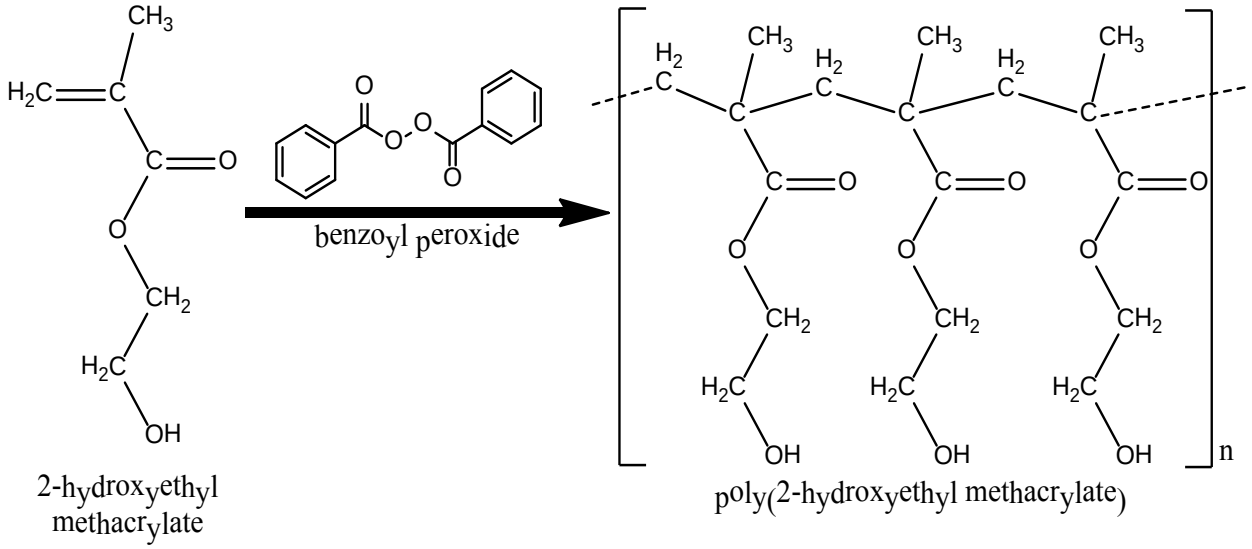

Figure IV. 2: Polymerization reaction scheme of HEMA in presence of BPO

Carboxymethylation of the pellets was done as follows: pellets were washed with deionized water for 30 min and soaked in 0.5 M bromoacetic acid in a 2 M NaOH solution overnight at room temperature and under gentle agitation. Pellets of the carboxymethylated polymer (pHEMA-CM) were washed five times (10 min each) in deionized water and dried in an oven at 60 °C until use.

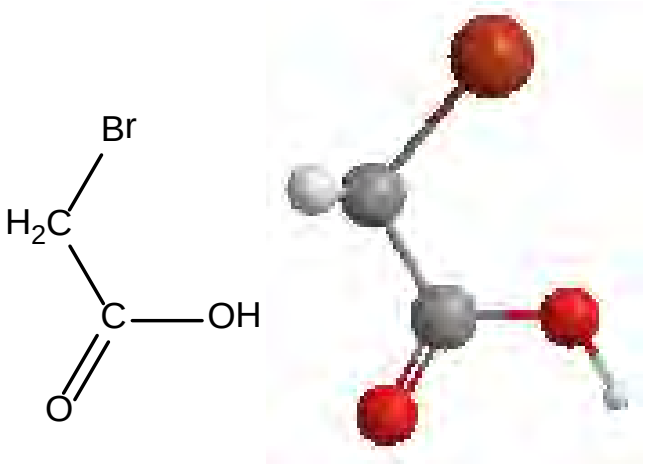

Figure IV. 3: Linear and 3D model of bromoacetic acid structure

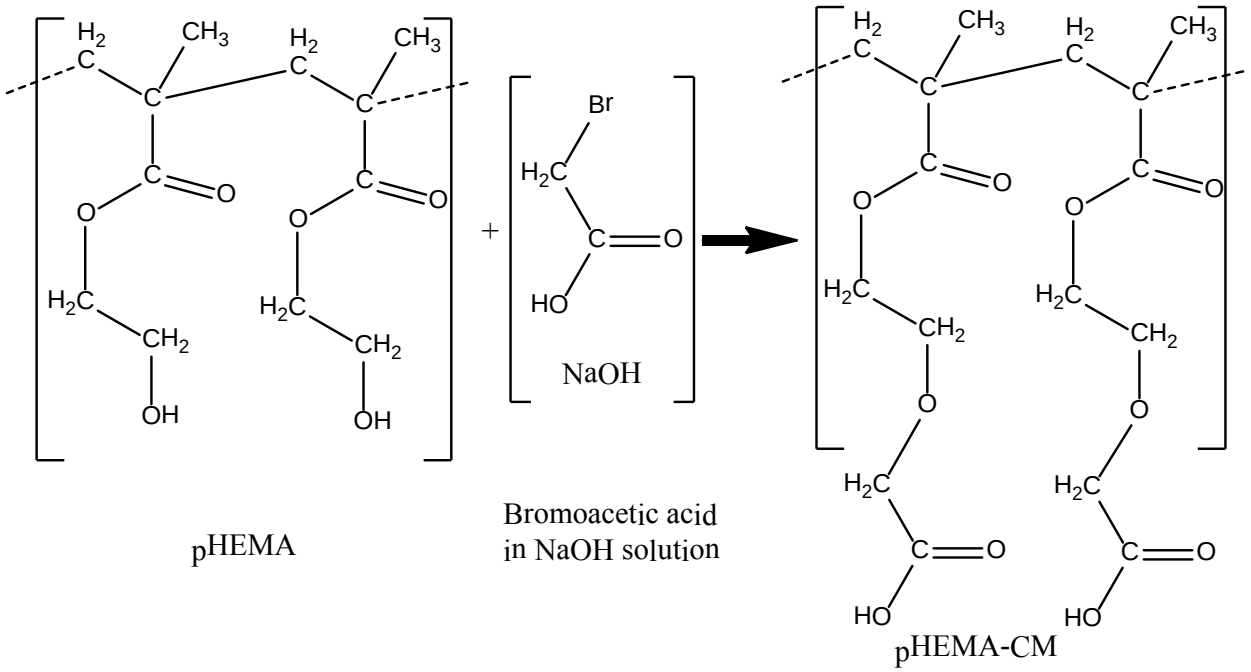

Figure IV. 4: Reaction scheme of pHEMA carboxymethylation

The success of carboxymethylation was assessed by using a modified Von Kóssa method. The von Kóssa method indirectly localizes calcium in tissue by detecting phosphate or carbonate ions. The sample is placed in 1% aqueous silver nitrate. Calcium cations are replaced by silver, with transformation of $Ca_3(PO_4)_2$ to Ag_3PO_4 and $CaCO_3$ to Ag_2CO_3. Both silver salts are subsequently reduced to the metal. The reaction is more easily achieved by placing the staining dish under a 100W light bulb or on a window sill. The calcified sample is blackened

in about 15 minutes and is sharply delineated. The next step is to immerse the sample for a few minutes in a sodium thiosulfate solution, which removes silver that has complexed with protein and would eventually darken with storage of the uncalcified sample.

In the modified method, pellets were soaked in $AgNO_3$ 5% in deionized water for 10 min in the dark. They were then rinsed three times in deionized water in order to remove the unreacted reagent. Silver atoms bound to the carboxymethyl residues were reduced with 5% sodium thiosulphate in deionized water. The reaction occurs immediately and the pellets were washed in deionized water and dried at 37 °C.

Incubation of pellets in synthetic body fluids

A standard synthetic body fluid (SBF 1.5X) mimicking the lymph fluid was prepared by dissolving the corresponding quantities of salts NaCl, $NaHCO_3$, KCl, K_2HPO_4, $MgCl_2$ $(H_2O)_6$, $CaCl_2$ $(H_2O)_2$, Na_2SO_4 into demineralised water at 37 °C accord to Yamada et al. The *p*H of this body fluid was *p*H 7.4, and it was achieved by using a buffer solution of tris(hydroxymethyl) aminomethane (TRIS) and hydrochloric acid (HCl). The composition (verified on a Technicon SMA analyzer) was as follows: Na^+- 213.28 mM; Ca^{2+} - 3.73 mM; Mg^{2+} - 2.25 mM; HCO_3^- - 6.3 mM; Cl^- - 212.31 mM; HPO_4^{2-} - 1.35 mM; SO_4^{2-} - 0.75 mM; K^+: 4.85 mM. Pellets of pHEMA-CM were immersed in capped Falcon tubes filled with SBF 1.5X. Pellets were let to soak in a humidified oven at 37 °C, with 5% CO_2 for five days to allow the formation of hydroxyapatite globules at their surface. Then, the pellets were randomly allocated in one of the following groups: (i) pellets incubated with SBF served as controls; (ii) pellets incubated with SBF enriched with 20 µg/L Al^{3+}; (iii) pellets immersed in SBF enriched with 40 µg/L Al^{3+}; (iv) pellets incubated with 60 µg/L Al^{3+}. The Al^{3+} ions were provided by dissolving $AlCl_3$ in the SBF (Sigma–Aldrich). Three additional groups of pellets were incubated with freshly cut pieces of commercial Al foil (food grade, 16 µm in thickness): (v) pellets immersed in SBF containing one piece of 60 mm x 20 mm Al foil (total mass: 33 ± 5mg); (vi) pellets incubated in SBF containing two pieces of 30 mm x 20 mm Al foil and (vii) pellets incubated in SBF containing six pieces of 20 mm x 10 mm aluminum foil. Between these three groups, the overall surface and mass of Al foil was maintained constant, only the number of pieces and as such the exposed cutting surface changed. Pellets were incubated for a 21 day-period at 37°C in a humidified oven with an inflowing air containing 5% CO_2. The medium was replaced every two days. At the end of the incubation period, pellets were rinsed in deionized water 3 times for 10 min to remove any non-crystallized ions. Eighty-four pellets were used for the entire study and twelve pellets were allocated in each group. The following analyses were conducted in triplicate.

Chemical analysis

Pellets were transferred into 1 ml of 0.2 M HCl for 24 h to allow complete dissolution of the mineral deposits. The fluid was then collected and used to determine the amount of free ions on an automated Hitachi 917 spectrophotometer (Roche, France) with standardized clinical reagents for calcium (Calcium Infinity TM Arsenazo III) and phosphate (the reduced phosphomolybdate method) obtained from the manufacturer. Al concentration was determined by Inductively Coupled Plasma Atomic Emission Spectrometry, ICP-AES (Jobin-Yvon JY-238 Ultrace, HORIBA Jobin-Yvon, Longjumeau, France). Measurements were performed on the fluid obtained from three disks incubated in the same conditions, and the mean ± standard deviation (SD) of the triplicate was considered.

Scanning electron microscopy (SEM) and energy-dispersive X-ray analysis (EDX)

Pellets to be examined by SEM were processed as previously described. Briefly, they were dehydrated and carbon-coated with a MED 020 device (Bal-Tec, Balzers, Liechtenstein). SEM was performed on an EVO LS10 (Carl Zeiss, Nanterre, France) microscope equipped with an energy-dispersive X-ray microanalysis machine (INCA XMAX, Oxford Instruments, Oxford, UK). In order to determine the composition of the mineral deposits, EDX was performed by point analysis. The methods explore several micrometers in thickness. Based on SEM photographs, a number of 50 mineral deposits were measured for each group; the size of the Ca/P deposits was done using the ImageJ freeware (NIH, Bethesda, MD).

Statistical analysis

Statistical analysis was done with Systat statistical software, release 13 (Systat, San José, CA). All results are expressed as mean ± SD. The Kruskal-Wallis non-parametric ANOVA test was used to compare the differences between the groups. Results were considered significant when $p < 0.05$. When the result of ANOVA was significant, comparison between groups was obtained by the Conover-Inman *post-hoc* test.

Results

Chemical analysis

Pellets did not vary in shape or weight under standardized polymerization conditions. They were translucent and their mean weight was 190 mg ± 5%, without significant differences between groups. Pellets of pHEMA did not react with silver nitrate and remained translucent. On the other hand, pellets of pHEMA-CM were strongly bound to silver and appeared heavily blackened at the end of the reaction (Figure IV. 5).

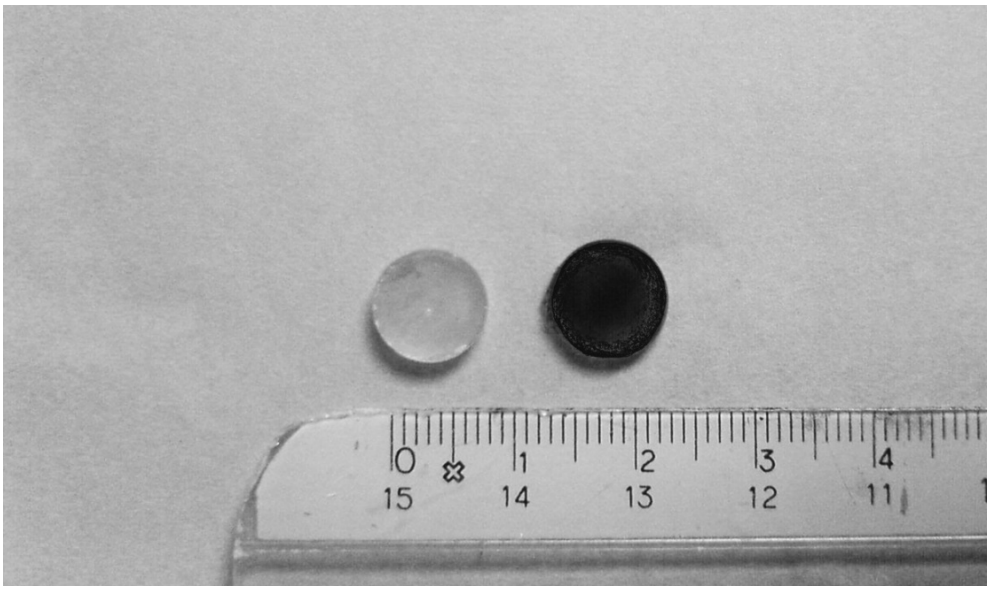

Figure IV. 5: The Von Kóssa reaction performed on the pellets: pellet of pHEMA remained translucent - left side; pellet of pHEMA-CM has strongly bound silver nitrate - right side

When incubated in SBF enriched with Al ions, there were significant differences between Al ion groups and controls for chemical analysis (Table IV. 1 and Figure IV. 6). As expected, the amount of Al^{3+} was dose-dependently increased as compared with untreated controls ($p<0.05$). On the other hand, the amount of calcium and phosphorus were significantly reduced as the dose of aluminum increased. As a consequence, the Al/Ca ratio was markedly increased in a dose-dependent manner. The Ca/P ratio tended to decrease, however it did not reached significance when compared with untreated controls (Kruskal-Wallis ANOVA: 10.476, p=0.106).

The presence of Al foil pieces in the SBF also dramatically affected the chemical composition of the mineral. Indeed, a marked augmentation in aluminum concentrations and Al/Ca ratio were observed in all groups. Furthermore, the Ca2+ and PO_4^{3-} content were dose-dependently reduced in these conditions as well as the Ca/P ratio.

Table IV. 1: Concentrations of Al^{3+}, Ca^{2+} and PO_4^{3-} in pHEMA-CM pellets incubated with 1.5× body fluid enriched with Al^{3+} (0, 20, 40, and 60 µg/L) or in presence of aluminum foil (one piece 60x20 mm; two pieces 30x20 mm; 6 pieces 20x10 mm; thickness of 16 µm and total mass of 33 ± 5 mg).

Source of aluminum	Al^{3+} µM/mg of pHEMA	Ca^{2+} µM/mg of pHEMA	PO_4^{3-} µM/mg of pHEMA	Al^{3+}/Ca^{2+}	Ca^{2+}/PO_4^{3-}
(i) - none	0.020 ± 0.003	86.1 ± 0.3	52.0 ± 0.2	< 0.001	1.66 ± 0.013
ii) Al^{3+} 20 µg/L	0.155 ± 0.007*	86.2 ± 20.01	52.5 ± 12.0	< 0.001	1.64 ± 0.008
iii) Al^{3+} 40 µg/L	0.245 ± 0.046*	49.8 ± 18*	31.5 ± 10.1*	0.006 ± 0.001*	1.58 ± 0.030*
iv) Al^{3+} 60 µg/L	0.679 ± 0.261*	6.0 ± 1.6*	3.9 ± 1.2*	0.013 ± 0.011*	1.53 ± 0.036*
v) Al foil 1x60x20	0.052 ± 0.007*	29.3 ± 11.6*	19.6 ± 8.0*	0.001 ± 0.000*	1.49 ± 0.018*
vi) Al foil 2x30x20	0.043 ± 0.003*	18.9 ± 12.1*	12.6 ± 2.5*	0.007 ± 0.008*	1.51 ± 0.445*
vii) Al foil 6x10*20	0.042 ± 0.007*	8.0 ± 4.2*	5.3 ± 8.8*	0.013 ± 0.002	1.50 ± 0.039*

*: $p<0.05$ *vs*. untreated

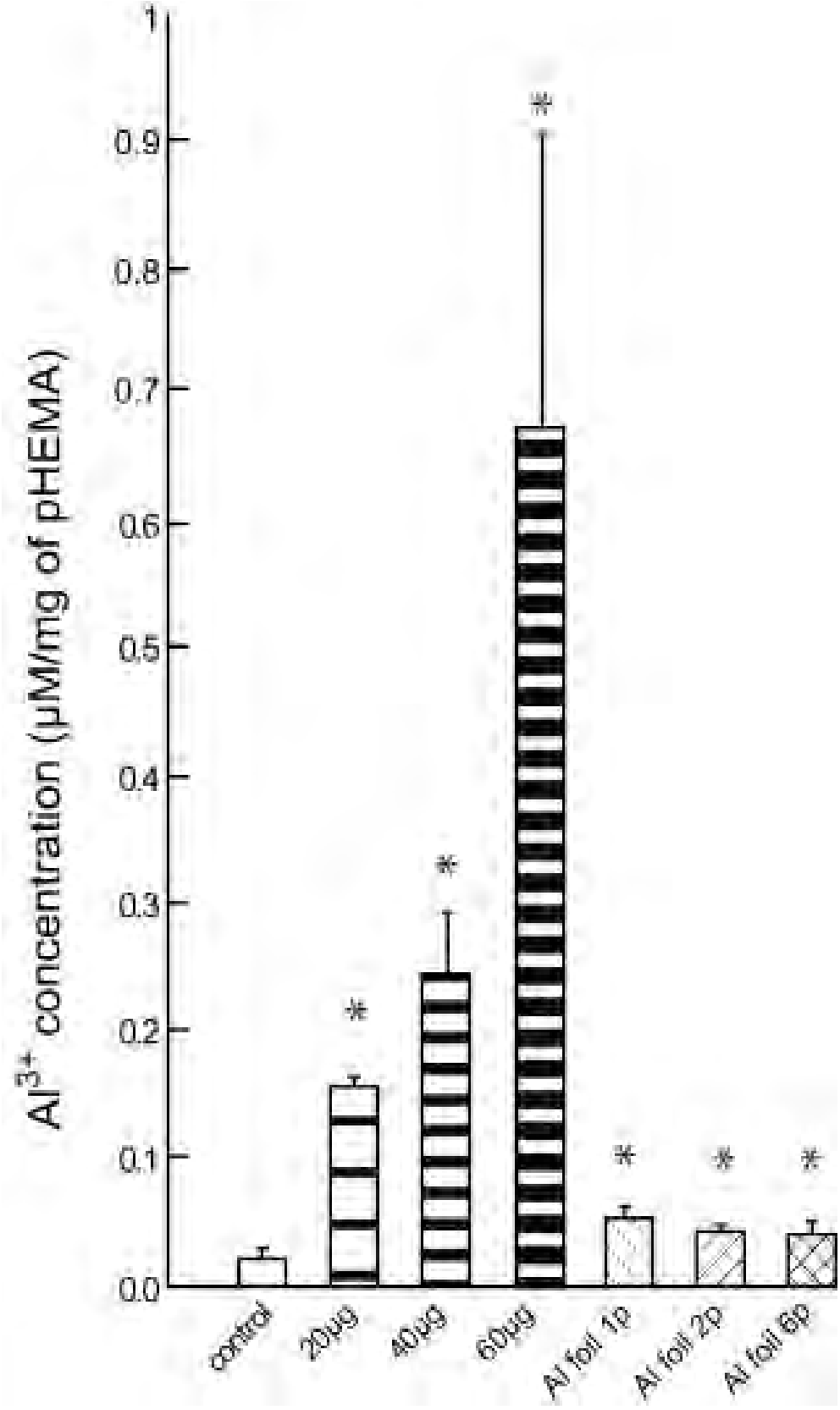

Figure IV. 6: Amount of Al^{3+} ion in the mineral deposits deposited at the surface of pHEMA-CM pellets and dissolved in HCl.

Scanning electron microscopy

After incubation in SBF, a white layer composed of mineralized nodules was clearly seen at the surface of the pHEMA-CM pellets by SEM (Figure IV. 2A). Mineralized nodules had a round shape (calcospherites) made of elementary tablets or plates of hydroxyapatite, packed together with a mean diameter of 8.19 ± 0.14 µm (Figure IV. 2H). Significant differences were observed in the diameter and shape of mineral deposits between untreated and Al ions-treated pellets. Indeed, although a white deposit composed of calcium and phosphorus was evidenced at the surface of pHEMA disks incubated with aluminum ions, it was not composed of typical calcospherite but rather appeared as mineralized plates emerging from the polymer surface. This aspect corresponds to the nucleation areas of hydroxyapatite during the first incubation period followed by a complete arrest during the second incubation time. As such, no measurement were possible.

Al foils were composed of pure aluminum without contaminants (Figure IV. 1C). Polymer disks immersed in SBF enriched with Al foil pieces also presented a mineralized layer at their surface. With one and two pieces of aluminum foil, some calcospherites were observed at the surface of the polymer disks but with a significant reduction in their diameters as compared with controls (4.43 ± 0.07 µm and 3.26 ± 0.1 µm respectively, $p<0.001$ and $p<0.001$ respectively Figure IV. 2H). However, polymer disks incubated in SBF in the presence of six aluminum pieces displayed plate-like mineral deposits similar to those observed with the aluminum ion concentrations.

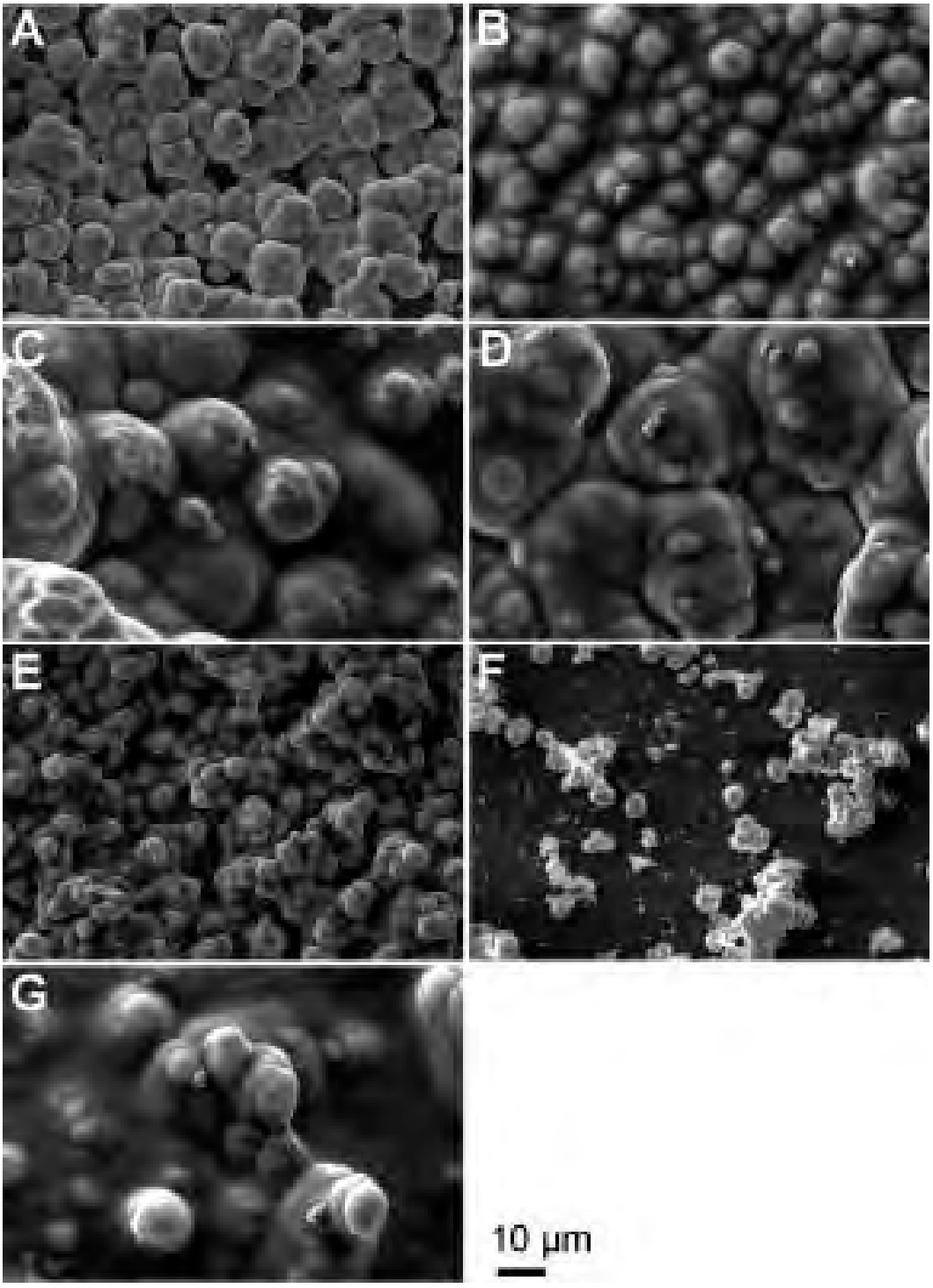

Figure IV. 7 (A-G): Characterization of mineral deposits at the surface of pHEMA-CM after incubation with SBF 1.5X. Mineral deposits are detected in untreated controls in the form of calcospherites (A) and in disk incubated in the presence of 20 µg/L Al^{3+} (B), 40 µg/L Al^{3+} (C), 60 µg/L Al^{3+} (D), 1 piece (60 x 20 mm) (E), 2 pieces (30 x 20 mm) (F) and 6 pieces of aluminum foil (10 x 20 mm) (G). Calcospherites are visible in A, E and F.

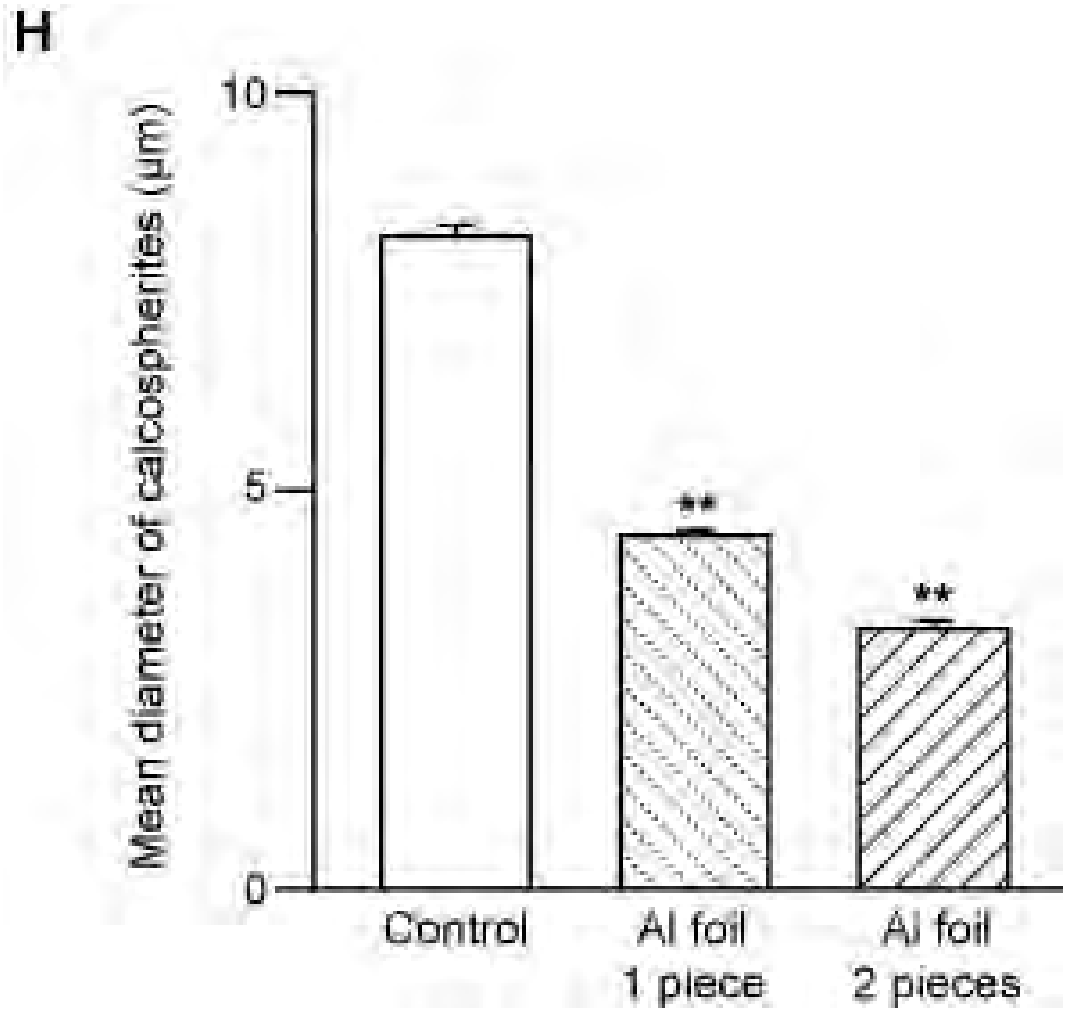

Figure IV. 7H: Characterization of mineral deposits at the surface of pHEMA-CM after incubation with SBF 1.5X. H) the mean diameter of calcospherites observed in A, E and F. **: $p<0.001$ vs. untreated.

Energy dispersive x-ray analysis reveals the presence of aluminum only at the highest concentration in aluminum ion groups and on disks incubated with six pieces of aluminum foil (Figure IV. 8).

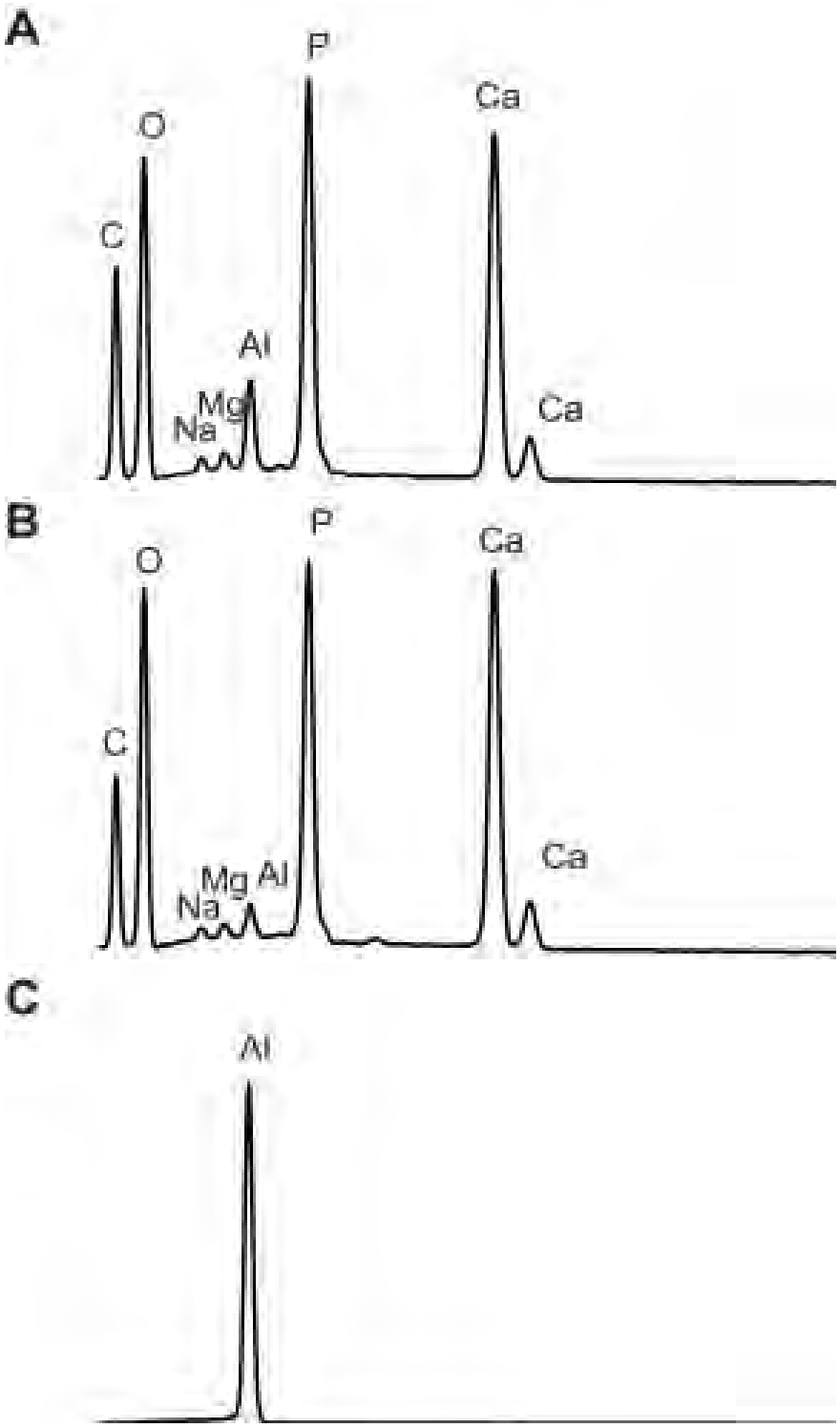

Figure IV. 8: Figure 8: EXD analysis of polymer disks incubated in the presence of 60 µg/L of Al^{3+} (A) or 6 pieces of aluminum foil (B). The EDX spectrum of a native Al foil is provided in (C).

DISCUSSION

Hydroxyapatite is a critical component of the bone matrix and any alteration of the mineral potentially leads to dramatic alteration of quality of the bone matrix and hence resistance to fracture. Mineral growth on pHEMA-CM is a non-cellular model mimicking the mineralization of woven bone observed in the growing skeleton, fracture callus and metaplasia. In this model, we have repeatedly shown that mineralization is independent of any cellular machinery or protein. This model has been developed to test drug efficacy (bisphosphonates), cell adherence, and protein interaction during bone crystal growth. *In vitro*, we have previously documented abnormal hydroxyapatite organization with several metals known to influence mineralization: strontium, iron, cobalt, chromium and nickel. In the present study, $AlCl_3$ was added in a TRIS-HCl buffered solution at *p*H equal to 7.4 and the majority of Al ions were complexed with hydroxyphosphate/phosphates.

First of all, it appeared that Al ions mediated a significant inhibition of mineral deposit at the surface of pHEMA-CM disks dose-dependently. Furthermore, as Al^{3+} reduces mineralization, we derived the Al^{3+}/Ca^{2+} index to assess the incorporation of Al^{3+} in the mineral composition. The augmentation of Al ions in SBF resulted in an increased Al incorporation into the mineral and thus led to structural modifications of the mineral deposits. These deposits no longer appeared with a calcospherite shape, but rather with mineral plates emerging from the polymer surface. Because of such an intense inhibition of mineralization, it was not possible to evaluate the Al containing mineral with other methods such as X-ray Diffraction or X-ray fluorescence spectrometry.

To simulate the *in vivo* release of Al ion from implanted biomaterials containing aluminum, we incubated pieces of freshly cut Al foils. This represented an easy way to introduce a large amount of Al ions from a material in a limited incubation period. In regenerative biomedicine, the use of TA6V (a titanium alloy containing 6% aluminum and 4% vanadium) is common to prepare orthopedic prosthesis or some types of dental implants. The release of Al from TA6V has been documented *in vivo* in the microenvironment of baboons which had a segmental bone replacement with TA6V devices. However, because of the reduced amount of Al in this alloy, it would have necessitate a considerable incubation time to evaluate this effect by using pieces of TA6V. In addition, Ti can be released from TA6V and is also known to have harmful effects. Al release from biomaterials containing high amounts of Al have been presented: cases of Al encephalopathy have been well documented with an Al-containing cement and prostheses coated with Al plasma-spray impair mineralization at their contact. Extracellular fluids coming in contact with metallic biomaterials contain many anions (Cl^-, PO_4^{3-}, HCO_3^-, SO_4^{2-}), cations (Na^+, Ca^{2+}, Mg^{2+}), dissolved oxygen, free radicals, proteins etc. and represent a highly corrosive environment which has a Cl^-concentration equivalent to ⅓ of that of seawater and an oxygen concentration equal to ¼ of that of the air. The body temperature also increases the capacity of these corrosive liquids. In addition, the SBF

composition (*p*H, buffering) frequently undergoes local fluctuations. The high amounts of phosphates are very corrosive for Al which has a marked affinity for the PO_4^{3-} ions. Incubation of polymer disks with aluminum foils in SBF resulted in surface oxidation leading to a mineralization inhibition and Al incorporation into the mineral deposit. Noteworthy is the presence of calcospherites observed at the surface of polymer disk with one or two piece of aluminum foils. Nevertheless, incorporation of Al^{3+} into the mineral lattice led to dramatic alterations in calcospherites size. As the possible exposed area of aluminum increased, inhibition of mineralization and mineral alterations occurred with aluminum foils.

A study in the early 80's which was conducted on 21 patients which were selected based on radiologic osteomalacia and/or suspicion of aluminum intoxication and skeletal lesions of osteitis fibrosa strongly suggested that aluminum can interfere with normal mineralization. In the patient group of osteomalacic uremic bone tissue who have been exposed to aluminum-containing dialysis fluid, the preferentially localization of aluminum was at the junction of mineralized bone and osteoid tissue, where the bone mineral is normally first deposited. In rats receiving drinking water enriched with Al chloride, a decrease in the bone mineral density was observed after 150 days but no histological control of the mineralization degree was available. In this study, aluminum was passively incorporated in hydroxyapatite and interfered with crystal size growth independently of any cellular, hormonal, or protein intervention.

Scanning electron microscopy showed a direct effect of aluminum on the crystal growth, a finding previously described by crystal modeling and in synthetic hydroxyapatites. Although the presence of metal elements in bone, such as iron, cobalt, chromium, nickel, aluminum or lead, especially in humans with metallic implants, has been well documented, the precise toxicity mechanisms remain largely unknown. In a human study on the effects of aluminum on bone localization, the range of Al^{3+} found in bone was between 25 to 130 ppm.

Recently, Al was found to induce osteoblast apoptosis which can explain the reduction of bone mass in patients with Al intoxication associated with cessation of the mineralization process.

One limitation of this study is linked to the acellular system used to assess the direct effect of Al^{3+} on mineral deposition. Physiologically, bone mineralization is a complex phenomenon involving a protein pattern, deposited by bone cells that allow clear spaces for mineralization initiation and growth. The effects of aluminum on bone cells and as such protein pattern has not been investigated in the present study and represent additional mechanisms explaining the bone loss associated with Al ingestion.

Conclusions.

Al ions significantly inhibited hydroxyapatite growth at the surface of pHEMA-CM and completely modified the morphology of calcospherites, first by decreasing their mean

diameter, then by converting them in less structured calcified plates. A very similar observation was reported in the same model with tiludronate, a bisphosphonic compound used as an antiosteoclastic drug. Inhibition of calcification as well as calcospherites changing into less-structured plates were observed. We also evidenced this severe alteration of the newly-formed mineral with incorporation of Al ions into the mineral lattice by SEM and EDX. Al interfered with mineralization when it was provided in the SBF as ion. It can also be released from the foil, although the metal is passivated by a layer of aluminum oxide.

CONCLUDING REMARKS AND PERSPECTIVES

The research as presented in this thesis, has focused on investigating various biomaterials in what regards their suitability for tissue engineering.

The first part of the PhD programme focused on obtaining various biopolymer structures and assessing their physico-chemical and mechanical properties. The following structures were prepared and obtained: films, microparticles, fibers, tubes and microporous structures. The conclusions of this first phase can be summarized as follows:

1. PHBV microspheres can be obtained very easily in any size range by vary the concentration of the polymer solution concentration or/and stirring speed or/and surfactant solution concentration.
    a. The obtained microparticles can be used as drug delivery system or for tissue reconstruction based on polymer biodegradability.
    b. For drug delivery application there is an issue regarding the polymer solvent which is chloroform and the substance which must be delivered should dissolve in this or to form a surfactant-like solution to play the role of PVA or DDS.
    c. If necessary a sieving operation can be employed in order to reduce polydispersity of the microspheres and to obtain a certain diameter size range.

2. PHBV films were also obtained and further studied as potential scaffolds for bone reconstruction implants. PHBV films were obtained using spin-coating and drop-casting method.
    a. The films obtained using spin-coating method are very thin (under 10 mm in thickness).
    b. The drop-casting method was used for to obtain both of porous and unporous films. The thickness of the films was in range of 30-50 mm if the solvent was left to evaporate free under the atmosphere and could reach the 2 mm in thickness if the solvent was evaporated at slow rates. When the solvent was evaporated at slow rates by covering the Petri dish the films can be obtained from thin (10 mm) to thick (2 mm) modifying the concentration of the solution. This also allows obtaining reproducible films.
    c. A mineralization test was performed on a PHB film. The results (using SEM images) have shown a poor amount of mineral deposit on the surface of PHB films.

3. For PHA films, a study was carried out on the surface modification by plasma treatment.
    a. This preliminary study allowed the determination of the experimental procedure of plasma treatment leading to the best wettability of the polymer film surface.
    b. The values of the contact angles increase with the storage time and the value of the free surface energy decrease with the same storage time. Nevertheless, they do not equalize the initial values before treatment, even not after 3 months.
    c. This study offered an excellent perspective for the functionalization of PHAs films by low pressure plasma treatment.

4. We investigated and set up a laboratory technique for the manufacture of PHB tubes. These tubes were proposed to be used as surgical drains in the Emergency Hospital "Floreasca", and afterwards potentially in other Romanian hospitals.

Also during this phase of the programme (on characterization of physico-chemcial and mechanical properties of biopolymer-based structures), but during my work at the Angers University, I contributed to a study aiming at developing new morphometric methods to characterize porous materials:

- Connectivity of the pore was measured by computing the interconnectivity index and the star volumes on 2D sections obtained by microCT.
- These parameters, based on Euclidean geometry, were refined by measuring the complexity of the pore size and their interconnectivity with measurements based on fractal geometry (Kolmogorov and Minkowski–Bouligand fractal dimensions) and the newly described fractal parameters lacunarity and succolarity.
- Non-linear relationships exist between these descriptors of porosity and the amount of the materials constituting the pore throats.
- Fractal descriptors constitute a very promising approach in this field and should be further used to better characterize porous materials.
- These parameters can be applied to non-homogeneous and anisotropic materials and may help in designing new types of scaffolds to allow a better invasion of the grafted materials by vascular sprouts and progenitor cells.

5. A small part of the research focused on the properties of blends made from PHB reinforced with treated cellulose/wood fibers (fillers) for other applications (e.g. packaging), given their special mechanical properties. To determine the effect of filler type on PHBV blends, mechanical, thermal and rheological characteristics of each formulations were performed.

a. To obtain films of PHB or PHB blended with treated cellulose/wood fibers a melting-press method was employed, leading to a 1mm thickness films.
b. This method can have the disadvantage of heating the polymer at the melting point during film formation, which can cause its degradation.
c. Overall, the results indicated that the blends containing PHB and cellulose fibers exhibit enhanced mechanical properties compared with those containing PHB and wood fibers, especially regarding tensile strength. This suggests that cellulose fibers are superior to wood fibers in terms of physico-mechanical properties.
d. The torque measurements for all blends performed have shown that the viscosity of molten wood fiber/cellulose fiber is lower than that of molten PHB. The melting temperature decreased with increasing filler content for all blends.
e. The findings are therefore expected to provide a framework for the future development of trials at laboratory and pilot scale in order to obtain items such as tomato yarn, packaging for agriculture by extrusion and molding injection technologies.

In the second part of my PhD programme, I assessed the biocompatibility characteristics of the PHBV films, PHBV fibers, silk fibroin and cellulose fibers.

1. The PHBHV8% films have a hydrophobic character resulting from the high value of the contact angle. The best porosity was achieved with sodium chloride, but this porous film has an increased cytotoxicity. The idea that the porous structures favor a higher cell adhesion is not sustained by the results with porous polyester films.
2. PHBV fibers obtained by wet spinning method appeared to be a very convenient form to test the cytocompatibility of the material *in vitro*. Their diameters offer a large surface to cells to adhere, similar to the surface they encounter when apposed onto a bone trabeculae. PHBV fibers appeared to be degradable by the J774.2 macrophage cell line *in vitro*. This method to produce fiber make the surface with a certain roughness, which is known to favor the adherence of cells, particularly osteoblasts. Probably due to this microstructure they were also colonized by SaOs2 osteoblast-like cell which can spread and develop onto their surface. However, the material is soft, and does not favor bone apposition *in vivo*. Other applications are currently under study in our laboratory as a coating material or in other types of tissues.

3. Silk-fibroin based materials were obtained by grafting with Ce4+ different synthetic monomers (AMPSA, HEMA-AMPSA, DEAEMA) onto the silk-fibroin.

    a. FTIR-ATR and SEM analyses performed on grafted fibers confirmed the grafting monomers AMPSA, HEMA-AMPSA and DEAEMA onto the silk surface.

b. The results of the study on mineralization of grafted silk fibroin indicated that grafted fibroin with acidic and amine groups has the potential to induce apatite deposition on its surface in a biomimicking solution, in this case 1xSBF.
c. The presence of calcospherites was observed on silk samples grafted with HEMA / IA after incubation in synthetic body fluid, respectively Ca and P solutions. The presence of calcospherites and the apatite nucleation may be attributed to the existence of acidic and amine groups from the silk fibers. Hydroxypatite formation on fibroin fiber can be accelerated by prior treatment with an aqueous solution containing calcium ions, such as a $CaCl_2$ solution, having a concentration of 1 M or more.
d. The best results were obtained for the modification of silk fibroin with IA-HEMA mixture following a PSK initiation.
e. These findings support the use of these hybrid materials based on grafted silk fibers and HA as bone substitutes. Further research is needed in order to completely elucidate the chemical nature of the formed copolymers, the grafting mechanism and the biological behavior.

Finally, ***a separate part of the research focused on investigating the effects of Al ions on hydroxyapatite growth on PHEMA-CM***.

- Al ions significantly inhibited hydroxyapatite growth at the surface of pHEMA-CM and completely modified the morphology of calcospherites, first by decreasing their mean diameter, then by converting them in less structured calcified plates.

- A very similar observation was reported in the same model with tiludronate, a bisphosphonic compound used as an antiosteoclastic drug.

- We also evidenced this severe alteration of the newly-formed mineral with incorporation of Al ions into the mineral lattice by SEM and EDX.

- Al interfered with mineralization when it was provided in the SBF as ion. It can also be released from the foil, although the metal is passivated by a layer of aluminum oxide.

- These findings support the preliminary conclusion that Al is detrimental to bone mineralization and as a consequence, on biopolymeric implants. However further research is needed to elucidate the mechanisms.

Bibliography

1. De Boer, J., et al., *Tissue Engineering*. 2008: Elsevier Science.
2. Jenkins, M., M. Institute of Materials, and Mining, *Biomedical Polymers*. 2007: Woodhead Pub. and Maney Pub.
3. Ham, A.W. and D.H. Cormack, *Ham's histology*. 1987: Lippincott.
4. Baron, R., *Anatomy and ultrastructure of bone. In: Primer on the metabolic bone diseases and disorders of mineral* 1999: Lippincott Williams & Wilkins. 502.
5. Lian, J.B., et al., *Bone formation: osteoblast lineage cells, growth factors, matrix proteins and the mineralization process. In:Primer on the metabolic bone diseases and disorders of mineral metabolism*. 1999: Lippincott Williams & Wilkins.
6. Aubin, J.E., J.B. Lian, and G.S. Stein, *Bone formation: maturation and functional activities of osteoblast lineage cells. In: Primer on the metabolic bone diseases and disorders of mineral metabolism*. 1999: Lippincott Williams & Wilkins.
7. Ross, F.P., *Osteoclast biology and bone resorption. In: Primer on the metabolic bone diseases and disorders of mineral metabolism*. 1999: Lippincott Williams & Wilkins.
8. Suda, T., et al., *Modulation of osteoclast differentiation and function by the new members of the tumor necrosis factor receptor and ligand families.* Endocr Rev, 1999. **20**(3): p. 345-57.
9. Williams, D.F., *The Williams Dictionary of Biomaterials*. 1999: University of Chicago Press.
10. Chapekar, M.S., *Tissue engineering: challenges and opportunities.* J Biomed Mater Res, 2000. **53**(6): p. 617-20.
11. Khan, Y., et al., *Tissue engineering of bone: material and matrix considerations.* J Bone Joint Surg Am, 2008. **90 Suppl 1**: p. 36-42.
12. Moore, W.R., S.E. Graves, and G.I. Bain, *Synthetic bone graft substitutes.* ANZ J Surg, 2001. **71**(6): p. 354-61.
13. Meinel, L., et al., *Silk implants for the healing of critical size bone defects.* Bone, 2005. **37**(5): p. 688-98.
14. Takeuchi, A., et al., *Deposition of bone-like apatite on silk fiber in a solution that mimics extracellular fluid.* J Biomed Mater Res A, 2003. **65**(2): p. 283-9.
15. Fleisch, H., *Bisphosphonates in Bone Disease: From the Laboratory to the Patient*. 2000: Elsevier Science.
16. Hing, K.A., *Bone repair in the twenty-first century: biology, chemistry or engineering?* Philos Trans A Math Phys Eng Sci, 2004. **362**(1825): p. 2821-50.
17. Miller, M.D., *Review of orthopaedics*. 2004: W. B. Saunders.
18. Doblaré, M., J.M. García, and M.J. Gómez, *Modelling bone tissue fracture and healing: a review.* Engineering Fracture Mechanics, 2004. **71**(13–14): p. 1809-1840.
19. Borer, K.T., *Physical activity in the prevention and amelioration of osteoporosis in women : interaction of mechanical, hormonal and dietary factors.* Sports Med, 2005. **35**(9): p. 779-830.
20. Datta, H.K., et al., *The cell biology of bone metabolism.* J Clin Pathol, 2008. **61**(5): p. 577-87.

21. Buckwalter, J.A., et al., *Bone Biology.* The Journal of Bone & Joint Surgery, 1995. **77**(8): p. 1256-1275.
22. Legros, R., N. Balmain, and G. Bonel, *Age-related changes in mineral of rat and bovine cortical bone.* Calcif Tissue Int, 1987. **41**(3): p. 137-44.
23. Field, R.A., et al., *Bone composition in cattle, pigs, sheep and poultry.* J Anim Sci, 1974. **39**(3): p. 493-9.
24. Bertazzo, S., C.A. Bertran, and J.A. Camilli, *Morphological Characterization of Femur and Parietal Bone Mineral of Rats at Different Ages* Key Engineering Materials, 2006. **309-3011**: p. 11-14.
25. Bertazzo, S., C.A. Bertran, and J.A. Camilli, *Morphological and Dimensional Characteristics of Bone Mineral Crystals.* Key Engineering Materials, 2006. **309-3011**: p. 3-6.
26. Vigorita, V.J., B. Ghelman, and D. Mintz, *Orthopaedic pathology*. 2008: Wolters Kluwer Health/Lippincott Williams and Wilkins.
27. Rosen, C.J., J.E. Compston, and J.B. Lian, *Primer on the Metabolic Bone Diseases and Disorders of Mineral Metabolism*. 2009: Wiley.
28. Termine, J.D., *Non-collagen proteins in bone.* Ciba Found Symp, 1988. **136**: p. 178-202.
29. Marcus, R., et al., *Fundamentals of Osteoporosis*. 2009: Elsevier Science.
30. Everts, V., et al., *The bone lining cell: its role in cleaning Howship's lacunae and initiating bone formation.* J Bone Miner Res, 2002. **17**(1): p. 77-90.
31. Sapir-Koren, R. and G. Livshits, *Bone mineralization and regulation of phosphate homeostasis.* IBMS BoneKEy, 2011. **8**(6): p. 286-300.
32. Blumenthal, N.C., *Mechanisms of inhibition of calcification.* Clin Orthop Relat Res, 1989(247): p. 279-89.
33. Glimcher, M.J., *A basic architectural principle in the organization of mineralized tissues.* Clin Orthop Relat Res, 1968. **61**: p. 16-36.
34. Raggio, C.L., B.D. Boyan, and A.L. Boskey, *In vivo hydroxyapatite formation induced by lipids.* J Bone Miner Res, 1986. **1**(5): p. 409-15.
35. Byrappa, K. and T. Ohachi, *Crystal Growth Technology*. 2003: Springer.
36. Stancu, I.C., et al., *Synthesis of methacryloyloxyethyl phosphate copolymers and in vitro calcification capacity.* Biomaterials, 2004. **25**(2): p. 205-213.
37. Cao, H., et al., *Materials design and modification on amide-based composites for hydrogen storage.* Progress in Natural Science: Materials International, 2012. **22**(6): p. 550-560.
38. Dorozhkin, S.V., *Nanosized and nanocrystalline calcium orthophosphates.* Acta Biomaterialia, 2010. **6**(3): p. 715-734.
39. Ratner, B.D., et al., *Biomaterials Science: An Introduction to Materials in Medicine*. 2004: Elsevier Science.
40. Park, J.B. and R.S. Lakes, *Biomaterials: an introduction*. 1992: SPRINGER VERLAG GMBH.
41. Khadka, D.B. and D.T. Haynie, *Protein- and peptide-based electrospun nanofibers in medical biomaterials.* Nanomedicine, 2012. **8**(8): p. 1242-62.
42. Davis, J.R., *Handbook of Materials for Medical Devices*. 2003: ASM International.

43. Shi, D., *Biomaterials and Tissue Engineering*. 2004: Springer.

44. Park, J.B. and J.D. Bronzino, *Biomaterials: Principles and Applications*. 2002: Taylor & Francis.

45. Basu, B., D.S. Katti, and A. Kumar, *Advanced Biomaterials: Fundamentals, Processing, and Applications*. 2010: Wiley.

46. Heimann, R.B., *Classic and Advanced Ceramics*. 2010: Wiley.

47. Kokubo, T., H.-M. Kim, and M. Kawashita, *Novel bioactive materials with different mechanical properties.* Biomaterials, 2003. **24**(13): p. 2161-2175.

48. Ige, O.O., L.E. Umoru, and S. Aribo, *Natural Products: A Minefield of Biomaterials.* ISRN Materials Science, 2012. **2012**: p. 20.

49. Kokubo, T., *Bioactive glass ceramics: properties and applications.* Biomaterials, 1991. **12**(2): p. 155-63.

50. Ueki, K., et al., *Effect of self-setting alpha-tricalcium phosphate between segments for bone healing and hypoaesthesia in lower lip after sagittal split ramus osteotomy.* J Craniomaxillofac Surg, 2012. **40**(4): p. e119-24.

51. Gilding, D.K. and A.M. Reed, *Biodegradable polymers for use in surgery—polyglycolic/poly(actic acid) homo- and copolymers: 1.* Polymer, 1979. **20**(12): p. 1459-1464.

52. Woodfield, T.B., et al., *Design of porous scaffolds for cartilage tissue engineering using a three-dimensional fiber-deposition technique.* Biomaterials, 2004. **25**(18): p. 4149-61.

53. Hutmacher, D.W., et al., *Mechanical properties and cell cultural response of polycaprolactone scaffolds designed and fabricated via fused deposition modeling.* J Biomed Mater Res, 2001. **55**(2): p. 203-16.

54. Mikos, A.G., et al., *Host response to tissue engineered devices.* Adv Drug Deliv Rev, 1998. **33**(1-2): p. 111-139.

55. Bonassar, L.J. and C.A. Vacanti, *Tissue engineering: the first decade and beyond.* J Cell Biochem Suppl, 1998. **30-31**: p. 297-303.

56. Blaine, G., *THE USES OF PLASTICS IN SURGERY.* The Lancet, 1946. **248**(6424): p. 525-528.

57. Figueiredo, Z.M.B. and J.F. Kennedy, *Progress in biomedical polymers. Edited by C. G. Gebelein and R. L. Dunn, Plenum Press, New York, 1990. pp, 406, price $8950 ($107.40 outside US and Canada). ISBN 0-306-43523-3.* Polymer International, 1991. **26**(3): p. 203-203.

58. Griffith, L.G., *Polymeric biomaterials.* Acta Materialia, 2000. **48**(1): p. 263-277.

59. Ramakrishna, S., et al., *Biomedical applications of polymer-composite materials: a review.* Composites Science and Technology, 2001. **61**(9): p. 1189-1224.

60. Shtilman, I., *Polymeric Biomaterials*. 2003: VSP.

61. Ratner, B.D., et al., *Biomaterials Science: An Introduction to Materials in Medicine*. 2012: Elsevier Science.

62. Williams, D.F., *On the mechanisms of biocompatibility.* Biomaterials, 2008. **29**(20): p. 2941-2953.

63. Anderson, J.M., A. Rodriguez, and D.T. Chang, *Foreign body reaction to biomaterials.* Semin Immunol, 2008. **20**(2): p. 86-100.

64. Nilsson, B., et al., *Can cells and biomaterials in therapeutic medicine be shielded from innate immune recognition?* Trends Immunol, 2010. **31**(1): p. 32-8.

65. Anderson, J.M., *Biological responses to materials.* Annual Review of Materials Research, 2001. **31**: p. 81-110.

66. Helmus, M.N., *Biomaterials in the Design and Reliability of Medical Devices*. 2003: Landes Bioscience/Eurekah.com.

67. Cincu, C., et al., in *Biomateriale Polimerice si Aplicatii Medicale*. 2009, Politehnica Press.

68. Doi, Y., A. Segawa, and M. Kunioka, *Biosynthesis and characterization of poly(3-hydroxybutyrate-co-4-hydroxybutyrate) in Alcaligenes eutrophus.* International Journal of Biological Macromolecules, 1990. **12**(2): p. 106-111.

69. Doi, Y., S. Kitamura, and H. Abe, *Microbial Synthesis and Characterization of Poly(3-hydroxybutyrate-co-3-hydroxyhexanoate).* Macromolecules, 1995. **28**(14): p. 4822-4828.

70. Freier, T., et al., *In vitro and in vivo degradation studies for development of a biodegradable patch based on poly(3-hydroxybutyrate).* Biomaterials, 2002. **23**(13): p. 2649-2657.

71. Lee, S.Y., *Bacterial polyhydroxyalkanoates.* Biotechnology and Bioengineering, 1996. **49**(1): p. 1-14.

72. Freier, T., *Biopolyesters in Tissue Engineering Applications*, in *Polymers for Regenerative Medicine*, C. Werner, Editor. 2006, Springer Berlin Heidelberg. p. 1-61.

73. Baptist, J.N. and J.B. Ziegler, *METHOD OF MAKING ABSORBABLE SURGICAL SUTURES FROM POLY BETA HYDROXY ACIDS* 1965, W. R. Grace Co., New York, N.Y., 5 April corporation of Connecticut November Drawing. (OCR): USA.

74. Bonfield, W., *Composites for bone replacement.* Journal of Biomedical Engineering, 1988. **10**(6): p. 522-526.

75. Duvernoy, O., et al., *A Biodegradable Patch used as a Pericardial Substitute after Cardiac Surgery: 6- and 24-Month Evaluation with CT.* Thorac cardiovasc Surg, 1995. **43**(05): p. 271-274.

76. Hazari, A., et al., *A resorbable nerve conduit as an alternative to nerve autograft in nerve gap repair.* British journal of plastic surgery, 1999. **52**(8): p. 653-657.

77. Ljungberg, C., et al., *Neuronal survival using a resorbable synthetic conduit as an alternative to primary nerve repair.* Microsurgery, 1999. **19**(6): p. 259-264.

78. Novikov, L.N., et al., *A novel biodegradable implant for neuronal rescue and regeneration after spinal cord injury.* Biomaterials, 2002. **23**(16): p. 3369-3376.

79. Kunze, C., et al., *In vitro and in vivo studies on blends of isotactic and atactic poly (3-hydroxybutyrate) for development of a dura substitute material.* Biomaterials, 2006. **27**(2): p. 192-201.

80. Shum-Tim, D., et al., *Tissue engineering of autologous aorta using a new biodegradable polymer.* The Annals of Thoracic Surgery, 1999. **68**(6): p. 2298-2304.

81. Sodian, R., et al., *Tissue engineering of a trileaflet heart valve-early in vitro experiences with a combined polymer.* Tissue Eng, 1999. **5**(5): p. 489-94.

82. Stock, U.A., et al., *Patch augmentation of the pulmonary artery with bioabsorbable polymers and autologous cell seeding.* The Journal of thoracic and cardiovascular surgery, 2000. **120**(6): p. 1158-1167.

83. Hoerstrup, S.P., et al., *Tissue engineering of small caliber vascular grafts.* European Journal of Cardio-Thoracic Surgery, 2001. **20**(1): p. 164-169.

84. Sodian, R., et al., *Evaluation of Biodegradable, Three-Dimensional Matrices for Tissue Engineering of Heart Valves.* ASAIO Journal, 2000. **46**(1): p. 107-110.

85. Martin, D.P. and S.F. Williams, *Medical applications of poly-4-hydroxybutyrate: a strong flexible absorbable biomaterial.* Biochemical Engineering Journal, 2003. **16**(2): p. 97-105.

86. Deng, Y., et al., *Study on the three-dimensional proliferation of rabbit articular cartilage-derived chondrocytes on polyhydroxyalkanoate scaffolds.* Biomaterials, 2002. **23**(20): p. 4049-4056.

87. Wang, Y.-W., Q. Wu, and G.-Q. Chen, *Attachment, proliferation and differentiation of osteoblasts on random biopolyester poly(3-hydroxybutyrate-co-3-hydroxyhexanoate) scaffolds.* Biomaterials, 2004. **25**(4): p. 669-675.

88. Chung, C.W., et al., *Poly(ethylene glycol)-grafted poly(3-hydroxyundecenoate) networks for enhanced blood compatibility.* International Journal of Biological Macromolecules, 2003. **32**(1–2): p. 17-22.

89. Dufresne, A. and M. Vincendon, *Poly(3-hydroxybutyrate) and Poly(3-hydroxyoctanoate) Blends: Morphology and Mechanical Behavior.* Macromolecules, 2000. **33**(8): p. 2998-3008.

90. Marois, Y., et al., *Mechanism and rate of degradation of polyhydroxyoctanoate films in aqueous media: A long-term in vitro study.* Journal of Biomedical Materials Research, 2000. **49**(2): p. 216-224.

91. Gogolewski, S., et al., *Tissue response and in vivo degradation of selected polyhydroxyacids: Polylactides (PLA), poly(3-hydroxybutyrate) (PHB), and poly(3-hydroxybutyrate-co-3-hydroxyvalerate) (PHB/VA).* Journal of Biomedical Materials Research, 1993. **27**(9): p. 1135-1148.

92. Webb, A.R., J. Yang, and G.A. Ameer, *Biodegradable polyester elastomers in tissue engineering.* Expert Opinion on Biological Therapy, 2004. **4**(6): p. 801-812.

93. Dawes, E.A. and P.J. Senior, *The Role and Regulation of Energy Reserve Polymers in Micro-organisms*, in *Advances in Microbial Physiology*, A.H. Rose and D.W. Tempest, Editors. 1973, Academic Press. p. 135-266.

94. Engelberg, I. and J. Kohn, *Physico-mechanical properties of degradable polymers used in medical applications: A comparative study.* Biomaterials, 1991. **12**(3): p. 292-304.

95. Avella, M., E. Martuscelli, and M. Raimo, *Review Properties of blends and composites based on poly(3-hydroxy)butyrate (PHB) and poly(3-hydroxybutyrate-hydroxyvalerate) (PHBV) copolymers.* Journal of Materials Science, 2000. **35**(3): p. 523-545.

96. Scandola, M., et al., *Study of the crystal phase and crystallization rate of bacterial poly(3-hydroxybutyrate-co-3-hydroxyvalerate).* Macromolecules, 1992. **25**(5): p. 1405-1410.

97. Luo, S., D.T. Grubb, and A.N. Netravali, *The effect of molecular weight on the lamellar structure, thermal and mechanical properties of poly(hydroxybutyrate-co-hydroxyvalerates).* Polymer, 2002. **43**(15): p. 4159-4166.

98. Renstad, R., S. Karlsson, and A.-C. Albertsson, *Influence of processing parameters on the molecular weight and mechanical properties of poly(3-hydroxybutyrate-co-3-hydroxyvalerate).* Polymer Degradation and Stability, 1997. **57**(3): p. 331-338.

99. Savenkova, L., et al., *Mechanical properties and biodegradation characteristics of PHB-based films.* Process Biochemistry, 2000. **35**(6): p. 573-579.

100. Baltieri, R.C., L.H. Innocentini Mei, and J. Bartoli, *Study of the influence of plasticizers on the thermal and mechanical properties of poly(3-hydroxybutyrate) compounds.* Macromolecular Symposia, 2003. **197**(1): p. 33-44.

101. Kunze, C., et al., *Anti-inflammatory prodrugs as plasticizers for biodegradable implant materials based on poly(3-hydroxybutyrate).* Journal of Materials Science: Materials in Medicine, 2002. **13**(11): p. 1051-1055.

102. Labrecque, L.V., et al., *Citrate esters as plasticizers for poly(lactic acid).* Journal of Applied Polymer Science, 1997. **66**(8): p. 1507-1513.

103. Choi, J.S. and W.H. Park, *Effect of biodegradable plasticizers on thermal and mechanical properties of poly(3-hydroxybutyrate).* Polymer Testing, 2004. **23**(4): p. 455-460.

104. Freier, T., C. Kunze, and K.P. Schmitz, *Solvent removal from solution-cast films of biodegradable polymers.* Journal of Materials Science Letters, 2001. **20**(21): p. 1929-1931.

105. Abe, H., Y. Doi, and Y. Kumagai, *Synthesis and Characterization of Poly[(R,S)-3-hydroxybutyrate-b-6-hydroxyhexanoate] as a Compatibilizer for a Biodegradable Blend of Poly[(R)-3-hydroxybutyrate] and Poly(6-hydroxyhexanoate).* Macromolecules, 1994. **27**(21): p. 6012-6017.

106. Abe, H., I. Matsubara, and Y. Doi, *Physical Properties and Enzymic Degradability of Polymer Blends of Bacterial Poly[(R)-3-hydroxybutyrate] and Poly[(R,S)-3-hydroxybutyrate] Stereoisomers.* Macromolecules, 1995. **28**(4): p. 844-853.

107. Scandola, M., et al., *Polymer Blends of Natural Poly(3-hydroxybutyrate-co-3-hydroxyvalerate) and a Synthetic Atactic Poly(3-hydroxybutyrate). Characterization and Biodegradation Studies.* Macromolecules, 1997. **30**(9): p. 2568-2574.

108. El-Taweel, S.H., et al., *Stress–strain behavior of blends of bacterial polyhydroxybutyrate.* Journal of Applied Polymer Science, 2004. **94**(6): p. 2528-2537.

109. Gassner, F. and A.J. Owen, *Physical properties of poly(ϐ-hydroxybutyrate)-poly(ε-caprolactone) blends.* Polymer, 1994. **35**(10): p. 2233-2236.

110. Immirzi, B., et al., *Blends of biodegradable polyesters by reactive blending: preparation, characterisation and properties.* Journal of Materials Science, 1999. **34**(7): p. 1625-1639.

111. Abe, H., et al., *Physical Properties and Enzymic Degradability of Poly(3-hydroxybutyrate) Stereoisomers with Different Stereoregularities.* Macromolecules, 1994. **27**(21): p. 6018-6025.

112. Zhao, K., et al., *Polyhydroxyalkanoate (PHA) scaffolds with good mechanical properties and biocompatibility.* Biomaterials, 2003. **24**(6): p. 1041-1045.

113. Kusaka, S., T. Iwata, and Y. Doi†*, *Microbial Synthesis and Physical Properties of Ultra-High-Molecular-Weight Poly[(R)-3-Hydroxybutyrate].* Journal of Macromolecular Science, Part A, 1998. **35**(2): p. 319-335.

114. Park, J.W., Y. Doi, and T. Iwata, *Uniaxial Drawing and Mechanical Properties of Poly[(R)-3-hydroxybutyrate]/Poly(l-lactic acid) Blends.* Biomacromolecules, 2004. **5**(4): p. 1557-1566.

115. Doyle, C., E.T. Tanner, and W. Bonfield, *In vitro and in vivo evaluation of polyhydroxybutyrate and of polyhydroxybutyrate reinforced with hydroxyapatite.* Biomaterials, 1991. **12**(9): p. 841-847.

116. Wang, Y.-W., et al., *Evaluation of three-dimensional scaffolds made of blends of hydroxyapatite and poly(3-hydroxybutyrate-co-3-hydroxyhexanoate) for bone reconstruction.* Biomaterials, 2005. **26**(8): p. 899-904.

117. Wang, Y.-W., Q. Wu, and G.-Q. Chen, *Reduced mouse fibroblast cell growth by increased hydrophilicity of microbial polyhydroxyalkanoates via hyaluronan coating.* Biomaterials, 2003. **24**(25): p. 4621-4629.

118. Saito, T., et al., *In vivo and in vitro degradation of poly(3-hydroxybutyrate) in pat.* Biomaterials, 1991. **12**(3): p. 309-312.

119. Taylor, M.S., et al., *Six bioabsorbable polymers: In vitro acute toxicity of accumulated degradation products.* Journal of Applied Biomaterials, 1994. **5**(2): p. 151-157.

120. Shishatskaya, E.I. and T.G. Volova, *A comparative investigation of biodegradable polyhydroxyalkanoate films as matrices for in vitro cell cultures.* Journal of Materials Science: Materials in Medicine, 2004. **15**(8): p. 915-923.

121. Cheng, G., Z. Cai, and L. Wang, *Biocompatibility and biodegradation of poly(hydroxybutyrate)/poly(ethylene glycol) blend films.* Journal of Materials Science: Materials in Medicine, 2003. **14**(12): p. 1073-1078.

122. Schmack, G., et al., *Effect of electron irradiation on the properties of poly(3-hydroxybutyric acid) fibres and their in vitro degradation.* Polymer Degradation and Stability, 2004. **83**(3): p. 467-472.

123. Rivard, C.-H., et al., *Fibroblast seeding and culture in biodegradable porous substrates.* Journal of Applied Biomaterials, 1995. **6**(1): p. 65-68.

124. Zhang, D.M., et al., *Wettability improvement of bacterial polyhydroxyalkanoates via ion implantation.* Surface and Coatings Technology, 2000. **131**(1–3): p. 350-354.

125. Nitschke, M., et al., *Low pressure plasma treatment of poly(3-hydroxybutyrate): Toward tailored polymer surfaces for tissue engineering scaffolds.* Journal of Biomedical Materials Research, 2002. **59**(4): p. 632-638.

126. Yang, X., K. Zhao, and G.-Q. Chen, *Effect of surface treatment on the biocompatibility of microbial polyhydroxyalkanoates.* Biomaterials, 2002. **23**(5): p. 1391-1397.

127. Zhao, K., et al., *Effect of lipase treatment on the biocompatibility of microbial polyhydroxyalkanoates.* Journal of Materials Science: Materials in Medicine, 2002. **13**(9): p. 849-854.

128. Hu, S.G., C.H. Jou, and M.C. Yang, *Protein adsorption, fibroblast activity and antibacterial properties of poly(3-hydroxybutyric acid-co-3-hydroxyvaleric acid) grafted with chitosan and chitooligosaccharide after immobilized with hyaluronic acid.* Biomaterials, 2003. **24**(16): p. 2685-2693.

129. Piddubnyak, V., et al., *Oligo-3-hydroxybutyrates as potential carriers for drug delivery.* Biomaterials, 2004. **25**(22): p. 5271-5279.

130. Saad, B., et al., *Cell response of cultured macrophages, fibroblasts, and co-cultures of Kupffer cells and hepatocytes to particles of short-chain poly[(R)-3-hydroxybutyric acid].* Journal of Materials Science: Materials in Medicine, 1996. **7**(1): p. 56-61.

131. Nebe, B., et al., *Structural alterations of adhesion mediating components in cells cultured on poly-β-hydroxy butyric acid.* Biomaterials, 2001. **22**(17): p. 2425-2434.

132. Gurav, N. and S. Downes, *A qualitative in vitro evaluation of the degradable materials poly(caprolactone), poly(hydroxybutyrate) and a poly(hydroxybutyrate)-(hydroxyvalerate) copolymer.* Journal of Materials Science: Materials in Medicine, 1994. **5**(11): p. 784-787.

133. Torun Köse, G., et al., *Poly(3-hydroxybutyric acid-co-3-hydroxyvaleric acid) based tissue engineering matrices.* Journal of Materials Science: Materials in Medicine, 2003. **14**(2): p. 121-126.

134. Köse, G.T., et al., *Macroporous poly(3-hydroxybutyrate-co-3-hydroxyvalerate) matrices for bone tissue engineering.* Biomaterials, 2003. **24**(11): p. 1949-1958.

135. Tesema, Y., D. Raghavan, and J. Stubbs, *Bone cell viability on collagen immobilized poly(3-hydroxybutrate-co-3-hydroxyvalerate) membrane: Effect of surface chemistry.* Journal of Applied Polymer Science, 2004. **93**(5): p. 2445-2453.

136. Zheng, Z., et al., *Effects of crystallization of polyhydroxyalkanoate blend on surface physicochemical properties and interactions with rabbit articular cartilage chondrocytes.* Biomaterials, 2005. **26**(17): p. 3537-3548.

137. Deng, Y., et al., *Poly(hydroxybutyrate-co-hydroxyhexanoate) promoted production of extracellular matrix of articular cartilage chondrocytes in vitro.* Biomaterials, 2003. **24**(23): p. 4273-4281.

138. Zheng, Z., et al., *Induced production of rabbit articular cartilage-derived chondrocyte collagen II on polyhydroxyalkanoate blends.* Journal of Biomaterials Science, Polymer Edition, 2003. **14**(7): p. 615-624.

139. Foster, L.J.R., S.M. Davies, and B.J. Tighe, *Centrifugally-spun polyhydroxybutyrate fibres: Effect of process solvent on structure, morphology and cell response.* Journal of Biomaterials Science, Polymer Edition, 2001. **12**(3): p. 317-336.

140. Ostwald, J., et al., *In-vitro-Kultivierung von Zellen der respiratorischen Schleimhaut auf Matrizes aus Kollagen, Poly-L-Laktid (PLLA) und Polyhydroxybuttersäure (PHB).* Laryngo-Rhino-Otol, 2003. **82**(10): p. 693-699.

141. Tezcaner, A., K. Bugra, and V. Hasırcı, *Retinal pigment epithelium cell culture on surface modified poly(hydroxybutyrate-co-hydroxyvalerate) thin films.* Biomaterials, 2003. **24**(25): p. 4573-4583.

142. Malm, T., et al., *Enlargement of the Right Ventricular Outflow Tract and the Pulmonary Artery with a New Biodegradable Patch in Transannular Position.* European Surgical Research, 1994. **26**(5): p. 298-308.

143. Volova, T., et al., *Results of biomedical investigations of PHB and PHB/PHV fibers.* Biochemical Engineering Journal, 2003. **16**(2): p. 125-133.

144. Shishatskaya, E.I., et al., *Tissue response to the implantation of biodegradable polyhydroxyalkanoate sutures.* Journal of Materials Science: Materials in Medicine, 2004. **15**(6): p. 719-728.

145. Löbler, M., et al., *Biomaterial patches sutured onto the rat stomach induce a set of genes encoding pancreatic enzymes.* Biomaterials, 2002. **23**(2): p. 577-583.

146. Löbler, M., et al., *Biomaterial implants induce the inflammation marker CRP at the site of implantation.* Journal of Biomedical Materials Research, 2002. **61**(1): p. 165-167.

147. Knowles, J.C. and G.W. Hastings, *In vitro and in vivo investigation of a range of phosphate glass-reinforced polyhydroxybutyrate-based degradable composites.* Journal of Materials Science: Materials in Medicine, 1993. **4**(2): p. 102-106.

148. Luklinska, Z.B. and W. Bonfield, *Morphology and ultrastructure of the interface between hydroxyapatite-polyhydroxybutyrate composite implant and bone.* Journal of Materials Science: Materials in Medicine, 1997. **8**(6): p. 379-383.

149. Leenstra, T.S., J.C. Maltha, and A.M. Kuijpers-Jagtman, *Biodegradation of non-porous films after submucoperiosteal implantation on the palate of Beagle dogs.* Journal of Materials Science: Materials in Medicine, 1995. **6**(8): p. 445-450.

150. Gotfredsen, K., L. Nimb, and E. Hjørting-hansen, *Immediate implant placement using a biodegradable barrier, polyhydroxybutyrate-hydroxyvalerate reinforced with polyglactin 910. An experimental study in dogs.* Clinical Oral Implants Research, 1994. **5**(2): p. 83-91.

151. Unverdorben, M., et al., *A Polyhydroxybutyrate Biodegradable Stent: Preliminary Experience in the Rabbit.* CardioVascular and Interventional Radiology, 2002. **25**(2): p. 127-132.

152. Lootz, D., et al., *Laser cutting: influence on morphological and physicochemical properties of polyhydroxybutyrate.* Biomaterials, 2001. **22**(18): p. 2447-2452.

153. Zhang, L., C. Xiong, and X. Deng, *Biodegradable polyester blends for biomedical application.* Journal of Applied Polymer Science, 1995. **56**(1): p. 103-112.

154. Doi, Y., et al., *Hydrolytic degradation of microbial poly(hydroxyalkanoates).* Die Makromolekulare Chemie, Rapid Communications, 1989. **10**(5): p. 227-230.

155. Jendrossek, D., A. Schirmer, and H.G. Schlegel, *Biodegradation of polyhydroxyalkanoic acids.* Applied Microbiology and Biotechnology, 1996. **46**(5-6): p. 451-463.

156. Winkler, F.K., A. D'Arcy, and W. Hunziker, *Structure of human pancreatic lipase.* Nature, 1990. **343**(6260): p. 771-774.

157. Yasin, M., S.J. Holland, and B.J. Tighe, *Polymers for biodegradable medical devices: V. Hydroxybutyrate-hydroxyvalerate copolymers: effects of polymer processing on hydrolytic degradation.* Biomaterials, 1990. **11**(7): p. 451-454.

158. Holland, S.J., et al., *Polymers for biodegradable medical devices: II. Hydroxybutyrate-hydroxyvalerate copolymers: hydrolytic degradation studies.* Biomaterials, 1987. **8**(4): p. 289-295.

159. Li, H. and J. Chang, *In vitro degradation of porous degradable and bioactive PHBV/wollastonite composite scaffolds.* Polymer Degradation and Stability, 2005. **87**(2): p. 301-307.

160. Mitomo, H., et al., *Radiation-induced degradation of poly(3-hydroxybutyrate) and the copolymer poly(3-hydroxybutyrate-co-3-hydroxyvalerate).* Polymer Degradation and Stability, 1994. **45**(1): p. 11-17.

161. Carswell-Pomerantz, T., et al., *Mechanistic Studies on the Radiation Chemistry of Poly(hydroxybutyrate)*, in *Irradiation of Polymers*. 1996, American Chemical Society. p. 11-27.

162. Bibers, I. and M. Kalnins, *Control of biopolymer poly-β-hydroxybutyrate characteristics by γ-irradiation.* Mechanics of Composite Materials, 1999. **35**(2): p. 169-178.

163. Miyazaki, S.S., et al., *Biodegradable polymeric films based on microbial poly(3-hydroxybutyrate). Effect of gamma-radiation on mechanical properties and biodegradability.* Macromolecular Symposia, 2003. **197**(1): p. 57-64.

164. Bledzki, A.K., J. Gassan, and M. Heyne, *Auswirkungen von Sterilisationsverfahren auf biologisch abbaubare Kunststoffe.* Die Angewandte Makromolekulare Chemie, 1994. **219**(1): p. 11-26.

165. Behrend, D., K.P. Schmitz, and A. Haubold, *Bioresorbable Polymer Materials for Implant Technology.* Advanced Engineering Materials, 2000. **2**(3): p. 123-125.

166. Olsen, L., et al., *Urethral Reconstruction with a New Synthetic Absorbable Device.* Scandinavian Journal of Urology and Nephrology, 1992. **26**(4): p. 323-326.

167. Kalangos, A. and B. Faidutti, *Preliminary clinical results of implantation of biodegradable pericardial substitute in pediatric open heart operations.* The Journal of thoracic and cardiovascular surgery, 1996. **112**(5): p. 1401-1402.

168. Nkere, U.U., et al., *Pericardial Substitution After Cardiopulmonary Bypass Surgery: A Trial of an Absorbable Patch.* Thorac cardiovasc Surg, 1998. **46**(02): p. 77-83.

169. Mosahebi, A., et al., *Retroviral labeling of Schwann cells: In vitro characterization and in vivo transplantation to improve peripheral nerve regeneration.* Glia, 2001. **34**(1): p. 8-17.

170. Mosahebi, A., et al., *Effect of Allogeneic Schwann Cell Transplantation on Peripheral Nerve Regeneration.* Experimental Neurology, 2002. **173**(2): p. 213-223.

171. McKay Hart, A., M. Wiberg, and G. Terenghi, *Exogenous leukaemia inhibitory factor enhances nerve regeneration after late secondary repair using a bioartificial nerve conduit.* British journal of plastic surgery, 2003. **56**(5): p. 444-450.

172. Young, R.C., G. Terenghi, and M. Wiberg, *Poly-3-hydroxybutyrate (PHB): a resorbable conduit for long-gap repair in peripheral nerves.* British journal of plastic surgery, 2002. **55**(3): p. 235-240.

173. Knowles, J.C. and G.W. Hastings, *In vitro degradation of a PHB/PHV copolymer and a new technique fop monitoring early surface changes.* Biomaterials, 1991. **12**(2): p. 210-214.

174. Knowles, J.C., F.A. Mahmud, and G.W. Hastings, *Piezoelectric characteristics of a polyhydroxybutyrate-based composite.* Clinical Materials, 1991. **8**(1–2): p. 155-158.

175. Kostopoulos, L. and T. Karring, *Augmentation of the rat mandible using guided tissue regeneration.* Clinical Oral Implants Research, 1994. **5**(2): p. 75-82.

176. Vainionpää, S., et al., *Biodegradable fixation of rabbit osteotomies.* Acta Orthopaedica, 1986. **57**(3): p. 237-239.

177. Kostopoulos, L. and T. Karring, *Guided bone regeneration in mandibular defects in rats using a bioresorbable polymer.* Clinical Oral Implants Research, 1994. **5**(2): p. 66-74.

178. Kramp, B., et al., *Polyhydroxybuttersäure (PHB)-Folien und -Platten zur Defektdeckung des knöchernen Schädels im Kaninchenmodell.* Laryngo-Rhino-Otol, 2002. **81**(05): p. 351-356.

179. Galego, N., et al., *Characterization and application of poly(β-hydroxyalkanoates) family as composite biomaterials.* Polymer Testing, 2000. **19**(5): p. 485-492.

180. Boeree, N.R., et al., *Development of a degradable composite for orthopaedic use: mechanical evaluation of an hydroxyapatite-polyhydroxybutyrate composite material.* Biomaterials, 1993. **14**(10): p. 793-796.

181. Li, H. and J. Chang, *Fabrication and characterization of bioactive wollastonite/PHBV composite scaffolds.* Biomaterials, 2004. **25**(24): p. 5473-5480.

182. Ni, J. and M. Wang, *In vitro evaluation of hydroxyapatite reinforced polyhydroxybutyrate composite.* Materials Science and Engineering: C, 2002. **20**(1–2): p. 101-109.

183. Saad, B., et al., *DegraPol-Foam: A Degradable and Highly Porous Polyesterurethane Foam as a New Substrate for Bone Formation.* Artificial Organs, 2000. **24**(12): p. 939-945.

184. Tsujimura, H., *Metamorphosis of wing motor system in the silk moth, Bombyx mori L. (Lepidoptera: Bombycidae): Anatomy of the sensory and motor neurons that innervate larval mesothoracic dorsal musculature, stretch receptors, and epidermis.* International Journal of Insect Morphology and Embryology, 1988. **17**(4–5): p. 367-380.

185. Khan, M.M.R., et al., *Structural characteristics and properties of Bombyx mori silk fiber obtained by different artificial forcibly silking speeds.* International Journal of Biological Macromolecules, 2008. **42**(3): p. 264-270.

186. Koushic, U. and H. Sonia, *A Comparitive Study on Silk Dyeing with Acid Dye and Reactive Dye.* INTERNATIONAL JOURNAL OF ENGINEERING & TECHNOLOGY, 2010. **10**(6): p. 6.

187. Cao, Y. and B. Wang, *Biodegradation of silk biomaterials.* Int J Mol Sci, 2009. **10**(4): p. 1514-24.

188. M, M., T. K, and N.K. S, *The silk proteins, sericin and fibroin in silkworm, Bombyx mori Linn.* Caspian Journal of Environmental Sciences, 2007. **5**(5): p. 14.

189. Vaithanomsat, P. and V. Kitpreechavanich, *Sericin separation from silk degumming wastewater.* Separation and Purification Technology, 2008. **59**(2): p. 129-133.

190. Yamada, H., et al., *Preparation of undegraded native molecular fibroin solution from silkworm cocoons.* Materials Science and Engineering: C, 2001. **14**(1–2): p. 41-46.

191. Nagarkar, S., et al., *Structure and gelation mechanism of silk hydrogels.* Phys Chem Chem Phys, 2010. **12**(15): p. 3834-44.

192. Zhou, C.Z., et al., *Fine organization of Bombyx mori fibroin heavy chain gene.* Nucleic Acids Res, 2000. **28**(12): p. 2413-9.

193. Inoue, S., et al., *Silk fibroin of Bombyx mori is secreted, assembling a high molecular mass elementary unit consisting of H-chain, L-chain, and P25, with a 6:6:1 molar ratio.* J Biol Chem, 2000. **275**(51): p. 40517-28.

194. Altman, G.H., et al., *Silk-based biomaterials.* Biomaterials, 2003. **24**(3): p. 401-416.

195. Monti, P., et al., *Raman spectroscopic characterization of Bombyx mori silk fibroin: Raman spectrum of Silk I.* Journal of Raman Spectroscopy, 2001. **32**(2): p. 103-107.

196. Li, M., et al., *Structure and properties of silk fibroin-poly(vinyl alcohol) gel.* Int J Biol Macromol, 2002. **30**(2): p. 89-94.

197. Li, M., M. Ogiso, and N. Minoura, *Enzymatic degradation behavior of porous silk fibroin sheets.* Biomaterials, 2003. **24**(2): p. 357-365.

198. Shen, Y., M.A. Johnson, and D.C. Martin, *Microstructural Characterization of Bombyx mori Silk Fibers.* Macromolecules, 1998. **31**(25): p. 8857-8864.

199. Monti, P., et al., *Raman spectroscopic studies of silk fibroin from Bombyx mori.* Journal of Raman Spectroscopy, 1998. **29**(4): p. 297-304.

200. Chen, X., et al., *Conformation transition kinetics of regenerated Bombyx mori silk fibroin membrane monitored by time-resolved FTIR spectroscopy.* Biophys Chem, 2001. **89**(1): p. 25-34.

201. He, S.J., R. Valluzzi, and S.P. Gido, *Silk I structure in Bombyx mori silk foams.* Int J Biol Macromol, 1999. **24**(2-3): p. 187-95.

202. Furuzono, T., et al., *Chemical modification of silk fibroin with 2-methacryloyloxyethyl phosphorylcholine. II. Graft-polymerization onto fabric through 2-methacryloyloxyethyl*

isocyanate and interaction between fabric and platelets. Biomaterials, 2000. **21**(4): p. 327-333.

203. Ifrim, S., *Matasea naturala*. 1998, Bucuresti: Ed. Ceres.

204. Sashina, E.S., et al., *Structure and solubility of natural silk fibroin.* Russian Journal of Applied Chemistry, 2006. **79**(6): p. 869-876.

205. Valluzzi, R. and S.P. Gido, *The crystal structure of Bombyx mori silk fibroin at the air–water interface.* Biopolymers, 1997. **42**(6): p. 705-717.

206. Huemmerich, D., U. Slotta, and T. Scheibel, *Processing and modification of films made from recombinant spider silk proteins.* Applied Physics A, 2006. **82**(2): p. 219-222.

207. Lu, Q., et al., *Water-insoluble silk films with silk I structure.* Acta Biomaterialia, 2010. **6**(4): p. 1380-1387.

208. Kuduğ, E. and İ.I.o. Technology, *Use Of Fibroin/Hyaluronic Acid Matrices As A Drug Reservoir In Iontophoretic Transdermal Delivery*. 2004: İzmir Institute of Technology, İzmir.

209. Mukhamedzhanova, M.Y., D.B. Takhtaganova, and T.S. Pak, *Properties of Concentrated Solutions of Fibroin and Its Derivatives.* Chemistry of Natural Compounds, 2001. **37**(4): p. 377-380.

210. Jiang, C., et al., *Mechanical Properties of Robust Ultrathin Silk Fibroin Films.* Advanced Functional Materials, 2007. **17**(13): p. 2229-2237.

211. Chen, H., X. Hu, and P. Cebe, *Thermal properties and phase transitions in blends of Nylon-6 with silk fibroin.* Journal of Thermal Analysis and Calorimetry, 2008. **93**(1): p. 201-206.

212. Lee, Y. and A.O.o.t.U. Nations, *Silk reeling and testing manual[*1999: Food and Agriculture Organization of the United Nations.

213. Hu, X., D. Kaplan, and P. Cebe, *Effect of water on the thermal properties of silk fibroin.* Thermochimica Acta, 2007. **461**(1–2): p. 137-144.

214. Wilhelm, E. and T.T.M. Letcher, *Heat Capacities: Liquids, Solutions and Vapours*. 2010: ROYAL SOC OF CHEMISTRY.

215. Motta, A., L. Fambri, and C. Migliaresi, *Regenerated silk fibroin films: Thermal and dynamic mechanical analysis.* Macromolecular Chemistry and Physics, 2002. **203**(10-11): p. 1658-1665.

216. Murphy, A.R. and D.L. Kaplan, *Biomedical applications of chemically-modified silk fibroin.* Journal of Materials Chemistry, 2009. **19**(36): p. 6443-6450.

217. Chen, X., et al., *Regenerated Bombyx silk solutions studied with rheometry and FTIR.* Polymer, 2001. **42**(25): p. 09969-09974.

218. Makaya, K., et al., *Comparative study of silk fibroin porous scaffolds derived from salt/water and sucrose/hexafluoroisopropanol in cartilage formation.* Journal of Bioscience and Bioengineering, 2009. **108**(1): p. 68-75.

219. Ohgo, K., et al., *Preparation of non-woven nanofibers of Bombyx mori silk, Samia cynthia ricini silk and recombinant hybrid silk with electrospinning method.* Polymer, 2003. **44**(3): p. 841-846.

220. Um, I.C., et al., *The role of formic acid in solution stability and crystallization of silk protein polymer.* International Journal of Biological Macromolecules, 2003. **33**(4–5): p. 203-213.

221. Wang, X., et al., *Fibrous proteins and tissue engineering.* Materials Today, 2006. **9**(12): p. 44-53.

222. Kaplan, D.L., *Fibrous proteins—silk as a model system.* Polymer Degradation and Stability, 1998. **59**(1–3): p. 25-32.

223. Zhang, Q., S. Yan, and M. Li, *Silk Fibroin Based Porous Materials.* Materials, 2009. **2**(4): p. 2276-2295.

224. Cilurzo, F., et al., *An investigation into silk fibroin conformation in composite materials intended for drug delivery.* International Journal of Pharmaceutics, 2011. **414**(1–2): p. 218-224.

225. Shi, P. and J.C.H. Goh, *Release and cellular acceptance of multiple drugs loaded silk fibroin particles.* International Journal of Pharmaceutics, 2011. **420**(2): p. 282-289.

226. Oliveira, A.L., et al., *Aligned silk-based 3-D architectures for contact guidance in tissue engineering.* Acta Biomaterialia, 2012. **8**(4): p. 1530-1542.

227. Acharya, C., B. Hinz, and S.C. Kundu, *The effect of lactose-conjugated silk biomaterials on the development of fibrogenic fibroblasts.* Biomaterials, 2008. **29**(35): p. 4665-75.

228. Gotoh, Y., et al., *Preparation of lactose–silk fibroin conjugates and their application as a scaffold for hepatocyte attachment.* Biomaterials, 2004. **25**(6): p. 1131-1140.

229. Wang, Y., et al., *The synergistic effects of 3-D porous silk fibroin matrix scaffold properties and hydrodynamic environment in cartilage tissue regeneration.* Biomaterials, 2010. **31**(17): p. 4672-4681.

230. M, R.R., *Innovative and Multidirectional Applications of Natural Fibre, Silk - A Review.* Academic Journal of Entomology, 2009. **2**(2): p. 5.

231. Shi, P. and J.C.H. Goh, *Self-assembled silk fibroin particles: Tunable size and appearance.* Powder Technology, 2012. **215–216**(0): p. 85-90.

232. Vasconcelos, A., A.C. Gomes, and A. Cavaco-Paulo, *Novel silk fibroin/elastin wound dressings.* Acta Biomaterialia, 2012. **8**(8): p. 3049-3060.

233. Schneider, A., et al., *Biofunctionalized electrospun silk mats as a topical bioactive dressing for accelerated wound healing.* Acta Biomaterialia, 2009. **5**(7): p. 2570-2578.

234. Teng, W., J. Cappello, and X. Wu, *Physical crosslinking modulates sustained drug release from recombinant silk-elastinlike protein polymer for ophthalmic applications.* J Control Release, 2011. **156**(2): p. 186-94.

235. Madduri, S., M. Papaloïzos, and B. Gander, *Trophically and topographically functionalized silk fibroin nerve conduits for guided peripheral nerve regeneration.* Biomaterials, 2010. **31**(8): p. 2323-2334.

236. Altman, G.H., et al., *Silk matrix for tissue engineered anterior cruciate ligaments.* Biomaterials, 2002. **23**(20): p. 4131-41.

237. Mandal, B.B. and S.C. Kundu, *Calcium alginate beads embedded in silk fibroin as 3D dual drug releasing scaffolds.* Biomaterials, 2009. **30**(28): p. 5170-5177.

238. Garcia-Fuentes, M., et al., *Silk fibroin/hyaluronan scaffolds for human mesenchymal stem cell culture in tissue engineering.* Biomaterials, 2009. **30**(28): p. 5068-5076.

239. Gandhi, M., et al., *Post-spinning modification of electrospun nanofiber nanocomposite from Bombyx mori silk and carbon nanotubes.* Polymer, 2009. **50**(8): p. 1918-1924.

240. H, Z.Z., O. K, and A. T, *Preparation and characterization of regenerated Bombyx mori silk fibroin fiber with high strength.* Express Polymer Letters, 2008. **2**(12): p. 5.

241. Li, G., et al., *Surface modification and functionalization of silk fibroin fibers/fabric toward high performance applications.* Materials Science and Engineering: C, 2012. **32**(4): p. 627-636.

242. Fan, H., et al., *In vivo study of anterior cruciate ligament regeneration using mesenchymal stem cells and silk scaffold.* Biomaterials, 2008. **29**(23): p. 3324-3337.

243. Wei, W., et al., *Bio-inspired capillary dry spinning of regenerated silk fibroin aqueous solution.* Materials Science and Engineering: C, 2011. **31**(7): p. 1602-1608.

244. Wang, M., et al., *Production of Submicron Diameter Silk Fibers under Benign Processing Conditions by Two-Fluid Electrospinning.* Macromolecules, 2006. **39**(3): p. 1102-1107.

245. Horan, R.L., et al., *In vitro degradation of silk fibroin.* Biomaterials, 2005. **26**(17): p. 3385-3393.

246. Kardestuncer, T., et al., *RGD-tethered silk substrate stimulates the differentiation of human tendon cells.* Clin Orthop Relat Res, 2006. **448**: p. 234-9.

247. Tudora, M.R., et al., Chem. Bull. "Politehnica" Univ. Timișoara, 2010. **55(69)**(1): p. 82-85.

248. Wei, K., et al., *Multiwalled carbon nanotubes incorporated bombyx mori silk nanofibers by electrospinning.* Journal of Polymer Research, 2011. **18**(4): p. 579-585.

249. Kang, M., P. Chen, and H.-J. Jin, *Preparation of multiwalled carbon nanotubes incorporated silk fibroin nanofibers by electrospinning.* Current Applied Physics, 2009. **9**(1, Supplement): p. S95-S97.

250. Liu, H., et al., *Modification of sericin-free silk fibers for ligament tissue engineering application.* Journal of Biomedical Materials Research Part B: Applied Biomaterials, 2007. **82B**(1): p. 129-138.

251. Mandal, B.B. and S.C. Kundu, *Cell proliferation and migration in silk fibroin 3D scaffolds.* Biomaterials, 2009. **30**(15): p. 2956-2965.

252. Zhang, Q., et al., *Preparation of uniaxial multichannel silk fibroin scaffolds for guiding primary neurons.* Acta Biomater, 2012. **8**(7): p. 2628-38.

253. Nazarov, R., H.J. Jin, and D.L. Kaplan, *Porous 3-D scaffolds from regenerated silk fibroin.* Biomacromolecules, 2004. **5**(3): p. 718-26.

254. Kim, H.J., et al., *Influence of macroporous protein scaffolds on bone tissue engineering from bone marrow stem cells.* Biomaterials, 2005. **26**(21): p. 4442-52.

255. Tamada, Y., *New process to form a silk fibroin porous 3-D structure.* Biomacromolecules, 2005. **6**(6): p. 3100-6.

256. Zhou, J., C. Cao, and X. Ma, *A novel three-dimensional tubular scaffold prepared from silk fibroin by electrospinning.* International Journal of Biological Macromolecules, 2009. **45**(5): p. 504-510.

257. Kim, U.J., et al., *Three-dimensional aqueous-derived biomaterial scaffolds from silk fibroin.* Biomaterials, 2005. **26**(15): p. 2775-85.

258. Vepari, C. and D.L. Kaplan, *Silk as a biomaterial.* Progress in Polymer Science, 2007. **32**(8–9): p. 991-1007.

259. Uebersax, L., H.P. Merkle, and L. Meinel, *Insulin-like growth factor I releasing silk fibroin scaffolds induce chondrogenic differentiation of human mesenchymal stem cells.* Journal of Controlled Release, 2008. **127**(1): p. 12-21.

260. Yan, L.-P., et al., *Macro/microporous silk fibroin scaffolds with potential for articular cartilage and meniscus tissue engineering applications.* Acta Biomaterialia, 2012. **8**(1): p. 289-301.

261. Wang, Y., et al., *The synergistic effects of 3-D porous silk fibroin matrix scaffold properties and hydrodynamic environment in cartilage tissue regeneration.* Biomaterials, 2010. **31**(17): p. 4672-81.

262. House, M., et al., *Cervical tissue engineering using silk scaffolds and human cervical cells.* Tissue Eng Part A, 2010. **16**(6): p. 2101-12.

263. Vepari, C.P. and D.L. Kaplan, *Covalently immobilized enzyme gradients within three-dimensional porous scaffolds.* Biotechnol Bioeng, 2006. **93**(6): p. 1130-7.

264. Szybala, C., et al., *Antiepileptic effects of silk-polymer based adenosine release in kindled rats.* Exp Neurol, 2009. **219**(1): p. 126-35.

265. Lu, Q., et al., *Cytocompatibility and blood compatibility of multifunctional fibroin/collagen/heparin scaffolds.* Biomaterials, 2007. **28**(14): p. 2306-13.

266. Lu, Q., et al., *Green process to prepare silk fibroin/gelatin biomaterial scaffolds.* Macromol Biosci, 2010. **10**(3): p. 289-98.

267. Lammel, A.S., et al., *Controlling silk fibroin particle features for drug delivery.* Biomaterials, 2010. **31**(16): p. 4583-91.

268. Wang, X., et al., *Silk nanospheres and microspheres from silk/pva blend films for drug delivery.* Biomaterials, 2010. **31**(6): p. 1025-35.

269. Wang, X., et al., *Silk microspheres for encapsulation and controlled release.* J Control Release, 2007. **117**(3): p. 360-70.

270. Li, C., et al., *Electrospun silk-BMP-2 scaffolds for bone tissue engineering.* Biomaterials, 2006. **27**(16): p. 3115-24.

271. Fini, M., et al., *The healing of confined critical size cancellous defects in the presence of silk fibroin hydrogel.* Biomaterials, 2005. **26**(17): p. 3527-36.

272. Zhao, J., et al., *Apatite-coated silk fibroin scaffolds to healing mandibular border defects in canines.* Bone, 2009. **45**(3): p. 517-27.

273. Zaharia, C., et al., *Characterization and deposition behavior of silk hydrogels soaked in simulated body fluid.* Materials Science and Engineering: C, 2012. **32**(4): p. 945-952.

274. Zhou, C., et al., *Application of rod-shaped cellulose nanocrystals in polyacrylamide hydrogels.* Journal of Colloid and Interface Science, 2011. **353**(1): p. 116-123.

275. Hibino, T., *New nanocomposite hydrogels containing layered double hydroxide.* Applied Clay Science, 2010. **50**(2): p. 282-287.

276. Haque, M.A., T. Kurokawa, and J.P. Gong, *Super tough double network hydrogels and their application as biomaterials.* Polymer, 2012. **53**(9): p. 1805-1822.

277. Mandal, B.B., S. Kapoor, and S.C. Kundu, *Silk fibroin/polyacrylamide semi-interpenetrating network hydrogels for controlled drug release.* Biomaterials, 2009. **30**(14): p. 2826-2836.

278. Atkinst, T.W. and S.J. Peacock, *In vitro biodegradation of polyhydroxybutyrate-hydroxyvalerate microcapsules exposed to Hank's buffer, newborn calf serum, pancreatin and synthetic gastric juice.* Journal of Microencapsulation, 1997. **14**(1): p. 35-49.

279. Ratner, B.D., et al., *In: Biomaterials science: An introduction to materials in medicine.* , B.D. Ratner, F.J. Schoen, and J.E. Lemons, Editors. 2004: San Diego: Elsevier. p. 1.

List of published papers and conference participations

PUBLISHED PAPERS

1. **C.-N. Degeratu**, G. Mabilleau,E. Aguado, R. Mallet, D. Chappard, C. Cincu, *In vitro and in vivo behavior of PHBV fibers obtained by a wet spinning method,* under review in Biomedical Materials (IF - 2.174)
2. **C.-N. Degeratu**, G. Mabilleau, C. Cincu, D. Chappard, *Aluminum inhibits the growth of hydroxyapatite crystals developed on a biomimic methacrylatic polymer,*2013, Article in press Journal of Trace Elements in Medicine and Biology, http://dx.doi.org/10.1016/j.jtemb.2013.05.004 (IF - 1.959)
3. M. N'Diaye, **C. Degeratu**, J.M. Bouler, D. Chappard, *Biomaterials porosity determined by fractal dimensions, succolarity and lacunarity on microcomputed tomographic images.* Materials Science and Engineering: C. 2013;33(4):2025-30 (IF - 2.404)
4. M. Armeanu, C. Zaharia, C. Cincu, **C.-N. Degeratu**, *Rheological Behaviour of Solutions of Polyacrylmide Modified by Mannich Reaction*, Revista de Chimie, 62 (4), pp.479-481 2011 (IF - 0.538)
5. M. Rapa, E. Grosu, **C. Degeratu**, A. Scheau, C. Stanescu, *Biodegradable Blends Prepared from Poly(3-hydroxybutyrate) and Wood/Cellulose Fibers,* Materiale Plastice 47 (4), pp. 503-508, 2010 (IF - 0.379)
6. M. Armeanu, C. Cincu, C. Zaharia, **C.-N. Degeratu**, R.-M.Tudora. *Active polymers for water treatment,* Materiale Plastice, 47(3), pp. 274-277, 2010 (IF - 0.379)
7. E. Mircea, C. Zaharia, C. Cincu, F. Miculescu, G. Hubcă, **C.-N. Degeratu**, *Natural fibers modified by chemical methods for application in bone* pathology, Politehnica University of Bucharest. Scientific Bulletin.Series B: Chemistry and Materials Science, 4, 2010

8. **C.-N. Degeratu**, C. Zaharia, M.R. Tudora, C. Tucureanu, G. Hubca, A. Salageanu, C. Cincu, *Influence of Porosity Upon Cells Adhesion on Polyhydroxyalkanoates Films,* Chemical Bulletin of "Politehnica" University of Timisoara 55(69), 2, pp. 189-192, 2010
9. M.R. Tudora, C. Zaharia, A. Diacon, **C.-N. Degeratu**, E. Mircea, C. Andronescu, C. Cincu, N. Preda and I. Enculescu, *Deposition of Bone-Like Hydroxyapatite on Grafted Fibroin Silk Fibers*, Chemical Bulletin of "Politehnica" University of Timisoara 55(69), 1, pp. 82-85, 2010

CONFERENCE PARTICIPATION

1. **C.-N. Degeratu**, C. Cincu, *Biomaterials based on polyester used as a bone reconstruction substitute,* Priorities of chemistry for a sustainable development – *PRIOCHEM - 8th Edition,* International symposium, October 25th – 26th , 2012, Bucharest, Romania – oral presentation
2. **C.-N. Degeratu**, C.Zaharia, A. Diacon, C. Cincu, B. Marculescu, M. R. Tudora *Functionalization Of Natural Polyester Films By Low-Pressure Oxygen Plasma Discharge And Their Medical Uses,* The 4th International Conference "Biomaterials, Tissue Engineering & Medical Devices " BiomMedD'2010, September 23-25, 2010, Sinaia, Romania – poster presentation
3. C. Cincu, C.Zaharia, A. Diacon, **C.-N. Degeratu**, *Biodegradable polyhydroxyesters with medical applications,*16th Romanian International Conference on Chemistry and Chemical Engineering, RICCCE16, Sinaia, Romania, 09-12 September 2009, poster
4. **C.-N. Degeratu**, C. Zaharia, M.R. Tudora, C. Tucureanu, G. Hubca, A. Salageanu, C. Cincu, *Influence of Porosity Upon Cells Adhesion on Polyhydroxyalkanoates Films*, 2nd International Conference on Chemistry and Chemical Engineering, May 27-29, 2010, Timisoara, Romania – oral presentation
5. M.-R. Tudora, C. Zaharia, A Diacon, **C.-N. Degeratu**, E. Mircea, C. Cincu, N. Preda, I. Enculescu, *Deposition of Bone-like Hydroxyapatite on Grafted Fibroin Silk Fiber*, 2nd International Conference on Chemistry and Chemical Engineering, May 27-29, 2010, Timisoara, Romania – oral presentation

Thèse de Doctorat

Cristinel-Nicolae DEGERATU

Structures de biopolymères pour la reconstruction de tissus biologiques

Biopolymer based structures for biological tissue reconstruction

Résumé

La thèse intitulée ***Structures de biopolymères pour la reconstruction de tissus biologiques***, structurée en 4 chapitres, présente la possibilité d'obtenir des structures biopolymériques qui peuvent être utilisées dans la reconstruction des tissus, notamment dans la reconstruction des tissus osseux.

Les objectifs spécifiques suivants ont été définis et suivis dans les chapitres 2, 3 et 4: 1) L'obtention de structures basées sur le PHA et des fibres naturelles, pour leur utilisation médicale - films, fibres, structures compactes et/ou poreuses, 2) Modification physique ou chimique des structures obtenues pour améliorer leur biocompatibilité, 3) Caractérisation biologique *in vitro* et *in vivo* des matériaux; 4) Etude de l'influence des métaux sur la minéralisation du tissu osseux.

Le Chapitre I résume les biomatériaux utilisés en génie tissulaire basé sur la littérature.

Le Chapitre II présente les différentes structures biopolymériques étudiées: films, microparticules, fibres, tubes et structures microporeuses et l'évaluation des propriétés physiques, chimiques et mécaniques des PHA et fibres naturelles et une étude sur la porosité en utilisant le microCT.

Le chapitre III traite de l'influence de la porosité sur l'adhésion cellulaire des films de PHA, une étude *in vitro* et le comportement *in vivo* des fibres de PHBV. La dernière partie inclut une étude sur la modification des fibres de fibroïne et de cellulose, pour améliorer leur minéralisation.

Le chapitre IV traite l'influence de l'aluminium sur la minéralisation osseuse. Cette étude a été motivée par les conclusions alarmantes des effets nocifs de l'aluminium sur la minéralisation osseuse.

La dernière section contient des observations finales et des perspectives.

Mots clés
biopolymères, reconstruction des tissus, polyhydroxyalkanoates, fibroïne de soie, porosité, pHEMA, prolifération cellulaire

Abstract

The thesis entitled ***Biopolymer based structures for biological tissue reconstruction***, structured in four chapters, aims to present the possibility of obtaining biopolymeric structures that can be used in tissue reconstruction, especially bone tissue reconstruction.

The following specific objectives were defined and followed in Chapters 2, 3 and 4: 1) Obtaining structures based on PHA and natural fibers, for medical purposes - films; fibers; blocks or other types of compact and/or porous structures; 2) Physical or chemical modification of the obtained structures to improve their biocompatibility properties; 3) Biological characterization of the materials *in vitro* and *in vivo*; 4) Study on the influence of metals on the mineralization of bone tissue.

Chapter I gives an overview of the biomaterials used in tissue engineering based on literature.

Chapter II presents the various biopolymer-based structures: films; microparticles; fibers; tubes and microporous structures. It includes the assessment of physical, chemical and mechanical properties of PHA and natural fibers and a study on porosity using microCT.

Chapter III discusses the influence of porosity on cell adhesion of polyhydroxyalkanoates films, a study on *in-vitro* and *in-vivo* behavior of PHBV fibers. The final part includes the results of a study concerning the modification of fibroin fibers and cellulose fibers with synthetic polymers, with the aim to enhance mineralization.

Chapter IV addresses the influence of aluminum on bone mineralization. This study was motivated by the alarming findings on the harmful effects of aluminum on bone mineralization.

The thesis ends with concluding remarks and perspectives.

Key Words
biopolymers; tissue engineering; polyhydroxyalkanoates; silk fibroin; porosity; pHEMA; simulated body fluid (SBF); cell proliferation.

Unité de recherche : ***GEROM*** *: Groupe d'Etudes sur le Remodelage Osseux et les bioMatériaux - UPRES EA 4658*
et Département des Bioresources et Science des Polymères - UPB Bucarest